Lawrence Berkeley National Laboratory
Recent Work

Title
Interpretation of Time Domain Electromagnetic Soundings near Geological Contacts

Permalink
https://escholarship.org/uc/item/0xj1c8p5

Author
Wilt, M.J.

Publication Date
1991-12-01

Lawrence Berkeley Laboratory
UNIVERSITY OF CALIFORNIA

EARTH SCIENCES DIVISION

Interpretation of Time Domain Electromagnetic Soundings near Geological Contacts

M.J. Wilt
(Ph.D. Thesis)

December 1991

DISCLAIMER

Interpretation of Time Domain Electromagnetic Soundings near Geological Contacts

Michael Joseph Wilt

(Ph.D. Thesis)

Engineering Geoscience
University of California

Earth Sciences Division
Lawrence Berkeley Laboratory
University of California
Berkeley, California 94720

December 1991

INTERPRETATION OF TIME DOMAIN ELECTROMAGNETIC

SOUNDINGS NEAR GEOLOGICAL CONTACTS

by

Michael Joseph Wilt

Abstract

Lateral changes in geology pose a serious problem in data interpretation for any surface geophysical method. Although many geophysical techniques are designed to probe vertically, the source signal invariably spreads laterally, so any lateral variations in geology will affect the measurements and interpretation. This problem is particularly acute for controlled source electromagnetic soundings because only a few techniques are available to interpret the data if lateral effects are present.

In this thesis we examine the effects of geological contacts for the time domain electromagnetic sounding method (TDEM). Using two simple two-dimensional models, the truncated thin-sheet and the quarter-space, we examine the system response for several commonly used TDEM sounding configurations. For each system we determine the sensitivity to the contact, establish how to the contact anomaly may be distinguished from other anomalies and, when feasible, develop methods for interpreting the contact geometry and for stripping the contact anomaly from the observed data. Since no numerical models were available when this work was started, data were collected using scale models with a system designed at the University of California at Berkeley. The models were assembled within a table-top modeling tank from sheets or blocks of metal using air or mercury as a host medium. Data

were collected with a computer-controlled acquisition system.

For a magnetic dipole source near the edge of a truncated sheet, induced currents propagating from the source are augmented on the conductive side of the contact and are decreased on the resistive side. The net anomalous current is a series of horizontal current loops centered at the edge. Anomalous current builds up at the contact during early and intermediate times and then seems to propagate back towards the source at later times as if it were reflected by the edge. The anomalous magnetic field near the edge decays exponentially at intermediate to late times.

We compared system responses for the truncated sheet and quarter-space models, using a fixed-loop variable-offset configuration, a grounded source variable-offset system (electric dipole), and a central induction system. Whereas for the inductive (loop) sources the contact anomaly does not appear until the induced currents have propagated from the source to the edge, for the electric dipole system the edge effect appears instantaneously and is present throughout time. With this system, currents are galvanically impressed into the earth so that electrical charge instantaneously appears at the conductivity interfaces. For all of the systems considered, we found that the contact anomaly was a function of the source dimensions, the distance from the source to the edge, and the conductance or conductivity of the model. The largest edge anomaly was observed with the electric dipole system; the smallest was observed with the central-loop configuration.

The simplest contact effect observed was with the central-loop configuration. For the vertical component it consists of a smooth level adjustment between the fields on either side of the edge. The horizontal field, which is zero over a layered model, develops a peak near the edge. If a profile of central-loop soundings is made over a contact and each decay curve is fitted to a one-dimensional model, the edge effect appears as a fictitious resistive layer that becomes shallower and more resistive as the soundings are made closer to the edge. We found the central-loop horizontal field to be diagnostic of the properties and location of the contact. Analysis of horizontal field transients yields simple expressions where the conductance or conductivity of the truncated sheet or quarter-space and the location of the contact may be determined from the transient peaks or their late-time decay characteristics. Profiles of horizontal fields are useful in determining contact dip and depth of overburden. For a two-

dimensional truncated sheet the horizontal and vertical field response may be collapsed into a single set of profiles if the fields are plotted against a normalized distance given by $R_n = \dfrac{R}{\mu St}$ where S is the sheet conductance, t is the lag time and R is the distance from the center of the loop to the contact. Using these normalized profiles it is possible to remove a contact anomaly from a profile of soundings. For the simple models considered, this contact stripping does not affect other anomalies of interest crossed by the profile. If horizontal fields are not measured in a central-loop profile, then much of the same information may be obtained by an analysis of the horizontal gradient of the vertical component.

Although the field cases examined here are typically much more complicated than the simple model response studied, the contact anomalies can be easily distinguished from other anomalies of interest by stripping the background layered model response from the data. The conductance and surface location of geological contacts may often be determined by applying the simple formulas developed in this thesis.

Acknowledgement

Table of Contents

CHAPTER 1 : INTRODUCTION

1.1 The Electromagnetic Sounding Method

With the electromagnetic (EM) sounding method we seek to obtain the subsurface distribution of electrical resistivity from measurements of electromagnetic fields on the surface of the earth. An EM sounding may be done by exploiting naturally occurring electromagnetic fields, as in the magnetotelluric and magnetovariometric methods or by supplying a man-made electromagnetic source, as in controlled-source electromagnetics (CSEM). Both methods are routinely applied to geophysical exploration problems; this thesis is concerned with CSEM.

Controlled-source electromagnetics was first proposed as a method for depth sounding by Slichter (1933). The first attempt at CSEM sounding was the ELTRAN method developed in the 1930's (Karcher and McDermott, 1935). ELTRAN utilized in-line electrical dipoles to measure electromagnetic "reflections" from layers of different conductivities. The method was used for about ten years in petroleum exploration but was largely abandoned when a series of scale model experiments revealed that reflections from deeper layers in sedimentary basins were undetectable due to wave dispersion caused by the low resistivity sediments (Yost, 1952; Orsinger and VanNostrand, 1954). Serious theoretical development in electromagnetic techniques did not begin until after World War II with parallel developments in the Soviet Union and the U.S. In the Soviet Union, EM induction in homogeneous half-space and layered half-space models was studied by Tikhonov (1946; 1950) and many others; much of this work is summarized in a book by Vanyan et al. (1968). In the United States, theoretical solutions were developed by Wait in a large number of papers (Wait, 1951 and 1955, for example) and Bhatttacharya (1957 a,b). The CSEM method was not used extensively for exploration in the U. S. until the early 1970's although in the Soviet Union it has been used for petroleum exploration continuously since the early 1950's. In the U.S. the drive for geothermal exploration spurred a mild resurgence of the technique in the early 1970's with exploration systems developed by Keller et al. (1974) and Morrison et al. (1978). Other recent applications in the western world have included groundwater exploration (Fitterman and Stewart, 1986), petroleum exploration (Keller et al. 1984), mineral

exploration (Spies, 1980; Buselli et al. 1985) and crustal conductivity studies (Nekut et al. 1977).

CSEM is an attractive method for depth sounding because measurements may be made with a fixed transmitter-receiver configuration. This has obvious logistic advantages and also minimizes the the effects of surface inhomogeneities which are evident when sources and receivers are frequently moved. CSEM sounding also has the advantage of a localized source, so that a distant large-scale structure does not significantly influence sounding results as it can with magnetotelluric sounding (Hermance, 1982).

There are two major systems used to acquire CSEM data: the frequency domain system (FDEM) and the time domain or transient method (TDEM). There are advantages and deficiencies associated with each system, these are discussed in Kaufmann and Keller (1983) and Hoversten and Morrison (1982). A brief summary of how each system operates is given below.

1.1.1 Frequency Domain Electromagnetic Sounding (FDEM)

For FDEM sounding, the electromagnetic coupling between a source and receiver is measured at a number of discrete frequencies, typically spanning several decades. The measured field consists of primary (generated) and secondary (induced) field components. A sounding may be made at a fixed transmitter-receiver separation by adjusting the transmitter frequency (parametric sounding) or by using a single frequency and varying the transmitter-receiver separation (geometric sounding). The penetration depth is a function of frequency, transmitter-receiver separation, and the conductivity distribution in the earth. For a homogeneous half-space, for example, the fields may be uniquely described in terms of an induction parameter B, which is given by

$$B = (\frac{\sigma\omega\mu}{2})^{1/2}R.$$

Here μ is the magnetic permeability, σ is the electrical conductivity, ω is the frequency, and R is the transmitter-receiver separation (Ryu et al. 1970). As the transmitter-receiver separation or the frequency is varied, the response is sampled over a range of induction numbers, and this constitutes a sounding. For a layered model the conductivity is a function of depth so the measurement of an EM field at different induction numbers corresponds to a measure of the conductivity of the earth at different depths. The maximum penetration at a particular frequency is limited by the plane wave skin

depth δ, which corresponds to the penetration for an infinite transmitter-receiver separation. This quantity is defined as the depth at which an EM plane wave is attenuated to $1/e$ of its surface value and is given by, $\delta = (2/\mu\omega\sigma)^{1/2}$.

Descriptions of useful FDEM systems are given in Wilt et al. (1983), Pridmore et al. (1976) and Duncan et al. (1984). FDEM systems developed to date have provided good penetration depth and high quality data but tend to be cumbersome and expensive to operate.

1.1.2 Time Domain Electromagnetic Sounding

The time domain (TDEM) method differs from FDEM in that the transmitted signal consists of a repetitive step-like waveform and measurements are made during the time when the transmitter is off. The step-function waveform is rich in frequency so that the complete recovery of the secondary field, or transient, constitutes a sounding. A useful model for the propagation of the induced current from a step change in transmitter current was proposed by Nabighian (1979). After the transmitter current from a loop source has been shut off, an induced ring current propagates downwards and outwards from the source with time in a manner analogous to a "smoke ring". The fields at early times, just after the transmitter has been shut off, are sensitive to the shallow layers since the induced current then lies just below the surface. At later times the current has penetrated deeper into the earth so the observed fields are also affected by the conductivity of the deeper layers.

Descriptions of practical time domain systems are given in Buselli et al. (1981), West et al. (1984), Keller et al. (1984), and MacNeill (1978). These systems are widely used for mineral, groundwater and geothermal exploration.

Theoretically, data obtained from time domain and frequency domain EM measurements contain equivalent information; they are related to each other through the Fourier transform. In practice, however, TDEM systems have two significant practical advantages over FDEM systems. The first advantage is that a sounding is made by the recovery of a single waveform instead of a sequence of waveforms spanning several decades; a sounding may therefore be made in less time. The second advantage is that measurements are made during the time that the transmitter is off so that there is no primary elec-

tromagnetic field to contend with. On the other hand, FDEM systems have the advantage that the measurements are made in discrete frequency bands so that cultural noise outside of the band of interest may be electronically filtered before the signals are recorded. This improves overall data quality.

1.1.3 CSEM Sounding Configurations

CSEM systems use may be configured in a variety of ways. Transmitters may be closed loops or grounded dipoles; receivers may be magnetometers, induction coils, or grounded wires. One of the advantages of the CSEM technique is the flexibility afforded by this variety of sources and receivers so that a specific system can often be assembled to solve a particular problem. The three most common configurations for CSEM sounding are the central-loop system, the fixed-loop system, and the electric dipole system. With the central-loop system an induction coil receiver is situated at the center of a square or circular loop transmitter. A variation of this system is the coincident-loop configuration which features a receiver loop coincident with the transmitter. These systems have the advantage of a low level of sensitivity to lateral conductivity variations, however, as only one sounding is taken for each loop transmitter position, they are slow to deploy. The fixed-loop system features multiple receiver positions for each transmitter loop set-up. EM field detectors which may be magnetometers, induction coils or grounded wires, are often arranged so that profiles may be made as well as soundings. This system is very popular for mineral and petroleum exploration. The electric dipole system differs from the fixed-loop configuration only in that an electric dipole (grounded wire) source is used instead of a loop transmitter. The magnetic field from an electrical dipole source is substantially stronger than that for a loop source so that soundings may be made at large transmitter-receiver separations; it is therefore a popular system for deep sounding. This system is very sensitive, however, to lateral conductivity variations (Wilt et al. 1986).

The difficulty in CSEM sounding lies in the complexity of the electromagnetic field about a loop or grounded wire source. The EM fields near a controlled source are easily computed only for a homogeneous or horizontally layered earth structure. Two- and three-dimensional resistivity distributions have been recently addressed but the existing numerical solutions are cumbersome and use large amounts of computer time (Lee and Morrison, 1985; Hohmann, 1988). For a number of problems, for

example the vertical contact at the surface, numerical solutions are still unavailable and these problems must be addressed with scale models (Frishchknecht, 1988).

Although the CSEM sounding method has significant potential for geophysical exploration the advancement of the method has been hindered by the lack of effective interpretational aids. For most users of the technique, two- and three-dimensional numerical codes are unavailable due to their complexity and high cost; this limits interpretation to one-dimensional models. As will be shown below, the use of one-dimensional models can result in an erroneous and misleading interpretation if two- or three-dimensional structures are present and have gone unrecognized.

One of the aims of this thesis is to aid in the recognition of two- and three-dimensional surface features in TDEM field data and for some simple cases either remove the effect of the surface feature or include it in the interpretation. The principal model used to this end is the two-dimensional surface geological contact.

1.2 CSEM Sounding near a Geological Contact

The induced currents from a CSEM transmitter travel outwards from the source as well as deep into the earth. For a dipole source over a homogeneous earth, for example, the current induced by step-function excitation moves almost twice as far laterally as it does vertically in a given time interval (Nabighian, 1979). This means that in doing a depth sounding, lateral changes in conductivity may affect the sounding more than the vertical conductivity changes that are sought. In some cases, the distortion from a geological contact will render the data uninterpretable. Of more concern, however, are the cases where field data can be fit to erroneous models. Such soundings can mislead the interpreter or cast doubt on the validity of other soundings from a survey when it is discovered that some of the interpretations are incorrect.

It is often very difficult to recognize two- or three-dimensional effects as their nature depends on the sounding configuration as well as the earth conductivity structure. For some sounding configurations lateral conductivity variations produce subtle effects, but for others the effects are more dramatic. It is often easier to recognize a contact effect if the soundings are plotted in profiles rather

than as individual decay curves at each observation point. In the next section several examples showing the effects of geological contacts in exploration problems are presented in this manner.

Figure 1.1, taken from Irvine and Staltari (1984), shows a set of TDEM time profiles measured with a fixed-separation horizontal loop system over the Brittania mineral prospect in Queensland, Australia. The loops are separated by 150 m and the data are plotted at a point halfway between them. The profiles show an abrupt anomaly near station 9700N which was initially interpreted as a steeply dipping massive sulfide conductor. Subsequent drilling and downhole EM surveys showed only weak mineralization and no deep EM anomaly, so further surveys were conducted to determine the cause of the surface EM anomaly. A series of three CSEM surveys and a Schlumberger resistivity sounding survey were done over the same line to accomplish this. Figure 1.2 is a coincident-loop TDEM profile over the same traverse as shown in Figure 1.1. The Schlumberger layered-model interpretation is shown with the geological section at the bottom of the illustration. The early-time plots from the SIROTEM profile show a voltage level change from east to west centered over station 1700N but little evidence of a deep conductor. This type of voltage level change is a typical response of the coincident-loop system to a discontinuous surface conductive layer (Wilt et al. 1986). The Schlumberger soundings confirmed that a shallow conductive layer abruptly thins at the northern end of the profile near station 1700N. Scale model studies have shown that for the fixed-separation or fixed-loop systems the response from an abrupt near surface contact appears very similar to that of a buried vertical conductor (Spies and Parker, 1984; Irvine and Staltari, 1984). This can be very troublesome as many mineral targets are located near geological contact zones so in many cases both responses are present (McCracken et al. 1986).

Once it has been recognized that lateral conductivity variations are affecting the data, not much can be done presently to correct the situation. In some cases, however, a strong conductor can overwhelm the surface variation. An example of this type in given in Figure 1.3, which shows a series of coincident-loop time profiles over the Teutonic massive sulfide ore body in Western Australia (Buselli et al. 1986). The early-time profiles show clear evidence of near surface conductivity variations but by later times the effect of the surface feature has been overwhelmed by the response of the deeper conductor. Analysis of the late-time portion of the response provided useful information on the
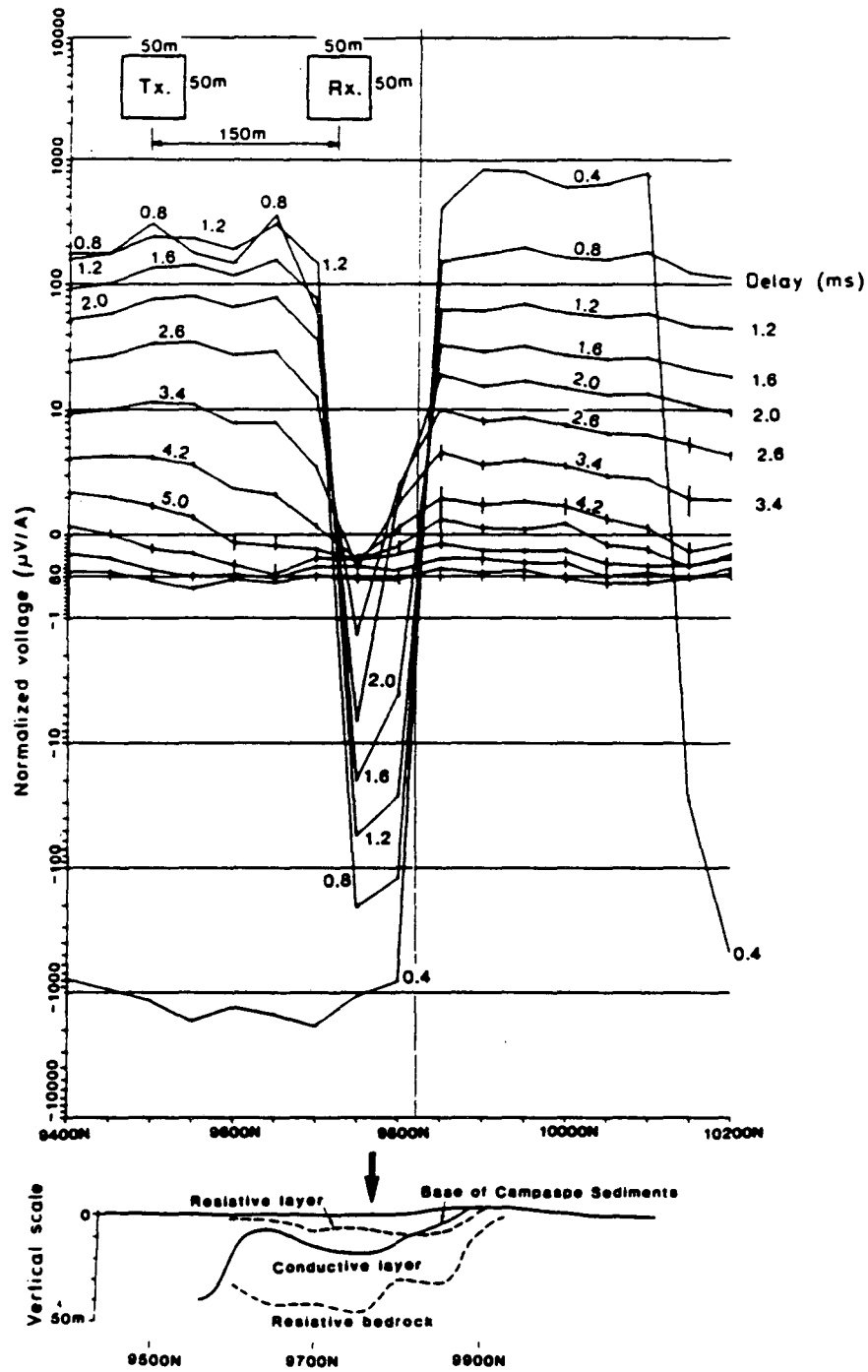
Figure 1.1   Time domain EM time profiles from a fixed-separation SIROTEM survey over the Brittania mineral prospect in Australia (after Irvine and Staltari, 1984). The schematic model shown at the base of the Figure is based on a geological model and Schlumberger resistivity soundings.
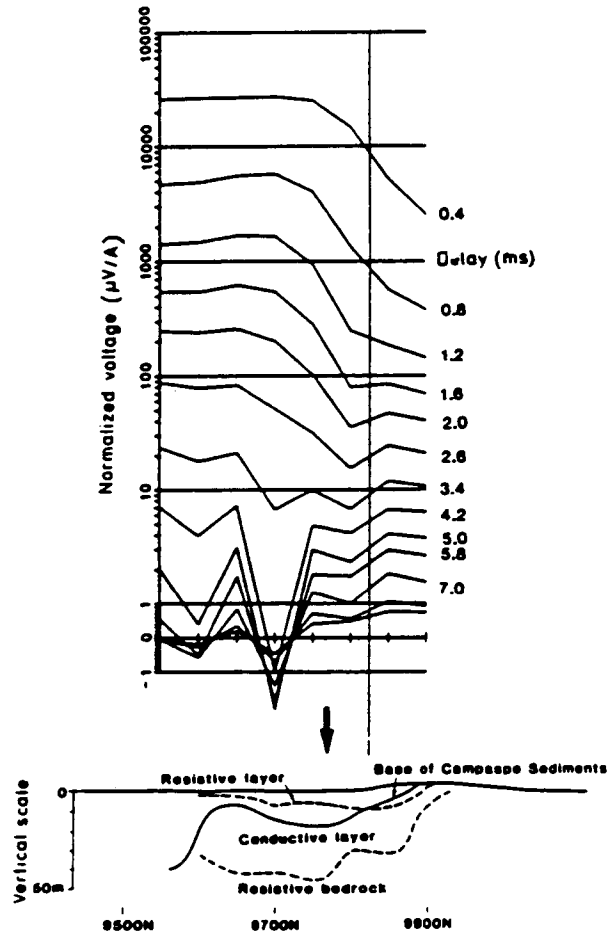
Figure 1.2 Coincident-loop time profiles for the prospect given in Figure 1.1 (after Irvine and Staltari, 1984).
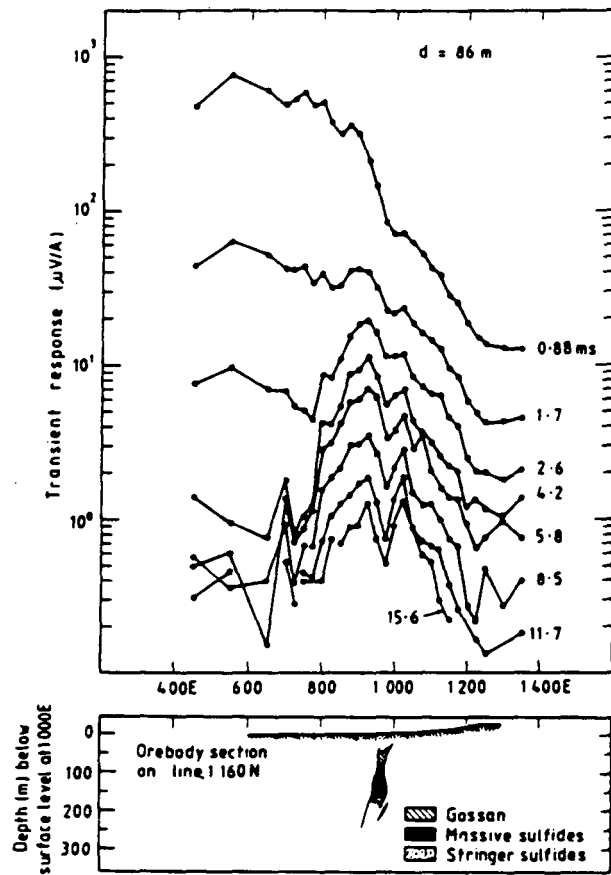
Figure 1.3 Coincident-loop SIROTEM profiles over the Teutonic massive sulfide ore body in Western Australia (after Busselli et al. 1987).

properties of the ore body without severe distortion (presumably) from the surface feature. The situation of a very good conducting deep target overwhelming the effect of surface variations is somewhat rare; it is a more common case to have the deeper response of the same magnitude as the surface feature, and in this case, separating one from the other is a more difficult task (McCracken et al. 1986).

In structural mapping the vertical resistivity section is sought over an area where lateral variations in conductivity are due to geological structure. Mapping these conductivity variations using one-dimensional models is a risky business that can yield unreasonable answers, especially near contacts. An example of a CSEM sounding over an approximately two-dimensional fault is shown in Figure 1.4 which contains coincident-loop soundings and the accompanying one-dimensional inversions for a profile in the Yucca Flats area at the Nevada test site (Frishknecht and Raab, 1984). The soundings have been converted to an apparent resistivity format using a formula given in Raab and Frishknecht (1983). Here we also show a dipole-dipole resistivity profile measured along the same line. The raw data shown in the upper part of the figure indicate discontinuities near stations TDEM 19 and TDEM 15. The interpreted profile of one-dimensional inversions clearly shows that near station TDEM 17, the inversions yield unreasonable resistivities and thicknesses from the layered models. Although the coincident-loop system has been shown to be relatively insensitive to surface contact effects, all of the EM sounding systems are affected to some degree in areas where the conductivity is changing (Wilt et al. 1986; Spies and Parker, 1984). In this case the overall structural characteristics are still evident from the one-dimensional inversions but much of the detail has been lost near the fault due to the distortion of the fields. It is worthwhile to note that the majority of this distortion occurs on the conductive side of the discontinuity; more will be said of this effect in Chapter 4.

These cases, all taken from the published literature, demonstrate that lateral variations in conductivity are a common problem in CSEM soundings and that they often affect the interpretation of collected data.

1.3 Layered Model Inversion of Central-Loop Sounding Data over a Quarter-Space

If CSEM soundings are collected in a profile across a vertical contact and the results are interpreted by fitting the measurements to layered models, then the interpretation will be distorted in some

Figure 1.4 Coincident-loop SIROTEM profiles and accompanying layered model inversions at Yucca Flats area of the Nevada Test Site (after Frischknecht and Raab, 1984).
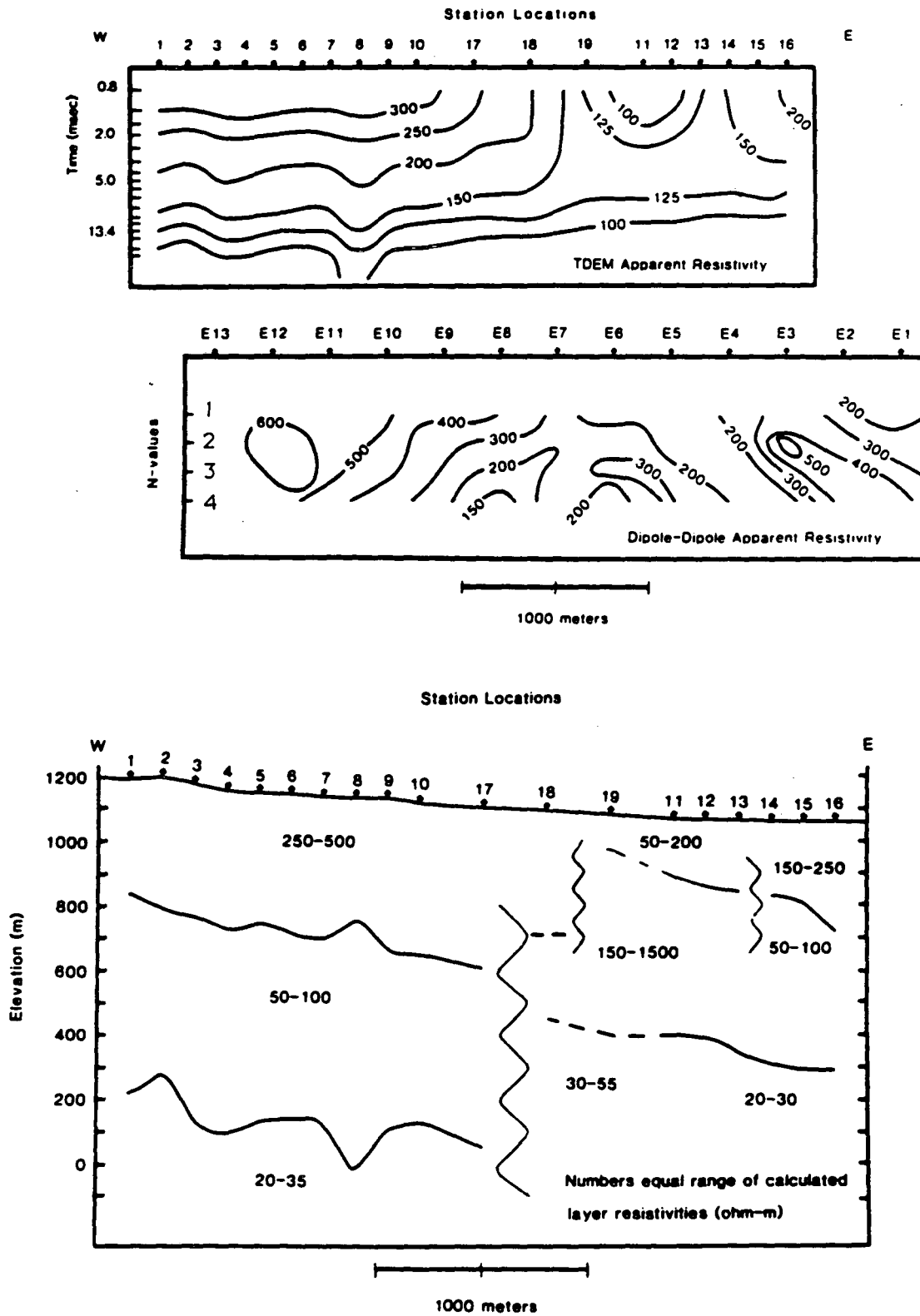
manner by the contact. Although the distortion will depend on the configuration used and the type of measurements made, it will also fundamentally depend on the parameters of the model. To illustrate this we made some scale model measurements across a quarter-space and interpreted the results using a layered model.

We considered a series of central-loop TDEM soundings collected along a single profile over a quarter-space. These data were individually fit to a series of layered models to determine how the contact effect manifests itself in the sounding interpretation. Soundings were made at the center of 250 m radius transmitter loops that were spaced 25-200 meters apart along a single profile orthogonal to the contact strike. The quarter-space was a 4.0 ohm-m block (aluminum) in contact with an infinitely resistive host (air). Vertical and horizontal magnetic fields measured at various times after current extinction are shown as a series of profiles in Figure 1.5. The vertical field transients at each station were fit to a layered model using FORTRAN code NLSTCI (Anderson, 1982). A three-layer model consisting of two 100m thick, 5 ohm-m layers overlying a 5.0 meter basement was used as a first guess for the inversion. Because the computer program requires an impulse response input (i.e., the time derivative of the field) and the scale model collects magnetic field the two data sets were initially incompatible. We therefore differentiated the scale model data numerically using a central-difference scheme. Although this added another layer of processing, it probably did not introduce significant noise or bias into the results.

In total, data for 18 stations were fit to layered models; details are given in Appendix 1, and the inversion results are plotted as a profile in Figure 1.6. For each sounding, the interpreted resistivity is plotted beneath the center of the loop at the center of the resolved layer. The layer boundaries are marked with a thick line. Note that none of the soundings actually resolved a three-layer model.

For soundings located farther than 700 m from the contact, the quarter-space resistivity was correctly determined (within 2 percent) by this process. Closer to the edge, however, the inversion begins to indicate a resistive layer at depth. For example, the sounding at 700 m from the contact indicates a 10 ohm-m layer at a depth of 280 m. At 500 m from the edge the resistive layer was 10 ohm-m and it was indicated at a depth of 240 m. At 300 m from the edge the layer was 32 ohm-m and only
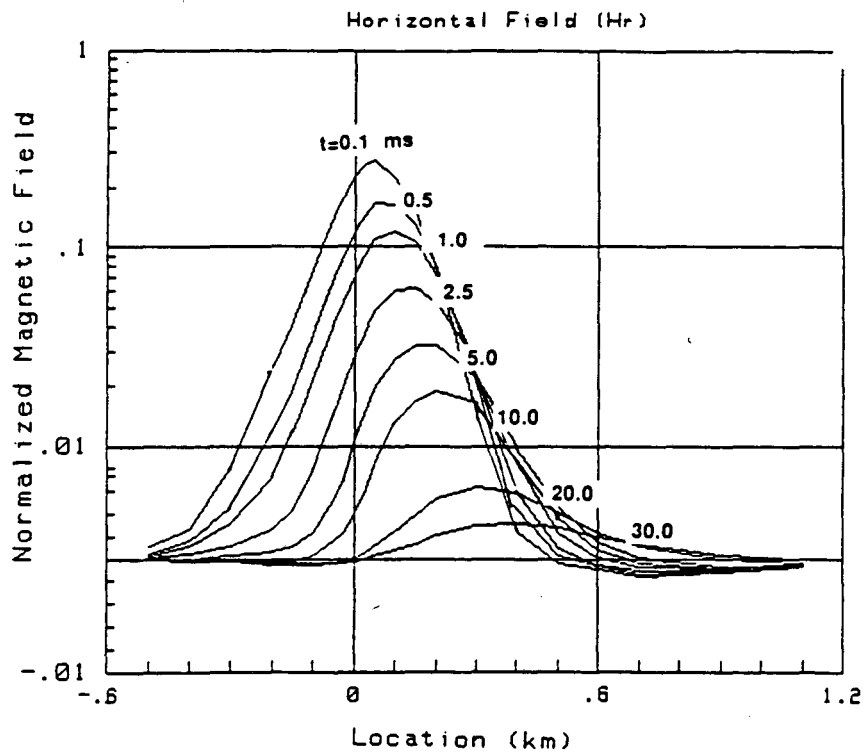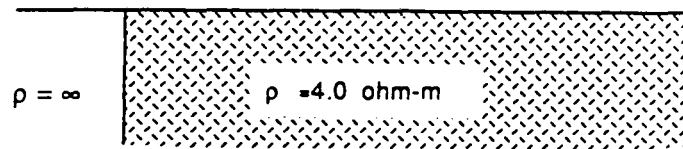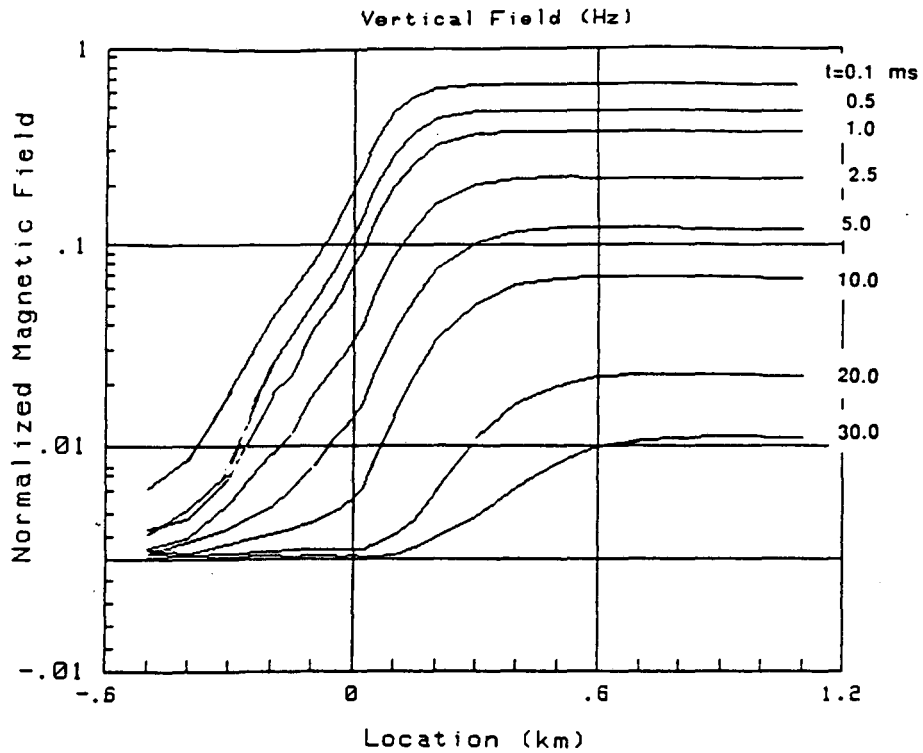
Figure 1.5 Vertical and horizontal magnetic field profiles over a quarter-space for various lag times after current extinction.

Layered model inversions

Station Location (km)

depth

| -0.2 | 0.0 | 0.1 | 0.2 | 0.3 | 0.4 | 0.5 | 0.7 | 0.9 |

100m   62   10.0   9.5   6.9   4.1   4.1   4.0   4.0   3.8   ohm-m

49   32

200m   28

9.5

300m   10.5

400m

Figure 1.6 Layered model inversion results from central-loop vertical field transients over a quarter- space.
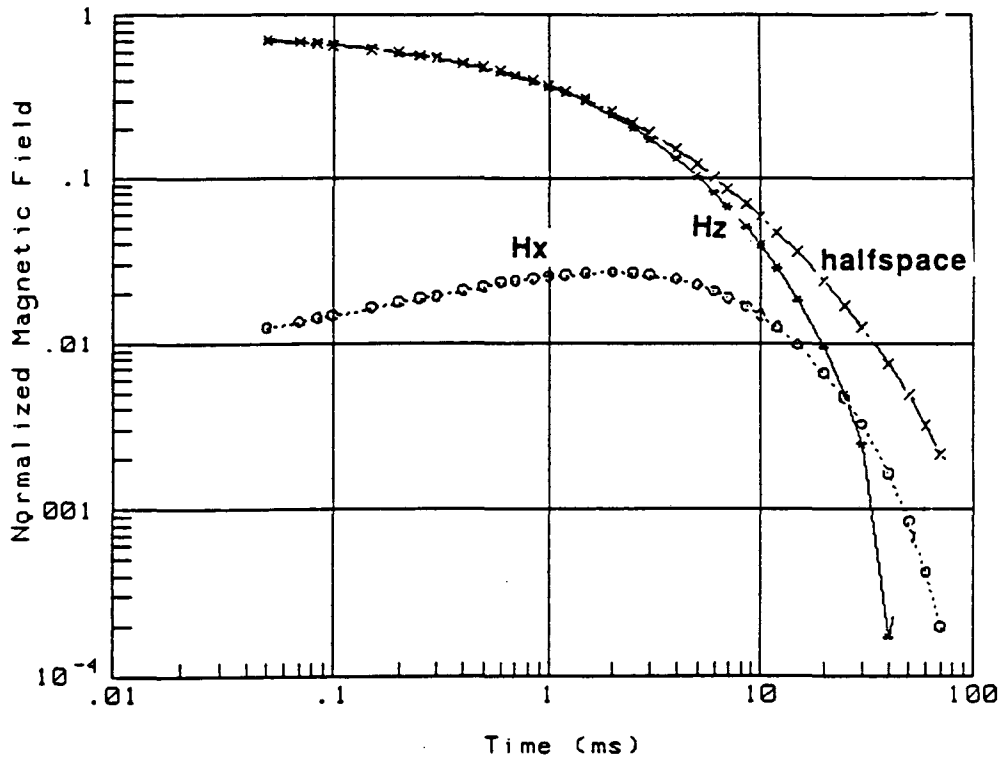
Figure 1.7 Vertical and horizontal field transients measured 300 m from the edge of a quarter-space,

and the transient for a homogeneous half-space.

170 m deep. For soundings collected within 100 m of the contact, part of the transmitter loop extended over the edge and even the resistivity at the surface was incorrectly determined. Across the contact, the layered models were indicative of a homogeneous half-space that progressively becomes more resistive as the soundings were taken further from the edge. At a distance past 300 m from the edge the inversion code could not fit the data to any layered model. Note that because the vertical fields are smoothly varying across a contact it was difficult to accurately determine the position of the contact on the basis of the layered model inversion results.

As shown above, for stations far from the edge, the contact effect is not evident until later times. For stations closer to the contact, the edge effect appears at earlier times and if part of the transmitter loop extends over the edge then the entire transient is affected. This behavior is explained by invoking Nabighian's smoke ring hypothesis. For stations some distance away from the contact the induced current is initially a symmetrical ring that propagates away from the source. When part of the current has reached the edge the symmetry is lost because this current cannot propagate further. At this time some of the field that normally has only a vertical component begins to develop a horizontal component as well. For stations closer to the edge, the induced current reaches the contact sooner and the contact effect appears earlier in time. The weakening of the vertical field (and development of the horizontal component) therefore occurs progressively earlier in time as the soundings are made closer to the edge. The layered model inversion interprets this effect as a (fictitious) resistive layer that becomes shallower and more resistive for transmitters closer to the edge.

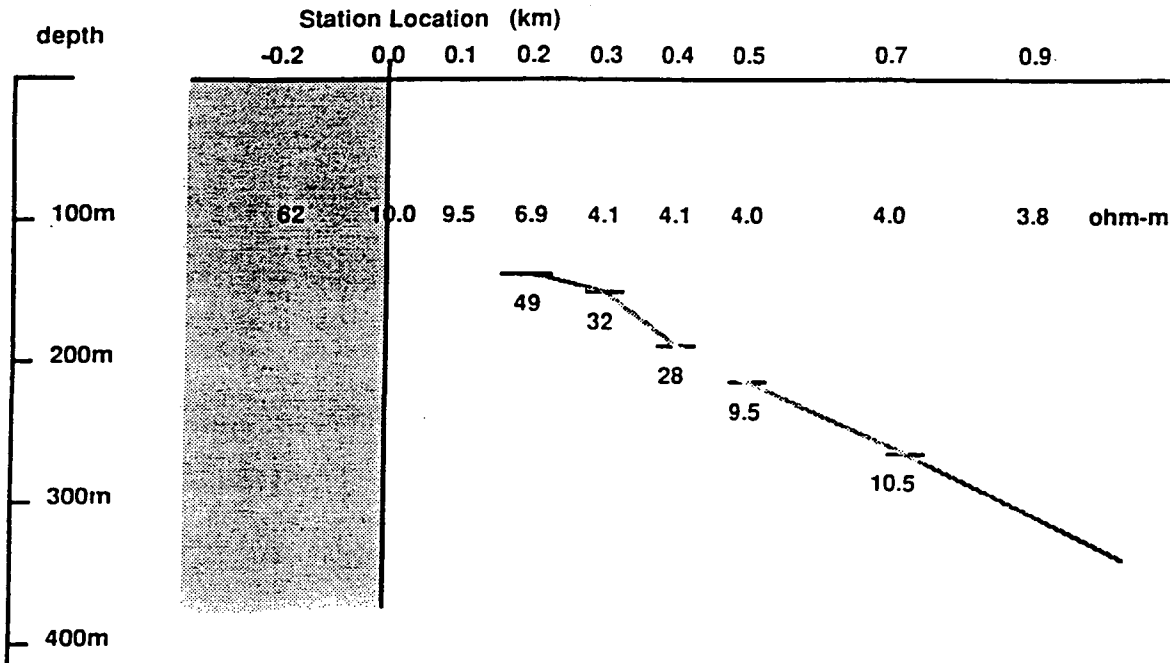Although for the central-loop system the contact effect is relatively benign as compared with the fixed-loop and electrical-dipole configurations (see Chapter 3), the distortion may still have a profound effect on interpretation. For example, a contact anomaly might mask a conductive target located near a geological boundary or distort a structural interpretation. It is therefore important that one recognizes the field signature of a contact before any interpretation of the data is made.

The horizontal fields are very good indicators of the presence of a nearby contact. Large horizontal fields strongly suggest that a layered interpretation should not be trusted. During lag times when the horizontal field is small, however, the vertical field data are not distorted and may be confidently fit to

layered models. As an example, the horizontal and vertical field for the sounding 300 m from the edge are shown in Figure 1.7, together with the transient for the homogeneous half-space. These transients show that the horizontal field develops a peak at a lag time of 3 ms, which is the time that vertical field transient begins to depart from the homogeneous half-space curve. In general we found that when the ratio H_x/H_z [which has been referred to as the TDEM tipper (Spies, 1988)] exceeded 0.2, the vertical field transient data cannot be confidently used in obtaining layered models.

1.4 Goals of This Thesis

The goals of this thesis are, first, to examine the effects of two-dimensional contacts for several commonly used CSEM sounding configurations and second to develop interpretational aids that allow for the structural interpretation of electromagnetic sounding data near a contact or for the removal of the contact effects from the data.

In Chapter 2 we describe the scale modeling system used to acquire the data. First, the mathematical basis for scale modeling is developed and, next, the relative merits of scale and numerical modeling are discussed. The time domain modeling system used for this study is then discussed in some detail, including a section on system calibration and comparison of scale model results to analytical and numerical models.

In Chapter 3 the effects of contacts on various CSEM sounding configurations are examined. First we consider the currents and fields for a dipole source over infinite and truncated thin-sheet models. Then using the central-loop, fixed-loop and electrical dipole systems, we describe the results for thin-sheet and quarter-space contact models. On the basis of these data, the responses of the three systems are compared to decide which configuration is the least sensitive to contact effects.

Chapter 4 deals with the interpretation of central-loop CSEM sounding data near contacts. In the first part of the chapter we examine the horizontal field at the center of the loop and develop means for using this data to determine the conductance or conductivity contrast and location of the edge. Contact models with a dipping interface, uniform overburden, and finite conductivity contrasts are also considered. We also show how a contact anomaly for a thin, discontinuous surface layer can be removed

from CSEM sounding data. Finally we examine the horizontal gradient of the vertical field and show how this quantity can in some cases be used in a similar manner as the horizontal field to extract information about the geological contacts.

In Chapter 5 we apply these principles to three field examples. The data, taken from published literature and unpublished field surveys, come from areas where the effects of a surface contact are evident. We apply some of the techniques discussed above to improve or add to the existing interpretation of the data. Chapter 6 is a short summary of the major conclusions of this thesis and a statement of future research needs.

In addition to the main text there are two appendices. Appendix 1 gives layered model inversion results for a series of central-loop soundings across a quarter-space contact. Appendix 2 contains data for a set of horizontal and vertical field profiles and transients over a thin-sheet contact.

CHAPTER 2: SCALE MODELING SYSTEM

2.1 Introduction

Scale modeling makes use of the law of similitude to relate a small laboratory system to its large scale physical analogue. In electromagnetic scale modeling the frequency or conductivity is increased to compensate for the reduction in size while still maintaining the same field relationships. We can substitute a block of aluminum for a 4 ohm-m shale body, for example, to produce an electrically equivalent model of the shale that is 10,000 times smaller. A 10 km by 10 km model may be reduced, therefore, to a square meter, a convenient size for a table top.

EM scale modeling has been done for a number of years chiefly by academic institutions and mining companies. Frequency domain scale models were developed to help interpret electromagnetic surveys used in mineral exploration (Frischknecht, 1971). Early models representing ore bodies typically consisted of metal sheets in air. The first studies that featured time domain scale modeling were reported by Yost (1952) and Orsinger and VanNostrand (1954). In these studies scale models were used in the development of a transient EM reflection technique. Complete treatments of the scale modeling method, including mathematical derivations and description of apparatus, are given in Sinclair (1948) and Frischknecht (1988). Spies (1980) derived scale modeling relations for time domain EM systems and used scale model results to help interpret field data in regions covered by conductive overburden. Dallal (1985) described time domain EM scale model results over edges and cavities using a unique "null-coupled" system. In his system only the time derivative of the horizontal field at the center of a horizontal loop transmitter was measured. This field is null-coupled to homogeneous or layered models but has impulsive field characteristics near inhomogeneities. West et al. (1984) describe scale modeling results for a step-response EM system (UTEM). With this system numerical and scale models are used to facilitate the interpretation of results for fixed-loop systems. The system used for the present study borrows from systems developed by Spies (1980), West et al. (1984), and Dallal (1985) although there are also several unique features.

2.2 Advantages of Scale Modeling

At the present time only a select group of EM model geometries can be handled with numerical methods. Electromagnetic fields over horizontally layered models may be routinely calculated (Morrison et al., 1969; Anderson, 1976). Those for spheres, spherical shells, and thin sheets are also easily done (Nabighian, 1971; Annan, 1974). More general two-dimensional and three-dimensional numerical codes are just becoming manageable (Lee and Morrison, 1985; Oristaglio and Hohmann, 1984 ; Newman et al. 1986). These codes are typically expensive to operate, however, and often have restrictions on the type of model and its dimensions. The scale model approach was chosen for the present study because none of the available numerical codes can be used to accurately calculate the electromagnetic fields near surficial geological contacts. Nevertheless a short discussion of the merits and deficiencies of numerical and scale modeling is useful.

The chief advantage of scale modeling is its versatility. With scale modeling, the EM response for virtually any type of model may be measured, with a predictable accuracy, for all EM system configurations. Unlike numerical models, three-dimensional laboratory models are often as easy to use as two-dimensional models. Once a system has been in use for some time, models results may be obtained at a predictable level of accuracy which, unlike numerical model data, is independent of the model. In fact, numerical codes are often tested against scale model data to ensure that the code is reliable. A final advantage is derived from the fact that scale model measurements are actually a field survey at a reduced scale. The fact that one can experiment with the system and model before field measurements are made often leads to a physical insight into the exploration problem.

Foremost among the disadvantages in scale modeling is the limited number of materials available for use in modeling. This limits the ability of scale models to approximate field situations. A second disadvantage is that models can be very cumbersome and difficult to alter. Because the models involve slabs or blocks of metals, machining of metals and transport using lifts and hoists are commonplace in scale modeling. Sometimes hazardous materials, such as mercury or lead, are involved, in which case special safety precautions are needed. In all cases a good deal of planning is necessary before a scale modeling project may be undertaken. Note that while long set-up times are usually required for scale

modeling, the actual measurement time is relatively short. For complex numerical modeling the inverse is usually true.

As more and more powerful numerical modeling codes become available and computers become more powerful and less expensive to operate, the role of electromagnetic scale modeling will diminish. But due to its inherent advantages, some scale modeling will continue to be done for some time.

2.3 Mathematical Basis for Scale Modeling

Spies (1980) describes two types of scale model systems, the first is based on geometric scaling while the other uses absolute scaling. In geometric scaling, typically only field ratios are obtained and only a dimensionless parameter, (δ) , is required to be the same for both the natural and the model systems. In absolute scaling actual field values are needed so an additional scale factor must be applied. In the present study field quantities are examined in terms of a free-space, or primary field, so only geometric scaling is necessary. In designing the system, however, absolute scaling was used to determine the expected amplitudes of the fields so that the various components could be designed accordingly.

The geometric scale model relations may be directly derived from Maxwell's equations (Grant and West, 1965),

$$\nabla \times H = J + \frac{\partial D}{\partial t} \tag{2.1}$$

$$\nabla \times E = -\frac{\partial B}{\partial t} \tag{2.2}$$

and the constitutive relations,

$$J = \sigma E \quad , \quad B = \mu H \quad , \quad D = \varepsilon E.$$

In these equations the fields are given as follows : H and E are the magnetic and electric fields, D is the displacement field, B is the magnetic induction and J is the current. The material properties are given by: σ, the conductivity; μ, the magnetic permeability; and ε, the electric permittivity. By requiring that both the model system, denoted by subscript m, and the natural system, subscript n, obey Maxwell's equations and assuming a linear relationship between the corresponding field components,

i.e., $H_m = aH_n$, a relation can be derived between the two systems. If displacement currents are

neglected $(\dfrac{\partial D}{\partial t} = 0)$, then equations (2.1) and (2.2) can be combined for each system into diffusion

equations.

$$\left[\nabla_n^2 - \sigma_n \mu_n \frac{\partial}{\partial t_n}\right] H_n = 0 \tag{2.3}$$

$$\left[\nabla_m^2 - \sigma_m \mu_m \frac{\partial}{\partial t_m}\right] H_m = 0$$

We can relate the ∇ operator from the natural to the model world by using the scale factor l ,

$$l = \frac{x_n}{x_m} = \frac{y_n}{y_m} = \frac{z_n}{z_m}.$$

Since ∇ has the dimensions of $1/L$, the spatial derivatives of the two systems can be related by,

$$\nabla_m = l\nabla_n \quad , \quad \nabla_m^2 = l^2 \nabla_n^2.$$

Inserting this relation into equation (2.3) and assuming a harmonic time dependence, $H = H_0 e^{i\omega t}$, we

can further simplify the relation.

$$\left[\nabla_n^2 - i\,\sigma_n\mu_n\,\omega_n\right] H_n = 0 \tag{2.4}$$

$$\left[\nabla_n^2 - \frac{i\,\sigma_m\mu_m\,\omega_m}{l^2}\right] H_m = 0.$$

Comparing these equations we can see that if $H_m = aH_n$, where a is a constant, then

$$l^2\sigma_n\mu_n\omega_n = \sigma_m\mu_m\omega_m. \tag{2.5}$$

The dimensionless scale parameter δ is therefore given by

$$\delta = \sigma\mu\omega l^2,$$

and for time domain systems this becomes,

$$\delta = \frac{\sigma\mu l^2}{t}. \tag{2.6}$$

In practice, the magnetic permeability for most earth and model materials permeability is equal to its

free-space value, so $\mu_n = \mu_m = \mu_0$. The scale modeling relations therefore usually involve length,

time, and conductivity scaling.

Equation (2.6) is the relation used for geometric scaling. If absolute fields are required then abso-

lute scaling is necessary and an additional factor must be applied (Spies, 1980). For our example the

absolute magnetic fields may be calculated from the model fields by applying the scale factor a, as in

$$a = \frac{H_n}{H_m} = \frac{\sigma_n l_n}{\sigma_m l_m}.$$ (2.7)

2.4 Description of the Scale Modeling System

The scale modeling system used in this study borrows heavily from previous systems. It uses a triangular current waveform similar to the UTEM system (West et al. 1984), and a computer controlled data acquisition system similar to that used by Spies (1980). By using the combination of a triangular current waveform, which is the integral of a square wave, and induction coil receivers which measure the time derivative of the magnetic field, the system measures a signal that is equivalent to the time varying magnetic field from a square-wave source (West et al. 1984). By adjusting the dc level of the receiver coil the signal appears similar to the magnetic field produced by a step change in transmitter current.

This system provides a convenient means for adjusting the amplitude of the primary (transmitted) signal. For resistive models where the induced signal decays rapidly, a higher frequency primary signal is used so that the primary field is larger and signal-to-noise ratios are maintained. For more conductive models where the signal decays more slowly, a lower frequency triangular waveform is used. The stepped magnetic field is used rather than the more commonly used time derivative (impulse response) for two reasons. First, because the magnetic field for a step excitation decays more slowly than its time derivative, the dynamic range demands on the system are lower and late-time data can be acquired more easily. Second, it is a simple task to compute the time derivative from the step response results whereas the calculation of the step response from an impulse response is much more difficult (Dallal, 1985).

The scale modeling system is schematically shown in Figure 2.1. The system largely consists of off-the-shelf electronic components and hand-wound transmitter and receiver coils. The triangle-wave signal is supplied by a Wavetek model 171 frequency synthesizer. Typically 6.5 Hz is used as the fundamental frequency although for more resistive models 65 Hz triangles are used. The power supply is a Crown model M-600 power amplifier with an essentially flat frequency response up to 20 KHz. This
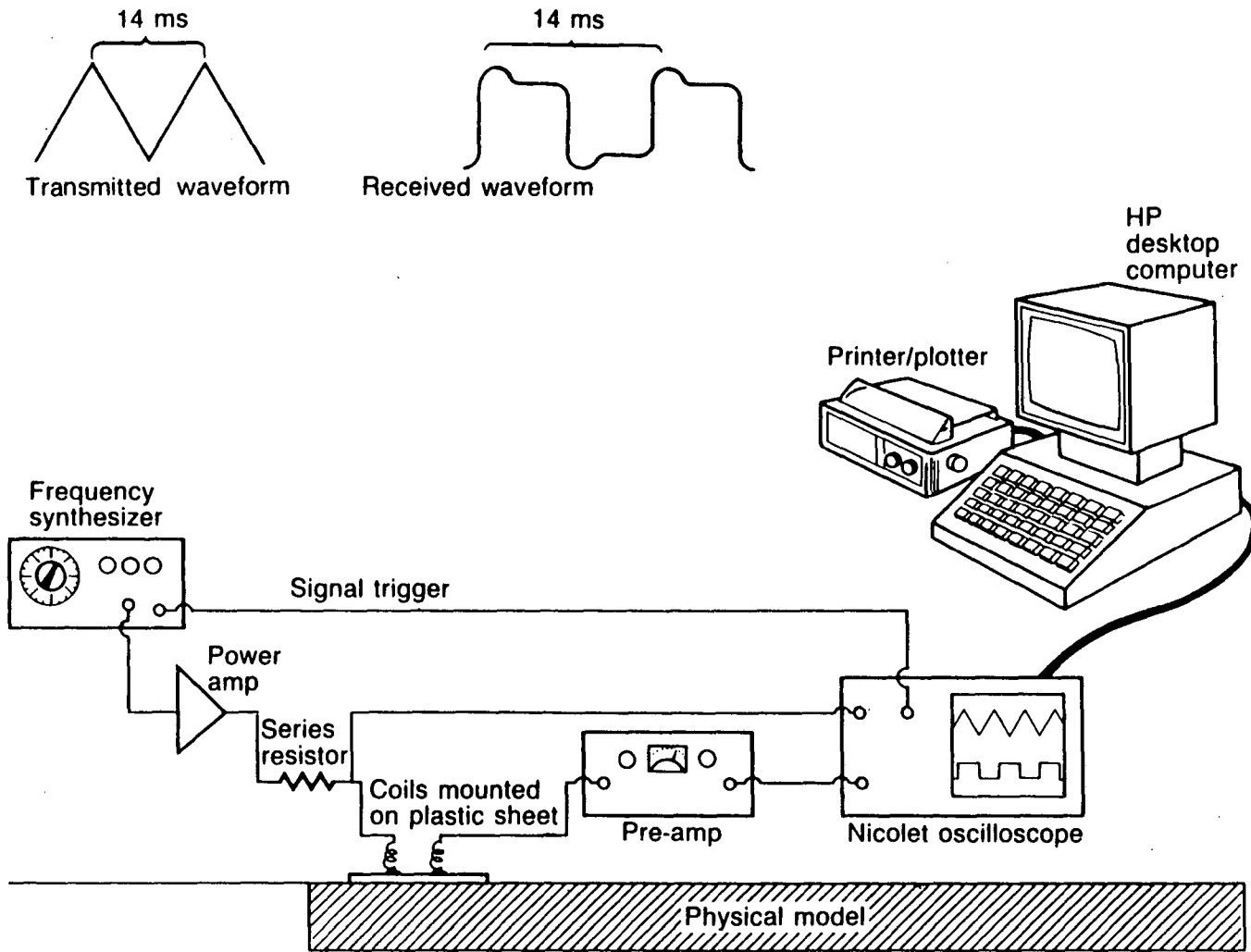
Figure 2.1 Schematic diagram of the scale modeling system.

broad-band capability is essential for time domain EM measurements to avoid the complexity of decon-volving a system response. The current is transmitted to hand-wound coils through a 12.5 ohm non-inductive power resistor. Wire-wound power resistors are not acceptable because their inductance causes an undesirable ramp in the transmitter current shut-off. This ramp can significantly alter the results from the assumed step response and it can only be removed by deconvolution. The transmitter is capable of supplying up to 20 amperes of current although in practice the current is maintained at about 5 amperes.

Receiver coils are hand-wound using 50 to 200 turns of no. 28 copper wire; for transmitter coils 10 to 30 turns of no. 14 wire are used. Vertical axis coils are wound around small segments of plastic tubing, 0.5 to 2.5 cm in radius, horizontal axis coils are wound around ferrite cores, 0.25 cm in radius. The ferrite cores typically increase the coil sensitivity by a factor of 4 or 5. The coils are connected to Princeton Applied Research (PAR) pre-amplifiers using shielded-twisted-pair cable. This type of cable is preferred to the more standard BNC cable which has a significant capacitance for lengths of several meters or longer. This capacitance, when coupled with the input impedance of the amplifier, can result in significant and undesirable low-pass filtering of the input signal. The pre-amp output is connected to a Nicolet model 4094 digital oscilloscope. The scope accepts a trigger from the signal generator to ini-tiate data collection, displays the incoming signals on the screen, and averages data from sequential sweeps before collection by the computer. The two-channel scope has a maximum sample rate of 100 KHz per channel, a memory of 32 Kbytes and a 15 bit word. There is sufficient dynamic range to eliminate the need for a time-varying amplifier gain (gain ranging) and sufficient memory to collect a time series from 10 microseconds to 80 milliseconds with each sweep. A single station typically requires 1 to 5 minutes of signal averaging to reduce the random noise to acceptable levels. The deci-sion to accept a station is usually determined from a visual inspection of the averaged time series.

The computer is a Hewlett Packard model 9816 desk-top with 512 K of internal memory. Data are transferred from the scope memory to the computer over the HPIB parallel interface. The computer code, written by the author in HP BASIC, averages the signal in logarithmically spaced time windows, normalizes the data by the primary magnetic field (when required) and keeps track of anomalous fields

by comparing results to measurements taken over homogeneous parts of the model. The program then plots results and stores data on 3 1/2 inch disks for later processing.

The time windows used in the scale model system are shown in Table 2.1. Note that the width of the windows ranges from 3 data points at the earliest time to more than 600 data points for the latest times. This increasing width is necessary with transient EM to maintain the signal-to-noise ratio as the signal level decreases at later lag times.

Table 2.1:

Scale Modeling System Time-Windows

Win #	Time(ms)	Time Span	No. pts	Win #	Time(ms)	Time span	No. pts
1	0.05	0.04-0.06	3	18	2.5	2.35-2.65	31
2	0.07	0.06-0.08	3	19	3.0	2.80-3.20	41
3	0.085	0.07-0.10	5	20	4.0	3.70-4.30	61
4	0.10	0.08-0.12	5	21	5.0	4.70-5.30	61
5	0.15	0.13-0.17	5	22	6.0	5.60-6.40	81
6	0.20	0.18-0.22	5	23	7.0	6.60-7.40	81
7	0.25	0.23-0.27	5	24	8.5	7.90-9.10	121
8	0.30	0.27-0.33	7	25	10.0	9.30-10.7	141
9	0.40	0.36-0.44	9	26	12.0	11.0-13.0	201
10	0.50	0.46-0.54	9	27	15.0	14.0-16.0	201
11	0.60	0.55-0.65	11	28	20.0	19.0-21.0	201
12	0.70	0.66-0.76	11	29	25.0	23.5-26.5	301
13	0.85	0.78-0.92	15	30	30.0	28.0-32.0	401
14	1.00	0.93-1.07	15	31	40.0	37.5-42.5	501
15	1.20	1.07-1.33	17	32	50.0	47.0-53.0	601
16	1.5	1.35-1.65	31	33	60.0	57.0-63.0	601
17	2.0	1.85-2.15	31	34	70.0	67.0-73.0	601

The models are made from sheets or blocks of aluminum, brass, lead or copper. Air is often used to represent a resistive host rock but when a conducting host material is needed mercury is used. Mercury is a valuable modeling material because it makes good electrical contact with many metals (i.e. copper, lead) without irregularities or gaps which affect the conductivity in the contact zone. Because it is both a hazardous and a dense substance, a system had to be designed for easy and safe assembly of models involving mercury. It was also required that the system have safeguards against the possible inhalation of mercury vapors during measurements.

Modeling is done in a 1 m by 2 m by 10 cm fiberglass-lined wooden tank situated atop a reinforced table and covered by a thin, removable sheet of clear plastic. The mercury is kept in a closed cylindrical container on a movable shop table adjacent to the modeling tank. When the solid metal components of the model are in place (they must be secured by screws to prevent them from floating in the mercury), the mercury table is raised above the level of the modeling tank with a hand crank. It is then drained into the tank through a section of tygon tubing until the desired level is reached, then the drain valve is closed. When the modeling session is complete, the table is lowered to a level below the tank and the mercury is drained from the modeling tank back into the storage vessel.

The modeling room is also equipped with fans to prevent the buildup of poisonous mercury vapors and the floor is painted with a chemical resistant paint.

Another feature of the system is a mechanical coil-mover which transports the transmitter and receiver coils across the model using a screw-gear. The screw gear is connected via bevel gears to a calibrated hand-crank. This simple device has allowed for more accurate and rapid placement of transmitter and receiver coils and has significantly improved productivity.

2.4.1 Noise Compensation

Because the scale modeling system was situated adjacent to a machine shop unwanted transient signals were often evident in the data and these could significantly affect the results. We also found that other sources of coherent noise internal to our system could contaminate some low-level signals. This was especially evident in the central-loop configuration because the late-time signals were very small.

For the central-loop system, where the transmitter-receiver separation is not a variable, we can compensate for common-mode noise using a simple technique. With this technique we connected an auxiliary (reference) transmitter coil in series with the modeling transmitter and situated it in free-space. A reference receiver coil is configured in the same manner as in the modeling system and measured on a separate channel. In this position, variations in reference receiver coil signal are sensitive only to fluctuations in the transmitter waveform and to external noise; the reference system is therefore useful in eliminating these effects from the data. The noise removal correction consists simply of subtracting

the observed variations in the reference receiver coil signal from the the modeling receiver coil signal; this is done in the computer. This simple procedure has reduced the noise levels for some configurations by more than 30 percent.

Although the same effect could be achieved by winding the reference coil in series opposition with the modeling system this would require two perfectly matched systems which is very difficult to achieve with hand-wound coils.

2.5 System Calibration and Measurement Error

The scale model system was calibrated component by component in the lab; the complete system was tested by comparing scale model data to analytical expressions for the thin-sheet and to numerical results for a homogeneous half-space.

The amplifiers and coils were calibrated in the lab using a Hewlett Packard model 3582A spectrum analyzer and a solenoid; calibration corrections are applied through computer software. The Nicolet oscilloscope was calibrated at the factory in Fremont, California.

A measure of the coil sensitivity may be given by the effective area of the coil (NAk), where N is the number of turns, A is the cross-sectional area, and $k = \mu/\mu_0$ is the increase in coil sensitivity caused by using permeable core material such as ferrite or mu-metal. The effective area of the 2.5 cm radius transmitter coils is 0.016 m^2 and the coils have an inductance of 0.9 millihenries (mH). For the receiver coils the effective areas range from 0.05 m^2 for the 0.5 cm coils to 0.5 m^2 for the 1.5 cm coils. The corresponding inductances range from 3 to 30 mH. The resonant frequency of all coils was measured to be greater than 250 KHz, which is well beyond the bandwidth of the system.

2.5.1 Analytical Comparison

A good test of a scale model system is to make measurements over simple models for which analytical solutions are available and compare the results to the analytical calculations. One such model is the thin-sheet.

Step-response magnetic fields from a vertical magnetic dipole source over a homogeneous thin-sheet model are described by well-known analytical expressions (Kaufmann and Keller, 1983). The

voltage induced in a coil at the center of a circular loop transmitter situated over a flat-lying thin sheet is given by;

$$V(a,t) = \frac{3N_t I M_r}{Sa^2} \frac{(bt/a + 2h/a)}{(1+(bt/a+2h/a)^2)^{5/2}}$$

(2.8)

where M_r is the effective receiver area, N_t is the number of turns on the transmitter coil, I is the transmitter current, S is the conductance of the sheet, h is the height of the transmitter and receiver, a is the radius of the transmitter loop and $b = 2/\mu S$.

Measurements were made using the central-loop configuration at a height of 6 mm over a 1.6 mm thick aluminum sheet, $(S = 3.52S)$. The scale-model data are differentiated numerically, using a central-difference scheme, so that the scale model results can be compared to the analytical model. The response of this model should approximate a thin-sheet except at early times (Kamenetskii, 1976).

In this case, as in virtually all of the illustrations that follow, the observed field values are normalized by the magnitude of the effective primary field at the moment of current extinction. Figure 2.2 shows a comparison of the scale model and analytical results for this model which indicates that the two agree to within one percent for all but the earliest lag times.

Another test for the scale modeling system is to compare measurements to numerical results for simple models. In this case a code written by Anderson (1976) was used for comparison with the scale model results. The code calculates impulse and step magnetic field responses for a vertical magnetic field at the center of a loop transmitter situated over a layered half-space. The program can also account for a transmitter current turn-off ramp and for the transmitters and receivers to be positioned above the model; both of these features are characteristics of this scale model system. A comparison between the scale and numerical model results for a 4 ohm-meter half-space model is given in Figure 2.3. The figure shows that the aluminum scale model data closely match the response for a half-space model with a resistivity of 4.1 ohm-meters, which is a good approximation of the conductivity of the aluminum model at a scale of 1:10,000. An upper (resistive) layer (64 m= 6.4 mm) thick with a resistivity of about 1700 ohm-m represents the air layer between the coil and the model surface.
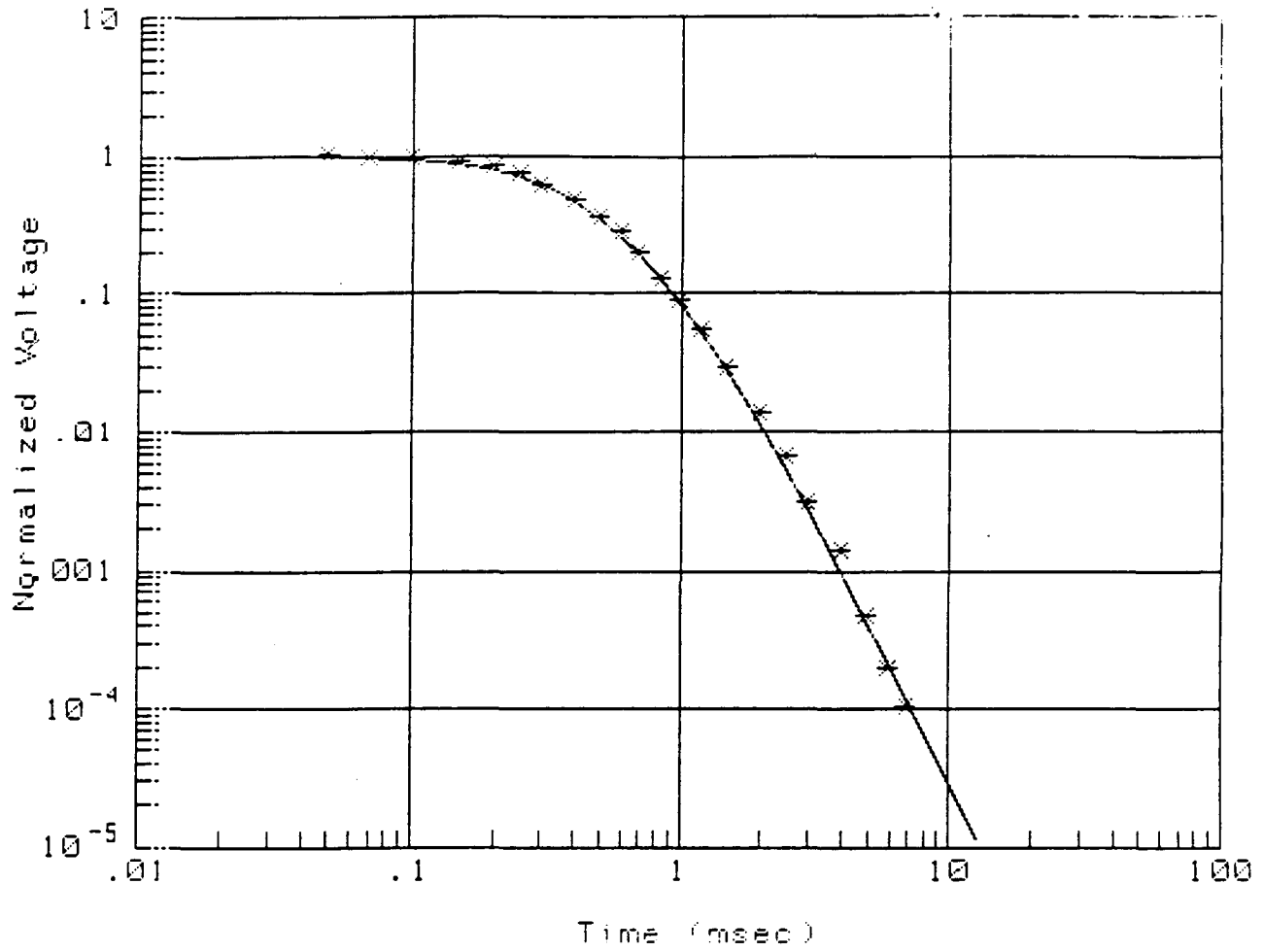
Figure 2.2 Comparison of analytical (solid line) and scale model results
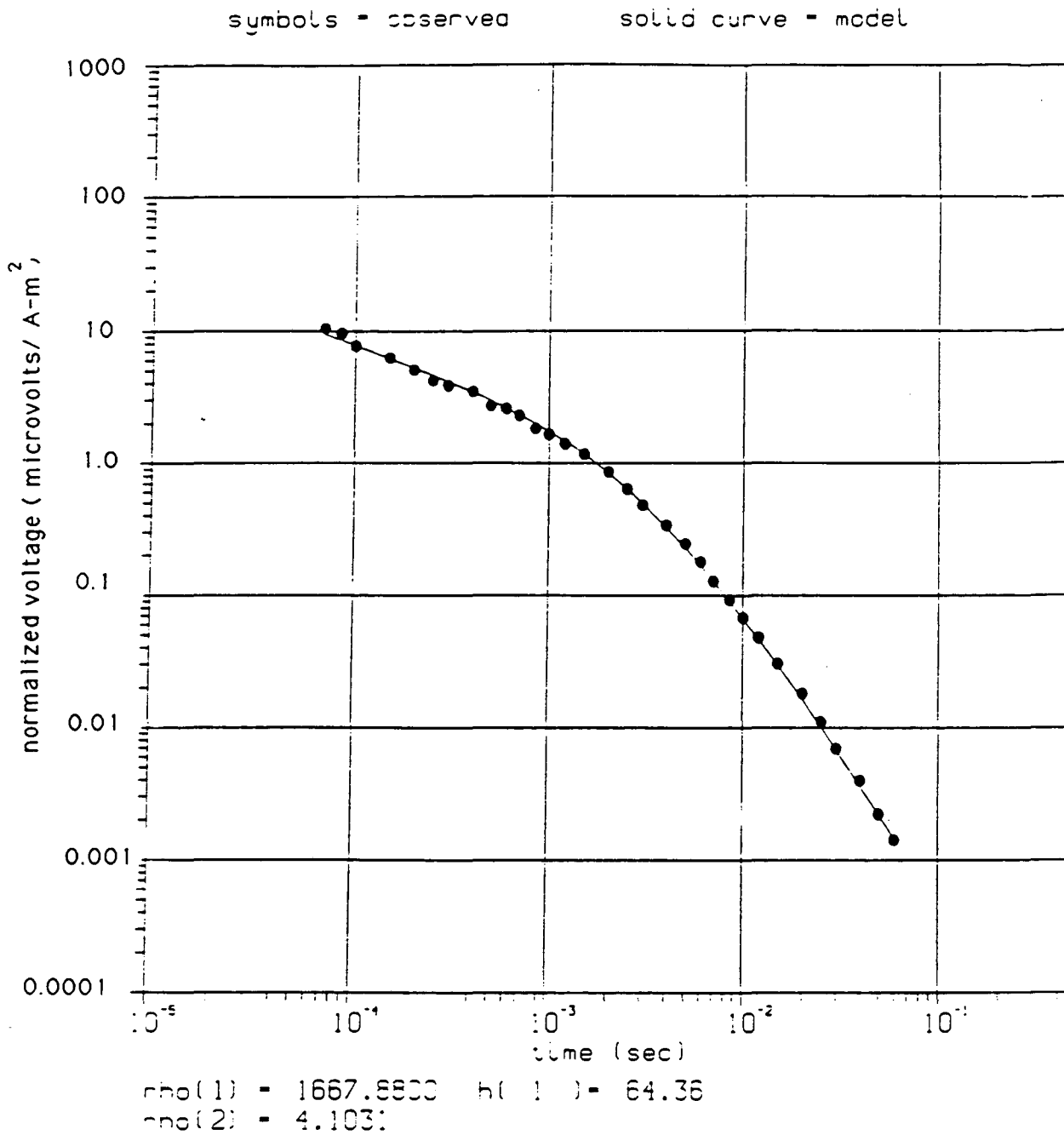
for central-loop sounding over a thin-sheet.

Figure 2.3 Comparison of numerical (solid line) and scale model results for central-loop sounding over a 4 ohm-meter half-space. The model parameters are derived from a least-squares inversion.

The good agreement between the scale and numerical data for this half-space model suggests that scale model measurements may also be used to determine the conductivity of materials. Techniques for doing this are described by Spies (1980) who measured transient decay curves over blocks of metals and used the late-time portion of the curves to deduce their conductivity. With this technique Spies measured the conductivity of various metallic materials to an accuracy of about 10 percent.

2.5.2 The Effects of Coil Height and Turn-off Ramp

Because the coils consist of up to several hundred turns of wire mounted on a plastic base, their effective average height is 5-7 mm above the model surface. At a scale of 1:10000 this translates to a height of 50-70 m. Results may be obtained at the model surface by taking measurements at two different heights and logarithmically extrapolating the data downwards (Spies, 1980). This procedure more than doubles the measurement time and more than triples the error level, so scale model data were not downward continued unless we were matching results to field data.

The current turn-off ramp of the scale model system is approximately an exponential function to lag times of 50 microseconds; at 100 microseconds the current has decreased to less than 0.5 percent of its value before current shut-off. This turn-off ramp is significantly steeper than commercial time-domain field systems such as Geonics EM-37 (McNeill,1982). The main effect of the ramp is to contaminate early-time data when the current has not been completely shut off; it does not have a significant effect on middle or late-time results. Although it is possible to remove the ramp effect from the data by deconvolution of the system response, it is a more common practice, especially in commercial systems, to convolve the primary field ramp with the numerical model used to fit the field results (Anderson, 1976). For this study the relatively sharp current ramp is not viewed as a significant problem and it is not removed from the data.

2.5.3 Measurement Error

In addition to external and system noise, the measurement error for the scale modeling system depends on the configuration used. For example, for the fixed transmitter systems the dominant sources of error are the uncertainty in the transmitter-receiver separation and the low signal levels at large

separations; for the central-loop system neither of these is important since the relative transmitter and receiver positions are fixed. In this case the dynamic range and external noise seem to be the most important factors. There is, therefore, some difficulty in assigning a general error level to the measurement system due to this dependence on configuration. Because of this we have chosen to focus our effort on determining the system noise level and the effective dynamic range. To accomplish this end a series of central-loop soundings were made over a 4 ohm-meter half-space model, and the differences between these repeated soundings is used as a measure of the system noise level. Figure 2.4 shows the decay curve for the sounding and the difference between two sequential measurements. The measurements were made using a 6.5 Hz source at a current of 6 amps; the radius of the transmitter loop was 2.5 cm (250 m at a scale of 1 to 10,000) and the signal was averaged for 5 minutes. For this model, the noise level is at least 30 dB below the decay curve out to 10 ms and it is 20 dB below this curve out to the latest time. The early-time noise level is shown to be about 10 microvolts, or 0.1 percent of the primary field; at late times the noise is below 1 microvolt. This reduction in noise level is primarily due to the greater signal averaging within the time windows at late time. Note that the decrease in noise is roughly proportional to the square-root of the increase in the number of sampling points per window (see Table 2.1). For most of the models in this study this level of noise is satisfactory. For subtle contact effects and more resistive models where the decay curve is sharper, the signal can easily fall below this noise level at late-times.
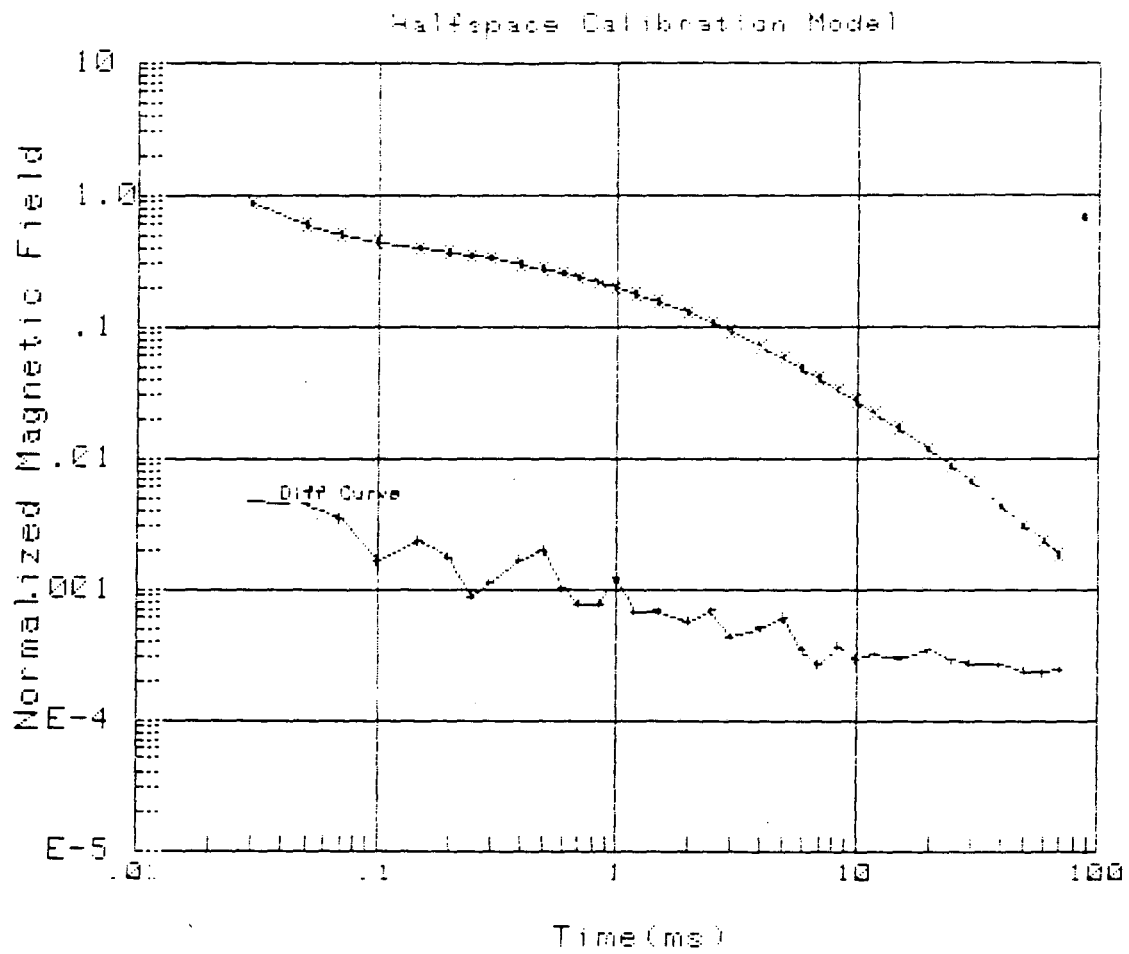
Figure 2.4 Relative signal and noise levels of the scale modeling system over a model of a 4 ohm-meter half-space.

CHAPTER 3: TRANSIENT ELECTROMAGNETIC FIELDS NEAR GEOLOGICAL CONTACTS

In this chapter we examine the electromagnetic effects of a surficial vertical geological contact for three commonly deployed ground-based EM systems. The primary goal is to inspect the fields near the edge to determine how the contact response is related to the system and model parameters. Secondly, the fields from the three systems are compared to determine which data set is the least affected by the contact and is therefore most amenable to one-dimensional interpretation. In addition to displaying observed fields over contact structures, some attempt is made to explain the secondary magnetic field behavior and to relate the observed anomalies to simple models.

Two simple two-dimensional models are used to examine the contact response: the truncated thin-sheet and the quarter-space (Figure 3.1). The truncated thin-sheet represents a discontinuous over-burden layer; the quarter-space represents a fault. The thin-sheet models are made from sheets of aluminum, brass or lead with a maximum thickness of 0.5 cm which corresponds to a scaled 50 m over-burden layer. The quarter-space models consist of a 5-cm-thick sheet of aluminum or copper. For the quarter-space models air is used as the host medium. Thin-sheet models can be examined in air or in a mercury host. The scale model system described in Chapter 2 was used to collect these data.

The three EM configurations used to study the contact effect are shown in plan view in Figure 3.2. These are the electrical dipole system (Figure 3.2a), the fixed-loop configuration (Figure 3.2b) and the central-loop system (Figure 3.2c). All are commonly used in mineral and petroleum exploration. With the fixed-loop system a large rectangular loop transmitter is installed in the area of interest and magnetic field receiver stations are occupied along profiles orthogonal to the long side of the loop. With the central-loop system, magnetic field measurements are made at the center of each transmitter loop. The electrical dipole system transmits signal through a long grounded wire and magnetic field receiver stations are located along profiles orthogonal to the orientation of the wire.

With each system we present magnetic field profiles made over the contact for various lag times (times after the extinction of the primary field). We also examine individual transients at various receiver locations. The field due to the contact is separated from the background response by
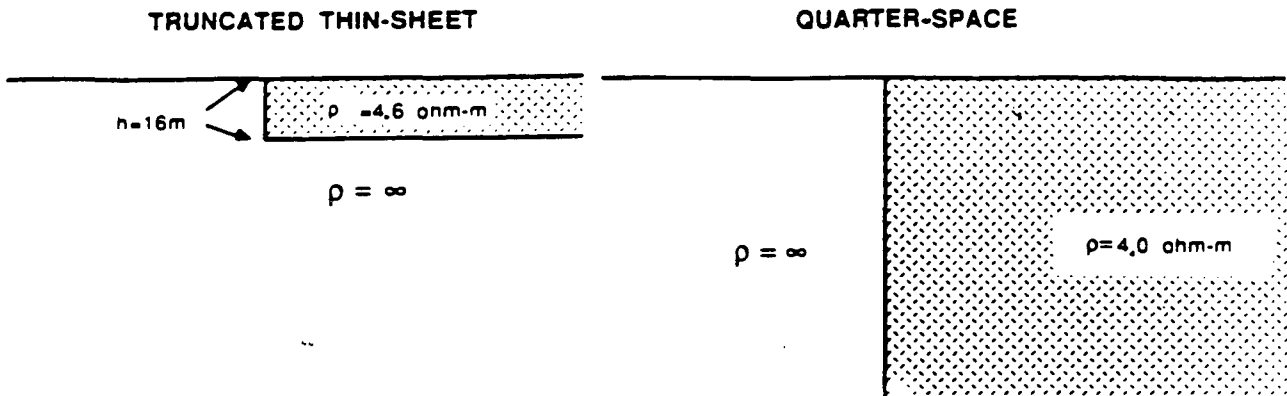
TRUNCATED THIN-SHEET

QUARTER-SPACE

$\rho = 4.6$ onm-m

$h=16m$

$\rho = \infty$

$\rho = \infty$

$\rho = 4.0$ ohm-m

Figure 3.1   Models used for the contact study.

section

Receivers

Receivers

HX coil

HZ coil

Transmitter Coil

Grounded Wire Transmitter

Transmitter Loop

a) Electrical Dipole System

b) Fixed Loop System

c)   Central-loop system
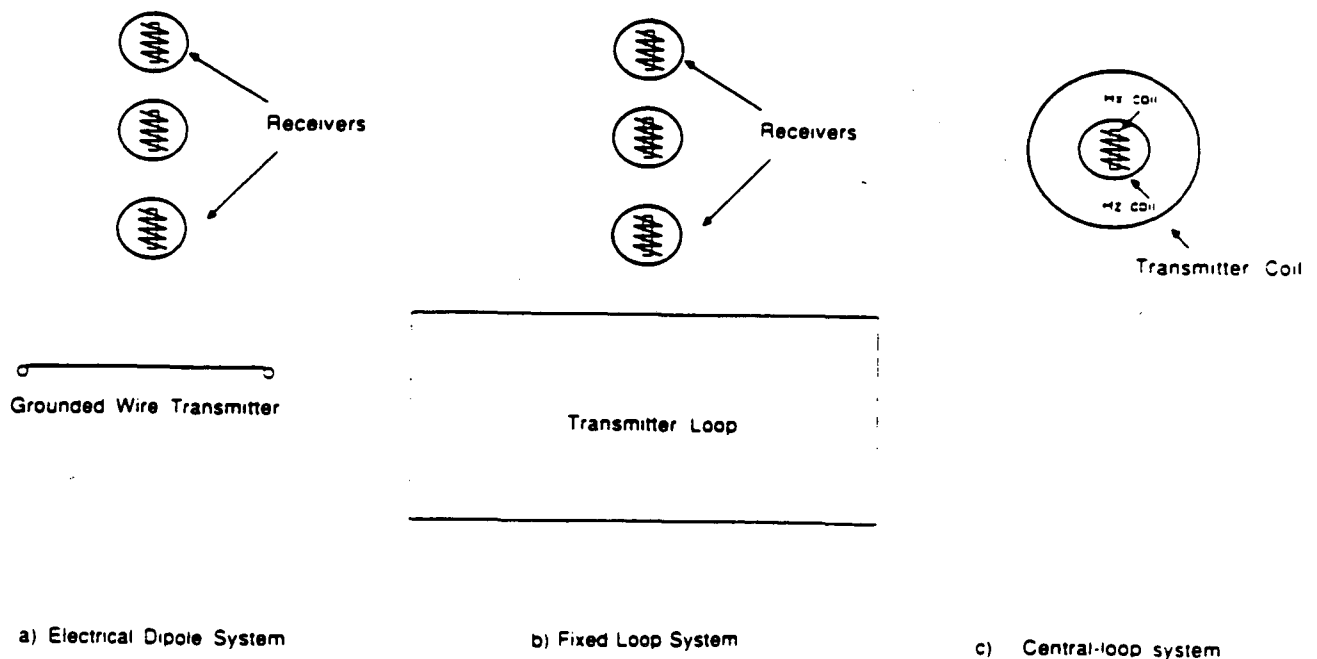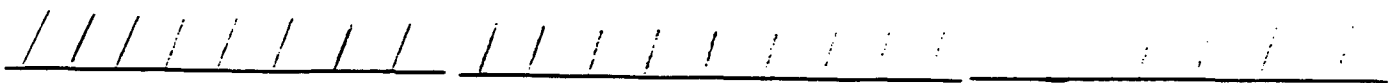
Figure 3.2   Configurations used in the contact study

plan view

subtraction and these data are presented as anomaly profiles or transients. From these results empirical relationships are developed that describe the contact effect.

3.1 Fields and Currents over a Truncated Sheet

Before considering field profiles over the contact models, it is useful to examine the fields and currents given by an analytical solution for the infinite horizontal thin-sheet. These results may then be compared to scale model measurements over a truncated sheet so that the fields and currents related to the contact can be better understood.

3.1.1 Electromagnetic Fields from a VMD on a Thin-Sheet

A thin-sheet is defined as an unbounded infinitely thin plate but with a finite conductivity-thickness product (conductance). It is a useful model for explaining the field behavior over thin conducting tabular bodies. The step-response electromagnetic fields for a vertical magnetic dipole source (VMD) over an infinite thin-sheet are described by well known analytic expressions. Derivations appear in Grant and West (1965) and Kaufmann and Keller (1983). The basis of the solution is that the governing equations and boundary conditions may be satisfied by replacing the sheet with a vertically oriented image dipole which is initially located an equal distance from the sheet but on the opposite side from the true source (Figure 3.3). After the source has been switched off the image moves downwards, away from the sheet, with a velocity inversely proportional to the conductance of the sheet. The fields on or above the sheet may be calculated from the image by using simple expressions for the electromagnetic fields of a magnetic dipole.

The general expressions in cylindrical coordinates for the vertical and radial magnetic fields and the azimuthal electrical field from a VMD over a thin-sheet are given below; the geometrical quantities are shown in Figure 3.3.

$$H_z(z,r,t) = \frac{M}{4\pi} \frac{r^2 - 2(bt + 2h - z)^2}{(r^2 + (bt + 2h - z)^2)^{5/2}},$$

(3.1)

$$H_r(z,r,t) = \frac{3M}{4\pi} \frac{r(bt + 2h - z)}{(r^2 + (bt + 2h - z)^2)^{5/2}},$$

(3.2)

Homogeneous Thin Sheet

Source Dipole

Receiver

r

h

z

+

S = sheet conductance
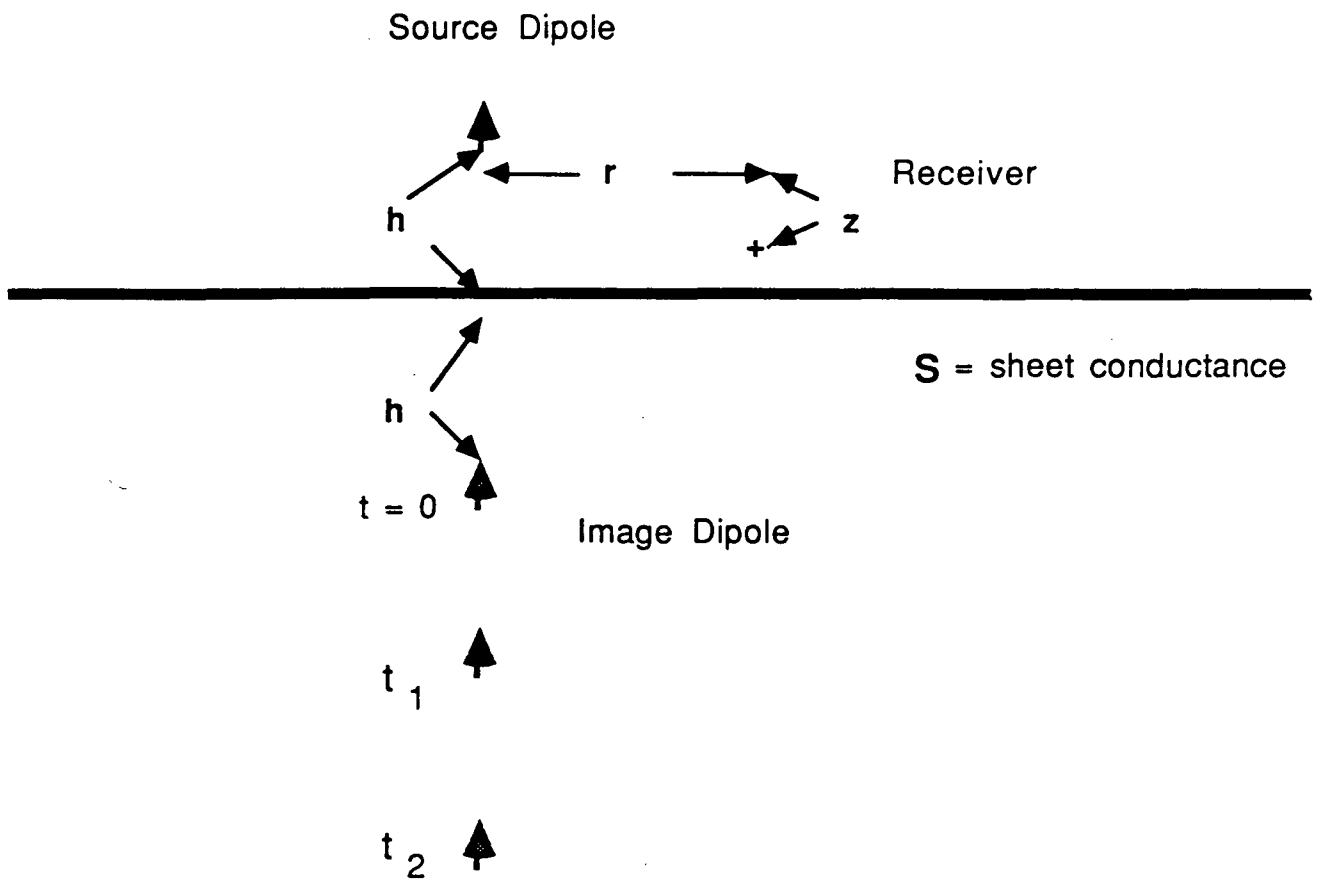
h

t = 0

Image Dipole

t₁

t₂

Figure 3.3 Geometrical parameters of the analytical solution for a homogeneous thin sheet.

$$E_\phi(r,t) = \frac{2}{S}H_r(r,t).\qquad\qquad(3.3)$$

where M is the dipole moment of the source, S is the conductance of the sheet in Siemens, and $b=2/\mu_0 S$, where μ_0 is the free-space magnetic permeability.

If the source and receiver are restricted to the surface of the sheet, which is the case for ground-based EM systems, the above expressions simplify further.

$$H_z(r,t) = \frac{M}{4\pi r^3}\frac{1-\dfrac{2b^2t^2}{r^2}}{(1+\dfrac{b^2t^2}{r^2})^{5/2}},\qquad\qquad(3.4)$$

$$H_r(r,t) = \frac{3M}{4\pi r^3}\frac{\dfrac{bt}{r}}{(1+\dfrac{b^2t^2}{r^2})^{5/2}},\qquad\qquad(3.5)$$

the induced current density in the sheet is given by

$$K_\phi(r,t) = SE_\phi(r,t) = \frac{3M}{2\pi r^3}\frac{\dfrac{bt}{r}}{(1+\dfrac{b^2t^2}{r^2})^{5/2}}\qquad\qquad(3.6)$$

Note that the current density in the sheet is twice the value of the radial magnetic field.

Asymptotic expressions for these equations at late-times, when $\dfrac{bt}{r}=\dfrac{2t}{\mu_0 Sr}\gg 1$, are given by

$$H_z(r,t)=\frac{M\mu_0^3 S^3}{16\pi t^3},$$

$$H_r(r,t) = \frac{3M\mu_0^4 S^4}{64\pi t^4}.$$

At late times magnetic fields and currents are therefore proportional to high powers of the conductance, inversely proportional to high powers of time, and are largely independent of the distance to the point of observation.

The voltage induced in a receiver loop located at the center of transmitter loop of dipole moment M_r and radius a at a height h above the sheet can be calculated by integrating E_ϕ in equation 3.4

around a loop of radius a and invoking the reciprocity principle. The result is:

$$V(a,t) = \frac{3M}{S} \frac{2h+\dfrac{bt}{a}}{(1+(2h+\dfrac{bt}{a})^2)^{5/2}}.$$ (3.7)

This expression was used in Chapter 2 to validate scale model measurements.

The display of the transient fields for separated dipoles can be facilitated by lessening their dependence on transmitter-receiver separation (see Equations 3.4 and 3.5). This can be done by normalizing the observations by the vertical magnetic field before current shut-off, or primary field

$H_0 = \dfrac{M}{4\pi r^3}$. The normalized equations can be further simplified by noting that the dimensionless

quantity $u = \dfrac{2t}{\mu_0 Sr}$ is common to all the field equations. With these simplifications Equations 3.4 and

3.5 reduce to

$$\frac{H_z(u)}{H_0} = \frac{1-2u^2}{(1+u^2)^{5/2}},$$ (3.8)

$$\frac{H_r(u)}{H_0} = \frac{3u}{(1+u^2)^{5/2}}.$$ (3.9)

By plotting the fields as a function of the normalized parameter u only one pair of curves is required to completely describe the transient field behavior over a thin-sheet. These are shown in Figure 3.4. Note that because of the logarithmic scale the data are all plotted as positive values. The negative values begin after the sharp notch in the plot which indicates the position of the zero crossing.

At small values of u (early times) the vertical secondary field assumes the value of the primary field at the instant of transmitter shut-off and begins to decay. The vertical field component at the observation point crosses zero as the induced current passes beneath the receiver; this occurs when the numerator in Equation 3.8 is zero.

$$u^2 = \frac{1}{2}, \quad or \quad u = \frac{2t}{\mu_0 Sr} = \frac{1}{2^{1/2}}.$$

At late-times the vertical field is negatively valued as it decays to zero with a slope of u^{-3}.

The radial magnetic field is zero before current shut-off and builds up to its maximum value approximately linearly with u; at large values of u it decays as u^{-4}. Because the induced current is

THIN SHEET RESPONSE
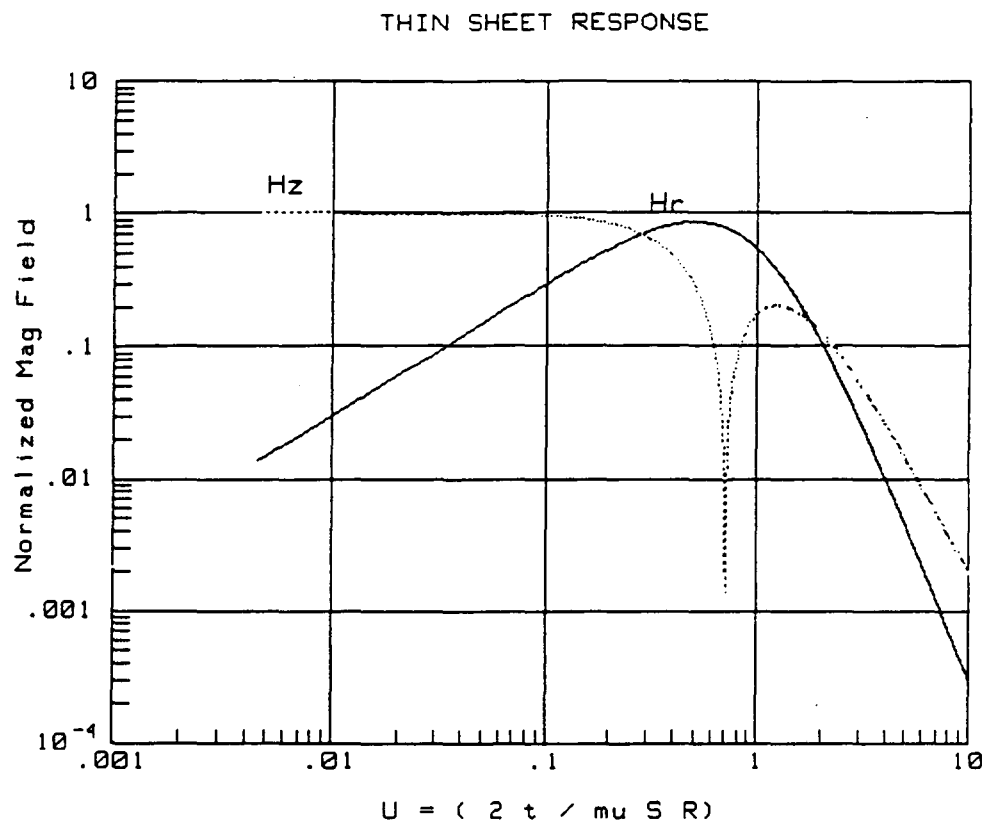
Figure 3.4 Normalized vertical and horizontal field transients plotted as a function of the parameter $u = \dfrac{2t}{\mu_0 SR}$. S is the sheet conductance, μ_0 is the free-space magnetic permeability and R is the source-receiver separation.

proportional to the radial field, the field maximum also corresponds to the maximum current density. The peak in the radial field transient curve (and also the induced current) may be determined by taking the derivative of Equation 3.8 with respect to u and setting it equal to zero

$$u_{max} = \frac{2t}{\mu_0 Sr} = \frac{1}{2}.$$ (3.10)

The position of the peak in the radial magnetic field (and azimuthal current) transient makes it possible to define a velocity for the induced current, where the velocity is defined as the movement of the peak position in the radial field transient away from the source in space and time. From equation 3.10 the velocity is a constant and given by

$$V_t = \frac{dr}{dt} = \frac{4}{\mu S}.$$

If the fields are again normalized by the value of the primary field before current shut-off, then the data shown in Figure 3.4 also describe the fields at particular lag times as a function of transmitter-receiver separation (profile presentation). This type of normalization is not appropriate, however, for describing the currents and fields as a function of transmitter-receiver separation, since it adjusts the field and current levels at each separation. The fields and currents are therefore best described by Equations 3.4 and 3.5.

Profiles of the absolute vertical and radial magnetic fields over an infinite thin-sheet for lag times from 0.05 ms to 2.0 ms are shown in Figure 3.5a and 3.5b. A transmitter with a unit dipole moment is used and the sheet has a conductance of 3.5 Siemens. The profile fields show the same general characteristics as the transient fields; the secondary vertical field equals the primary field at early times, crosses zero and decays at late times as r^{-3}. The sharp notch in the plot indicates the change in polarity. The radial field builds up to a peak proportional to time and decays at late times as r^{-4}.

We may obtain the peak value of the radial magnetic field as a function of transmitter-receiver separation by taking the spatial derivative in Equation 3.4 and and setting it equal to zero. In this case the current maximum occurs at a radial separation given by

$$r_{peak} = \frac{t}{\mu S}$$

and the corresponding velocity is

Vertical Magnetic Field (Hz)   S=3.5

a)

Radial Magnetic Field (Hr)   S=3.5

b)
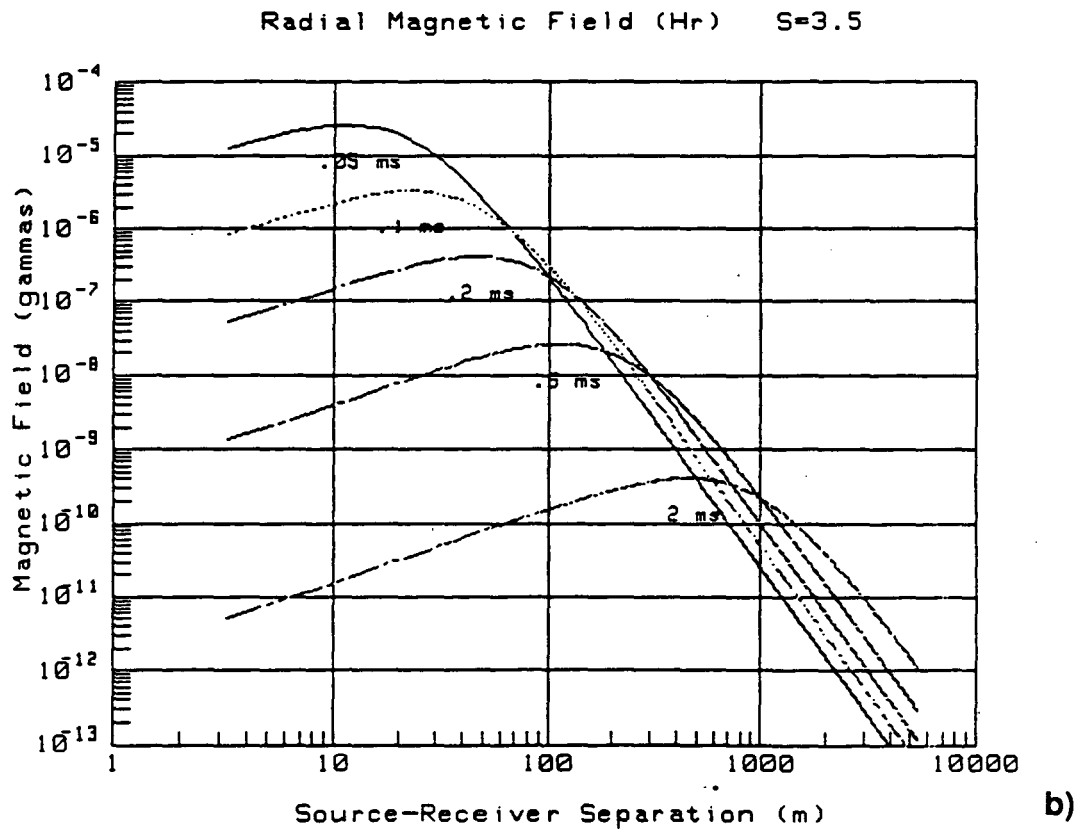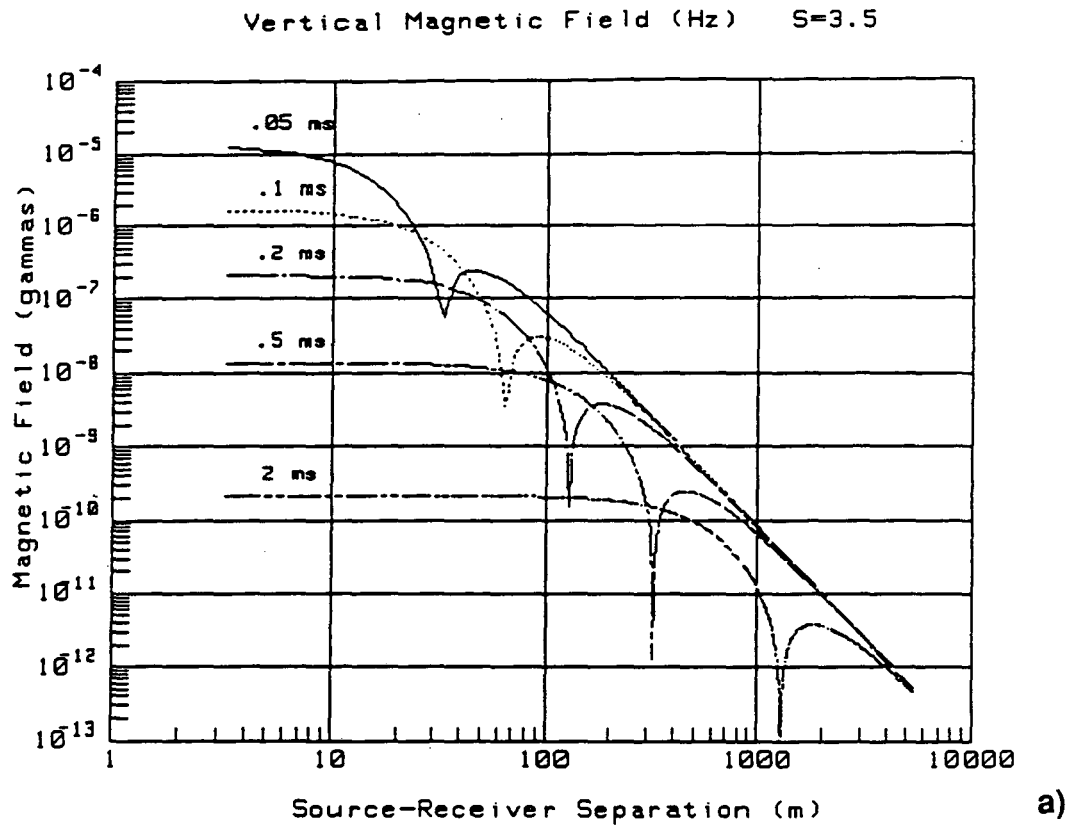
Figure 3.5 a) Vertical and b) horizontal magnetic fields over a thin-sheet as a function of source-receiver separation. The source is a vertical magnetic dipole with a unit moment; the sheet conductance is 3.5 S.

$$V_{prof} = \frac{1}{\mu S}.$$

Note that this velocity differs from the transient peak velocity by a factor of 4. The difference in these velocities is due to the $\frac{1}{r^3}$ dependence of the fields. If the fields had been normalized by the primary field, then the transient and profile velocities would be identical.

Finally, it is useful to examine the magnitude of the induced current at its peak value. This quantity is obtained by combining Equations 3.6 and 3.9 as follows:

$$J_{max}(t) = \frac{3M}{4\pi} \frac{\mu^3 S^3}{2^{1/2} t^3} \tag{3.11}$$

Note that this quantity displays a cubic dependence on the sheet conductance and time. This is similar to the late-time vertical field.

3.1.2 Truncated Sheet

The electromagnetic response for a VMD over a truncated sheet was investigated on scale models. Measurements were made for a series of thin aluminum sheets in air using three different transmitter positions for each model. Scale model data were collected as described in Chapter 2 using small and thin transmitter and receiver coils so that the experimental data closely approximated point measurements made at the surface of the sheet. In this case, the measurement of the horizontal field component is a good indication of the induced current in the sheet. The data are given either as normalized magnetic fields or as absolute fields for a source of unit dipole moment.

To determine if the scale model measurements for the truncated sheet can be compared to analytical results for the thin-sheet, analytical and scale model data must agree over parts of the model that resemble an infinite thin-sheet. To make this comparison we used a 1.6 mm sheet of aluminum, which scales to a layer 16 m thick with a resistivity of 4.65 ohm-m (S=3.5). Measurements were made at the center of the sheet where edge effects are unimportant. The radius of the transmitter coil was 50 m (5 mm) and receiver coils were less than half of this size.

The analytical and scale model results for this model, using a transmitter-receiver separation of 470 m, are shown in Figure 3.6. The figure shows an excellent agreement between the two data sets
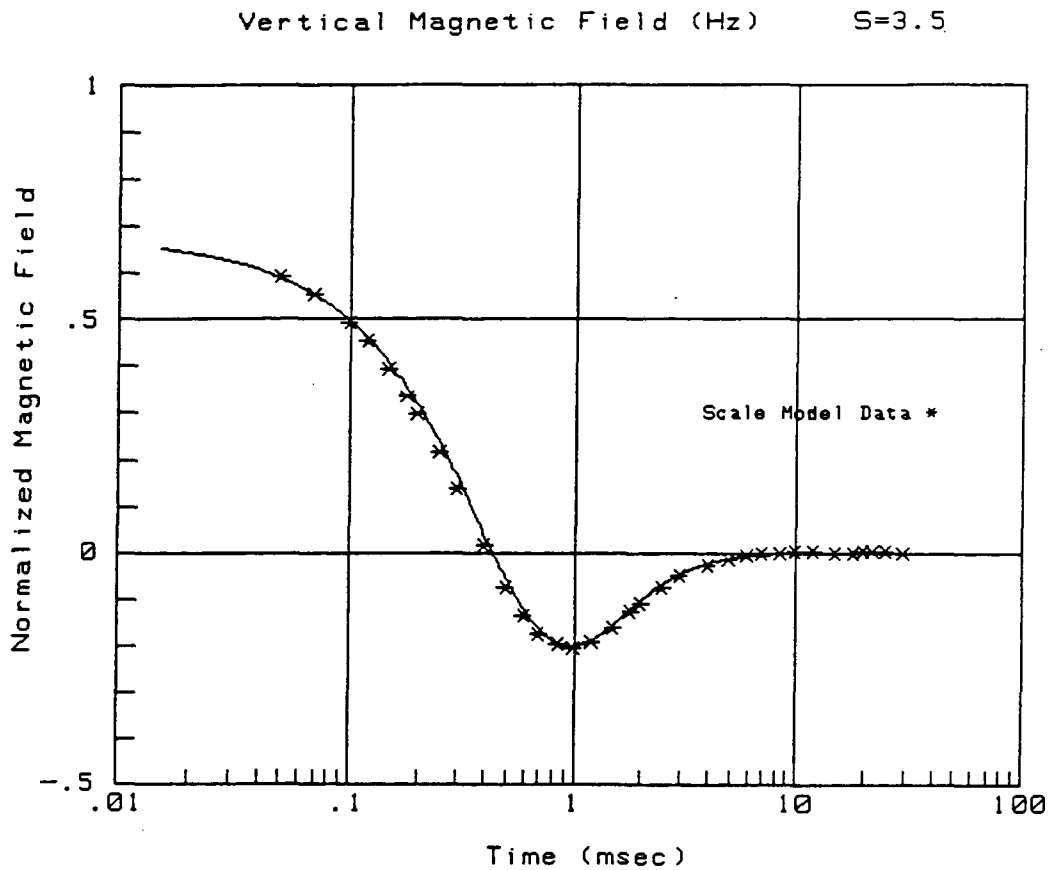
Figure 3.6 Comparison of scale model offset-dipole results over a 4.65 ohm-m 16 m thick sheet, and the analytical expression for a thin-sheet of the same conductance (3.5 Siemens). The source-receiver separation is 470 m.

for all lag times. At smaller separations we observed that the agreement was not as close. This is probably because the dipole field approximation breaks down at transmitter-receiver separations smaller than 8 loop radii (Spies, 1980).

Vertical and radial magnetic field profiles at lag times from 0.1-2.0 ms over a truncated sheet are shown in Figure 3.7. The transmitter is situated 1.5 km from the edge and receiver stations are located along a profile orthogonal to the contact, crossing the edge at 0 km. At early times, the vertical fields on opposite sides of the transmitter are similar; by 0.5 ms the fields over the contact are increased, with respect to the infinite side, forming a broad peak over the edge. During late time (not shown) this positive anomaly seems to broaden and diminish, until at the latest times it is not recognizable. The radial magnetic fields over the sheet are larger on the side of the transmitter nearest to the contact, as compared to the infinite side. As the contact is crossed into the nonconducting medium the radial field rapidly diminishes to zero. The maximum anomaly occurs during the intermediate times, when the amplitude of the field (and the induced current) is also largest.

For this case the early-time data are not particularly sensitive to the contact because the transmitter is located far from the edge and most of the induced current remains close to the source. By intermediate time more of the current has reached the contact and begins to accumulate since it may not flow across the boundary into the nonconducting host medium. At late-time the anomaly seems to dissipate and move back towards the source as the fields decay to zero.

To better visualize the contact effect it is useful to separate the infinite thin-sheet response from the total observed field. We define the contact anomaly ($H_{Zcont}(r,t)$, $H_{Rcont}(r,t)$) as the difference of these two quantities,

$$H_{Zcont}(r,t) = H_{Zobs}(r,t) - H_{Zsheet}(r,t) \qquad (3.12)$$

$$H_{Rcont}(r,t) = H_{Robs}(r,t) - H_{Rsheet}(r,t). \qquad (3.13)$$

The infinite thin-sheet response used in calculating the contact anomaly was measured with a scale model. Although this quantity could be calculated from Equations 3.4 and 3.5, the calculation is only valid for a dipole source.
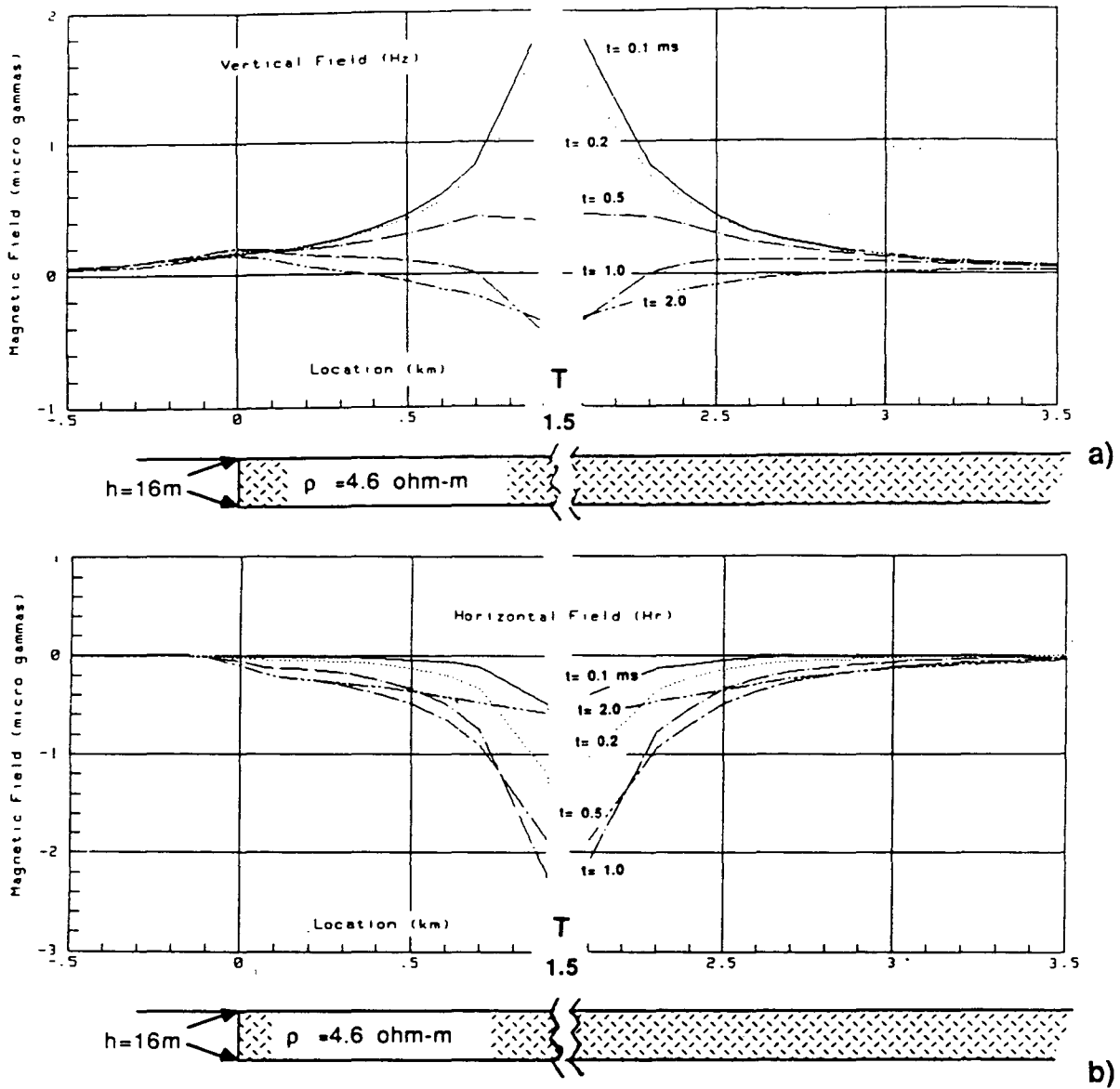
Figure 3.7 a) Vertical and b) horizontal magnetic field profiles over truncated and infinite thin-sheets. The source is a VMD with a unit dipole moment
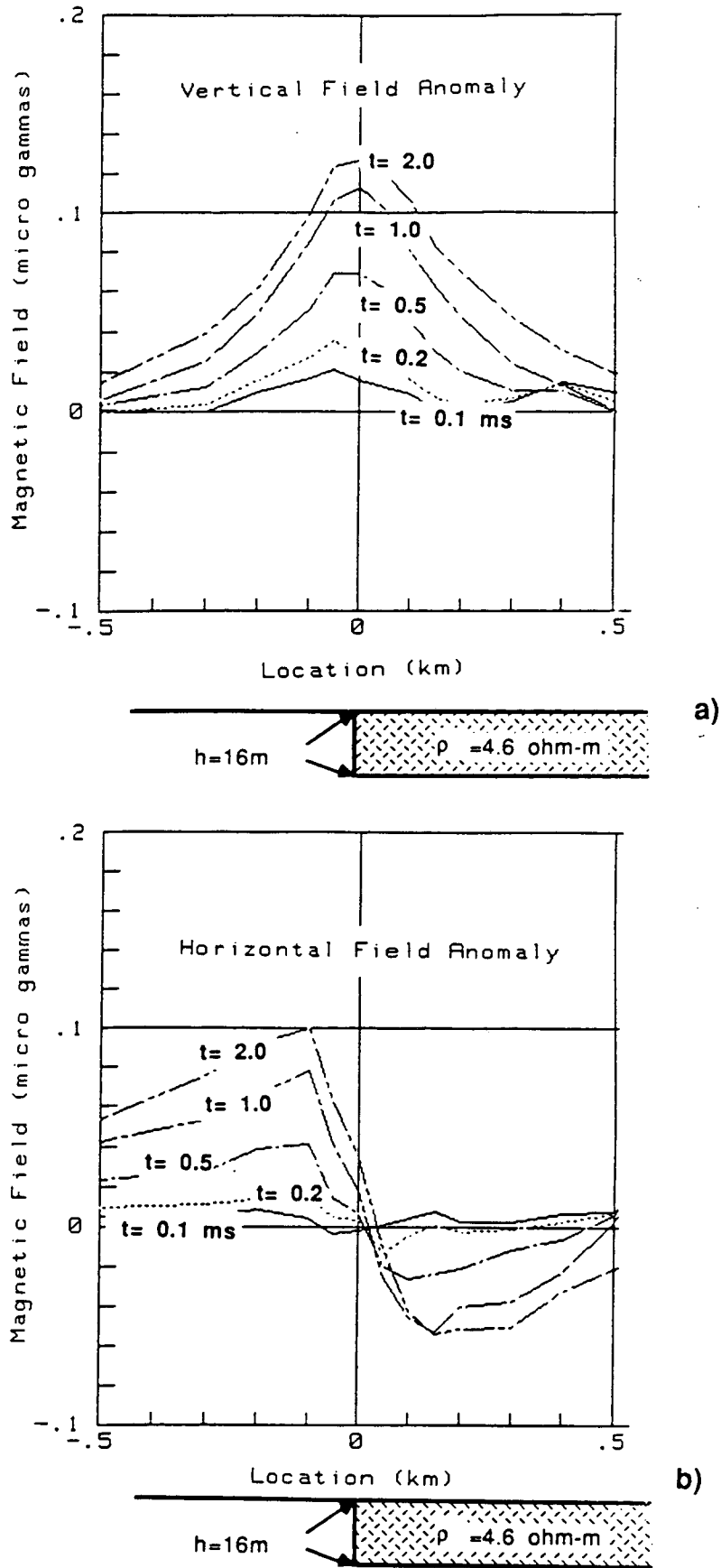
Figure 3.8 a) Vertical and b) horizontal magnetic field anomaly profiles over a truncated thin-sheet

model. The anomaly is defined as the difference between the truncated and infinite thin-sheet responses.

The anomaly profiles for the data in Figures 3.7 are presented in Figure 3.8. The shape of the vertical field anomaly (Figure 3.8a) is a broad peak centered over the contact. The radial field anomaly is a crossover with a negative lobe on the conductive side, a positive one on the free-space side and a zero-crossing at the contact. The resulting anomaly for both fields resembles the field of two straight parallel current-carrying wires of opposite polarity located equidistant from, but on opposite sides of the contact. This dual wire model may be an appropriate first order approximation for describing the contact anomaly which is defined as the observed data minus the infinite thin-sheet response. When compared to the infinite thin-sheet response The true excess current must reside on the conductive side of the contact but this means that there is a an apparent current deficiency of equal magnitude on the resistive side of the contact. The result is the symmetric and antisymmetric anomaly patterns observed across the contact.

The anomalous vertical and horizontal fields are shown as cross-sections in Figure 3.9; this is a useful presentation for observing the field behavior in space and time. At early times the two cross-sections indicate small but increasing field anomalies for each component with the maximum anomaly centered near the edge. At intermediate times, the position of the anomaly is more or less static as it reaches its maximum value and begins to decay. At late times, as the amplitude diminishes, the anomalies seem to broaden, and the position of the maximum and minimum peaks in the radial field anomaly move, away from the contact.

After measuring the anomalies for several truncated sheet models, using several transmitter positions for each model, the following observations are made: 1) The positions of the maxima and minima of the anomalous horizontal field are a function only of the distance from the source to the edge. These peaks occur on both sides of the edge at a distance from the contact equal to one tenth the distance from the source to the edge. 2) The peak anomaly for the truncated sheet occurs at a lag time governed by the velocity of the induced current in a infinite thin-sheet of the same conductance (Equation 3.10). The contact anomaly is greatest during the time required for the peak current in an infinite sheet to propagate the equivalent distance from the source to the edge. 3) The strength of the observed anomaly depends inversely on the cube of the distance from the source to the contact.
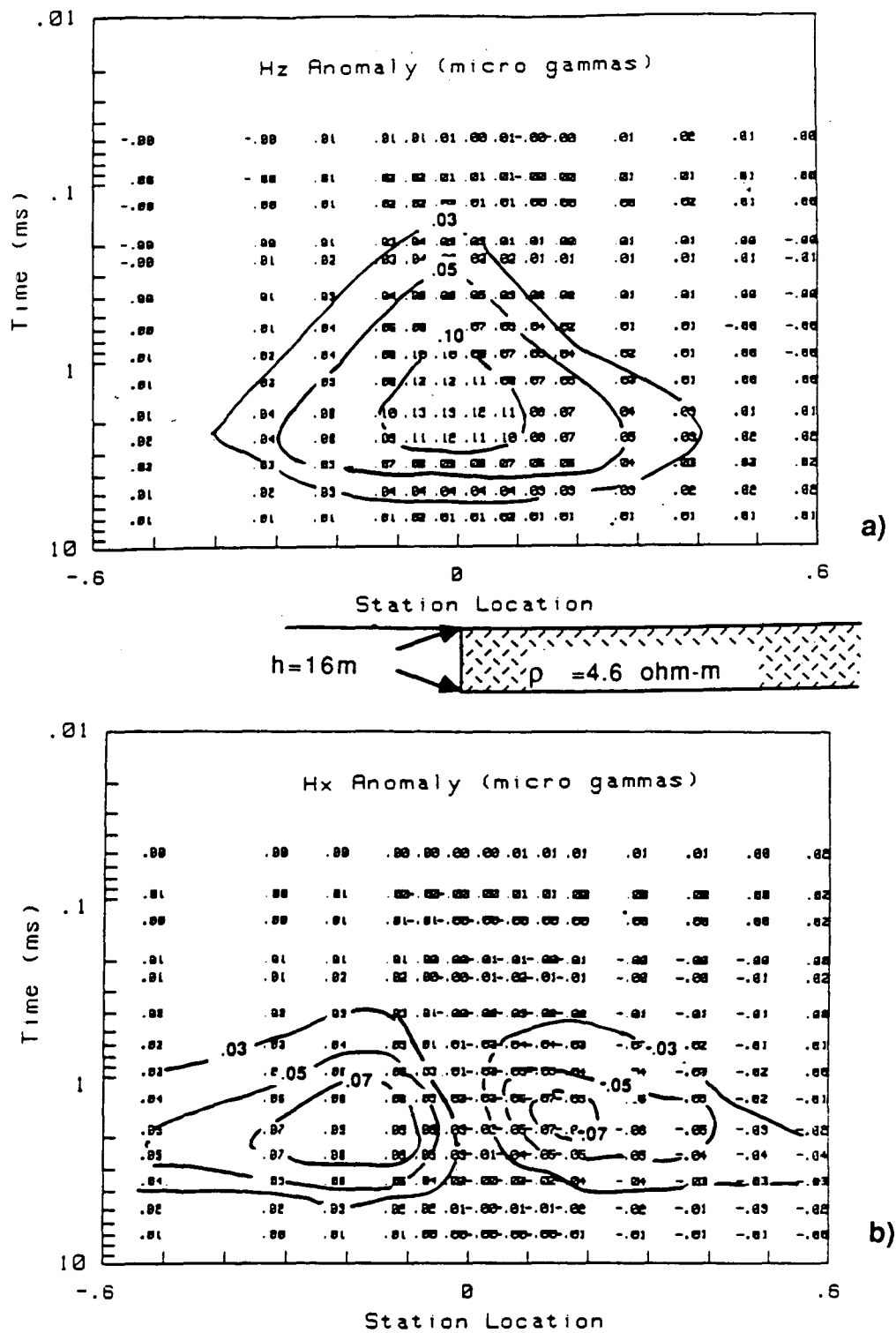
Figure 3.9 a) Cross sectional plots of the vertical magnetic field anomaly over a truncated sheet with a conductance of 3.5 S; the source position is 1.5 km. b) Cross-sectional plots of the horizontal magnetic field anomaly for the truncated sheet.

We can use the second and third observations to define a normalized time, t_n, and a normalized field, H_n, as was done for the infinite thin-sheet models.

$$t_n = \frac{t}{\mu SL} \qquad H_n = \frac{H}{M/4\pi L^3}, \qquad\qquad (3.13)$$

where L is the distance from the transmitter to the contact and M is the transmitter moment. The vertical and horizontal anomalous field sections as a function of the normalized parameters are shown in Figure 3.10. By plotting the fields for all the truncated sheet models as a function of these parameters, and the distance as a function of X/L, we obtain the generalized response for this type of model. The thin-sheet edge response for a dipole source is therefore completely represented by these profiles. For cases where superposition holds, such normalized profiles may be useful in removing a contact anomaly from field data.

3.1.2.1 Transient Fields

Vertical and horizontal field transients for two stations on a truncated sheet is shown in Figure 3.11a and b. The VMD transmitter has a unit dipole moment and is located 1.5 km from the edge. The first station is located 100 m away from the edge on the conductive side; the second is an equal distance from the source but located towards the center of the sheet.

The two vertical field transient curves are nearly identical at early times but by intermediate times the transient for the station near the edge decays much more slowly than that near the center of the sheet, and it does not change polarity. The vertical field transient near the edge does not cross zero because the contact prevents the majority of the current from flowing beneath the receiver. The horizontal field transients for the truncated and infinite thin-sheet models are quite similar in appearance (Figure 3.11b). The field near the contact is larger than the field over the homogeneous model and the peak occurs slightly earlier in time, but the general characteristics of the two transients are not greatly different.

The vertical and horizontal anomalous transients (i.e. difference between curves A and B) are shown on a semi-logarithmic plot in Figure 3.12. Both transients build to a maximum in proportion to the lag time and have a linear decay at late-times on the semi-logarithmic plot. This suggests that a

Normalized Hz Anomaly

a)

b)
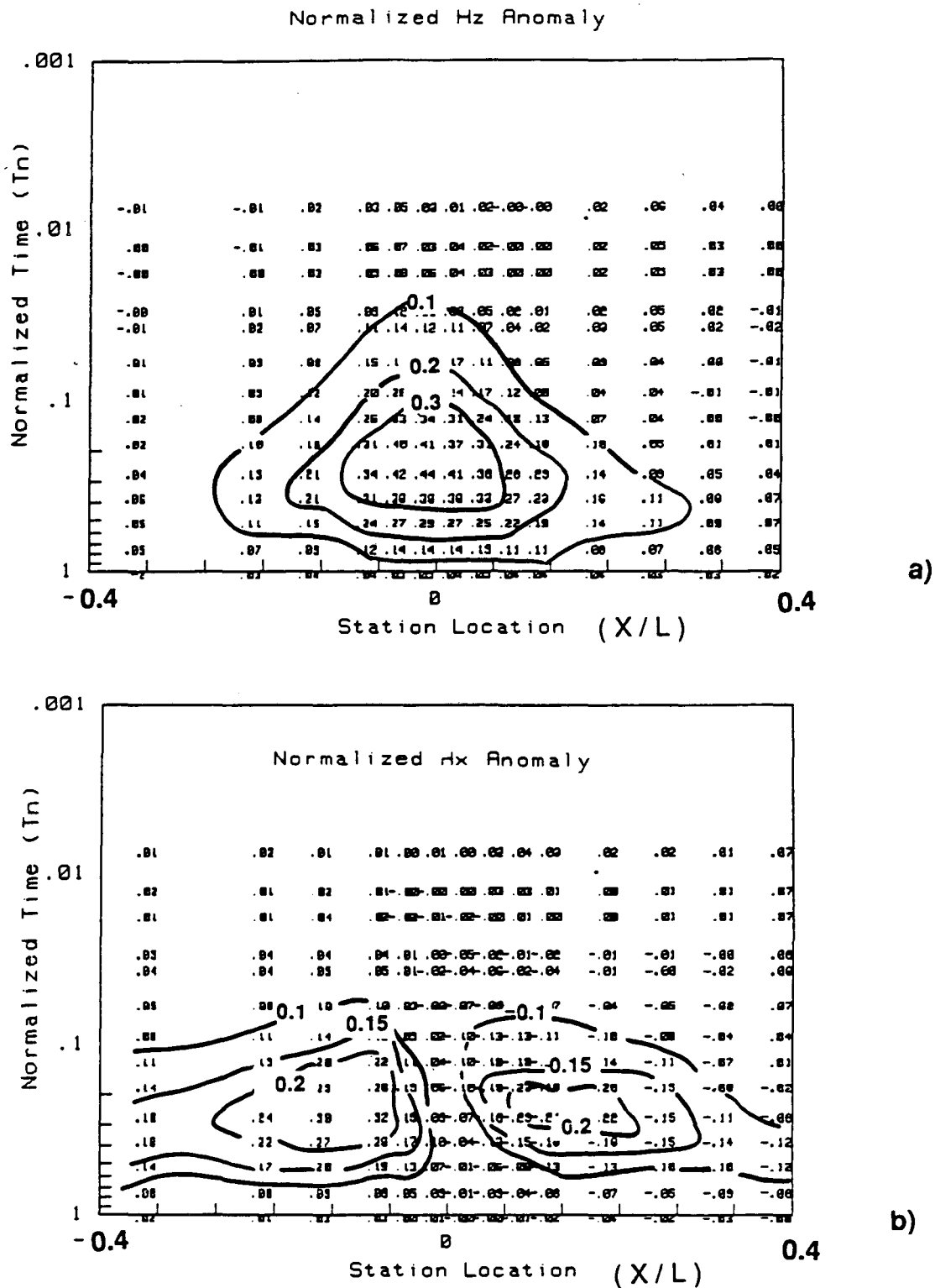
Figure 3.10 Normalized cross-sectional plots of a) anomalous vertical field and b) anomalous horizontal

field over a truncated sheet. The fields are normalized as $H_n = \dfrac{H}{M/4\pi X^3}$, the lag time is normalized

as $t_n = \dfrac{t}{\mu S L}$, where L is the distance from the source to the edge and X is the station location.
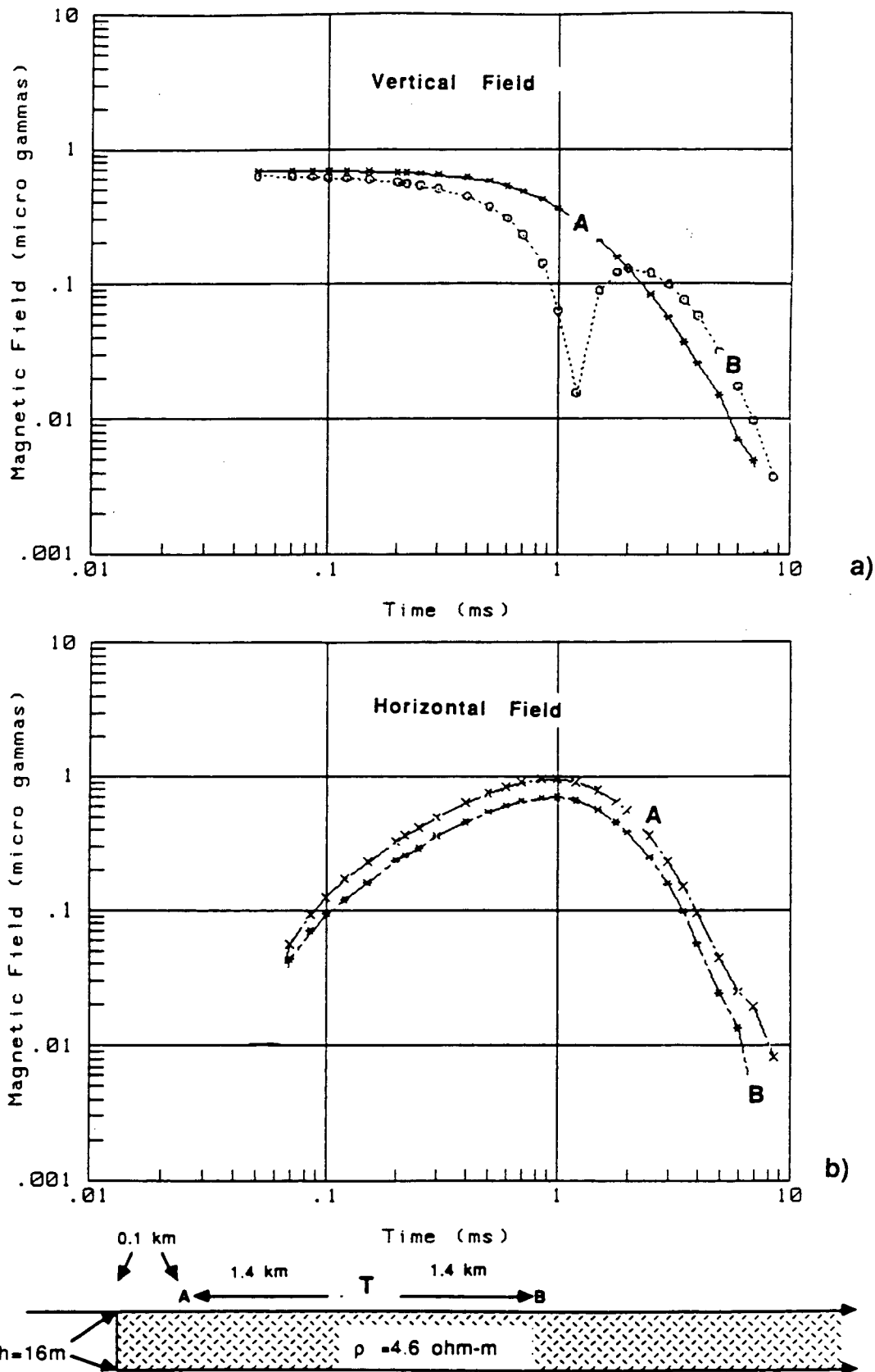
Figure 3.11 a) Vertical magnetic field transients for a station 100 m inwards from a thin-sheet contact

and a station an equal source-receiver separation located on an infinite thin-sheet. The source is a

VMD with a unit moment. b) Horizontal magnetic field transients for these same stations.
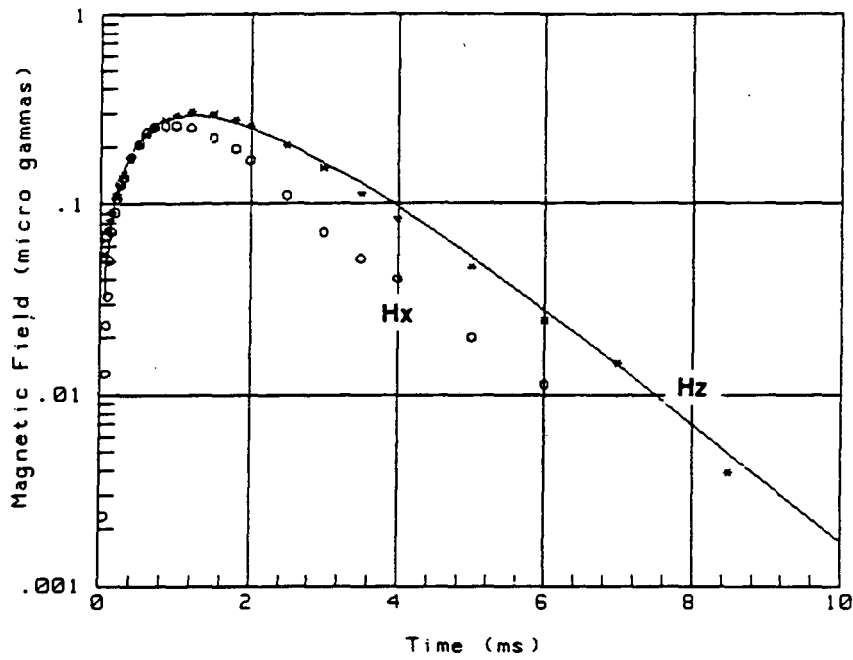
Figure 3.12 a) Vertical and horizontal magnetic field anomaly transients for fields shown in Figure 3.12. The anomaly is defined by the difference between the curves in Figure 3.11. The solid curve that fits the vertical field transient is an exponential function as given in equation 3.13.

simple exponential function may be used to represent the observations. For the vertical field anomaly transient the form of this function is given by

$$H_n(t) \approx K_1 t \mid L - D \mid^3 e^{-t/\tau} \qquad \tau = \frac{\mu S \mid L + D \mid}{4} \qquad (3.14)$$

$$H_n = \frac{H_0}{M / 4\pi L^3}$$

where t is lag time in seconds, L is the distance from the source to the edge and D is the distance from the measuring site to the contact in meters. The empirical constant K_1 is approximately equal to 0.001 $m^{-3} s^{-1}$.

In Figure 3.12 this function is fitted to the vertical field anomaly transient which can thus be approximated at all stations located within 200m of a thin-sheet contact for all of the models considered. No correspondingly simple formulation for the horizontal field transient was found.

3.1.2.2 Transient Peaks

To investigate the current distribution in a truncated sheet we examine the horizontal field transient peaks. Because the horizontal component in a thin sheet is a good measure of the induced current (see Section 3.1.1), the location and characteristics of its transient peaks on a truncated sheet should provide information on how the induced current propagates near the edge.

The position of the transient peaks for the infinite and the truncated thin-sheet models is plotted in Figure 3.13 for a transmitter 1.5 km from the contact. Near the source, and far from the edge, the transient peaks occur early in time and the peaks for the truncated sheet coincide with the infinite model. Both peaks occur at lag times proportional to the source-receiver separation (Equation 3.10). Beginning several hundred meters from the edge, the peaks over the truncated model become static in time while the maxima over the infinite sheet continue to move outward in time in proportion to the source-receiver separation.

These data indicate that the induced current in the truncated sheet slows near the edge, nearly becoming static. Because the current may not flow across the contact, it must either decay in place or move backwards towards the source. A look at the transient anomaly peaks can help to determine
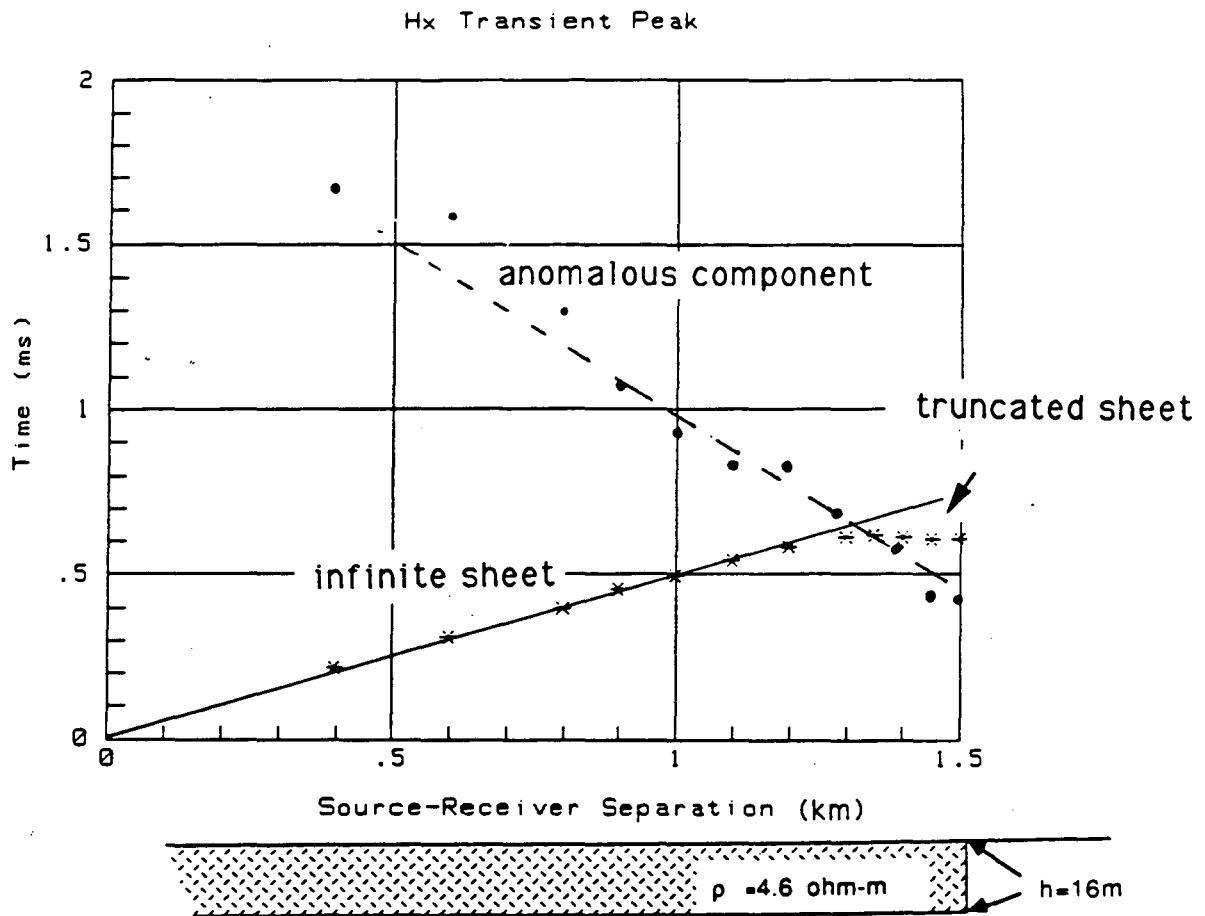
Figure 3.13 The horizontal field transient maximum as a function of source-receiver separation for thin-sheet (solid curve) and truncated sheet models (*). The contact is located 1.5 km from the source. The plot also shows the maximum in the anomalous field (see text), as a function of source-receiver separation.

which of these is occurring.

A plot of the anomalous horizontal field transient peaks, as defined in Equation 3.12, is shown in Figure 3.13. These data relate to the distribution of the anomalous current near the contact and can be represented by a line with a slope inverse to the transient peak data. That is, the anomalous component of the horizontal field transient peaks at later times at stations farther from the contact and at earlier times for stations near the edge. This suggests that after the induced current has reached the edge some of it is then scattered back towards the source, with approximately the same velocity. This means that at substantial distance from the contact there is a late-time anomaly due to current scattered back from the edge.

In summary, the induced current, for a dipole source over a truncated sheet, produces a broad positive anomaly in the vertical magnetic field and a crossover-type anomaly in the horizontal component. This field is reminiscent of a dual current filament or bifilar distribution. The peak anomalies occur in space as a function of the distance from the transmitter to the source and in time as a function of the velocity of the current in the sheet. The response can be reduced to a single set of profiles by normalizing the fields by their values prior to current shut-off, and plotting this data against a normalized time as given in Equation 3.13. The current initially propagates from the source towards the contact as it does for a infinite thin-sheet but several hundred meters from the edge, it begins to slow down and eventually becomes static. At later times the anomalous or scattered current moves inward towards the transmitter. Vertical and horizontal field anomaly transients near the contact build up to a peak at early times in proportion to time and then decay exponentially at intermediate to late times. This is similar to the field behavior for a confined body (Kaufmann, 1978).

3.2 Magnetic Fields over Truncated Sheet and Quarter-Space Models.

In this section we examine the magnetic field response for the thin-sheet and the quarter-space contact models (Figure 3.1) using three ground-based EM system configurations: the fixed-loop, the electrical dipole, and the central-loop system (Figure 3.2). The fixed-loop system, for this test, consists of a 400 m x 800 m rectangular loop transmitter, carrying a current of one ampere and centered 1.8 km from the edge, with the long axis parallel to the contact. Magnetic field measurements are made along

a single profile orthogonal to the contact strike. The electrical dipole transmitter is a 1-km-long wire oriented parallel to the contact and grounded at both ends. The wire carries one ampere of current and is located 1.8 km from the edge. The fields are measured along a single profile which is orthogonal to the wire, crossing it at its midpoint. The central-loop system uses a series of 250 m radius circular loop transmitters, each carrying a current of one amp, with measurements made at the center of each loop. The data are collected along a single profile, orthogonal to the contact, with station spacings ranging from 25 to 250 m.

3.2.1 Vertical Magnetic Field Profiles over a Truncated Sheet

Early-time vertical magnetic field profiles for the three systems over the truncated sheet are given in Figure 3.14a. For the fixed-loop and electrical dipole systems the data are displayed on both sides of the transmitter so that the fields over the contact can be compared to the fields over the continuous part of the model; the position of the transmitter is marked with a "T." Anomaly profiles, as defined in Equations 3.12 and 3.13, are shown at the bottom of the figure. The anomalies are displayed, at an expanded scale, only for stations near the edge (0 km). For the central-loop configuration the transmitter moves with each station so there is no dependence on transmitter-receiver separation. The anomaly for this system is therefore defined as the observed field less the field at the center of the sheet.

The early-time (0.1-0.3 ms) vertical magnetic fields for the fixed-loop configuration are not appreciably different on either side of the transmitter. This system is relatively insensitive to the contact at early times because little of the induced current has propagated very far from the source and the transmitter is a considerable distance from the edge. The early-time field amplitudes far from the source show the $\frac{1}{r^3}$ fall-off characteristic of a dipole source, but closer to the transmitter they attenuate more slowly with distance due to the large dimensions of the loop source. The early-time anomaly profiles (Figure 3.14b) show the development of a broad but very weak positive anomaly that increases in strength with time.

In contrast to the fixed-loop results the early-time vertical field profiles for the electrical dipole
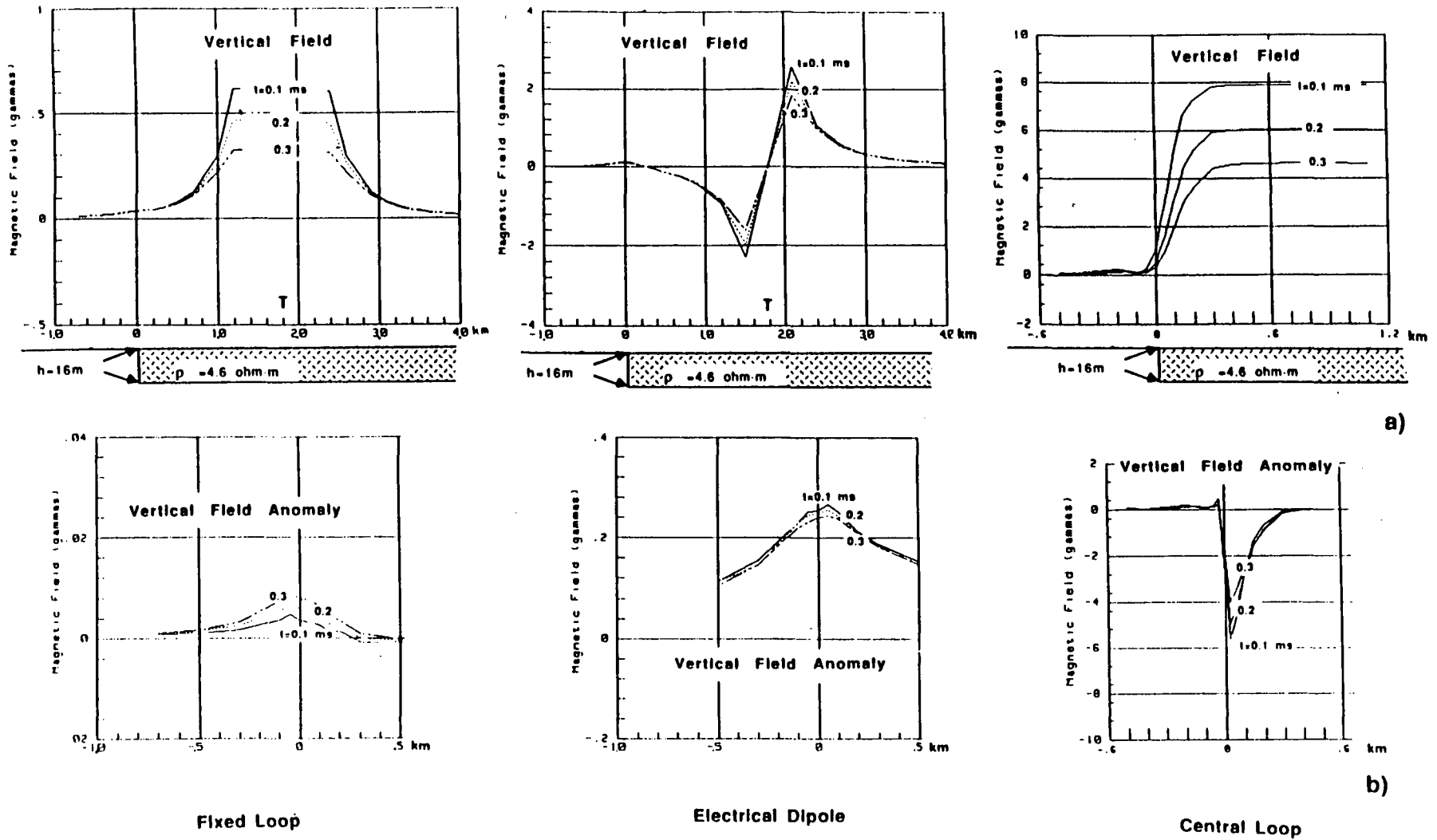
Figure 3.14 a) A plot of the early-time vertical fields over a truncated sheet for the fixed-loop, electrical dipole and central loop configurations. b) A plot of the vertical field anomaly over the edge, where the anomaly is defined as the difference between the fields on either side of the transmitter.

system show a large contact effect. The magnetic field changes polarity over the contact, passing through zero approximately 200 m inwards from the edge, and remaining at this opposite polarity over the contact. The early-time anomaly profiles for the electrical dipole source form a peak centered close to the edge (Figure 3.14b), with the maximum anomalous field more than twice as large as the primary field (because the polarity of the field is reversed).

Because the electrical dipole system impresses current into the medium, there is galvanic as well as inductive current flow, (galvanic currents are present in the medium before the transmitter has been shut off). In an electrically discontinuous medium, galvanic currents flow nonuniformly due to electrical charges that appear at the interfaces of bodies with contrasting conductivity; these currents are channeled into conducting regions and away from nonconducting bodies (Kaufmann, 1981; Nabighian, 1985). From the nonuniform distribution of these currents magnetic field anomalies are produced that shift the static magnetic field levels throughout the medium. Kaufmann (1981) noted that as secondary fields are produced by the collapse of the primary field, so are secondary fields created by the decay of the galvanic charges at the conductivity interfaces. The result is that for the electrical dipole system, the observed fields near a contact are due to a complex combination of galvanic and induced currents. For the truncated sheet, galvanic charges are located at the contact on the surface of the sheet. The anomalous fields are therefore very large near the edge due to the close proximity of the charges to the measurement point.

Early-time central-loop profiles over the truncated sheet show a smooth transition from the slow decay over the infinite sheet to the abrupt free-space response across the contact (Figure 3.14a). The transition at these early-times occurs almost completely within one loop radius of the contact. The anomalous vertical field for this system is a spike-like negative located adjacent to the contact on the conductive side (Figure 3.14b).

The intermediate and late-time vertical magnetic field profiles for the three systems are given in Figure 3.15a. At these times there is significant inductive current flow in the sheet and these plots reflect the movement and decay of this current. Note that the range of times on the plot varies from 0.5 to 10 ms for the fixed-loop system, to 0.5 to 4 ms for the central-loop and electrical dipole systems.
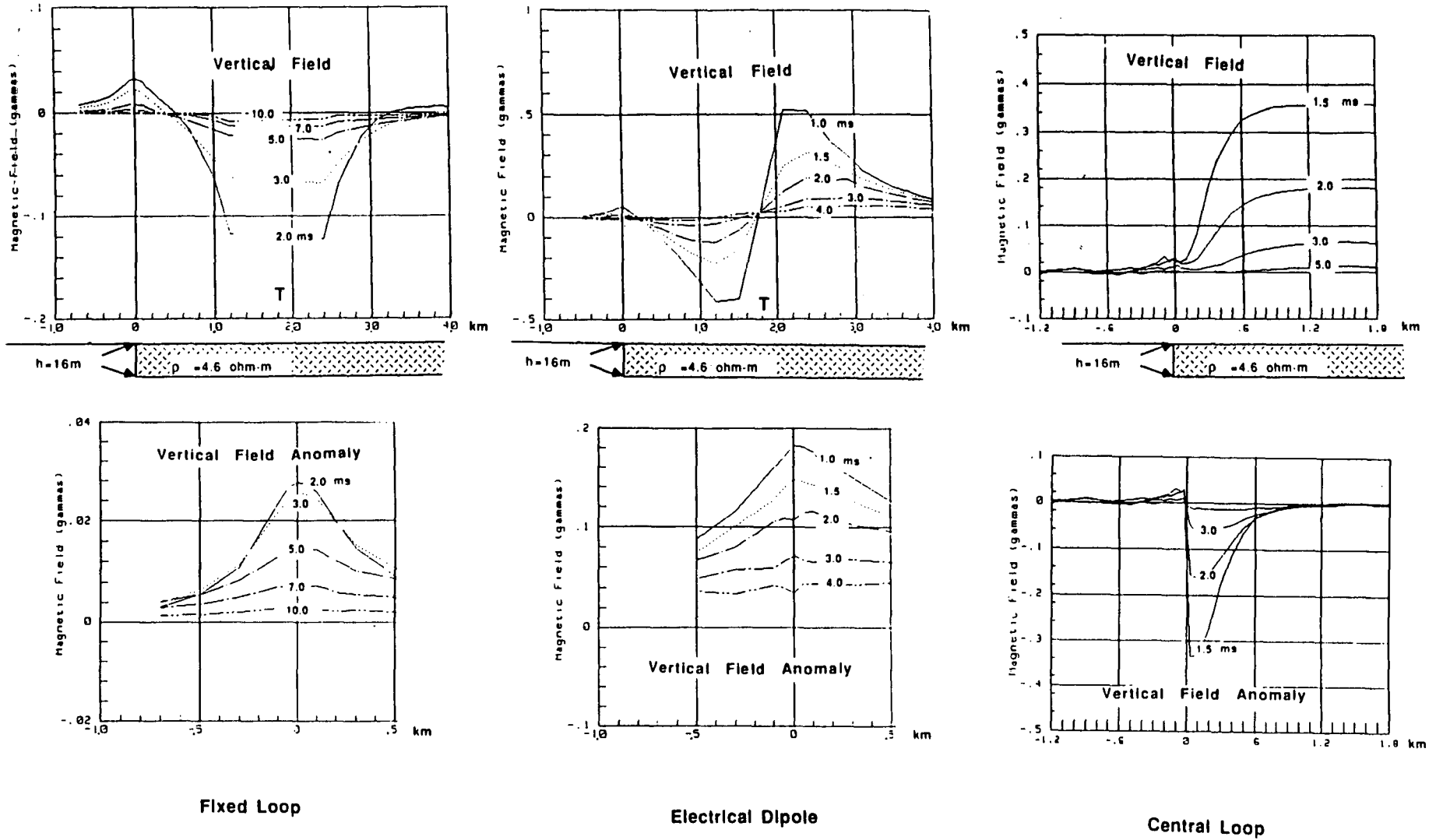
Figure 3.15 a) A plot of the vertical field for the three systems at intermediate and late times. b) The contact anomaly at intermediate and late times.

The intermediate-time fixed-loop profiles over the contact are very different from those over the infinite sheet. Near the contact the fields at different lag times switch polarity at a common point; they also decay more slowly than the fields over the infinite sheet. As shown in Sections 3.1 and 3.2 of this chapter, the zero crossings in the vertical field relate to the passage of induced current beneath the receiver. For an infinite thin-sheet the position of the crossover steadily moves outwards from the transmitter, occurring later in time at farther offset soundings (Equation 3.4). This is the case on the infinite side of the truncated sheet model (Figure 3.15), but on the side nearest the edge the zero-crossings begin to gather about 200 m inwards from the edge, and remain fixed at this position until late-time. This field behavior is reminiscent of the response of a vertical sheet-like conductor and has often been confused with this type of response (Spies and Parker, 1984).

At intermediate times, the vertical fields for the electrical dipole source decay monotonically in space and time over the infinite side, but the decay is more complex over the contact. The vertical field changes polarity about 200 m inwards from the contact and remains at this opposite polarity across the edge. At late times the fields revert back to the expected polarity.

The intermediate and late-time anomaly profiles for the fixed-loop system and early-time anomaly for the electrical dipole systems are both broad positives of approximately the same wavelength and centered near the contact. For the electrical dipole system, however, the maximum anomaly occurs early in time and begins to dissipate at later times. The maximum anomaly is more than twice as large as the primary field. For the fixed-loop source the maximum anomaly occurs at a time dependent on the distance from the source to the edge and is about the same magnitude as the observed field over the infinite sheet.

The central-loop contact effect at intermediate and late times appears again as a smooth adjustment in field level across the contact (Figure 3.15a). The adjustment distance gets progressively longer in proportion to the lag time and at the latest times some contact anomaly is evident more than 4 loop radii from the edge. At later times the vertical field also develops a small positive anomaly centered on the resistive side of the edge.

3.2.2 Horizontal Field Profiles over a Truncated Sheet

The early-time horizontal fields for the three systems over the truncated sheet are shown in Figure 3.16. Notice that for the fixed-loop system the polarity of the horizontal field reverses on opposite sides of the transmitter. The fields are symmetric, however, for the grounded source. For the central-loop system the observed field over a homogeneous or horizontally layered structure is entirely vertical and horizontal fields develop only near an inhomogeneity. The horizontal component for this system is therefore a purely anomalous field.

As with the vertical field, the fixed-loop horizontal field profiles do not have a significant early-time contact anomaly and the electrical dipole profiles have a large one (Figure 3.16b). The anomaly for both systems is a "crossover," with the negative lobe on the conductive side, the positive lobe on the free-space side, and the zero crossing directly on the contact. (Note that with the polarity convention adopted this negative anomaly is an enhancement of the field.)

For the central-loop system the early-time horizontal field profiles are sharply peaked anomalies centered on the conductive side of the contact. The peaks are larger, sharper and located closer to the contact at the earliest lag times and gradually diminish in amplitude, broaden and move inwards from the edge at later times.

The horizontal fields at intermediate and later times are shown in Figure 3.17. For the fixed-loop system the fields on each side of the transmitter are of a single polarity. Profiles for the electrical dipole system show a pattern of migrating crossovers similar in appearance to the fixed-loop vertical profiles. In this case, however, the crossovers do not gather near the contact but continue to migrate across it. At intermediate and later times the horizontal field anomalies for the fixed-loop and electrical dipole systems are both broad crossovers of approximately the same wavelengths (Figure 3.17b). The anomaly for the electrical dipole system, however, is several times larger than the fixed-loop anomaly.

For the central-loop system the horizontal field at intermediate and later times also form negative anomalies centered on the conductive side of the edge. At these times the anomalies are lower in amplitude, broader and situated further inwards from the contact than the early-time fields. Unlike the early-time fields the late-time profiles cross zero and develop a small positive anomaly over the contact.
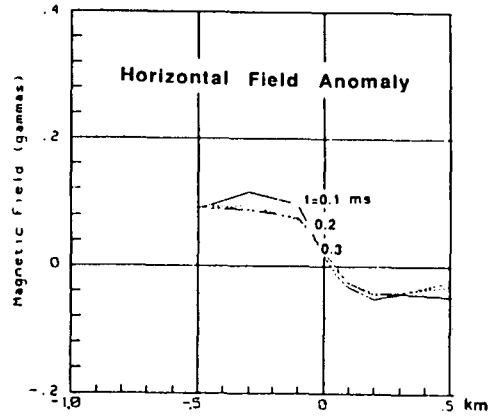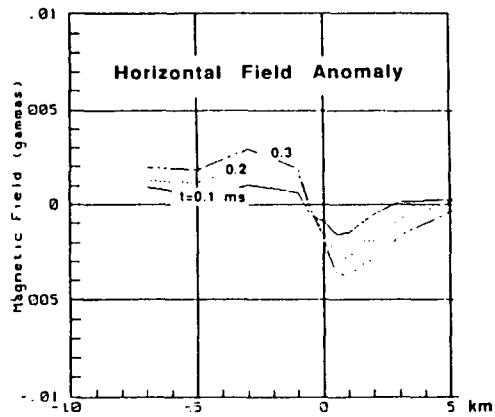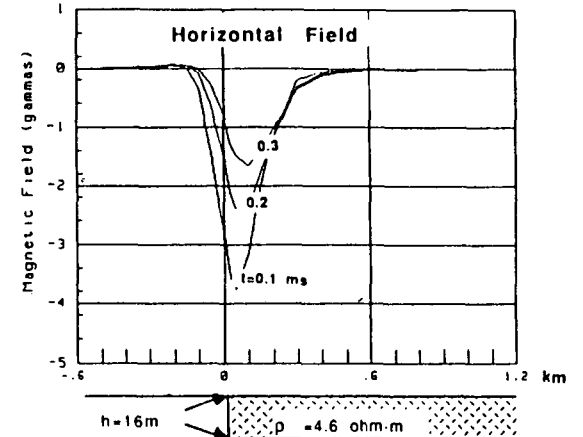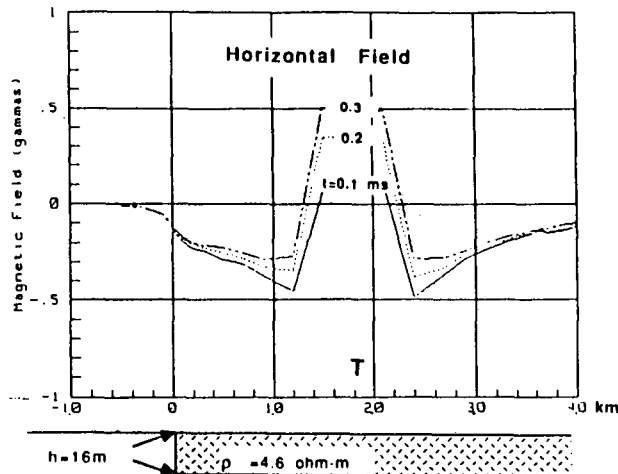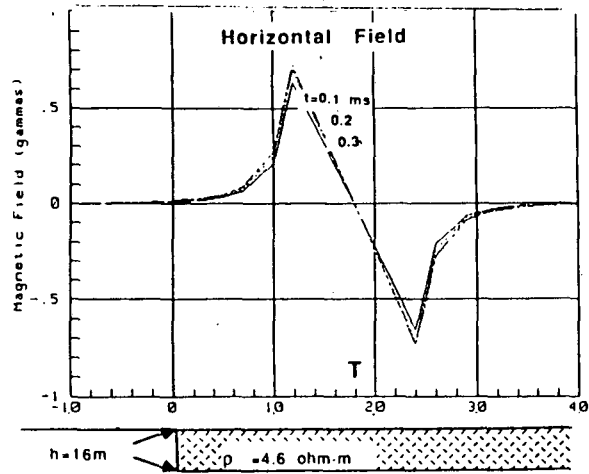
Fixed Loop

Electrical Dipole

Central Loop

Figure 3.16 a) A plot of the early time horizontal fields over a truncated sheet for the fixed-loop, electrical dipole and central-loop configurations. b) A plot of the horizontal field anomaly over the contact.
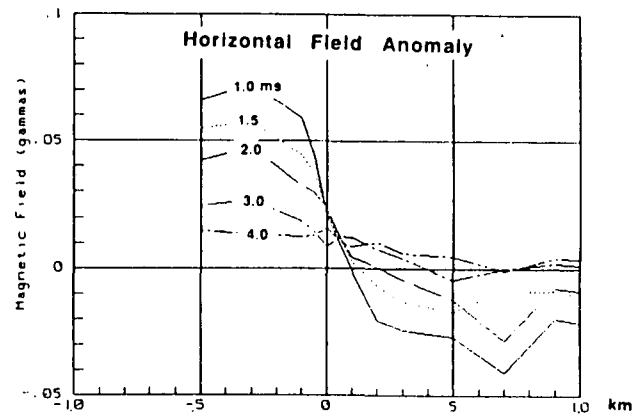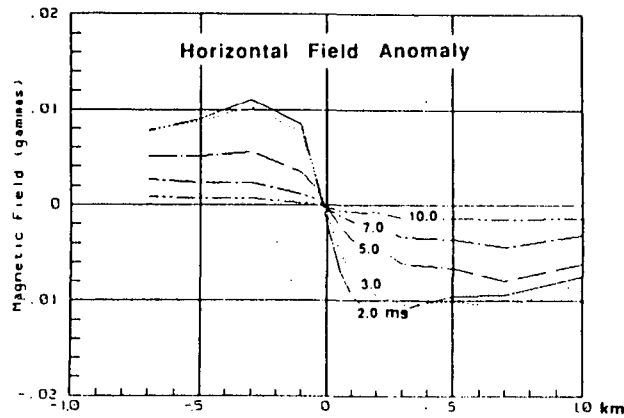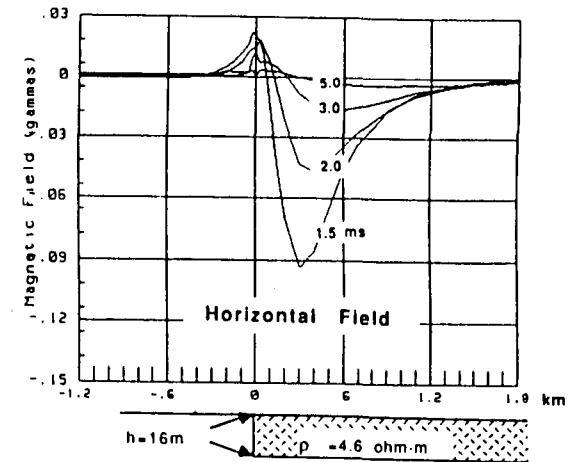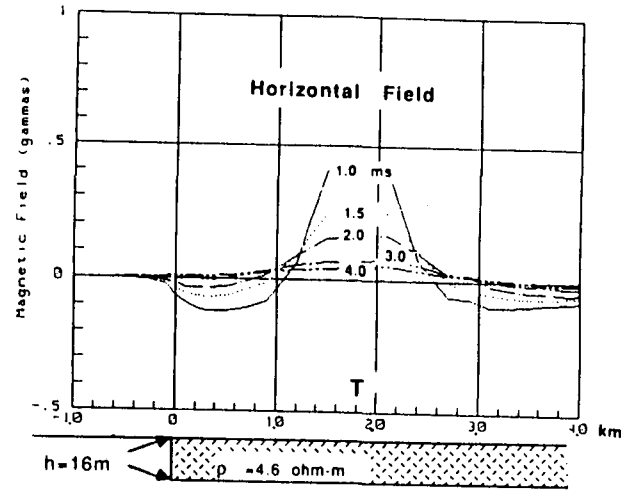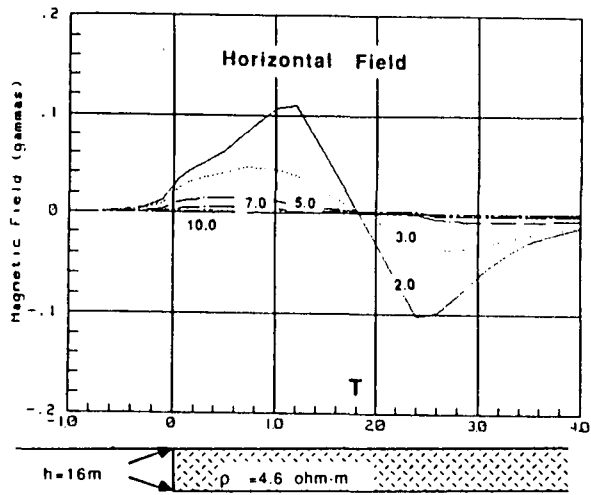
Fixed Loop **Electrical Dipole** **Central Loop**

Figure 3.17 a) A plot of the horizontal field for the three systems at intermediate and late times. b) The

contact anomaly at intermediate and late times.

64

3.2.3 Transient Fields over a Truncated Sheet

Vertical and horizontal field transients for the fixed-loop and electrical dipole systems are plotted for a station located 100 m inwards from the contact and for a station an equivalent distance from the source on an infinite thin-sheet (Figure 3.18). For the central-loop system the transient 100 m from the edge is plotted together with the transient at the center of the sheet.

For the fixed-loop source the vertical field transient near the contact initially increases in field strength until about 1.5 ms; it then monotonically decays to zero. At the center of the sheet the transient initially decreases in amplitude and changes polarity at about 2 ms, remaining at this opposite polarity until it decays to zero. The characteristic zero-crossing is due to the passage of the induced current beneath the receiver. The late part of the transient anomaly for this system (Figure 3.19b) can be represented by an exponential function whose time constant depends on the conductance of the sheet and the distances from the source and receiver to the edge. For the fixed-loop considered above the time constant was found to be

$$\tau = \frac{\mu S \, |L + D \,|}{3} \tag{3.15}$$

where L is the distance from the source to the edge and D is the distance from the measurement point to the edge. This is 25 percent larger than for the vertical magnetic dipole source, suggesting that the time constant is also a function of the source dimensions.

The vertical field transients for the electrical dipole system differ from each other in two respects (Figure 3.18b). First, the curves are shifted with respect to each other. Although this is not shown on the logarithmic plot, the transient near the contact has the opposite polarity from one at the same separation over an infinite sheet. Secondly, the curves have markedly different decay characteristics. Notice that the transient near the contact crosses zero at a lag time of 2 ms whereas the vertical field over the center of the model decays monotonically (Gunderson et al. 1986).
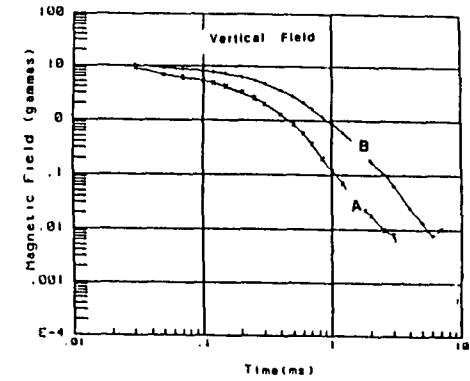
The electrical dipole system anomaly transient is plotted on semi-logarithmic paper in Figure 3.19a. This transient has a linear decay on the semi-logarithmic plot and can be represented by a simple exponential with a time constant given by
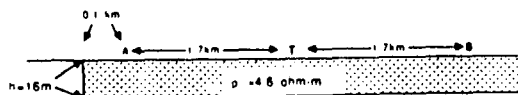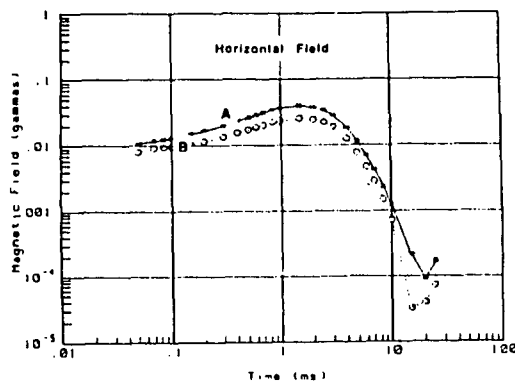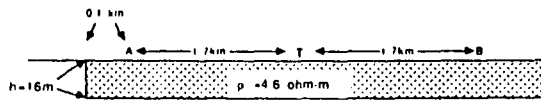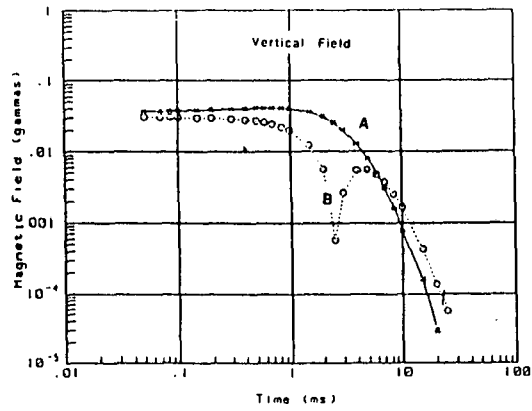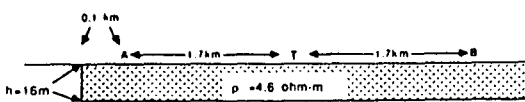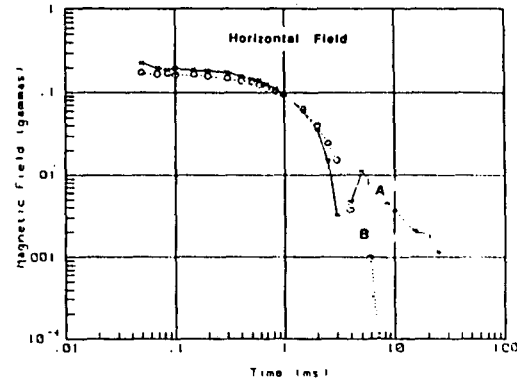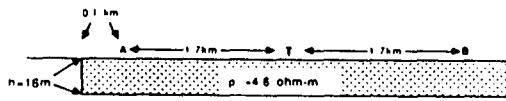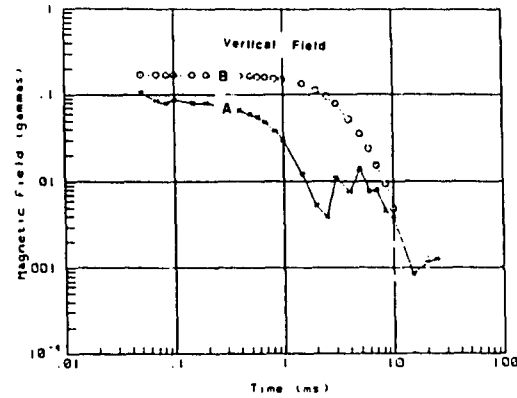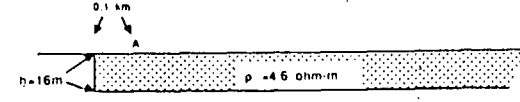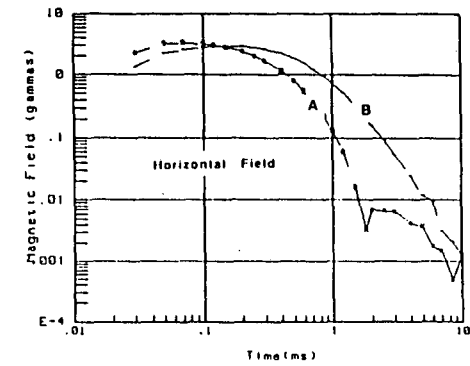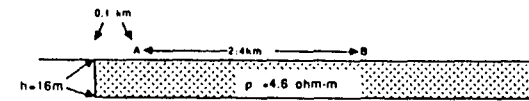
Fixed Loop   **Electrical Dipole**   **Central Loop**

Figure 3.18 Comparison of the vertical and horizontal field transients for the three systems for a station

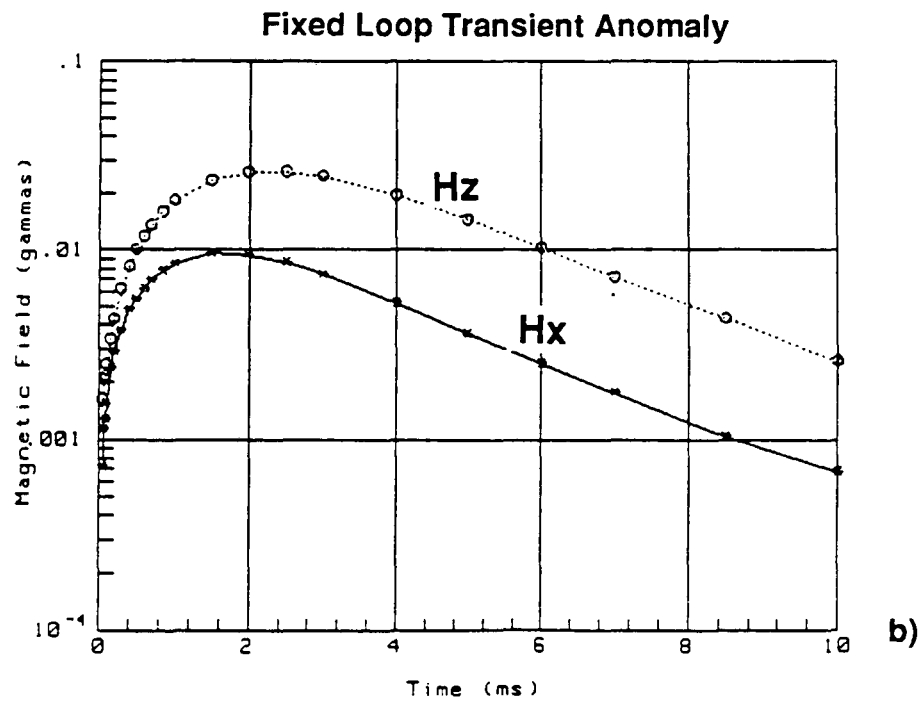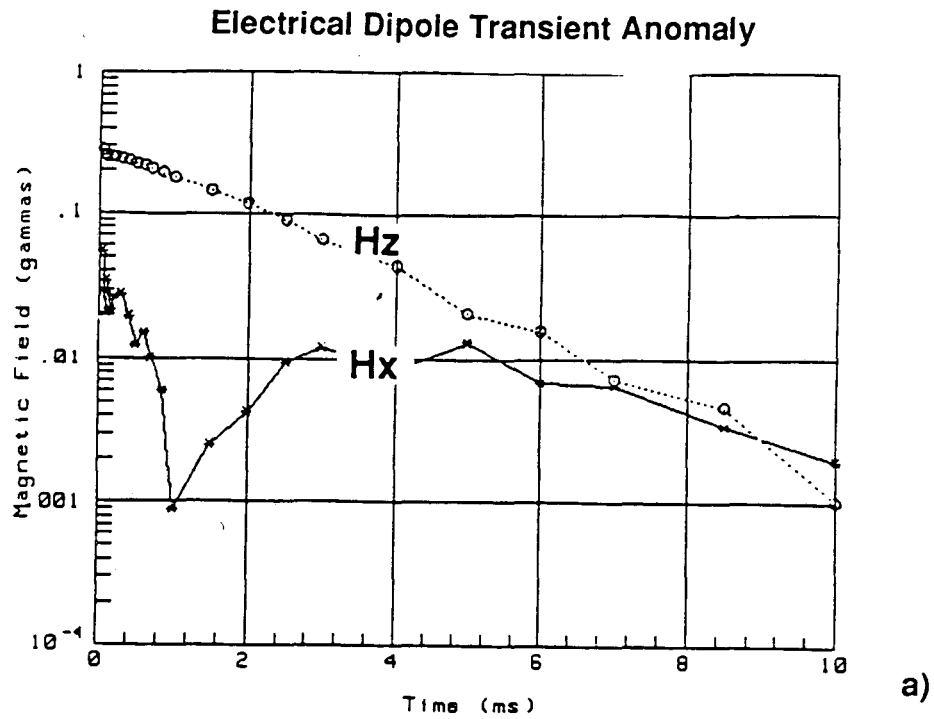100 m from the edge of a truncated sheet with those of a sheet of infinite extent.

Figure 3.19 Vertical and horizontal field anomaly transient for a station located 100m inwards from the edge of a truncated sheet for a) electrical dipole system and b) the fixed loop system.

$$\tau = \frac{\mu S \, |L+D|}{4}.$$

For stations located more than several hundred meters from the edge the dominant anomaly is the static shift discussed above. These data have similar decay characteristics to the infinite sheet transients but the observed fields are statically shifted throughout time. If a complete transient is obtained, however, it is often possible to interpret field data shifted in such a manner simply by adjusting the curve so that the early-time asymptote matches its expected free-space value and the late-time asymptote is zero (Newman, 1989). This data can then be fit to a one-dimensional model, often with good results.

For the central-loop system the vertical field transient near the edge decays noticeably faster than the transient at the center of the sheet (Figure 3.18). Both fields decay monotonically to zero but they are equal in magnitude only at early time.

The horizontal field transients for the three systems show less of an edge effect than was apparent with the vertical field data. For the fixed-loop system the horizontal field transient for the station nearest the edge is slightly larger but almost parallel with the transient for the station located near the center of the sheet. At early times the electrical dipole system transients are slightly larger in amplitude for the station near the contact as compared to the station over the continuous part of the sheet (Figure 3.18b). At 3 ms the transient near the contact crosses zero while the the one over the continuous part of the sheet decays monotonically to zero.

The horizontal field transient for the central-loop system (curve A) is shown with the vertical field contact anomaly (curve B) in Figure 3.18b. Both curves build up to a peak, at intermediate time, and then rapidly decay at intermediate to late time. The vertical field anomaly transient forms a peak slightly later in time and has a flatter late-time slope. The nature of these transients is examined further in Chapter 4.

In summary, the anomalies observed over a truncated sheet depend on the configuration, the source and receiver positions and the conductance of the sheet. With the electrical dipole system a large contact anomaly is observed beginning at the earliest times and persisting through late-time. This anomaly has a galvanic component that results in significant static field level shifts even for stations far removed from the edge, and an inductive component which alters the decay characteristics only for

stations nearest the edge. The anomalous field at the contact decays exponentially. For the fixed-loop system the contact anomaly develops with time in proportion to the distance from the source to the edge and the conductance of the sheet.

Although the magnitude and temporal characteristics of the contact anomaly differ for the electrical dipole and fixed-loop systems, the shape and wavelengths of the contact anomalies for the two systems are similar. This suggests that the contact anomaly develops mainly as a current channeling effect. With the electrical dipole system current is impressed into the medium, so there is therefore a contact anomaly even before the current is shut-off. For the fixed-loop system the contact anomaly is associated with the propagation of currents from the source to the edge, so the anomaly is only present during those times when the induced current is flowing near the edge. The contact effect is weaker with the fixed-loop system because the currents are attenuated by the medium as they propagate. Note that the contact anomaly for both systems appear similar even though the induced current in homogeneous models for these systems is quite different (Gunderson et al. 1986). This suggests that the anomaly is governed in large part by the configuration of the contact with respect to the source.

The vertical field contact effect for the central-loop system is a smooth level adjustment between the fields on either side of the edge. The adjustment distance gets progressively longer with time and a small positive anomaly develops near the contact, but the edge effect for this system is the simplest of those examined. The horizontal component at the center of a loop transmitter is a purely anomalous field, that is, it exists only near inhomogeneities. For the truncated sheet the early-time horizontal fields form sharply peaked profiles with the peaks located close to the edge; at later times the profiles are lower and broader with peaks centered further from the edge.

3.3 The Quarter-Space

The quarter-space model was prepared using a 5-cm-thick slab of aluminum located in an air host. At a scale of 1 to 10,000, the slab has a resistivity of 4.0 ohm-m. This model is somewhat problematic because the induced currents move slowly due to its high conductivity, so at large transmitter-receiver separations the transient does not develop until late in time. For a 4.0 ohm-meter homogeneous half-space, for example, the induced current from a magnetic dipole source requires approximately 50

ms to travel the 1.8 km from the source to the edge (Hohmann and Ward, 1988). With the existing instrumentation, however, we cannot recover the complete transient for long-offset soundings because of the weak signal. It is not feasible to assemble quarter-space models from less conductive materials, such as brass or lead, due to the increased thickness required and the accompanying increase in weight. A quarter-space of lead, for example, would be a slab more than 25 cm thick weighing more than two tons! To alleviate this problem we decided to use two source positions, one at 1.8 km from the edge, so that the quarter-space and truncated sheet results can be compared, and one closer to the edge so that we can examine the more fully developed transients.

The vertical field profiles for the fixed-loop system show significant transient character only for stations close to the source (Figure 3.20a). For lag times from 0.1 to 10.0 ms, and source-receiver separations greater than 500 m, the profiles collapse into one. This is due to the extremely slow propagation of the induced current in the quarter-space; at these lag times most of the current remains close to the loop so the field at distant points most closely resembles the primary field. The vertical field anomaly (Figure 3.20b) is very small at early times and it is broader than the anomaly observed over the truncated sheet. The anomaly steadily increases in magnitude until the latest measured times (10 ms) when it is about 20 percent of the primary field. Although this is far smaller than the maximum anomaly for the truncated sheet, note that by 10 ms the bulk of the current induced in the quarter-space is still concentrated near the source.

The vertical fields for electrical dipole system over the quarter-space have a strong contact anomaly that is present throughout time. As with the truncated sheet this anomaly is due to the accumulation of galvanic charges near the contact. The fields change polarity about 150 m inwards from the contact and remain at this reversed polarity over the edge. As with the fixed-loop system, there is little transient character to the fields except for stations near the source. The anomaly profiles (Figure 3.20b) show that the edge effect is much broader for this model than for the truncated sheet. The anomaly is centered 300 m from the contact, on the resistive side, rather than at the edge.

The anomalies over the quarter-space are broader than those over the truncated sheet because the induced (and galvanic) charges and currents are present at depth as well as at the surface. In fact, the
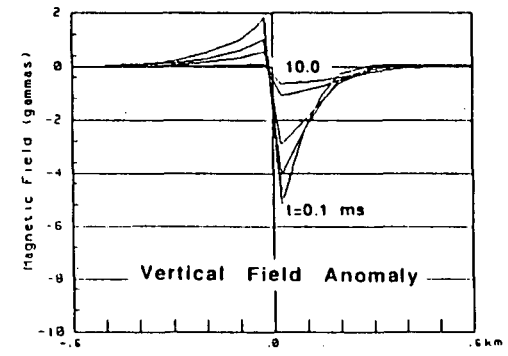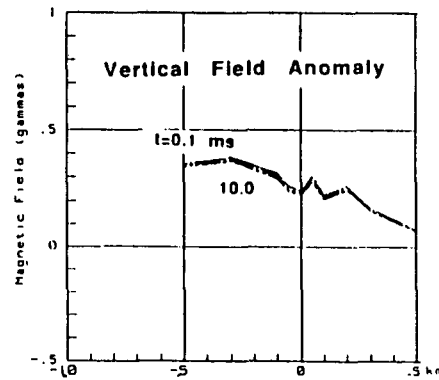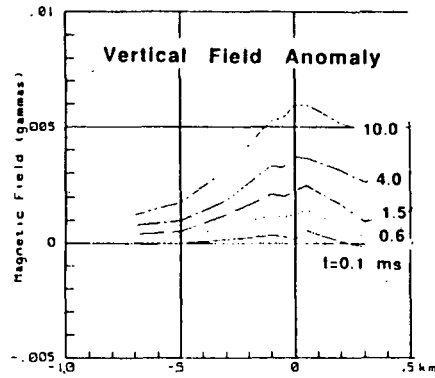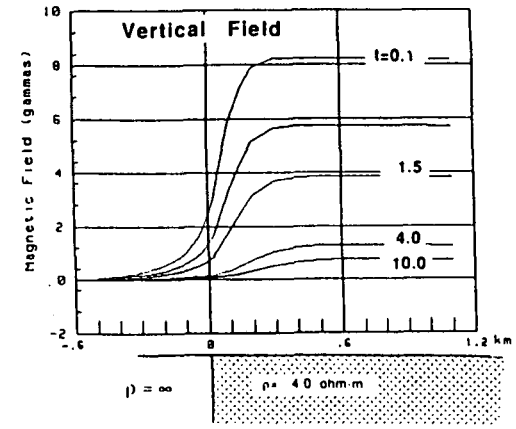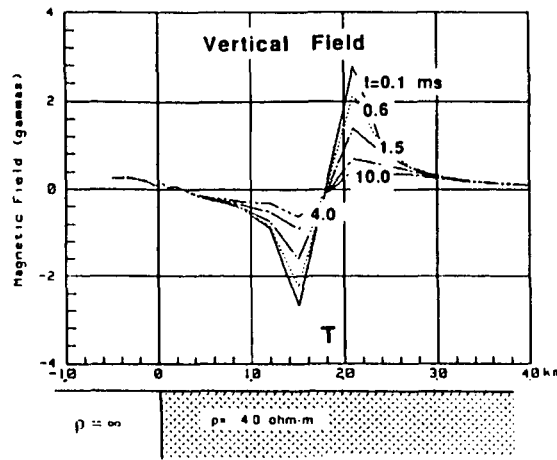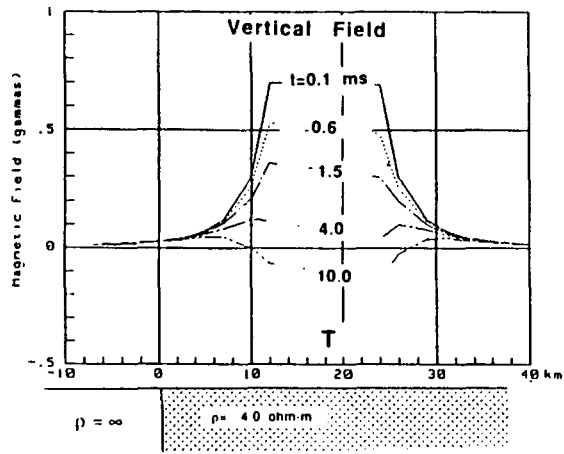
Figure 3.20 a) A plot of the vertical magnetic field over a quarter-space for the fixed-loop, electrical dipole and central-loop configurations. b) A plot of the vertical field anomaly over the contact, where the anomaly is defined as the difference between the fields on either side of the transmitter.

induced current for a dipole in a homogeneous half-space propagates at an angle of approximately 22 degrees from the horizontal (Nabighian,1979). Galvanic charges for a quarter-space model are also distributed along the contact at depth; the resulting greater separation of the charges from the measurement points causes the increased anomaly wavelength.

For the central-loop system the vertical field profiles over the quarter-space are similar to the truncated sheet results. The contact effect is a smooth adjustment between the fields on either side of the edge. Over the quarter-space, however, the fields decay slower and and the contact effect is more abrupt on the conductive side but more drawn out on the resistive side. Moreover the data do not show the development of the small positive anomaly over the contact as was observed for the truncated sheet.

The horizontal field profiles for the fixed-loop system show more transient behavior near the contact than the vertical fields do (Figure 3.21). The crossover anomaly is similar in character to the truncated sheet results but broader and lower in amplitude. For the electrical dipole system the horizontal field anomaly is a crossover of very low amplitude but of similar wavelength to the fixed-loop results. The horizontal field for the central-loop system appears similar to the truncated sheet data although the anomaly is sharper and the fields are of a single polarity.

3.3.1 Transient Fields over a Quarter-Space

Transient measurements were made for fixed-loop and electrical dipole transmitters located 1 km from the edge (Figure 3.22). As before, the receivers are located 100 m from the edge and at equal source-receiver separations over the infinite portion of the model.

For the fixed-loop system the two vertical sounding curves coincide at early time but they separate at intermediate time, with the transient near the edge decaying more slowly. The vertical field transients for the electrical dipole system are not very well developed; the curves just begin to decay at 10 ms. The transient curve near the edge has been statically shifted with respect to the homogeneous model. Although this curve has the expected polarity the amplitude is less than half of the equivalent half-space curve. For the central-loop system the transient near the edge is considerably smaller than the homogeneous curve throughout time.
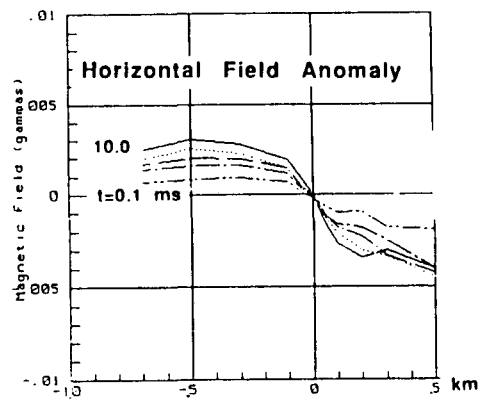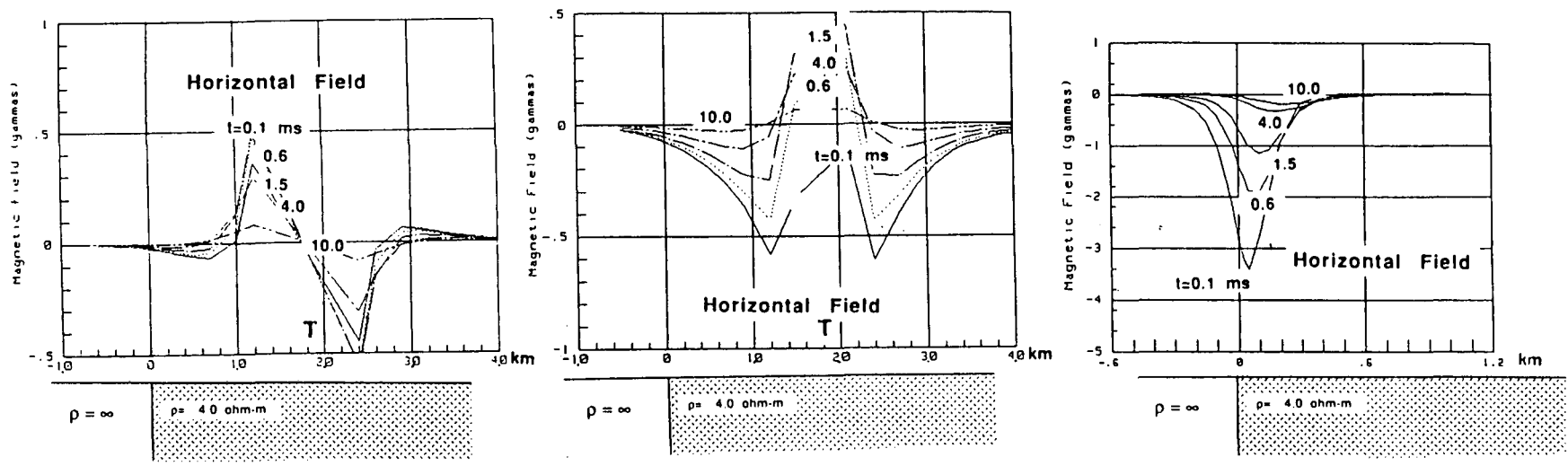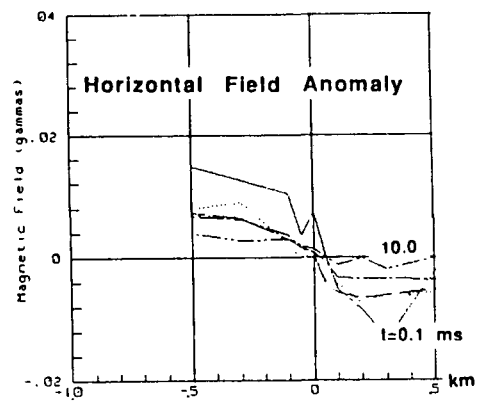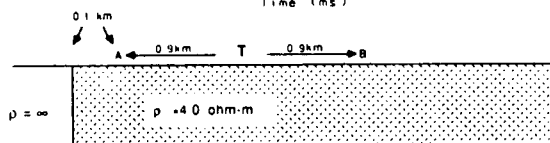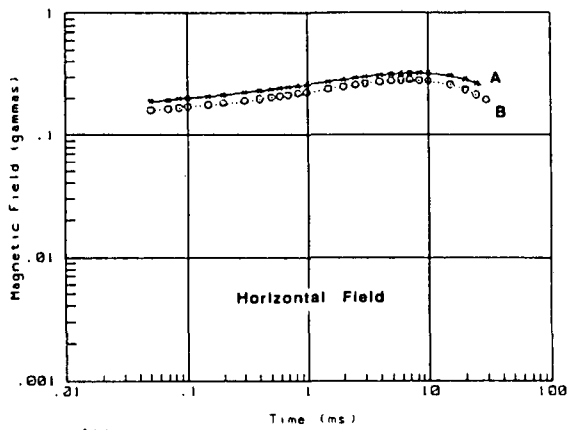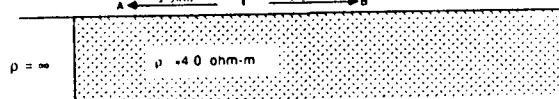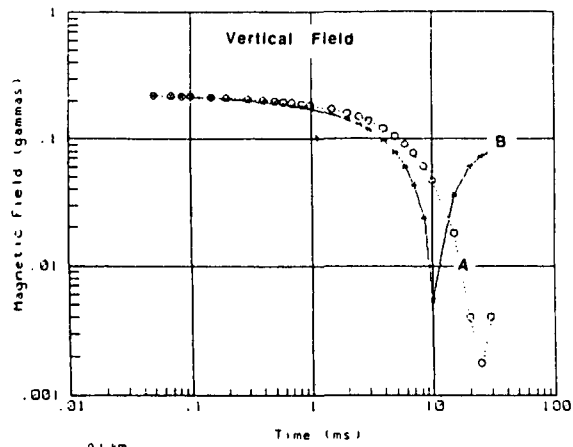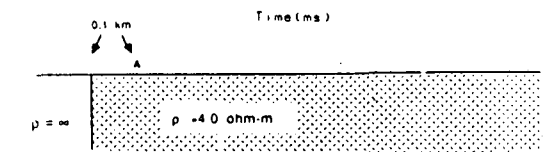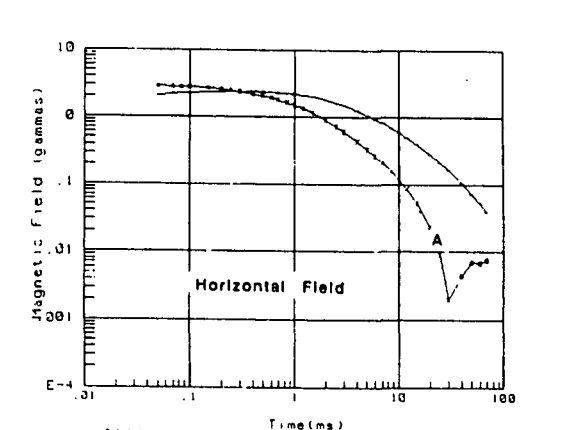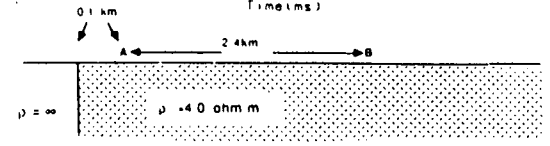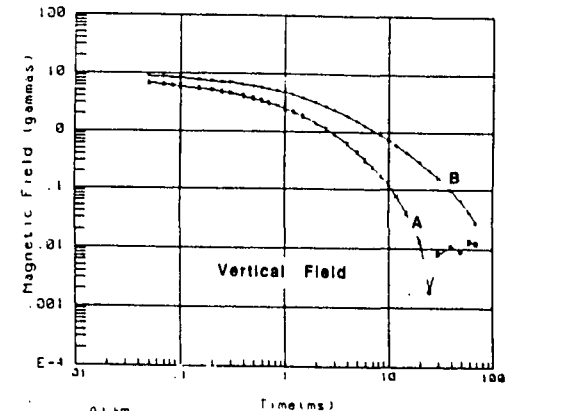
Figure 3.21 a) A plot of the horizontal fields over a quarter-space for the fixed-loop, electrical dipole and central-loop configurations. b) A plot of the horizontal field anomaly over the contact.
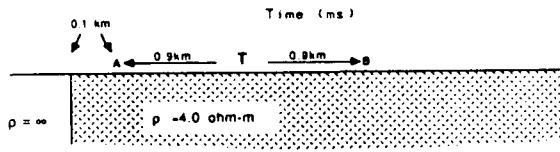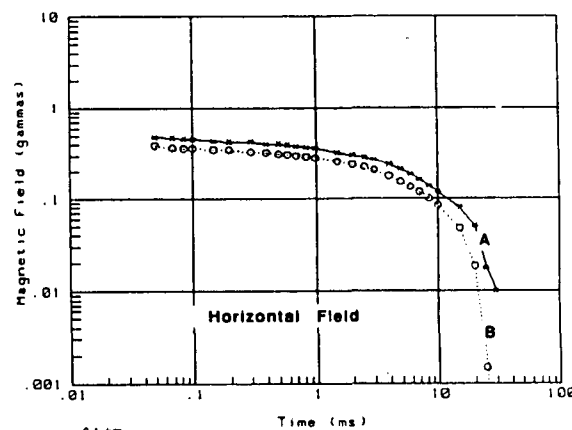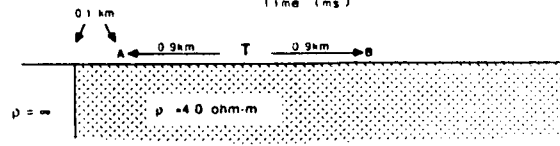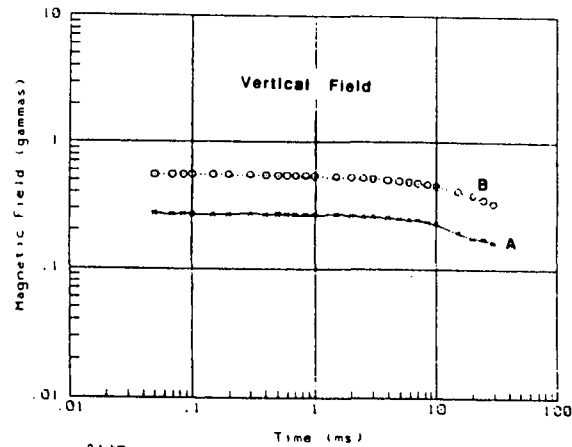
Figure 3.22 a) Vertical and b) horizontal field transients for a sounding 100 in meters from the edge of a quarter-space. The transmitter is located 1km from the edge.

The two horizontal field transient plots for the fixed-loop system are almost parallel throughout time with the curve near the edge consistently larger; both curves form a broad peak at about 10 ms. For the electrical dipole system the horizontal field transients decay faster than the vertical fields do. The two transients shown in Figure 3.22b are again sub-parallel except at the latest observation times. The central-loop horizontal field transient is a smooth curve that does not form a sharp peak which is in contrast to the field behavior over the truncated sheet.

The transient anomalies for the three systems over the quarter-space are similar to the truncated sheet results. The fixed-loop contact anomaly develops as the induced current propagates from the source to the edge. For the quarter-space this is much later in time than the truncated sheet and the anomaly is broader, although the shape and character of the anomaly are similar. The electrical dipole results for both models show a clear galvanic effect that shifts the field levels throughout time. The transient for this system over this model does not develop until very late in time, so complete transient behavior for the quarter-space model is unknown. For the central-loop system the contact effect over the quarter-space model is still basically a field level adjustment between the background fields across the contact. The adjustment distance is considerably shorter with the quarter-space model and the transition is smoother.

The quarter-space anomalies are generally much broader than the truncated sheet results and occur later in time. The charges and currents are now disseminated along the contact with depth as well as on the surface, leading to greater separation of anomalous currents and charges from the measurement points, which results is broader anomalies. The contact anomaly occurs later in time due to the progressive slowing of the current pulse with time. As this pulse propagates it also broadens, and this also leads to a broad contact anomaly.

3.4 Finite Contrast Models

Although the contact effect is well defined for the infinite contrast two-dimensional models described above, it is not clear that the same description holds for a finite conductivity contrast across the edge. To examine this situation several truncated sheet models with finite conductivity contrasts were assembled and measurement were made. These results are compared to the air-host models.

Finite contrast models are simple in concept but difficult to construct. Apart from the difficulty in finding materials that make a welded contact (see Chapter 2), several other factors must be considered. First, the materials across the contact must be similar in conductivity. Too great a conductivity contrast across the contact generates results that closely resemble air-host models so that the difference due to the finite contrast is not easily determined (Spies, 1981; Wilt et al. 1986). The material must also be sufficiently conductive so that a response can be measured over a broad range of time with the existing scale model system. This eliminates the use of lower conductivity host materials such as salt water.

A lead/mercury model is an ideal choice for its conductivity contrast (about 4 to 1) and for the bonding properties of mercury which are useful in making a welded contact. The weight of these materials and the relatively low conductivity (compared to the aluminum models thus far examined) make it impractical to study quarter-space models, but a truncated sheet is relatively easy to assemble.

For this test we used 0.60 cm sheet of lead in contact with an equal thickness of mercury. At a laboratory scale of 1 to 10,000 this corresponds to a 60 m thick layer with a resistivity of 25 ohm-m on one side of the contact and 100 ohm-m on the other. The response is compared to an identical model but with air as the host medium instead of mercury. The comparison is made for a fixed-loop system using a 400 m x 800 m source positioned 2.0 km from the edge. Central-loop finite contrast models are discussed in Chapter 4 where some of the techniques for contact interpretation are further developed.

Figure 3.23 shows vertical field and anomaly transients over the two models for a sounding 50 m inwards from the contact on the conductive side. In Figure 3.24 vertical field anomaly profiles over the two models are shown. The anomaly develops more slowly over the lead/mercury contact and reaches only 75 percent of its maximum value for the air host case. Note that the conductance contrast for the mercury host is 25 percent less than the air host model. The shape of the curves is similar, however, and at late-times their slopes are identical.

At early and intermediate times the contact anomaly over the mercury model is diminished because some of the induced current has crossed the contact into the less conducting medium. This is not possible in an air host. The shape for the two transients is virtually identical and can be fit, using
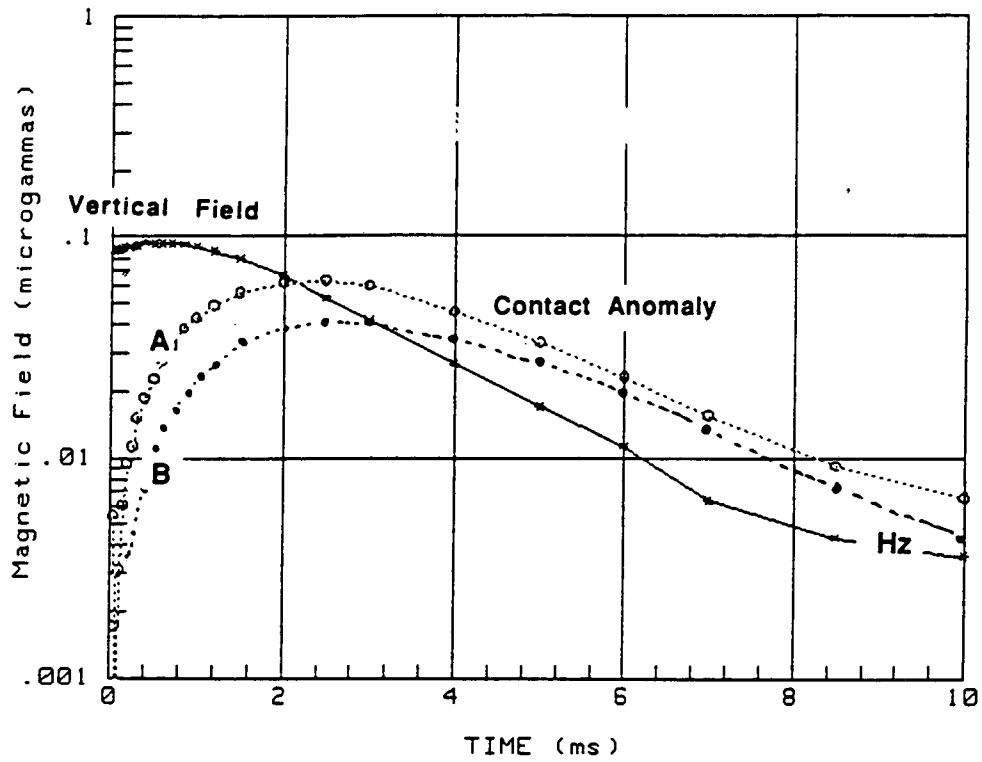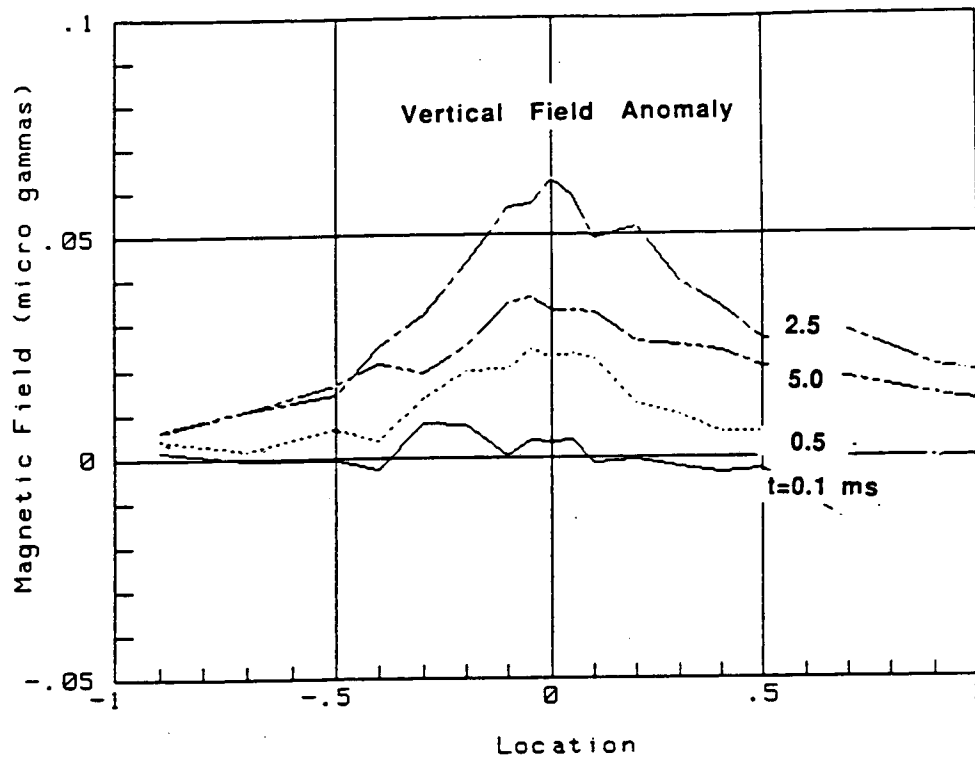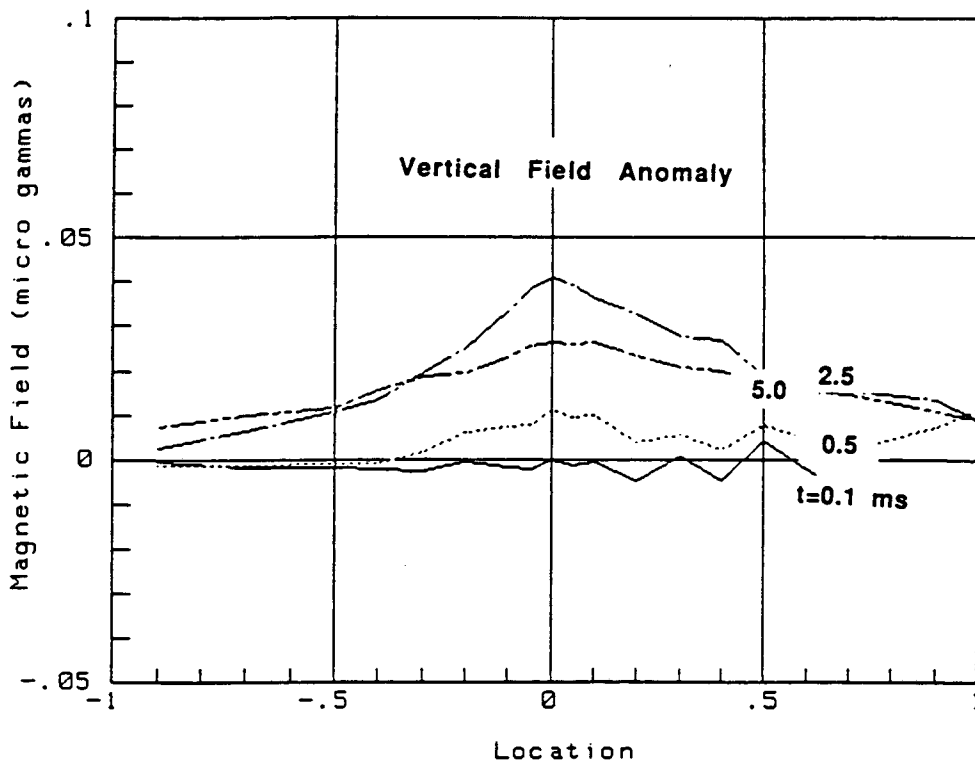
Figure 3.23 Vertical field and anomaly transients (Hz and curve A) for a station 50 m inwards from an

infinite contrast lead/air model and the anomaly transient (curve B) for an equivalent station over a

lead/mercury model.

Figure 3.24 a) Vertical field anomaly profiles for the air host truncated sheet model and b) the mercury host model.

Equation 3.18, to a model of a truncated sheet with a conductance of 2.4, which is equal to the conductance of the lead sheet. This means that in both cases the late-time data is sensing currents flowing in the lead, suggesting that these currents have propagated to the edge and have been scattered back towards the source.

3.5 Resolution of a Target Layer beneath a Truncated Contact

In the previous sections we showed that the contact effect for the three systems examined includes both galvanic and inductive components and is dependent on the transmitter and receiver positions and the conductance or conductivity contrast across the boundary. In spite of these complexities, it is clear that for the three systems considered the edge effect, as compared to the primary field strength, is greatest for the electrical dipole system and least for the central-loop configuration.

Of more concern when making sounding measurements, however, is the response of a deeper target layer as compared to the anomaly from a contact. The relative strengths of these signals will determine how effectively a deeper layer may be resolved if only a one-dimensional interpretation is made. It is therefore useful to determine the ratio of these two quantities, or the signal-to-geological noise ratio (SGNR).

An added complexity in determining the SGNR is the unknown interaction between currents induced in the deeper layer and those flowing at the surface. For deep targets this interaction is small and in general the two responses are additive. For shallower targets, however, there can be significant interaction between these currents and both responses are affected (Bartel and Becker, 1988). In general, we have found that when a target layer is present, the contact effect diminishes somewhat due to the increased current flow in the deeper layer.

For simplicity, let us assume that the two responses are additive. The SGNR is therefore defined as the target response beneath a continuous overburden layer divided by the edge effect with the deeper layer absent. As stated above this is a conservative estimate and generally will overestimate the anomaly for shallow target layers. It is a useful means, however, of comparing the relative contact and deeper layer responses for the three EM systems examined.

To determine the SGNR, we placed a 4.0 ohm-m 32 m thick (S=8.0) layer at a depth of 200 m beneath the surface contact model shown in Figure 3.1. The deep layer anomaly was measured by collecting field profiles over an infinite sheet with and without the deep layer and taking the difference between the readings.

The vertical and horizontal field deep layer and contact anomalies are plotted for the three configurations in Figure 3.25 for a sounding 100m from the edge. For the central-loop system only the vertical component is plotted since the horizontal field does not respond to a continuous deep layer.

The vertical field contact and deep layer anomaly transients for the fixed-loop system are both band-limited, that is, the maximum responses occur within a discrete time interval. As shown above, the maximum contact anomaly for this system occurs within a time window dependent on the position of the source and the conductivity of the medium; the same parameters also govern the time window of the deep layer response (Spies, 1989). For this model the peak response for both deep layer and contact anomalies occur at about 2 ms and are of about the same magnitude, although the contact anomaly is broader. For this case it would therefore not be possible to accurately determine the deep layer parameters without some form of contact removal.

For the electrical dipole system the deep layer anomaly is band-limited but the contact effect is not. The contact effect is greatest at early times and decays to small values by late time, when the deep layer response is significantly larger. The central-loop contact anomaly near the edge is initially much larger than the deep layer response but it also dies away quickly and by late time the deep layer response is larger.
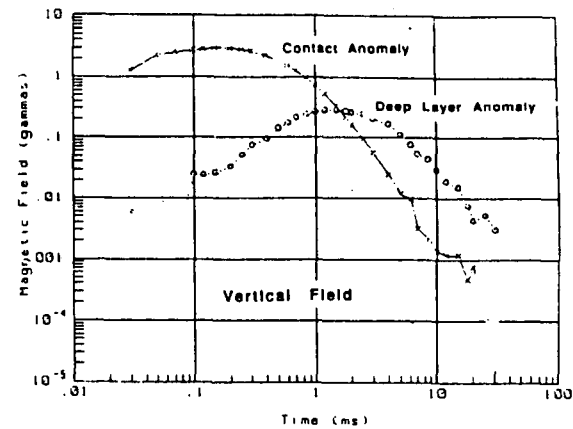
The maximum horizontal field contact and deep layer anomalies for the fixed-loop system occur during different times than the vertical field anomalies. The maximum contact response occurs earlier and the deep layer response is larger at later times. After 2.0 ms the deep layer response is considerably larger than the contact effect. For the electrical dipole system the horizontal component deep-layer response is larger throughout time than the contact effect. We showed, in Section 3.3, that the horizontal field contact anomaly for this system is small near the edge. This suggests that for this component a sounding near the edge would be a very effective means for obtaining the deep layer response.
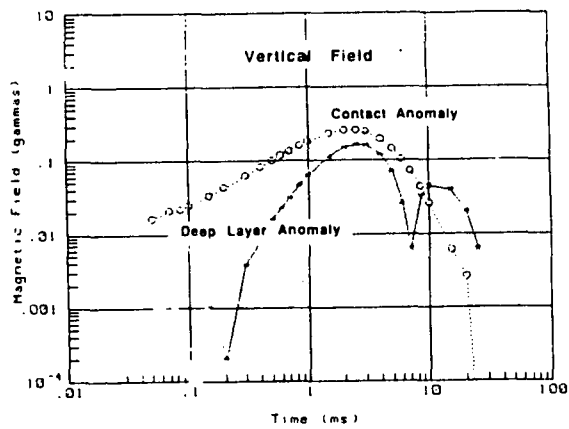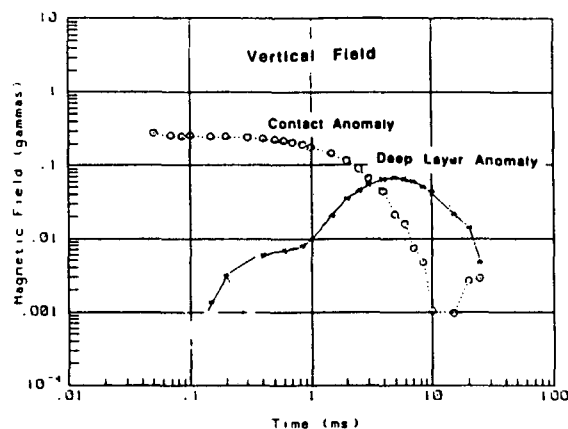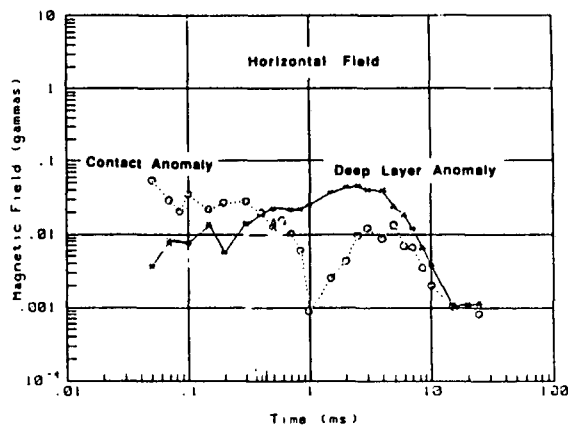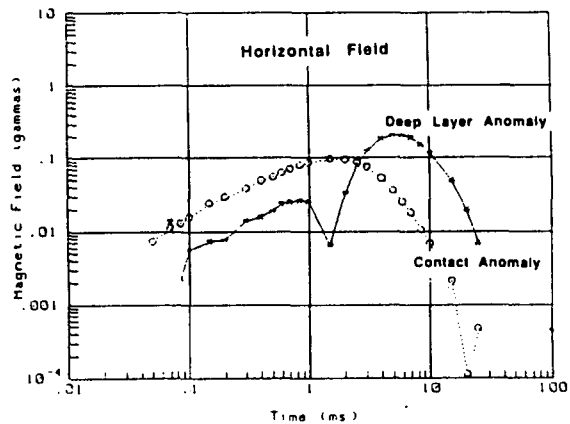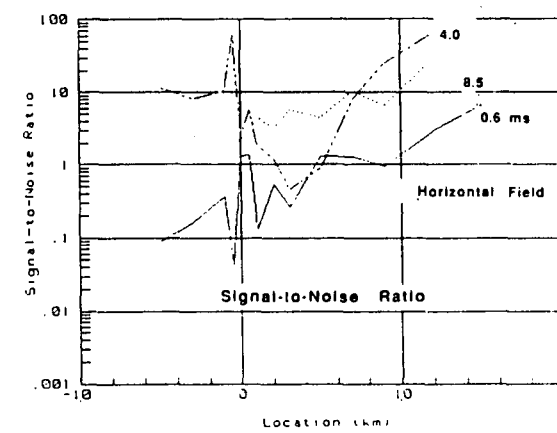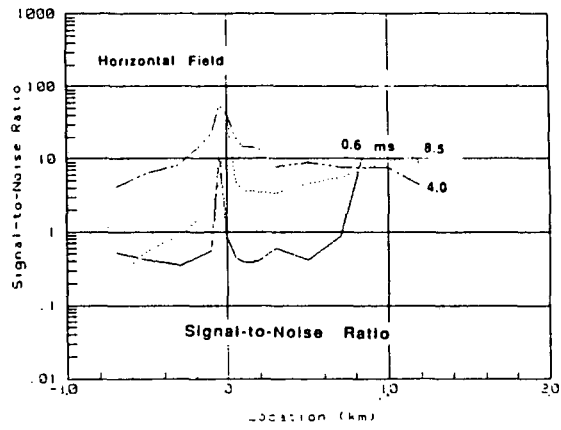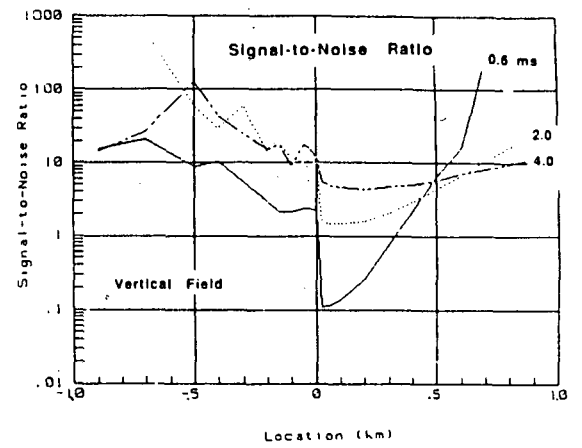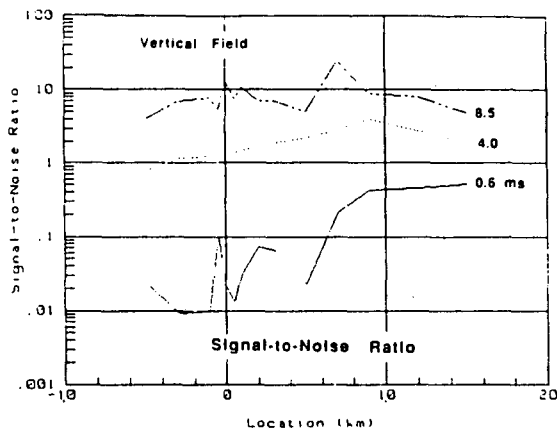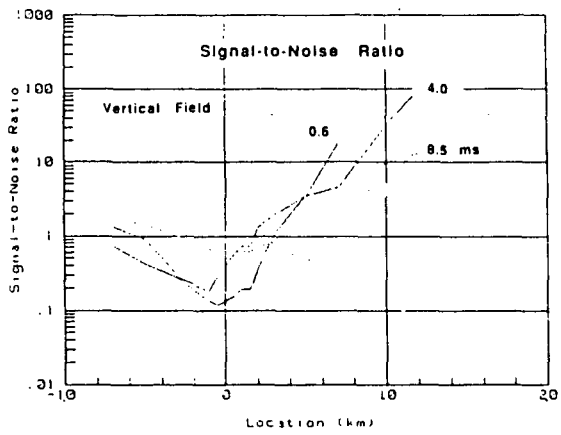
Figure 3.25 a) Vertical and b) horizontal field comparison of the contact anomaly transient and the deep layer anomaly for the three systems. The observation point is located 100 m inwards from the edge.

For this case the SNGR is the ratio of the two curves in Figure 3.25. This quantity is displayed in Figure 3.26 for each of the three systems at early time (0.6 ms), intermediate time (4.0 ms), and late time (8.5 ms). If we consider a SGNR of greater than 2 necessary to resolve the deeper target layer then we can define areas for each of the three systems where the deep layer response may be determined without removal of the contact anomaly.

The vertical field SGNR profiles for the fixed-loop system show that within 500 m of the contact it would not be possible to detect the deep layer without removing the effect of the contact. For the electrical dipole system the early-time vertical field SGNR is unfavorable within two kilometers of the edge but by late times the ratio is above 2 for all positions. For the central-loop system the ratio is unfavorable only in the region near the contact at early to intermediate times. The horizontal field SGNR for both the fixed-loop and electrical dipole systems show a region within 100m meters of either side of the contact where the ratio is favorable. This occurs because the horizontal field contact anomalies for these systems are small near the edge.

As compared to the deep layer response the contact effect for the electrical dipole system is larger than for the other systems studied. The SGNR for this system is small at early times and pervasive for all soundings within 2 km from the edge. It rapidly diminishes at later times, however, to below the deep layer response. The least affected system is the central-loop configuration where the effect is confined in the region near the edge. For the fixed-loop system the contact effect is intermediate between the two but the effect is broad and the maximum contact anomaly can occur during the time window desired for interpretation of the deeper layer.

When soundings are made near a geological contact it is clear that in some cases a one-dimensional inversion is not appropriate, but it is not always clear which soundings can be trusted. For a fixed-loop system we suggest that if the target parameters are approximately known, then it is possible to determine the source positions such that the contact effect during the time window of interest is minimal. Diagrams such as Figure 3.10 are useful in determining the most advantageous loop locations. If it is not possible to arbitrarily place loop sources then we suggest that near the contact the horizontal component be given more weight in layered model inversions.

Fixed Loop   **Electrical Dipole**   **Central Loop**

Figure 3.26 a) Vertical field and b) horizontal field Signal-to-geological-noise ratio (SGNR) for the

three systems. The ratio is defined as the deep layer response divided by the contact anomaly.

CHAPTER 4: INTERPRETATION OF CENTRAL-LOOP SOUNDINGS NEAR CONTACTS

In Chapter 3 we observed that of the three systems considered, the central-loop system produced the simplest contact anomaly. For the vertical field, the edge effect typically consists of a simple amplitude level adjustment across the contact. For the horizontal component, it is á bell-shaped anomaly centered near the edge on the conductive side. The edge effect is simple with this configuration because the measurement is made within each transmitter loop, so there is no dependence on source-receiver separation. In addition, for a homogeneous or layered earth, the field at the center of the loop transmitter is vertical. The development of a horizontal field component is therefore associated with inhomogeneous structure and analysis of this component may be diagnostic of the inhomogeneity.

In this chapter the central-loop contact response is examined in some detail for the truncated sheet and quarter-space models. The goal is to recognize a contact effect and either to include it in the interpretation or ro remove it from the data. In the first part of the chapter we examine the central-loop horizontal field over several simple models to obtain information about the contact. In the next part we describe how this information may be used to remove a contact anomaly from a data profile. The final section of this chapter concerns the horizontal gradient of the central-loop vertical field. This quantity is useful in interpreting central-loop data over contacts where horizontal fields are not available.

We consider three contact models (Figure 4.1): a surficial vertical contact where the conductivity and thickness of the conductive formation vary; a dipping quarter-space model where the contact dip angle ranges from 30 to 150 degrees and a vertical quarter-space covered with an overburden of variable thickness. The models, listed in Table 4.1, are constructed of sheets or blocks of metal whose conductivity was determined from manufacturers grade (where available) or from tables given in Spies (1980) and Frischknecht (1988).

Data were collected on the laboratory modeling system described in Chapter 2 using a scale factor of 10,000. Measurements were made within 250 m and 350 m loops using a current of 6 amps. For some of the models, observations were made at different heights above the surface. This was done to assess the effect of the system elevation on the data and when possible to extrapolate the results to

SURFICIAL CONTACT

p = ∞,100 ohm-m   h ρ=4-100 ohm-m

h=5-400m

$\rho=\infty$

a)

DIPPING CONTACT

h=250 m   φ=30-150   φ ρ=4.0 ohm-m

$\rho=\infty$

b)

CONTACT WITH OVERBURDEN

ρ= 4.0 ohm-m
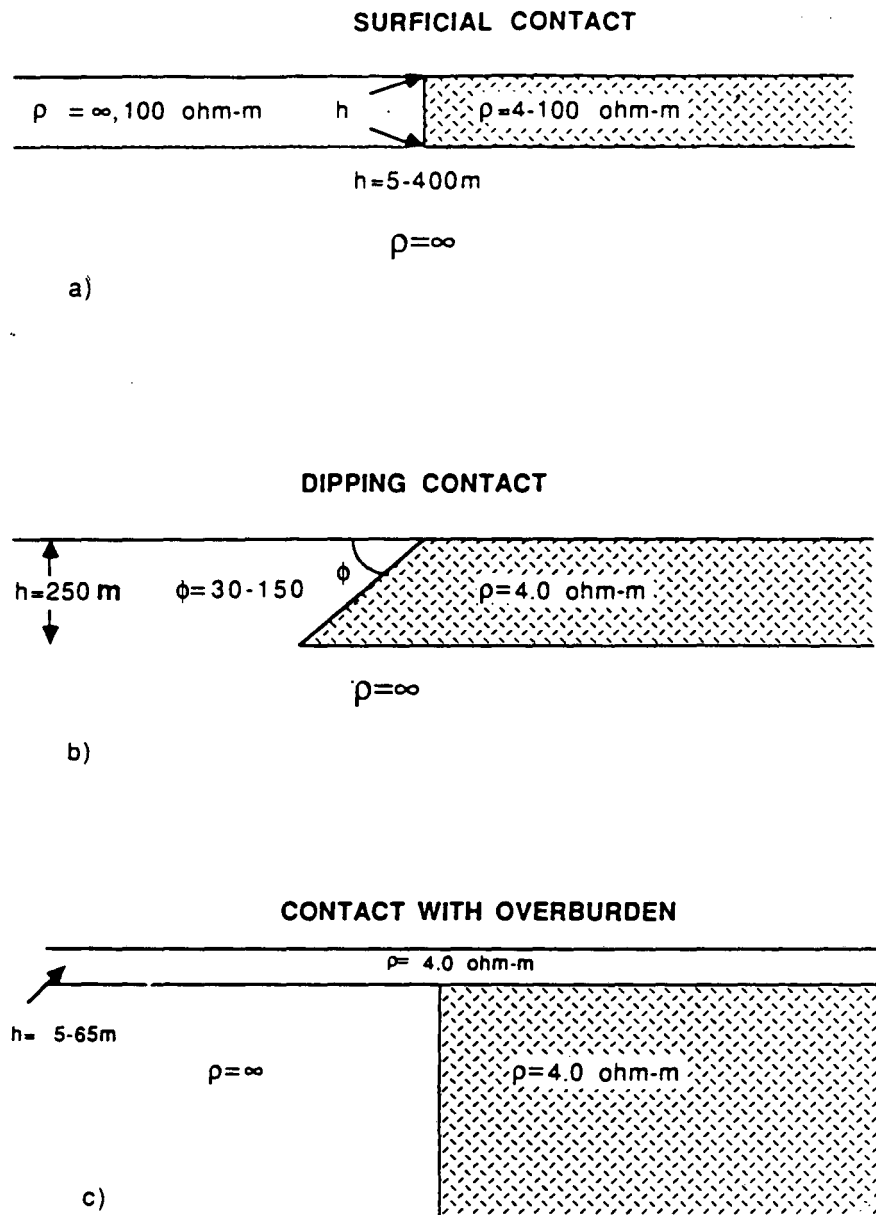
h= 5-65m

$\rho=\infty$ ρ=4.0 ohm-m

c)

Figure 4.1 Schematic representation of models used in this study.

the surface.

In Appendix 2 we list the vertical and horizontal field data and provide plots for a central-loop profile over a truncated sheet. These data may be of use when applying the interpretation techniques described later in this chapter.

4.1 Horizontal Fields near the Contact

As described earlier, for a homogeneous or layered medium, a step change in transmitter current from a loop source induces eddy currents that are azimuthally symmetric with respect to the source; the magnetic field at the center of the loop is vertical. Near geological inhomogeneities, however, the current pattern is distorted and the secondary field at the center of the loop now develops a horizontal component. For a two-dimensional inhomogeneity, the horizontal field is directed towards the structure and its time and spatial characteristics are related to the conductivity and geometry.

In Figures 4.2 and 4.3 we plot horizontal field decay curves and time profiles for model D (Table 4.1). The transient data are plotted on a semi-logarithmic scale; soundings are made at distances of 150, 300, and 500 meters from the contact on the conductive side. The profiles are given for observation times from 0.07 ms to 2.5 ms after current shut-off. Both sets of data are given as a percentage of the primary (vertical) magnetic field before current shut-off. (This normalization will be used, as necessary, throughout this chapter).

For stations close to the edge both profile and transient curves are sharply peaked early in time and have steep slopes; stations further from the contact peak later in time and have gentler slopes. The shape of the curves and the position of the peaks is related to the propagation of the induced currents in the medium. We suggested in Chapter 3 that the anomalous currents, responsible for the horizontal component, have propagated to the edge and have been reflected back towards the source. For stations near the edge the peak current should therefore occur early in time and the anomaly should have a high amplitude and be sharply peaked. For sources farther from the edge the anomaly is lower in amplitude and broader due to geometrical spreading, and attenuation and dispersion by the medium.

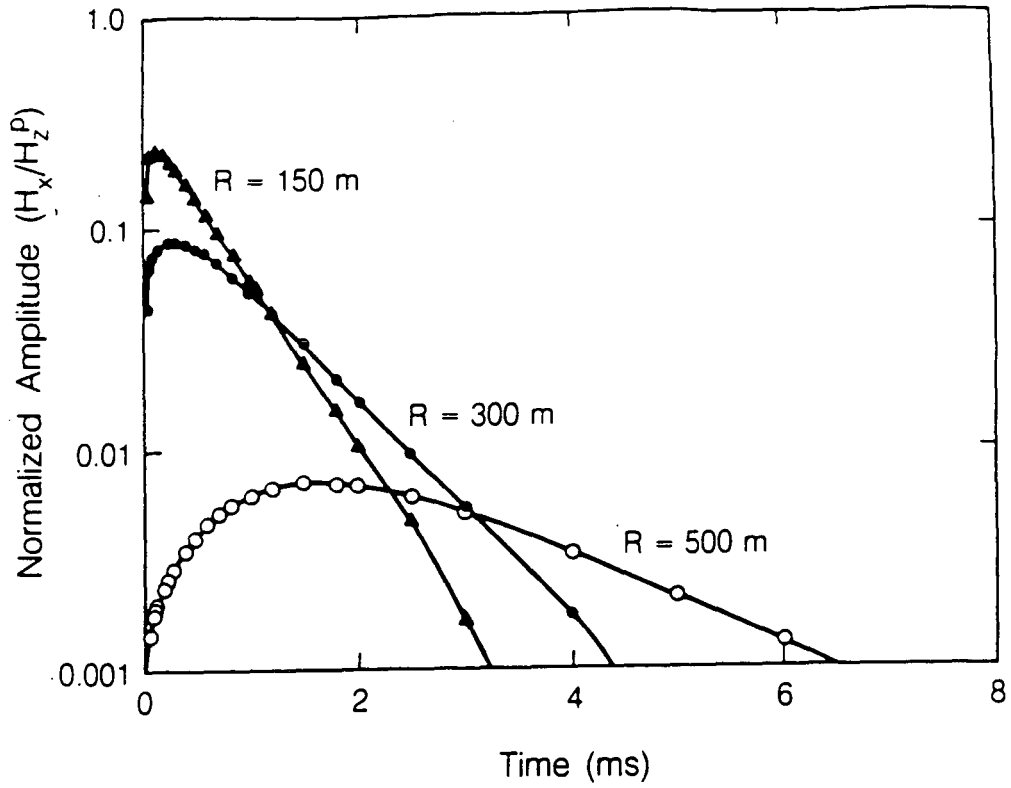We will show that the position and amplitude of the peaks and the late-time slope of the

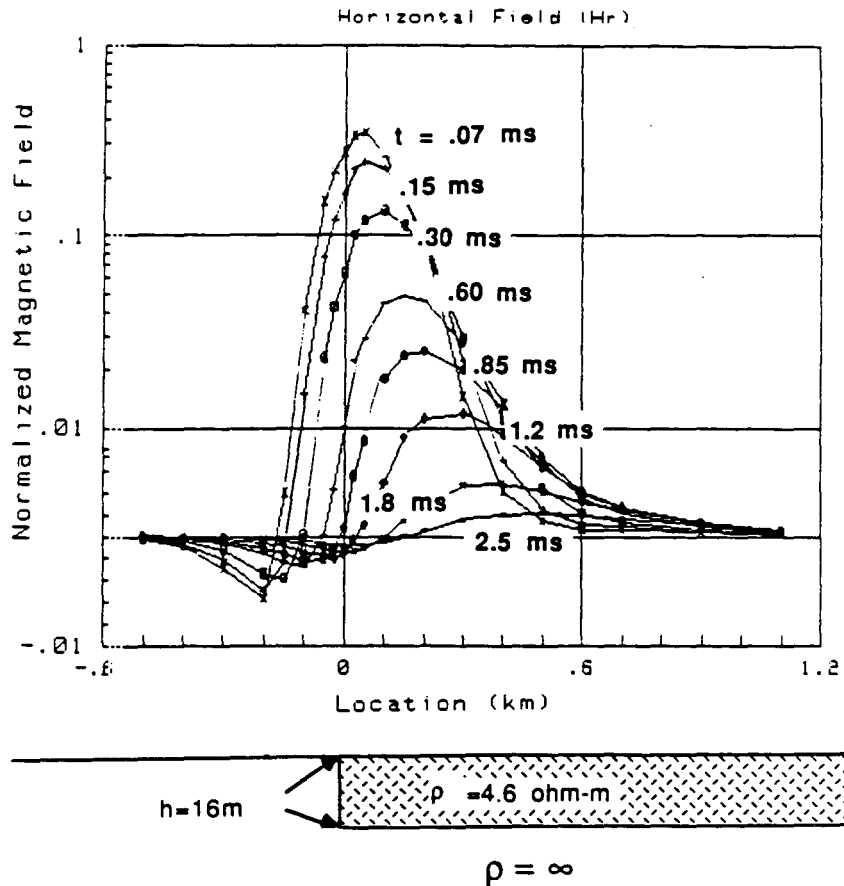Figure 4.2 Horizontal field transients 150, 300, and 500m from the edge of a truncated thin-sheet.

Figure 4.3 Central-loop horizontal magnetic field time profiles over a truncated sheet.

transients may be be used to determine the conductance (or conductivity) of the truncated layer, its dip and the distance from the source to the edge.

Table 4.1
Models Used in Contact Study

Surface Contact Models

Model	Material	Conductivity (S/m)	Thickness(m)	Conductance (S)
A	Lead	0.045	8.0	0.36
B	Lead	0.045	16.0	0.72
C	Aluminum	0.24	5.0	1.20
D	Aluminum	0.22	16.0	3.52
E	Brass	0.15	32.5	4.875
F	Brass	0.15	65.0	9.75
G	Aluminum	0.24	32.5	7.8
H	Aluminum	0.24	65.0	15.6
I	Aluminum	0.24	100.0	24.0
J	Aluminum	0.24	150.0	36.0
K	Aluminum	0.24	450.0	108.0
L	Copper	0.45	400.0	180.0

Finite Contrast Models:

Pb/Hg16	Lead/Mercury	0.045/0.01	16.0	0.72/0.16
Pb/Hg60	Lead/Mercury	0.045/0.01	60.0	2.70/0.60

Dipping Contacts:

Con30 (ϕ =30)	Aluminum	0.24	250.0	60.0
Con45 (ϕ =45)	Aluminum	0.24	250.0	60.0
Con60 (ϕ =60)	Aluminum	0.24	250.0	60.0
Con90 (ϕ =90)	Aluminum	0.24	250.0	60.0
Con120 (ϕ =120)	Aluminum	0.24	250.0	60.0
Con135 (ϕ =135)	Aluminum	0.24	250.0	60.0
Con150 (ϕ =150)	Aluminum	0.24	250.0	60.0

Contacts with Overburden:	ovbn/contact			
Ovbn5 (h=5m)	Alum/Alum	0.24/0.24	5.0	1.20
Ovbn16 (h=16m)	Alum/Alum	0.22/0.24	16.0	3.52
Ovbn32 (h=32.5m)	Alum/Alum	0.24/0.24	32.5	7.8
Ovbn65 (h=65m)	Alum/Alum	0.24/0.24	65.0	15.6

4.1.1 The Thin-Sheet Approximation

The analysis of the horizontal fields near a surficial contact simplifies considerably if the model can be approximated by a truncated thin-sheet. By definition, a thin-sheet is an infinitely thin layer with a finite conductivity-thickness product. The magnetic fields over many tabular bodies closely resemble the fields for a thin-sheet when the current density is approximately uniform across the thickness of the sheet. Similarly, a truncated thin-sheet may approximate a truncated layer when the induced current is uniform across the thickness of the layer. This occurs at later times, when the current has traveled some distance from the source.

To determine if the surface contact models considered qualify for the thin-sheet approximation we collected scale model data over a number of models listed in Table 4.1 using transmitter loops of 250 m and 350 m. The observed transients are then plotted against a normalized time given by,

$$t_{norm} = \frac{t}{\mu_0 Sa} \qquad (4.1)$$

where t is the time after current shut-off in seconds, μ_0 is the free-space magnetic permeability in H/m, S is the conductance of the layer in Siemens and a is the loop radius in meters (Figure 4.4). We plot these normalized transients for a station 300 m from the edge, on the conductive side. For these models, the decay curves merge at times when the thin-sheet approximation is valid. The figure indicates that for most of the models considered, the thin-sheet approximation is valid for normalized times $t_{norm} > 0.5$. Note that for the quarter-space (model K) the thin-sheet approximation may not be used.

This approximation differs somewhat from others cited in the literature. Dallal (1985), using similar methods and instrumentation, found that $t_{norm} > 2.0$ was a necessary condition for his truncated layer results to be equivalent to truncated thin-sheets. When only the vertical component is considered, the thin-sheet approximation is valid much later in time. Kamenetskii (1976) showed that over a homogeneous layer the thin-sheet approximation is valid for $t_{norm} > 7.0$. Spies (1981) showed that in addition to this condition it is also necessary for $a \gg d$, where a is the source loop radius and d is the depth of burial.

For the present study the reduction of the truncated surface layer models to truncated thin-sheets
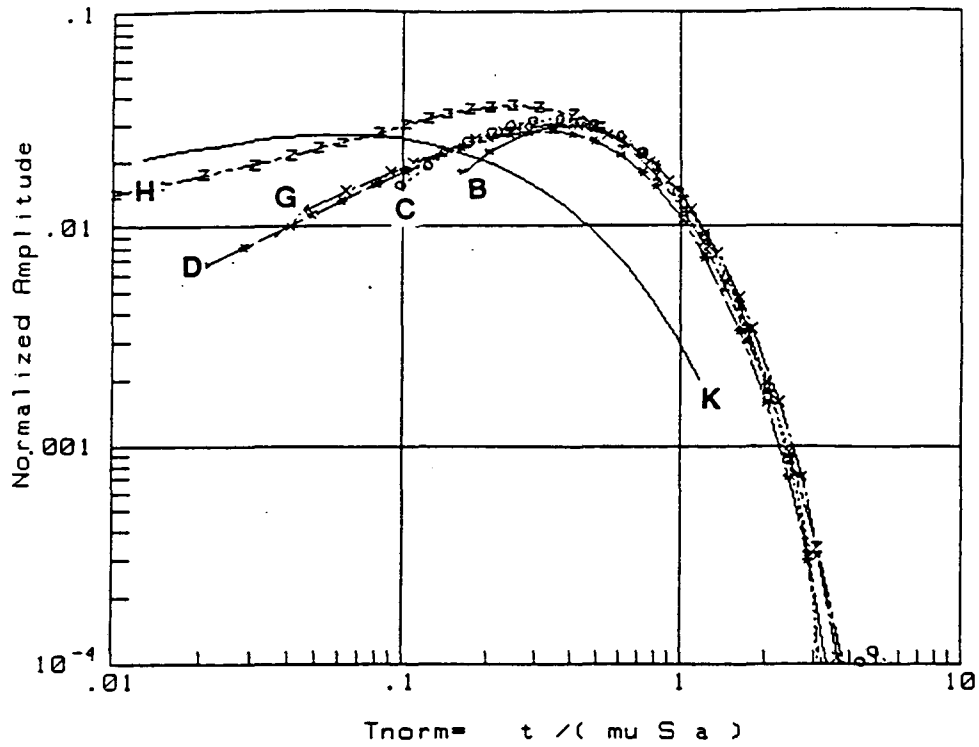
Figure 4.4 Normalized horizontal field decay curves for a sounding 300m from the edge. Plots are for models listed in Table 4.1.
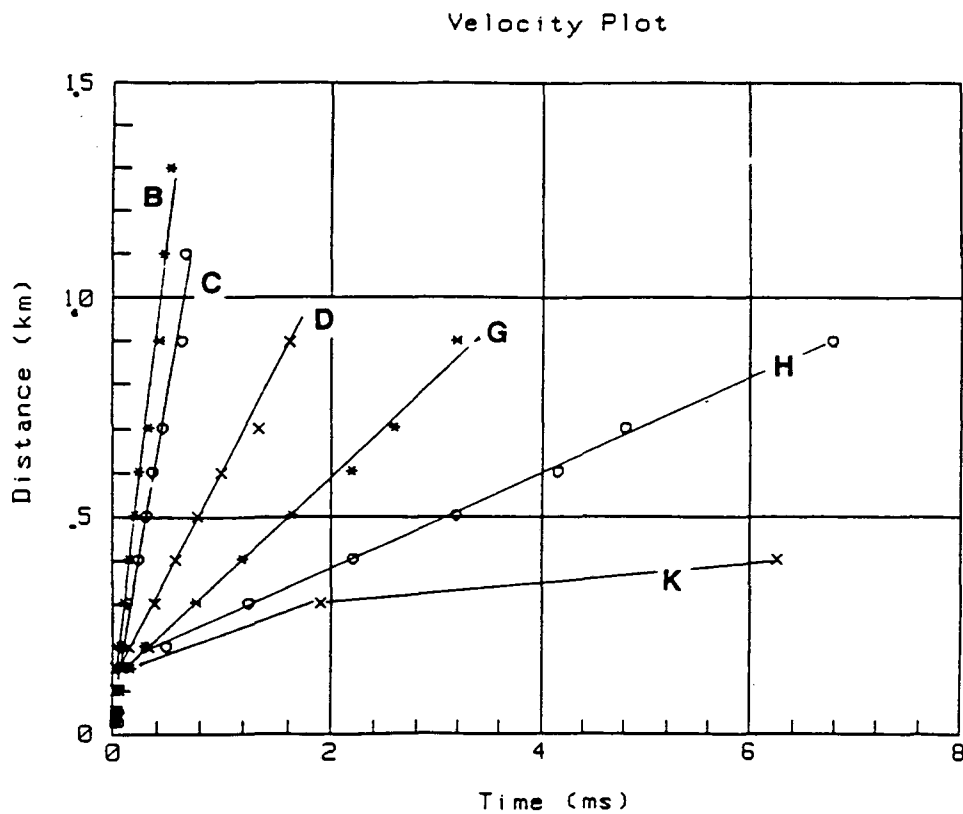

Figure 4.5 Horizontal field transient peak velocity for the models (A-K) shown in Table 4.1.

means that we have reduced the unknown parameters to two, the sheet conductance and the distance from the source to the edge. This step simplifies the analysis considerably.

4.1.2 Horizontal Field Transient Parameters

The conductance of a truncated sheet and distance to the edge may be determined from the characteristics of the central-loop horizontal field transient. For example in Figure 4.5 we plot the position of the horizontal field transient peak against time for several of the surface layer contact models shown in Table 4.1. Except for model K (the quarter-space), the curves are linear at later times with slopes inversely proportional to the conductance of the sheet. The slopes of these curves define the velocity of the horizontal field temporal peak. We have empirically found this velocity to be given by,

$$V = \frac{2}{\mu_0 S}.$$ (4.2)

Note that this is one half the expansion velocity of the induced ring current in an infinite thin-sheet.

In Chapter 3 we noted that the maximum contact anomaly from a fixed-loop source occurs near the edge at a time given by $t_{max} = \frac{\mu_0 SR}{4}$; this is the time required in an infinite sheet for the current to propagate from the source to the edge. Equation 4.2 suggests that it requires twice this long for the horizontal field at the center of the loop to develop a peak. This means that the temporal peak may be related to induced currents that propagate to the edge and have been reflected back. Equivalently, consider an image loop located at an equal distance from the edge but on the opposite side from the true source. Such an image would also generate horizontal fields in the source loop during these times.

Using the transient peak velocities as determined from any two field soundings, we can estimate the conductance of the surficial contact models from Equation 4.2. A comparison with the true conductance of the layers is given in Table 4.2; the calculated values for all but the thickest models agree to within a few percent of the true value. Note that for stations close to the edge the peak occurs at early time when the thin-sheet approximation is invalid. Near the edge the horizontal field peaks initially travel faster before approaching a constant velocity further from the edge.

Table 4.2
Comparison of Calculated and True Conductance and Conductivity

Model	Conductance	Conductance [eq. (4.2)]	Conductivity	Conductivity [eq.(4.6)]
A	0.36	0.32	-	-
B	0.72	0.75	-	-
C	1.2	1.16	-	-
D	3.52	3.5	-	-
E	4.875	4.4	-	-
F	9.75	9.6	-	-
G	7.8	8.0	-	-
H	15.5	15.6	-	-
I	24.0	25.0	-	-
K	-	-	0.24	0.25

The amplitude of the horizontal field transient peak may also be used to determine the model parameters. In Figure 4.6 we plot the peak amplitudes for a truncated sheet against normalized time (Equation 4.1). This master curve has been corrected for loop height (see Chapter 2.4) and is given in amps/meter for a single-turn loop carrying a current of one amp. After measurements using several loop radii we found that the observed horizontal field amplitude is largely independent of the loop size.

With this master curve, horizontal fields measured at the surface may be used to obtain the conductance of a truncated sheet. Before use the observed data must first be normalized such that the primary (pre shut-off) field is equivalent to that of the master curve. For an $n-turn$ loop of radius a carrying current I the normalizing (multiplication) factor is

$$N_f = \frac{0.002}{nI/2a}.$$

To use the master curve, simply match the observed horizontal field peak amplitude (adjusted for the primary field) to the corresponding point on the curve, and read the normalized time coordinate t_n of the match point. The conductance may be determined from

$$S = \frac{t_{obs}}{t_n \mu_0 a}.$$

Note that due to the thin-sheet assumption this curve is only valid for normalized times greater than 0.5.

Because each amplitude value in Figure 4.6 is associated with a particular distance as well as time coordinate, the data shown in Figure 4.6 may also be plotted against distance from the edge in
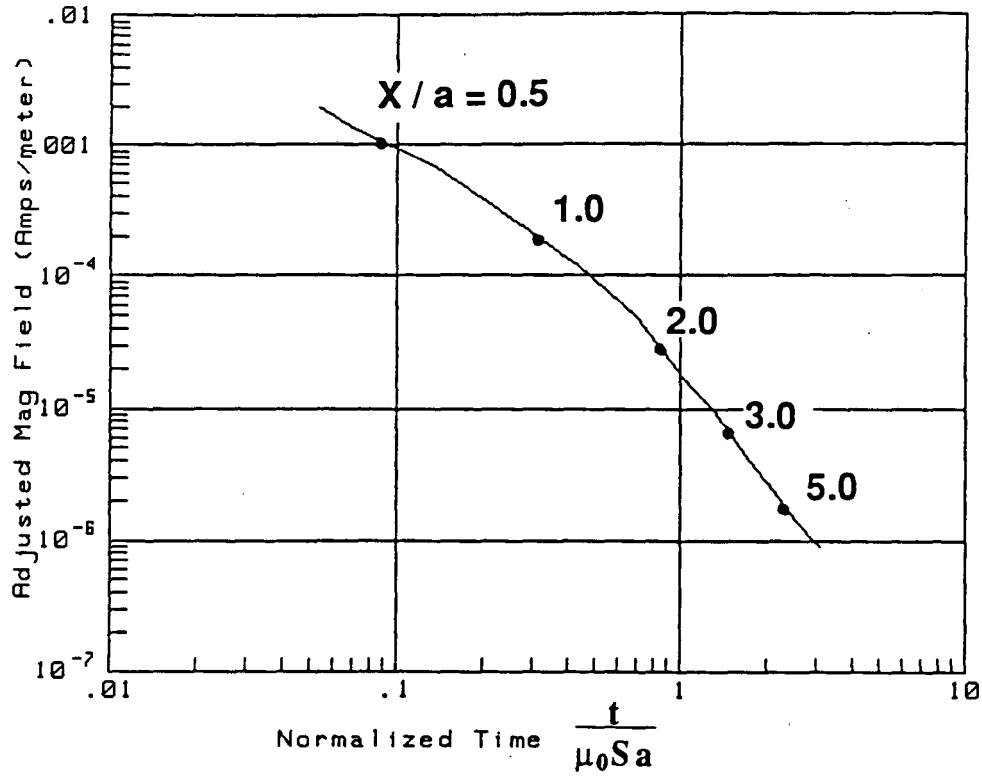
Figure 4.6 Transient peak amplitude maximum versus normalized time. The data has been corrected for loop height.
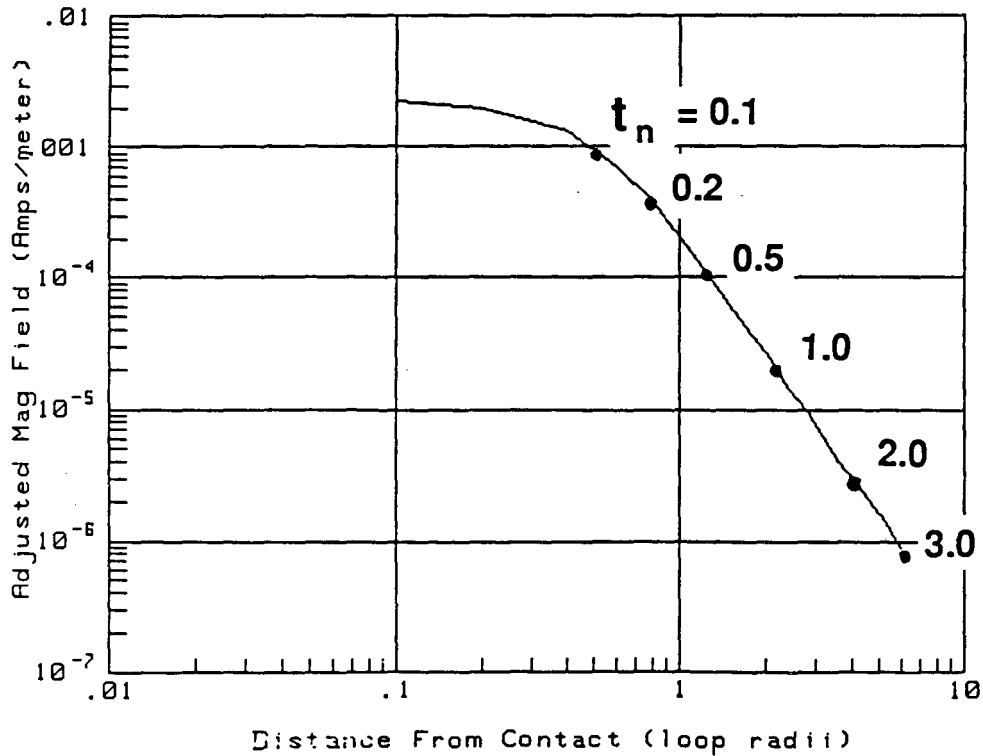

Figure 4.7 Transient peak amplitude versus distance from the edge, in loop radii.

units of loop radii (Figure 4.7). (Note that the information contained in Figures 4.6 and 4.7 is equivalent but the repetitive display allows for simpler use). Within one loop separation of the edge, the curve is relatively flat but at larger separations the field falls off with distance as $1/r^3$ which is a characteristic of a dipole source in free-space. The amplitude versus distance variation of the horizontal field maxima is a geometrical parameter that is largely independent of model type so this latter plot represents all truncated sheet and and quarter-space cases. The conductance of the truncated sheet and distance from the loop center to the edge may therefore be determined by measuring the amplitude at a single location and matching it to the appropriate position on Figures 4.6 or 4.7.

The slope of the transient decay curve after its peak is also useful in estimating contact parameters. Dallal (1985) showed that for an impulsive source the late-time horizontal field transients may be represented by a simple exponential function of the sheet conductance, the distance from the source to the edge and the loop radius. In Figure 4.8 we examine this relationship further for step-response excitation. In this plot the time constant for horizontal field transients is measured at various distances from the contact and the result is plotted against distance to the edge in units of loop radii. We have empirically found that the following functional relationship is representative of the data.

$$H_x(t) = H_0 e^{-t/\tau}, \quad \tau_1 = \frac{\tau}{\mu_0 Sa} = 0.4x/a + 0.1, \tag{4.3}$$

where τ is the measured time constant in milliseconds and τ_1 is the normalized time constant. If we know the conductance of the truncated sheet (by measuring the peak velocity, for example) then this formula allows us to compute the distance to the edge.

We have shown that the conductance of a surficial contact and the distance from the loop site to the edge may be obtained by two independent methods. With the first method these two parameters are obtained by matching the amplitude of the transient peak against two master curves, where normalized peak amplitudes are plotted against normalized time and distance to the edge. The second method is to determine the conductance from the velocity of the transient peak and to calculate the distance to the edge from the slope of the transient after the peak. The velocity may be determined by measuring the temporal position of the peak at two adjacent sites; the slope may be measured from either or both of the transients.
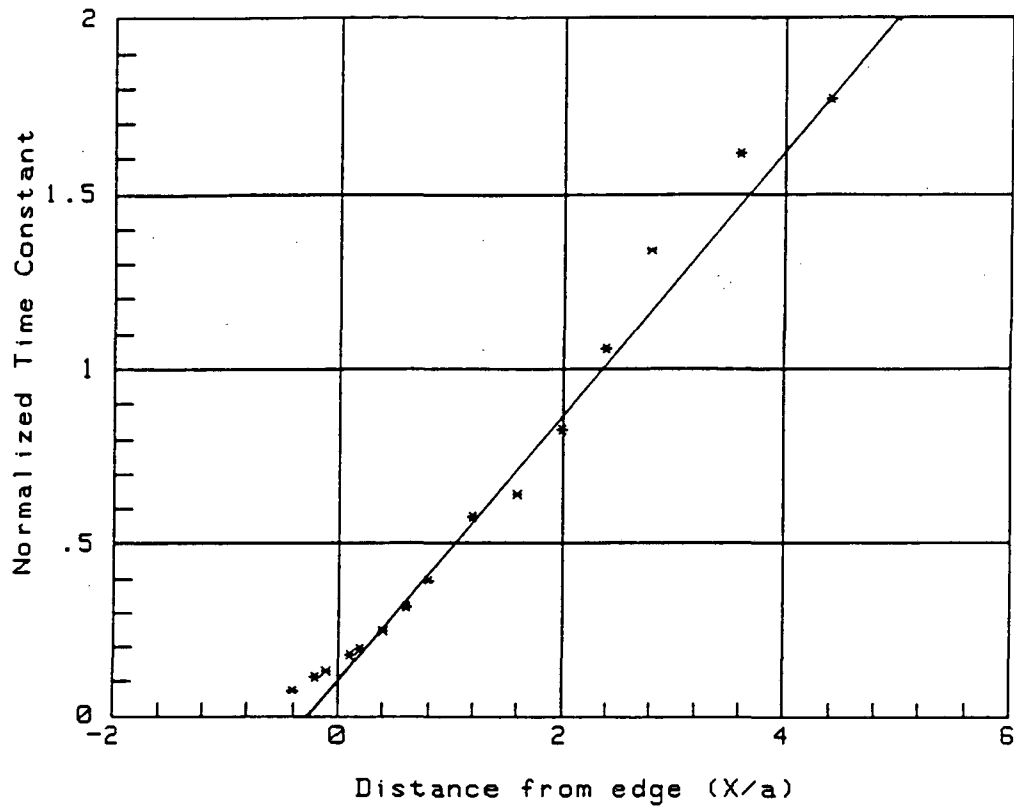
Figure 4.8 Normalized time constant as a function of distance from the edge in loop radii.

4.1.2.1 Horizontal Fields over a Quarter-Space Contact

We have shown that for a truncated sheet, where the current travels on the surface, the velocity of the transient peak is constant and inversely proportional to the sheet conductance. For a quarter-space the current propagates downwards as well as outwards and the velocity of the current pulse slows with time. Nabighian (1979) showed that over a homogeneous half-space the currents increase their radius with time as

$$R(t) = (\frac{4.37t}{\mu_0 \sigma})^{1/2}.$$ (4.4)

Their velocity of expansion is given by

$$V_R(t) = \frac{dR(t)}{dt} = (\frac{4.37}{4\mu_0 \sigma t})^{1/2}.$$ (4.5)

This velocity is therefore an inverse function of both the conductivity and the square root of time.

Horizontal field profiles and transient plots over a quarter-space are given in Figures 1.5 and 1.6. Based on the truncated-layer results we might expect that the horizontal field transient peak velocity over a quarter-space to have the same functional form as the expansion velocity of half-space currents. To test this assertion we plot the position of horizontal field transient peaks over two quarter-space models (U and L in Table 4.1) together with the horizontal position of the current in a homogeneous half-space, against the square root of time (Figure 4.9). The Figure indicates that 1) at distances exceeding two loop radii from the edge, the slope of the half-space current and the quarter-space transient peaks are linear with the square root of time and 2) the half-space current and quarter-space transient peaks for models of the same conductivity have the same slope.

Solving equation 4.5 for conductivity yields

$$\sigma = (\frac{4.37}{4\mu_0 t V_R(t)^2})$$ (4.6)

$$\sigma = \frac{4.37}{4\mu_0 p^2} \qquad p = \frac{dR(t)}{d(t^{1/2})}.$$

This means that we can determine the quarter-space conductivity by measuring the velocity of the transient peak, or equivalently, by measuring the slope, p, on a plot of the position of this peak versus the
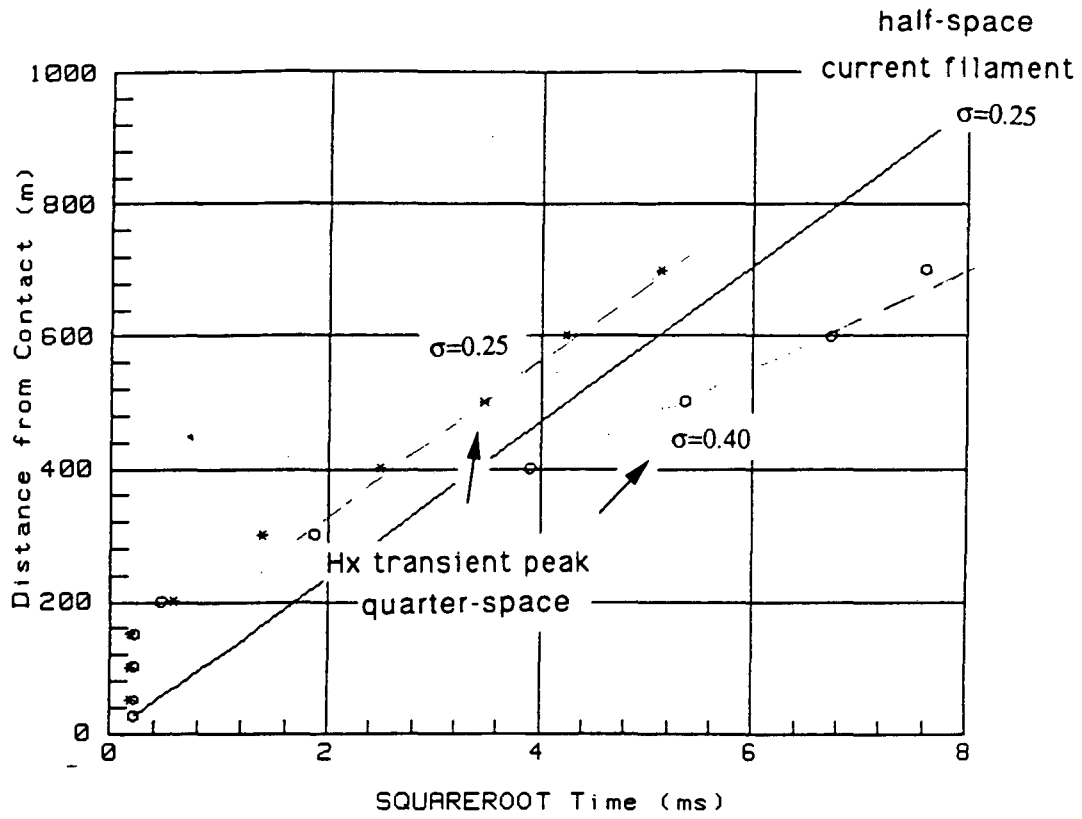
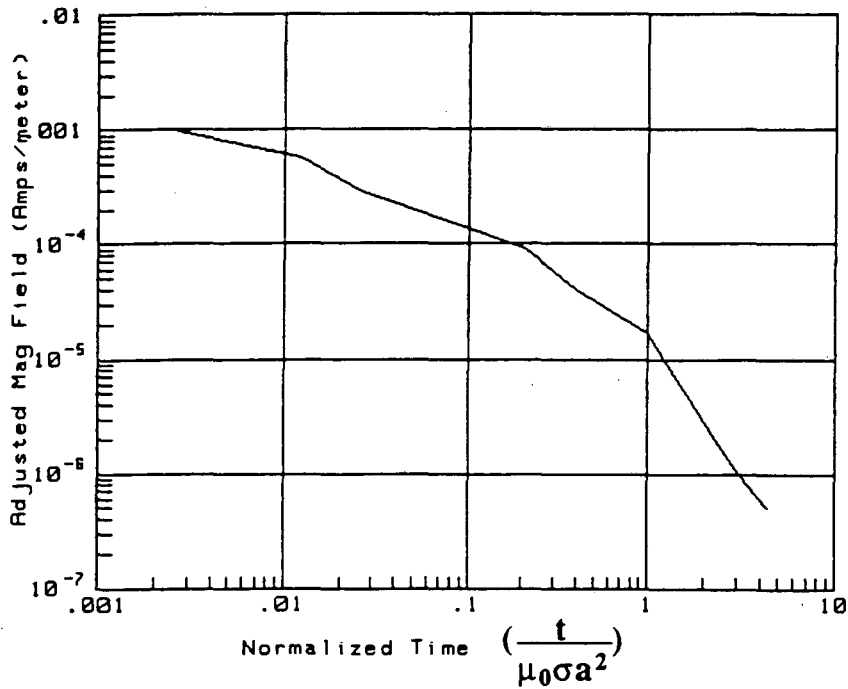Figure 4.9 Horizontal field transient peak velocity for a quarter-space.

Figure 4.10 Normalized horizontal field transient peak amplitude for a quarter-space.

square root of time. Note that this is only valid beyond approximately two loop radii from the edge.

We can also construct a master curve of the horizontal peak amplitudes for the quarter-space models much as we did for the truncated sheets. Plotting the quarter-space transient peak against normalized time, $t_{norm} = \dfrac{t}{\mu_0 \sigma a^2}$, results in a similar plot to the truncated sheet cases shown above (Figure 4.10). This master curve may be used for quarter-spaces in the same manner as Figure 4.10 is for truncated sheets. Note that the amplitude approximately decays as $t^{-3/2}$ instead of t^{-3} for the truncated sheet case.

Although the horizontal field transients for quarter-space and truncated sheet models appear similar to each other there are fundamental differences in the peak velocities and late-time characteristics. For practical field cases it may be necessary to make a series of soundings before it is clear whether an edge approximates a truncated sheet, a quarter-space or neither model. With three soundings, for example, one could determine whether the transient peak velocity is a constant, which would indicate a truncated sheet, or that it decreases with distance, which would suggest a quarter-space.

Remarks

If central-loop measurements are made over a truncated sheet of overburden or over a fault zone (that may be represented by a quarter-space) then the conductance or conductivity and distance to the edge can be determined from a few transient measurements. If a given case does not approximate either model then the above analysis does not apply. However for a fairly wide range of surficial contacts the response is similar to that of a truncated sheet if the station is far from the contact and it resembles that of a quarter-space when the station is near to the edge.

We have found that transient voltage data is typically more complex in character than the magnetic fields, particularly if the contact is dipping and/or is covered by an overburden layer (Dallal, 1985). For this reason we recommend that this data be integrated to obtain magnetic fields before analysis is performed. A simple technique for integrating the voltage data was described by Dallal (1985). With this method, the voltage transients are fitted at times later than some than t' to an exponential function. The observed data at early times are then numerically integrated, (t' to t),

using Simpson's rule and then added to the integral of the exponential function. The combined data, taken from from (t to ∞), represent the field quantity as a function of time.

$$H(t) = \int_{\infty}^{t} \frac{dH(t)}{dt} dt = H(t) - H(\infty) = H(t) \tag{4.7}$$

This method has the advantage of avoiding early-time noise due to a current shut-off ramp.

If one prefers to interpret the transient voltage instead of the magnetic field then a slightly different procedure is followed to determine the conductance and distance to the edge. Instead of obtaining the conductance from the temporal position of the transient peak we use the time of the zero-crossing. The peak that develops after the zero-crossing may be used in a similar manner to the horizontal field transient peak to determine the conductance and distance to the edge. Note that the slope of the decay curve after the primary peak the same for either the voltage or field transient. This quantity can therefore be used in either case to determine properties of the contact.

4.1.3 Analysis of Horizontal Field Profiles

If a series of central-loop soundings are collected in a line over a surficial contact then we can use the characteristics of the horizontal fields plotted as profiles for each observation time to determine the contact geometry and conductivity (see Figure 4.2.) For example, we can easily measure the amplitude and position of the horizontal field peaks as a function of lag time. These data may be used to determine the conductance or conductivity of the model as well as the contact dip and depth of overburden.

As an example, in Figure 4.11 we plot the amplitude of the horizontal field profile peak, $|H_{x,max}|$, against normalized time for a truncated sheet. This master curve may be used in a similar manner as the curve in Figure 4.7a to determine the conductance of the truncated sheet.

The position of the horizontal field maxima also have a simple form. If we plot the position of the peak field for a given observation time w observe that the curves are linear with slopes inversely proportional to the conductance of the sheet. The slope of these curves, which is a measure of the velocity of the profile peak, is given by
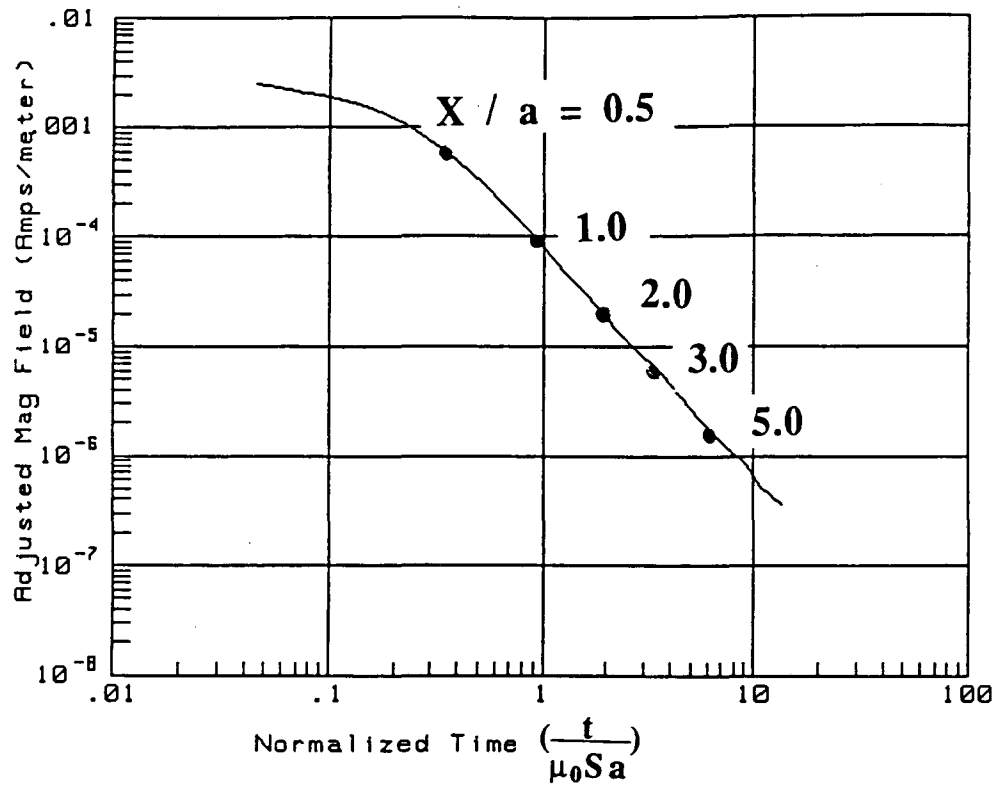
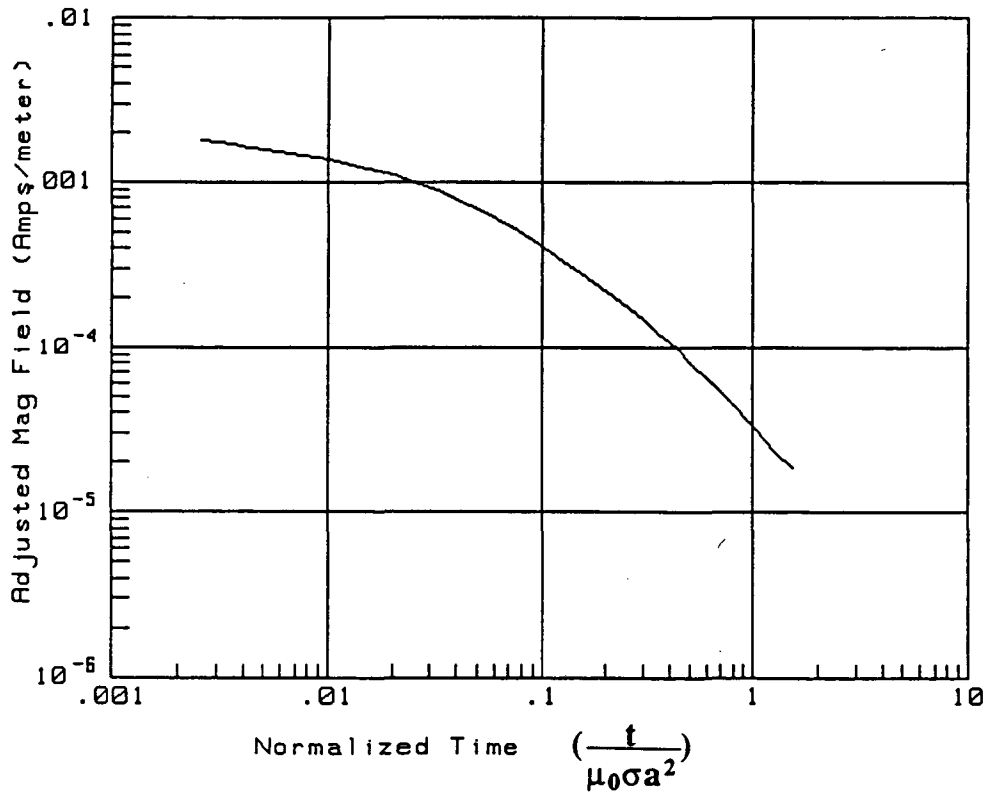Figure 4.11 Horizontal field profile maximum, $|H_{x,max}|$, over truncated sheet models.

Figure 4.12 Horizontal field profile maximum, $|H_{x,max}|$, over quarter-space models.

$$V_{prof} \approx \frac{0.7}{\mu_0 S} \qquad (4.8)$$

For the quarter-space models the horizontal field profile peaks decay as $t^{-3/2}$ which is a characteristic for the late-time vertical field transient over a homogeneous half-space (Nabighian, 1979, Figure 4.12). These data are normalized by plotting the amplitudes against $t_n = \frac{t}{\mu_0 \sigma a^2}$. This master curve may be used to obtain the conductivity for a quarter-space from a profile of central-loop measurements.

Analysis of the horizontal fields plotted as profiles provides more than simply an independent means of determining sheet conductance and distance to the edge. If a contact has a dipping face or is covered by a homogeneous overburden then the profiles offer a means of interpreting these characteristics as well. This is demonstrated below.

4.1.4 Dipping Quarter-Space Contacts

If the contact has a dipping face the central-loop horizontal fields are also somewhat affected by this parameter. To determine a relationship between the observed field and the contact dip, we collected central-loop data over a 250m thick 4.0 ohm-m dipping contact with dips from 30 to 150 degrees (Figure 4.1). Note that this data has not been corrected for the system elevation above the model which is estimated to be 60 m.

The vertical and horizontal fields for dips less than 90 degrees are plotted at lag times of 0.1ms and 10.0 ms in Figures 4.13 and 4.14. At early times the vertical fields for the models with a shallow dip are flatter than the fields for the vertically dipping case and the horizontal component develops lower and broader peaks. At late-times (Figure 4.14) the profiles are similar in appearance but the fields for the lower dip angles are shifted outwards (towards the edge) with respect to the field for the vertically dipping model. For dips greater than 90 degrees the horizontal and vertical field profiles (Figures 4.15 and 4.16) at early and late times are similar in appearance to the vertically dipping response but they are shifted inwards (away from the edge) as compared to the vertically dipping case. We have empirically found that, for dip angles from 30 to 150 degrees, the amount of lateral shift, (x), in the profiles may be related to the dip (ϕ) by ;
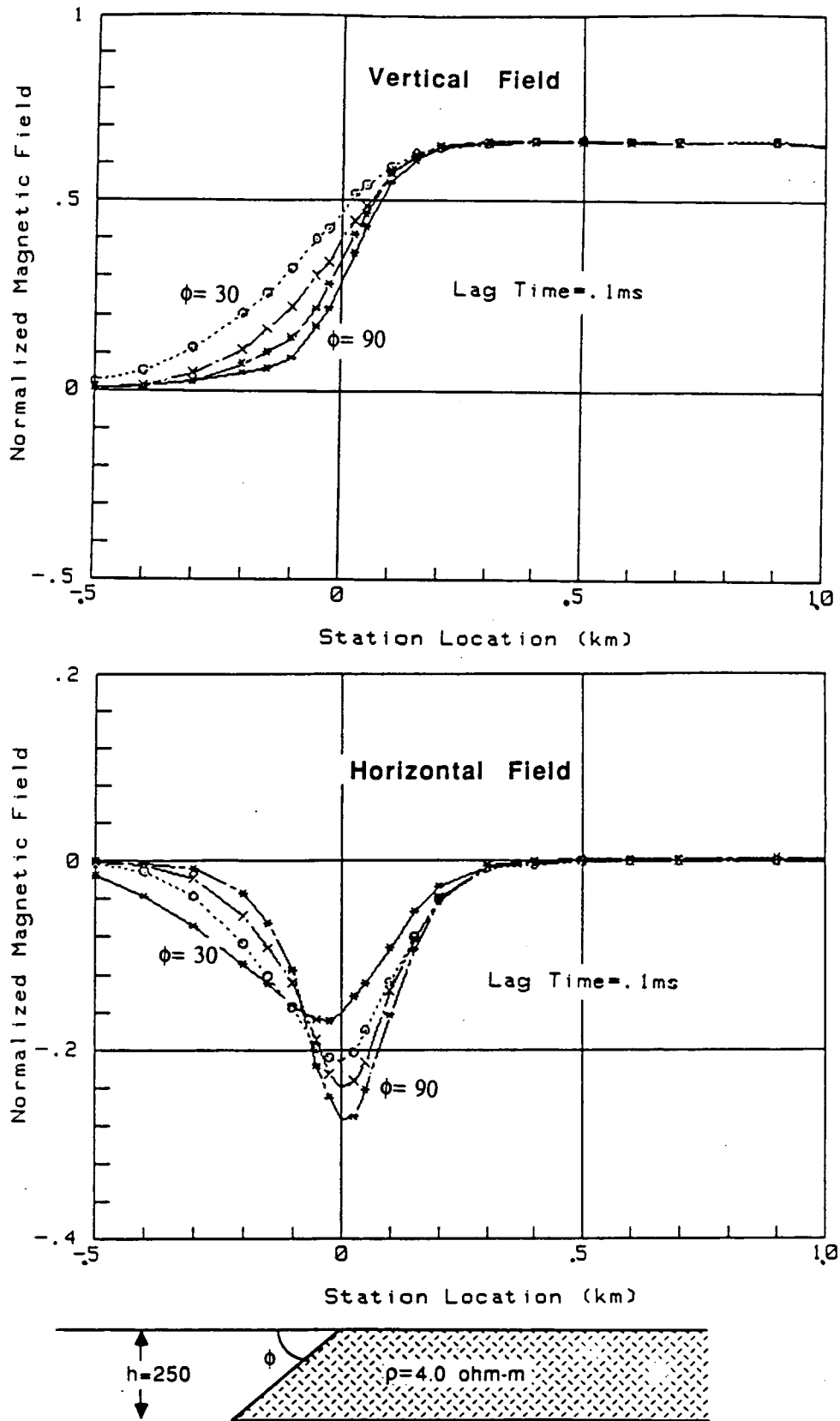
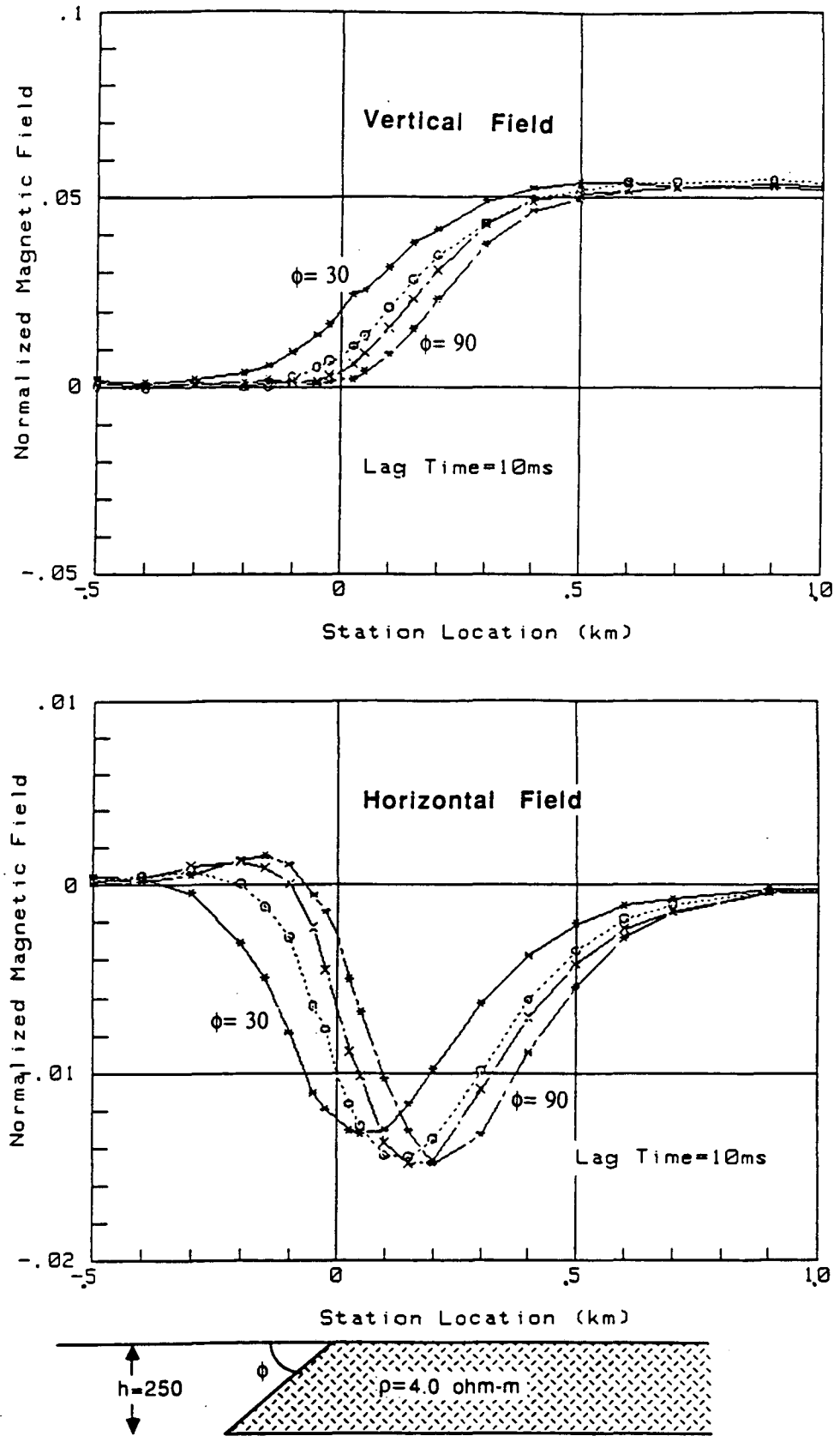Figure 4.13 Early time vertical and horizontal fields over dipping quarter-space models (Figure 4.1).

Figure 4.14 Intermediate time vertical and horizontal fields over dipping quarter-space models.
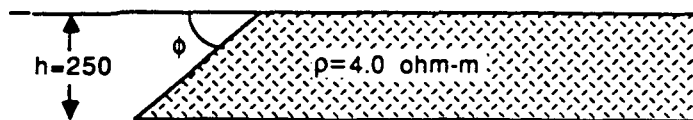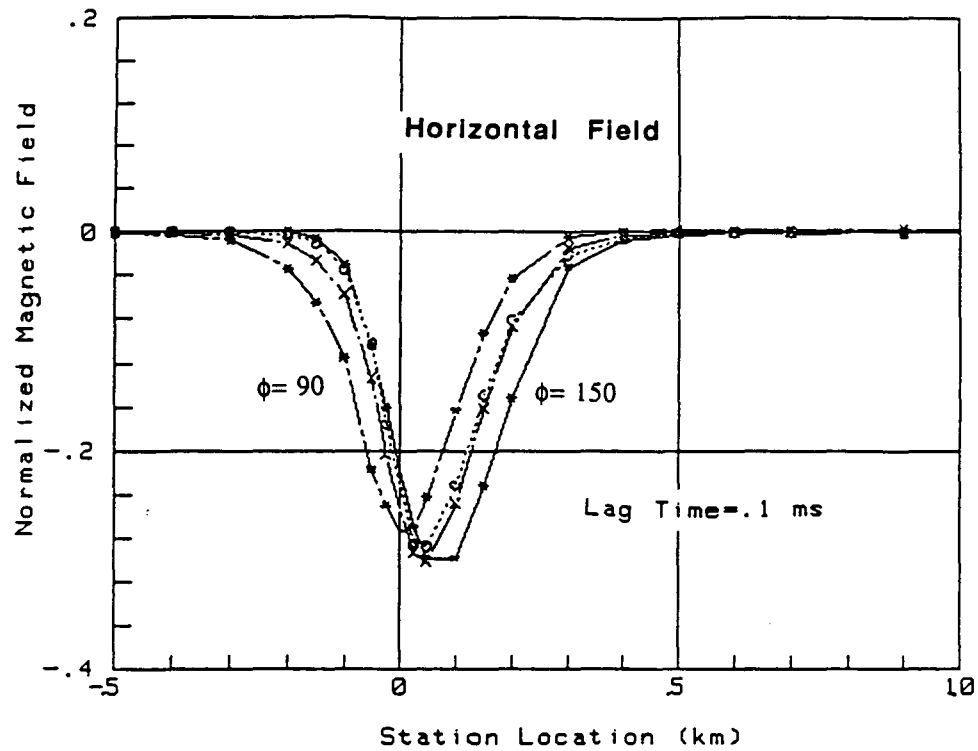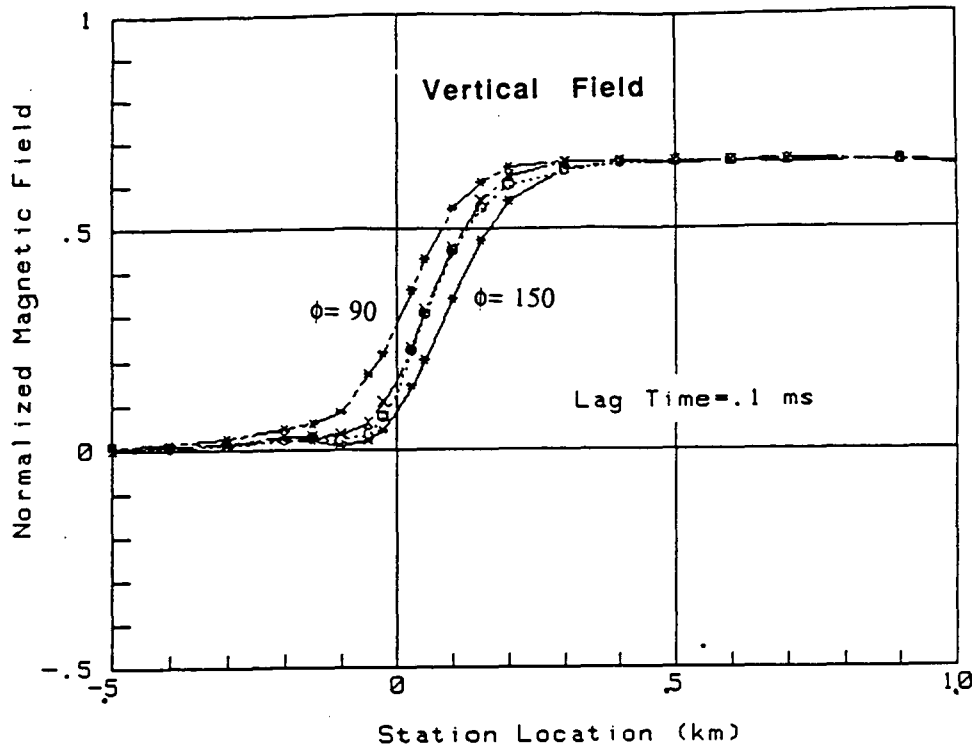
Figure 4.15 Early-time vertical and horizontal field profiles over dipping quarter-space models. The dips range from 90 to 150 degrees.
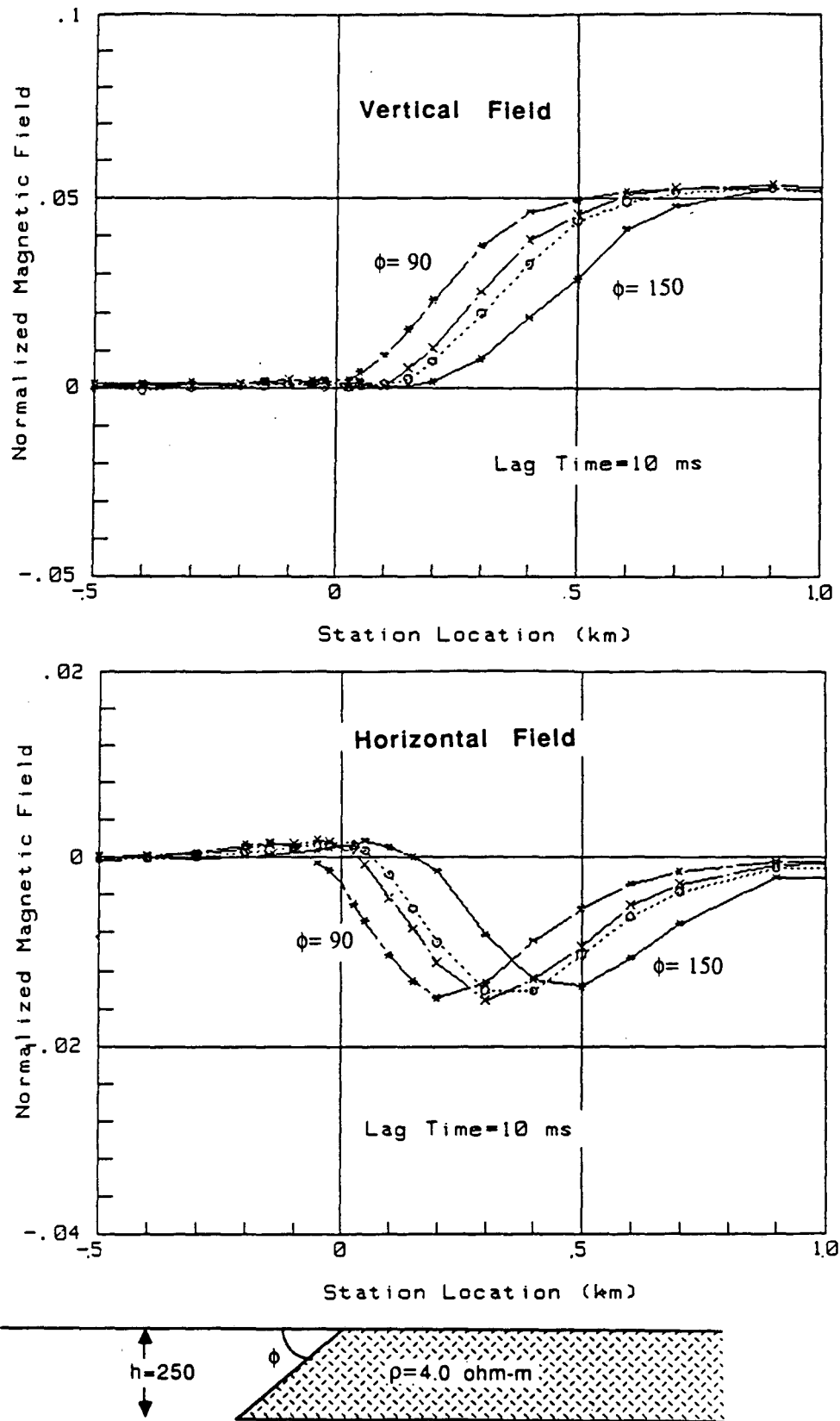
Figure 4.16 Intermediate-time vertical and horizontal fields over dipping quarter-space models.

$$H_x(x,\phi) \approx H_x(x(1 - \tan(90-\phi)), 90) \qquad (4.9)$$

For dips less than 90 degrees we found that the early-time peak amplitude is somewhat sensitive to the dip angle. We plot this amplitude $|H_{x,max}|$ against time for contact models with dips of 30, 45, 60 and 90 degrees in Figure 4.17. The curves are separate and parallel at early time but merge into one by about 2ms. At early time the contact models are sensed as a suite of dipping quarter-spaces and the responses are dependent on the dip. At later times the contact is sensed from far away and the fields respond to it as a single equivalent truncated sheet; the effect of dip is therefore unimportant. The conductance of the contact layer may therefore be obtained from a relation such as equation (4.3). (Note that no relation of the dip to the conductivity of the sheet could be established as only one set of models were measured.)

Using the results from the one model suite we have empirically found that for dip angles from, $(30° < \phi < 90°)$ the early time influence of the dip, ϕ, is given by,

$$\frac{|H_{x,max}(t,\phi)|}{|H_{x,max}(t,90°)|} = \sin\phi^{2/3}. \qquad (4.10)$$

For the shallow dipping contacts the early-time response seems to be more sensitive to the geometric configuration of the model than to its conductivity. This is a similar result to that reported in the literature for confined bodies (Kaufman, 1978).

For a shallow dipping contact, the dip may be resolved from a field profile using a two-step process. First the conductivity of the quarter-space (or sheet conductance) must be determined using one of the methods described above. Next the observed $|H_{x,max}|$ profile may be compared to the theoretical curve of Figure 4.11 or Figure 4.12. If the profile is dipping, the late-time data will match the curve but the amplitude of the early-time data will be shifted by an amount given by equation 4.10.

4.1.5 Contacts with Overburden

For quarter-space models covered with an overburden layer, the edge effect is not observed until the current has penetrated the surface layer and begins to flow in the quarter-space beneath. This effect is shown for early-time vertical and horizontal field profiles in Figure 4.18. For the thickest overburden
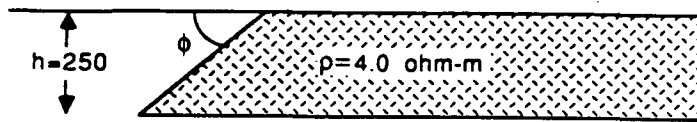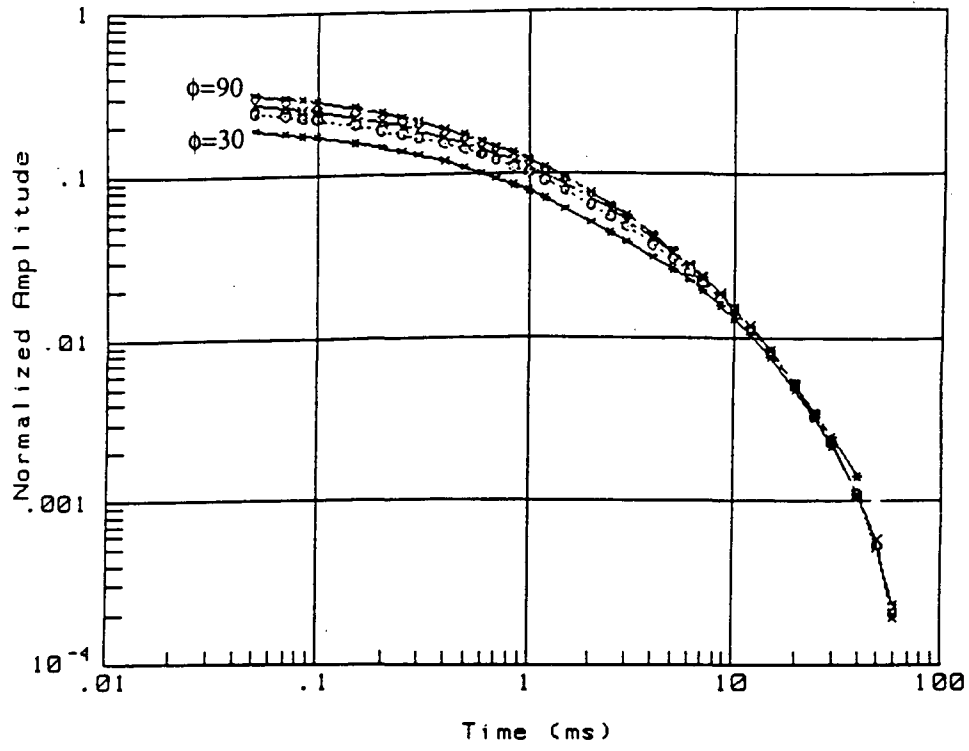
Figure 4.17 Plots of $|H_{x,max}|$ for dipping contact models. The dips range from 30 to 90 degrees.
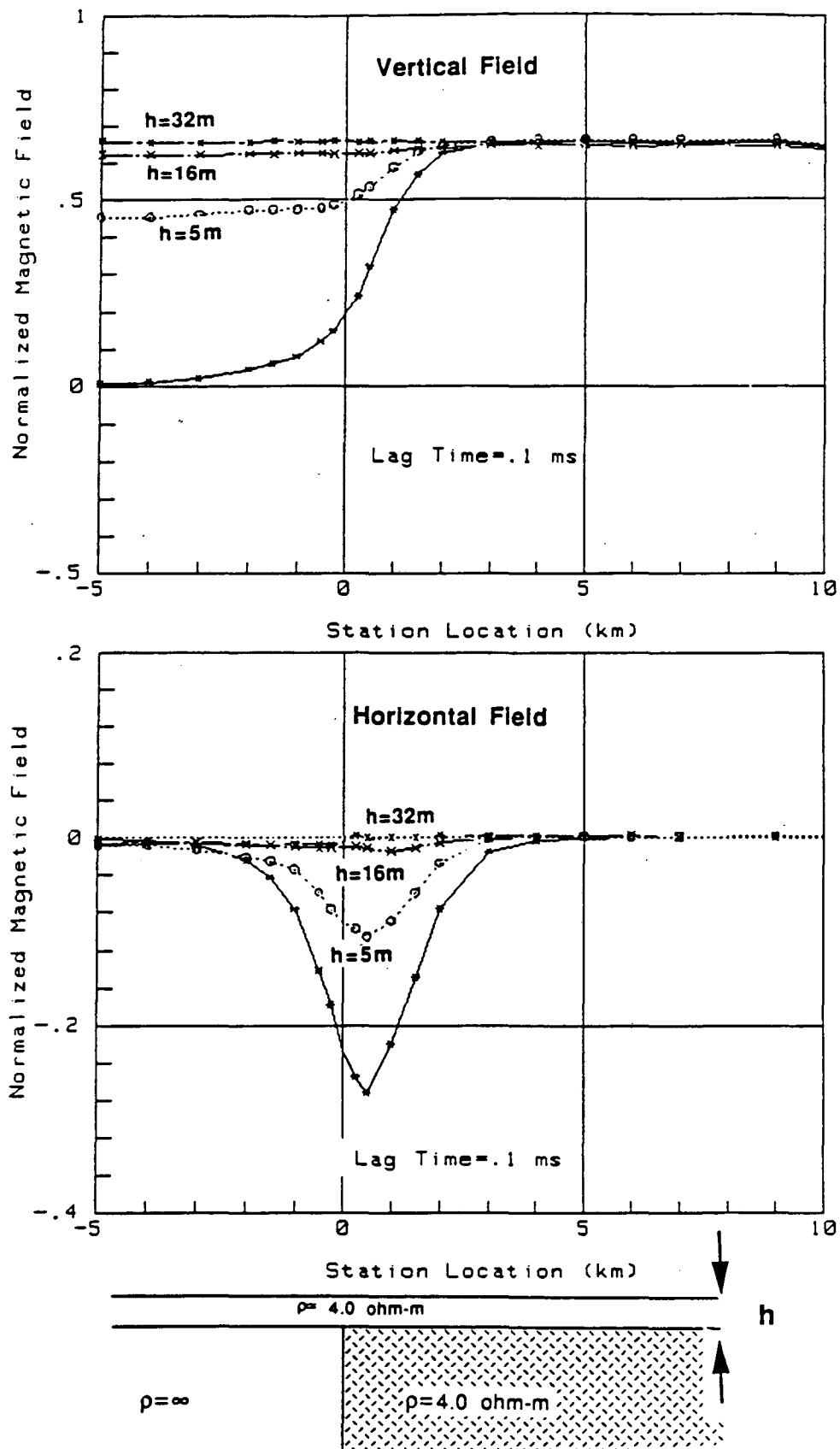
Figure 4.18 Early-time vertical and horizontal magnetic fields for quarter-spaces with overburden.

(h=32 m) the early-time vertical fields do not detect the contact at all, but the thinnest overburden case (h=5 m) shows a significant contact response. The horizontal field, for the 32 m overburden, is virtually zero but for the 5m overburden the response is significant; it is about one third the magnitude of the surficial quarter-space. At late times the contact response for all of the overburden models is virtually identical.

We find that for relatively thin overburden layers ($h<0.3a$), the peak amplitude of the horizontal field plotted as profiles $|H_{x,max}|$ is sensitive to the conductance of the overburden. In Figure 4.19 we plot $|H_{x,max}|$ against time on a logarithmic plot for a quarter-space model covered with overburden. The overburden is a 4.6 ohm-meter layer ranging in thickness from 0 to 65 m. At late times the curves merge but at early and middle times the plots are distinct. By late-time the induced current has completely penetrated the overburden layer so the response for all the models is identical. At early and middle times the current is either partially or totally confined within the overburden layer so the curves all have differing character. For these overburden models, the $|H_{x,max}|$ curves begin at a small value then build to a peak before merging at late times. Plotting the $|H_{x,max}|$ peak time against the conductance of the overburden we find that for all but the thinnest model (h= 5m) the two are linearly related. The conductance of the overburden is empirically given by

$$S_{obs} \approx \frac{1.5 t_{max}}{\mu_0 a}.$$

where the time t_{max} is the peak time in seconds. (Note that we cannot establish a relation of the overburden response to the conductivity of the host as only one set of models was measured.) The thickness of a homogeneous overburden layer may be calculated for this model if one knows its conductivity. This latter quantity may be determined from the vertical field transient.

4.1.6 Finite Contrast Models

If there is a finite resistivity contrast across the contact then the response is somewhat different from the infinite contrast models described above. Clearly, as the conductivity contrast across the boundary diminishes, the contact response will also be reduced but the nature of this adjustment is complex. To investigate the effect of a finite resistivity contrast on central-loop measurements, a truncated sheet
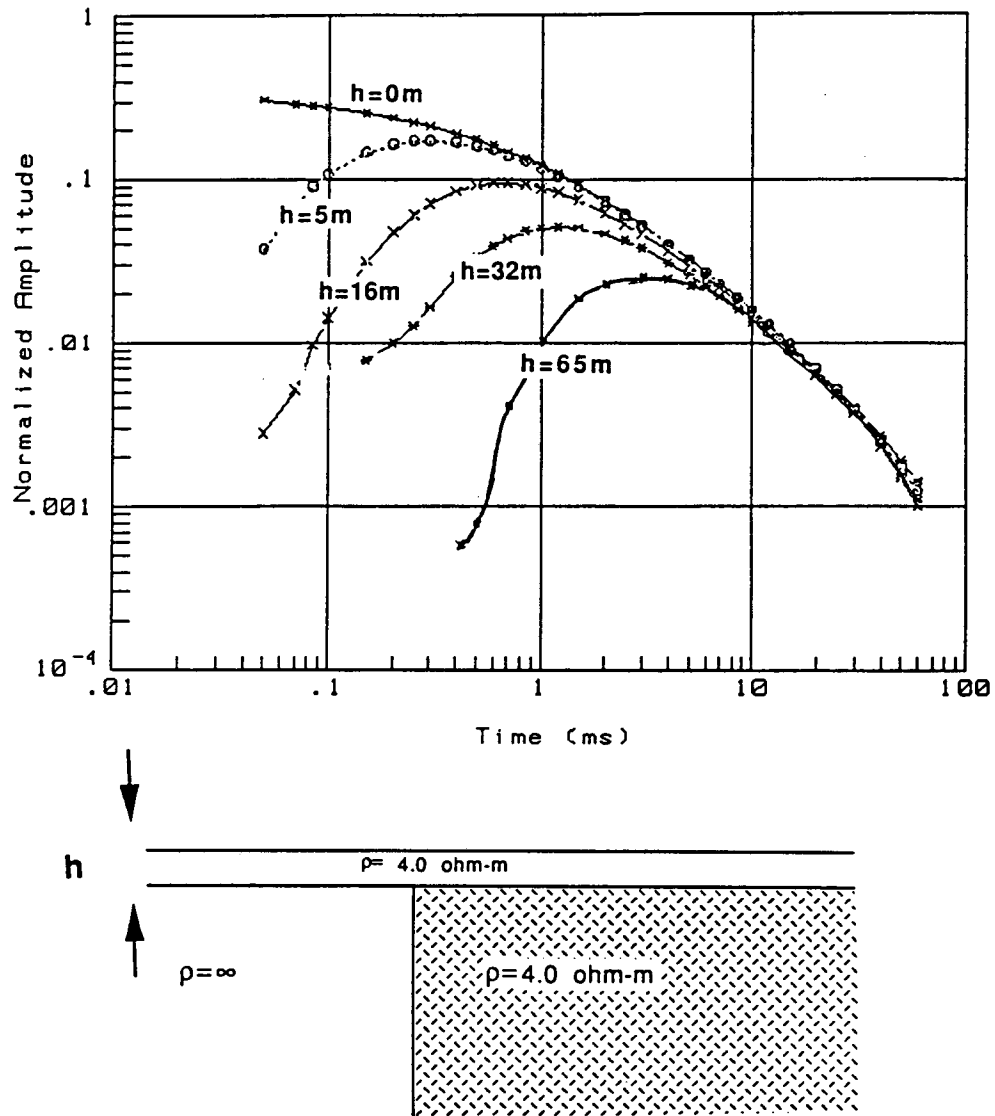
Figure 4.19 Plots of $|H_{x,max}|$ for quarter-space contact models with overburden.

model was constructed from a sheet of lead in contact with mercury. The model corresponds to a 16 m thick 22.5 ohm-m layer in contact with a 100 ohm-m layer of equal thickness. Measurements were also made over an equivalent infinite contrast model (lead/air) for comparison. As before, the system elevation is 60m above the model surface.

Vertical and horizontal magnetic fields time profiles are plotted for a lead/mercury model and the corresponding lead/air model in Figure 4.20. The central-loop vertical field profiles show a smooth level adjustment across the edge for the finite contrast model just as they do for the infinite contrast model. In the first case the fields do not fall to zero across the edge but, instead, asymptotically approach the value observed over an infinite sheet with the conductance of 0.16 (the value for the mercury pool). At later times, the vertical field over the resistive side of the contact is very small so there is little difference between the responses for the finite and infinite contrast models. The horizontal fields for a finite contrast model, shown in Figure 4.21, are similar in shape and wavelength to the those over the infinite contrast case but the amplitude of the curves is smaller throughout time and there are no zero-crossings. Analysis of the transient and profile peak velocities for the two models shows no difference. This is to be expected since in both cases the anomalous current is propagating in the same medium (lead). The only measurable difference between the profiles is the amplitude of the horizontal field peaks.

By plotting the peak horizontal field amplitudes ($|H_{x,max}|$) for the two models against lag time we can quantify this observed difference in amplitudes (Figure 4.22). In this plot it is clear that the horizontal field peak is consistently larger for the infinite contrast model and that the two curves are essentially parallel except at the earliest times. If we adjust the amplitude of the finite contrast model by the ratio of the conductance contrasts $\dfrac{0.72 \quad (Pb/air)}{0.56 \quad (Pb/Hg)}$ then we observe that the two curves now coincide (Figure 4.22b).

The horizontal field for the finite contrast model is therefore smaller by exactly the ratio in the conductance contrast. This suggests that part of the current is propagating across the boundary while the remaining current is being reflected back towards the source. As the conductance contrast across the boundary becomes smaller less of the current will be reflected and the horizontal field will therefore
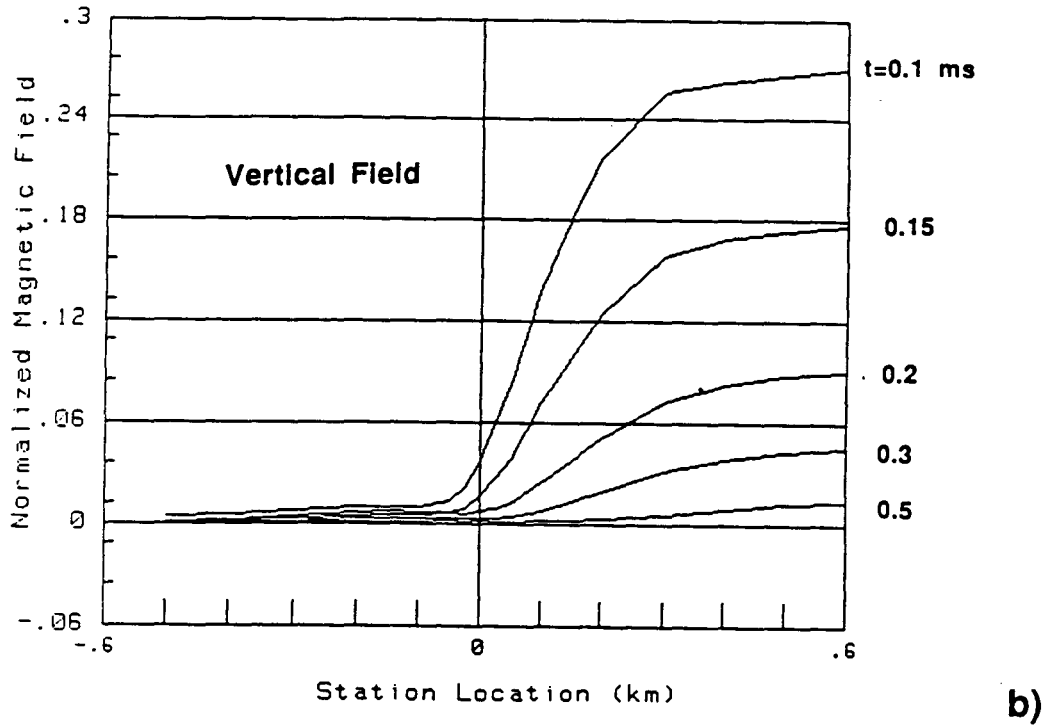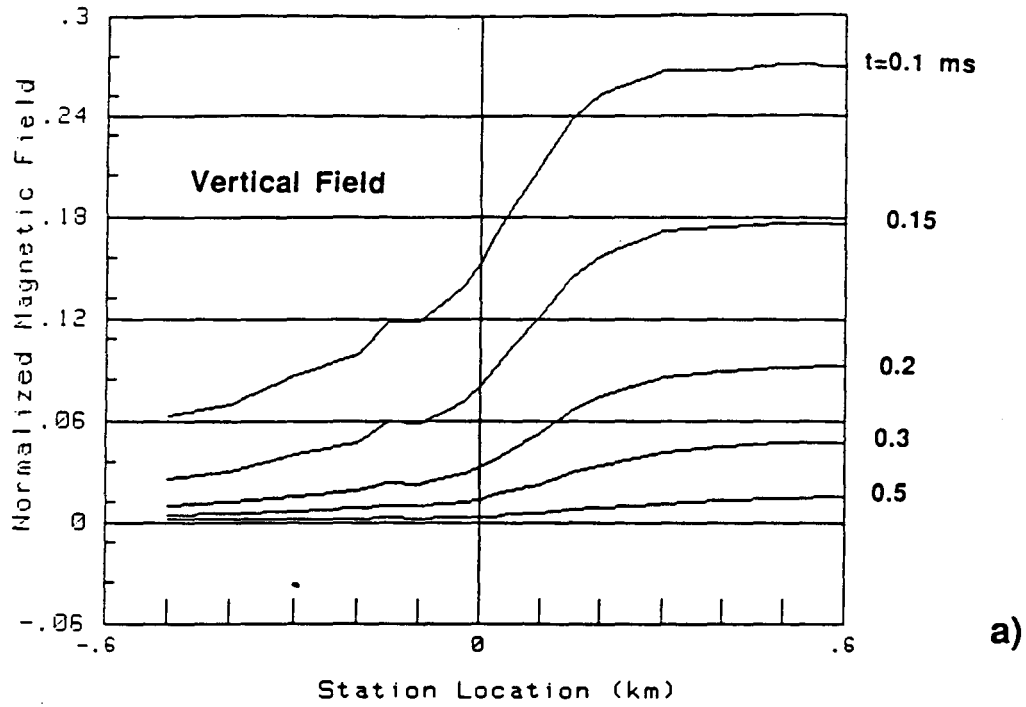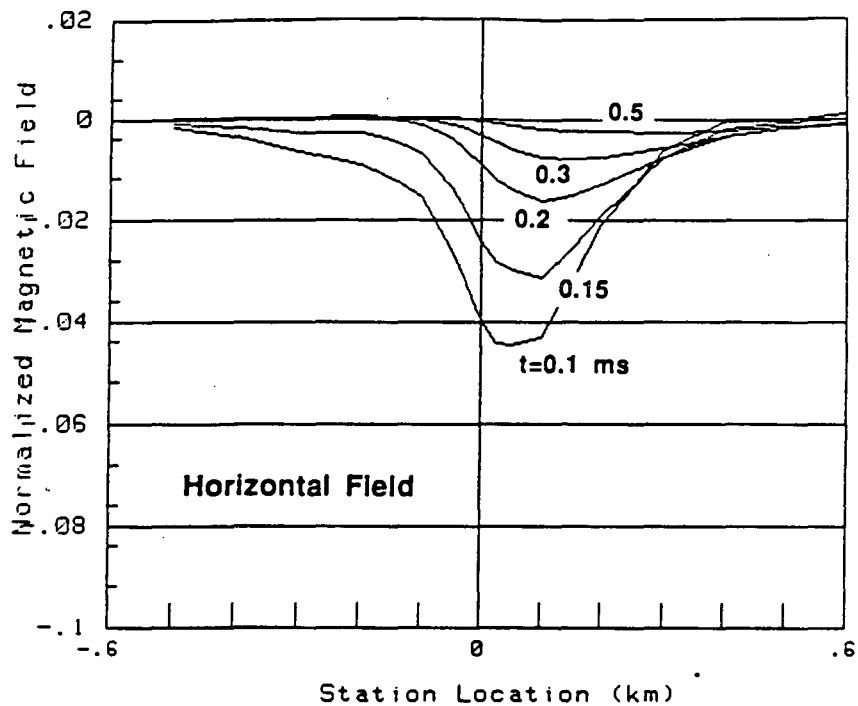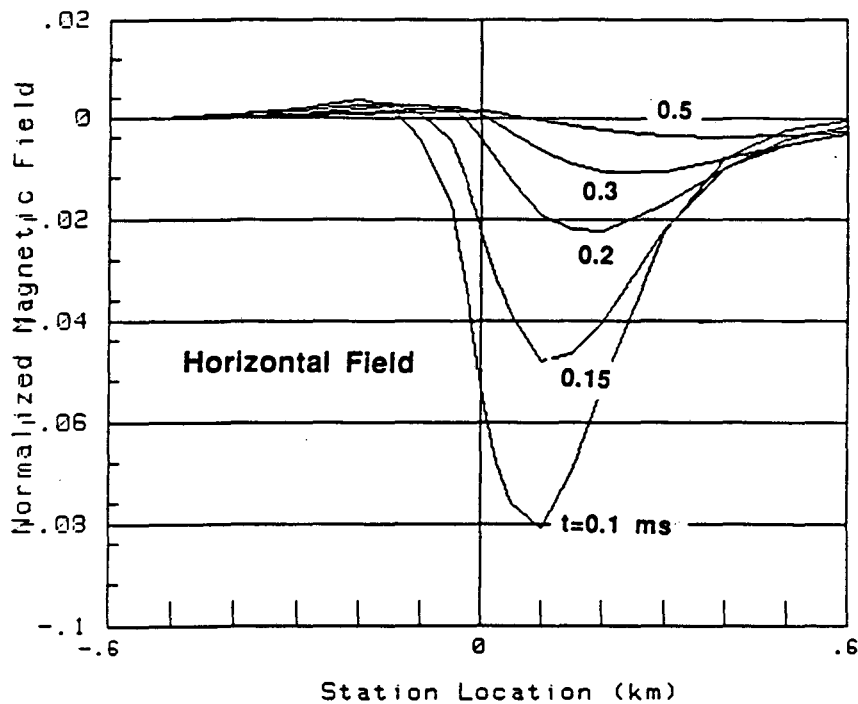
Figure 4.20 a) Vertical magnetic field time profiles for finite resistivity contrast truncated sheet models (Pb/Hg) and b) infinite resistivity contrast models (Pg/air).

Figure 4.21 a) Horizontal magnetic field time profiles for finite resistivity contrast truncated sheet models (Pb/Hg) and b) infinite resistivity contrast models (Pb/air).
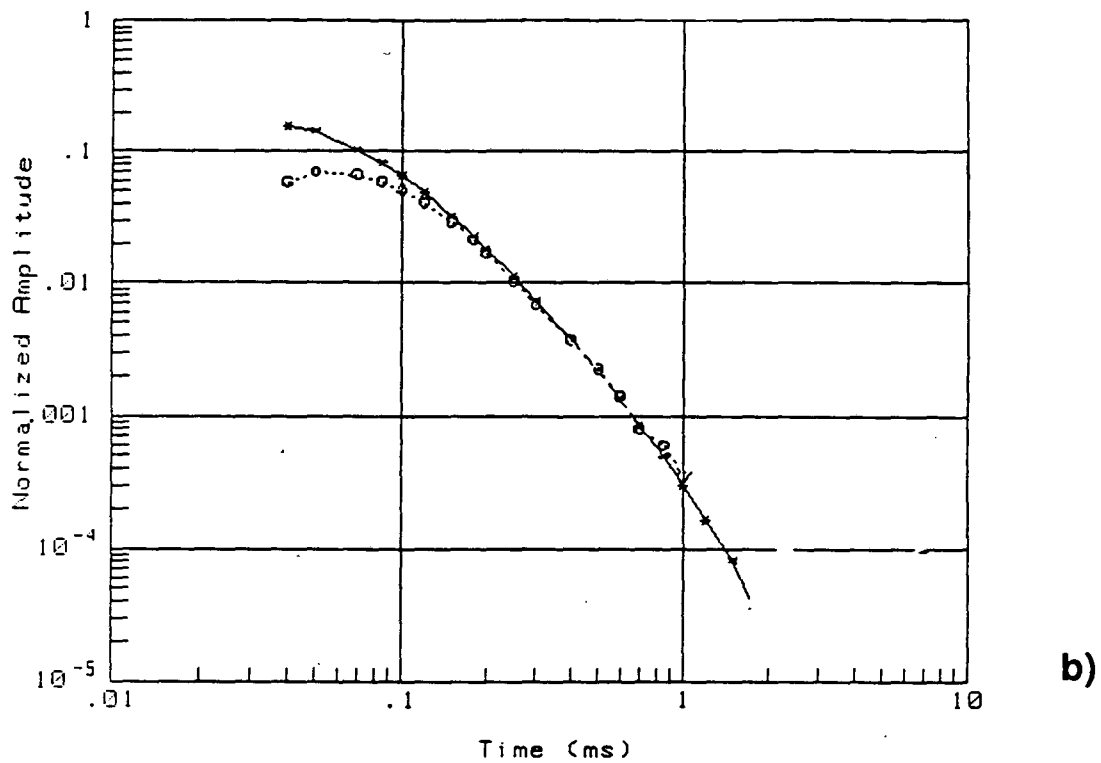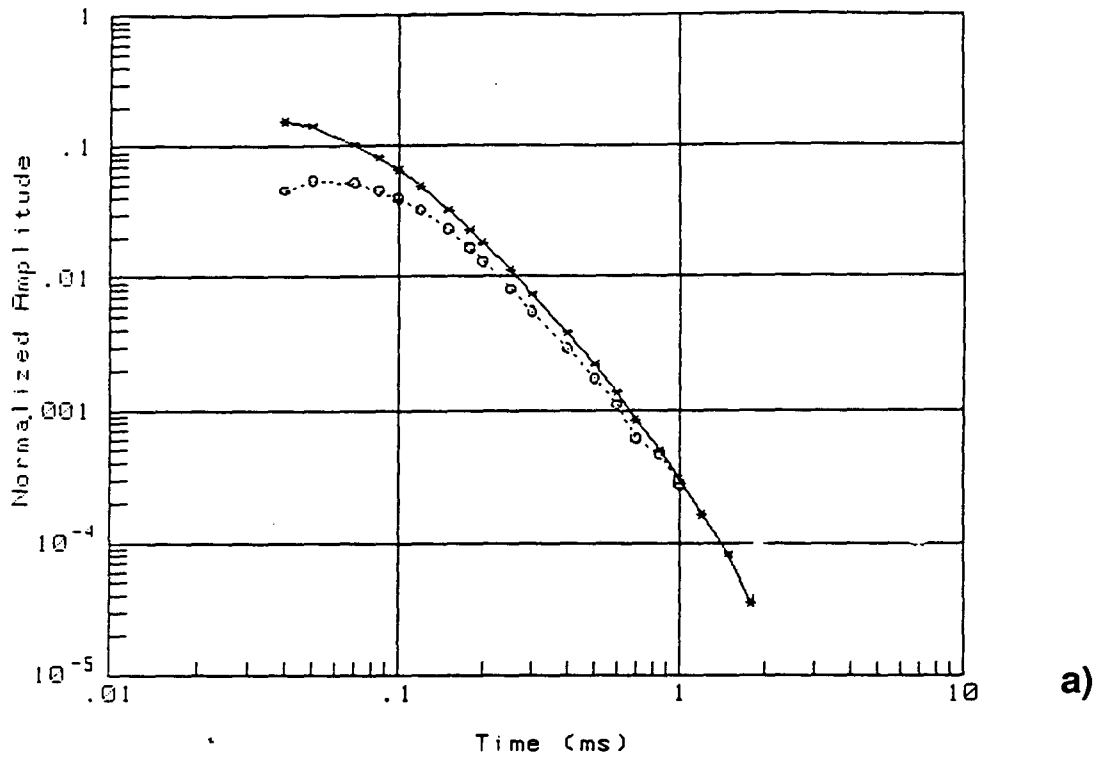
Figure 4.22 a) Plot of $|H_{x,max}|$ for finite and infinite contrast surface contact models (Pb/Hg), (Pb/air).

b) Same as a) except the amplitude for the finite contrast case is adjusted by the ratio in conductance

contrast for the two models $\dfrac{0.72 \quad (Pb/air)}{0.56 \quad (Pb/Hg)}$

decrease in amplitude until it vanishes for the case of no conductance contrast.

Note that for the finite contrast profile one may not use the $|H_{x,max}|$ data directly to obtain the conductance or conductance contrast by matching it to a curve such as Figure 4.11; doing so one will obtain a conductance of 0.66 instead of the correct value (0.72). To properly interpret this data you must first obtain the conductance on the more conductive side of the contact. This may be determined from the velocity of the transient peak or the velocity of the profile peak, which are sensitive only to the conductance, not the conductance contrast. Using this value to determine the abscissa, $t_n = \dfrac{t}{\mu_0 S a}$, the observed profile must be matched to the normalized profile in Figure 4.11 by sliding the curve verti-cally. The ratio of this vertical adjustment distance to the amplitudes on the normalized plot is then equal to the conductance contrast.

Summary

The above analysis shows that, for some simple two-dimensional contact models, the conductance or conductivity of a truncated surface layer and distance from the source to the edge may be determined from the horizontal component of central loop transient or profile measurements. If a full profile of soundings is obtained then the contact dip and overburden thickness may be obtained from the peak values of the horizontal component.

4.2 Contact Stripping

In Chapter 3 we showed how the presence of a surficial contact can distort the observed data making it difficult to either determine the properties of horizontal layers or to see through them to pros-pect for deeper bodies. It would therefore be advantageous to remove this effect from a sounding so that the deep structure can be properly resolved. With the central-loop method it is possible to separate the contact effect from other anomalies and remove it from the data; we show how this is accomplished below.

To properly interpret a vertical magnetic field sounding the contact effect must be separated from the observed data.

$$H_{z\ corr}(t) = H_{z\ obs}(t) - H_{z\ contact}(t) \tag{4.11}$$

For a central-loop sounding at a distance X from a contact, this may be written,

$$H_{z\ corr}(t) = H_{z\ obs}(t) - \int_X^\infty \frac{\partial H_z(t)}{\partial X} dX \tag{4.12}$$

where $\partial H_z(t) / \partial X$ is the derivative of the vertical field in the direction of the contact.

To remove a contact effect from a central-loop sounding an approximation for the derivative term in equation 4.12 must be calculated and subtracted from the data. Since for the central-loop configuration both the transmitter and receiver move for each sounding it is not clear from a practical sense how to approximate this quantity. We develop a relation to do this below.

For two-dimensional structures we can apply Ampere's law to derive a relation between the horizontal and vertical components of the magnetic field.

$$\nabla \times H = J \tag{4.13}$$

In rectangular coordinates, if we denote the y direction as the strike of the contact then we can use equation (4.15) to write the component of the current in this direction,

$$\frac{\partial H_x(t)}{\partial z} - \frac{\partial H_z(t)}{\partial x} = J_y. \tag{4.14}$$

In the air above the model, however, the current is zero so this expression reduces to,

$$\frac{\partial H_x(t)}{\partial z} = \frac{\partial H_z(t)}{\partial x}. \tag{4.15}$$

This relation suggests that the vertical derivative of the horizontal field may be substituted for the horizontal derivative of the vertical field in equation (4.12) to remove the contact effect.

Our strategy for using this expression is first to obtain $\partial H_x(t) / \partial z$ in generalized coordinates that include the conductance, S, of the surface contact layer and the distance to the edge, X. This allows the profiles for the truncated thin-sheet models to be reduced to a single set of curves. From these curves a set of correction curves can be derived by numerically approximating the integral in equation (4.12). This correction term can then be added to the observed data to remove the effect of the

surface contact. To apply these corrections to a field sounding, we must first use one of the methods described above to obtain the conductance S of the contact layer and the distance x from the source to the edge.

To obtain this vertical gradient we constructed a scale model coil system with an additional coil (gradient coil) situated 6 mm above the horizontal field sensor. The vertical derivative of the horizontal field is approximated by taking the difference between the horizontal field coil and gradient coil and dividing by the vertical separation. At a scale of 1/10,000 the gradient coil is approximately 60 m above the horizontal field sensor so this approximation will not be valid at times when the induced current is close to the transmitter. For thin sheet models of conductance less than 10 Siemens, however, the velocity of the induced current ring is greater than 300 meters / millisecond so this approximation will hold for these models except at early times.

In Figure 4.23a we plot $\partial H_x(t) / \partial z$ for model G in in Table 4.1 against a normalized distance, X_n , given by,

$$X_n = \frac{\mu SX}{t} \qquad (4.17)$$

In these coordinates, all $\partial H_x(t) / \partial z$ profiles for the truncated sheets collapse to a single set of curves. We can use these curves to obtain a set of correction curves by approximating the integral in equation (4.12) using Simpson's rule. The correction curves are given in Figure 4.23b.

To use this information to correct a field sounding we first determine the normalized distance X_n using the method described above. Knowing this we can obtain the correction values for the necessary observation times from Figure 4.23b. To test this scheme we apply it to some scale model data. Let us take a vertical field transient 200 m from a contact and compare it to one for a station 5 km from the edge (denoted *base*, in Figure 4.24a.) The difference between these transients is the anomaly due to the contact. As shown in Figure 4.24b, applying the correction curve to the transient near the edge almost completely eliminates the effect due to the contact.

We now take this process a step further and correct all of the soundings on a profile, station by station, to remove the contact effect from the data. By doing this we essentially strip away the contact
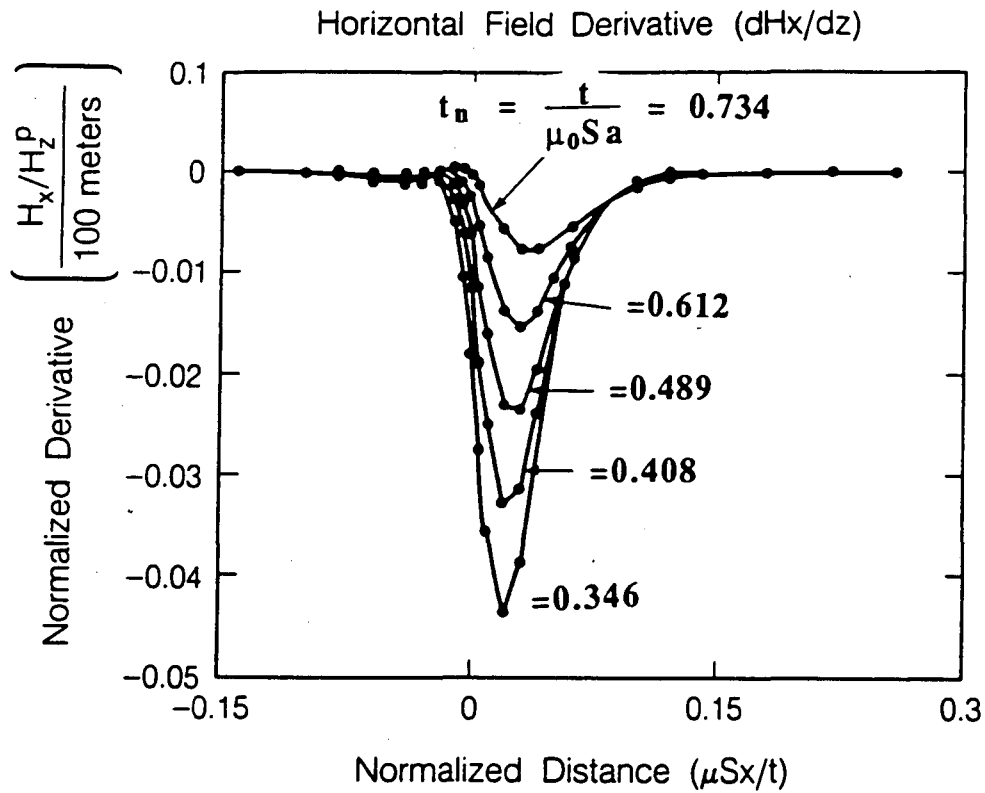
Horizontal Field Derivative (dHx/dz)

$$t_n = \frac{t}{\mu_0 S a} = 0.734$$

=0.612

=0.489

=0.408

=0.346

Normalized Derivative $\left(\dfrac{H_x/H_z^p}{100 \text{ meters}}\right)$

Normalized Distance (μSx/t)

Figure 4.23a Plot of $\partial H_x(t) / \partial z$ curves against normalized distance $X_n = \mu Sx/t$.

Contact Correction

$$t_n = \frac{t}{\mu_0 S a} = 0.346$$

=0.408

=0.489

=0.612

= 0.734

Normalized Magnetic Field (H_z/H_z^p)

Normalized Distance (μSx/t)
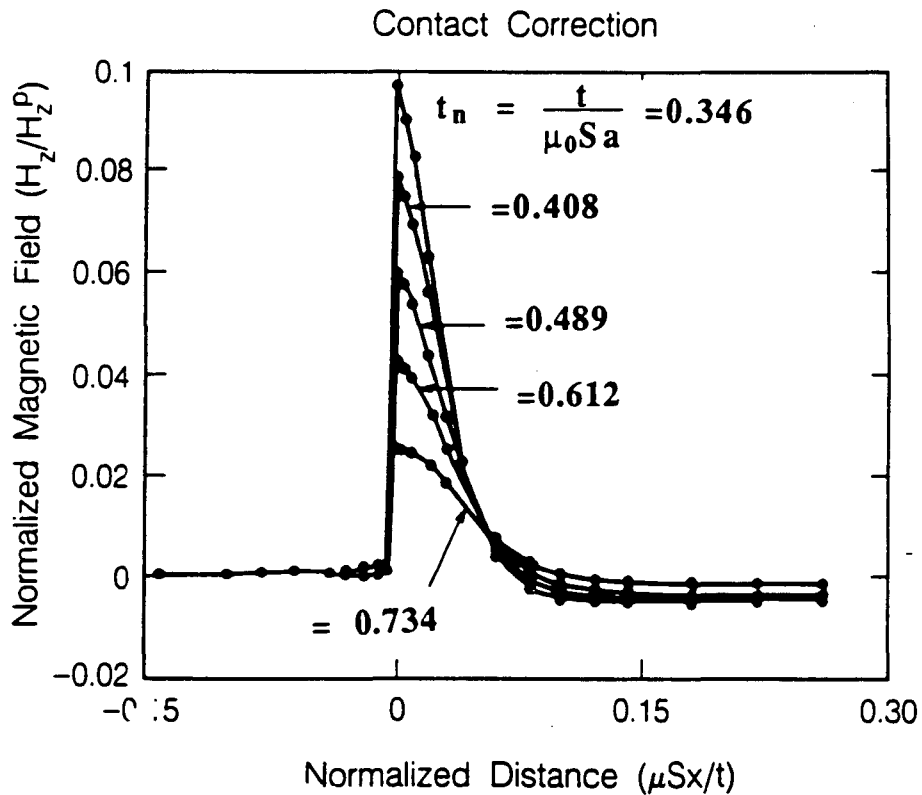
Figure 4.23b Plot of the correction curves for Figure 4.23a.
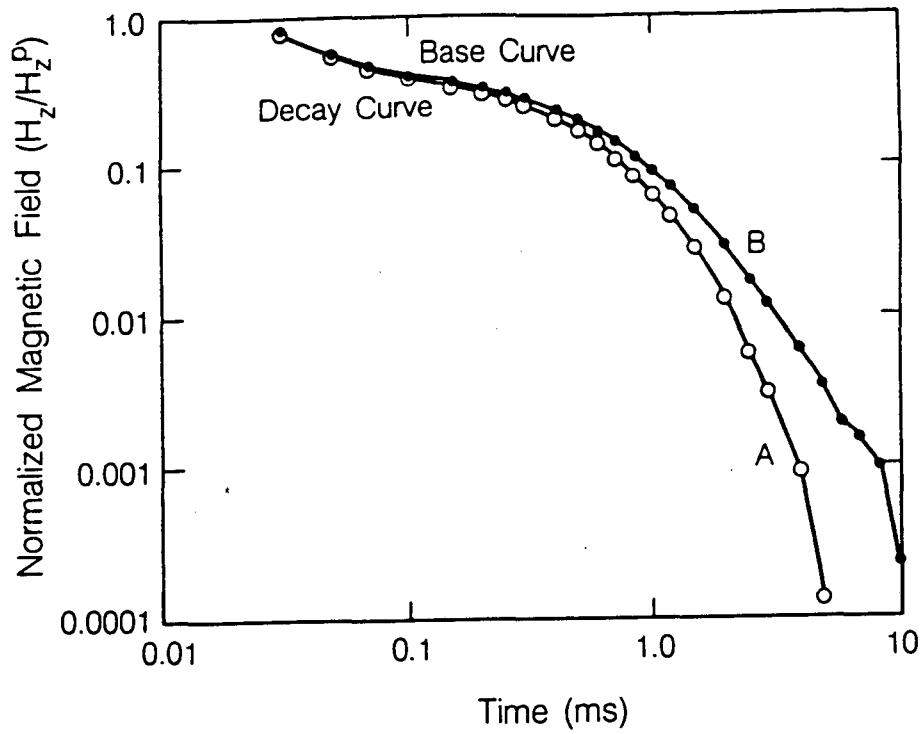
Figure 4.24a Vertical field sounding located 200m from the contact compared to a sounding *base*, 5 km from the edge. Soundings are for model G Table 4.1.
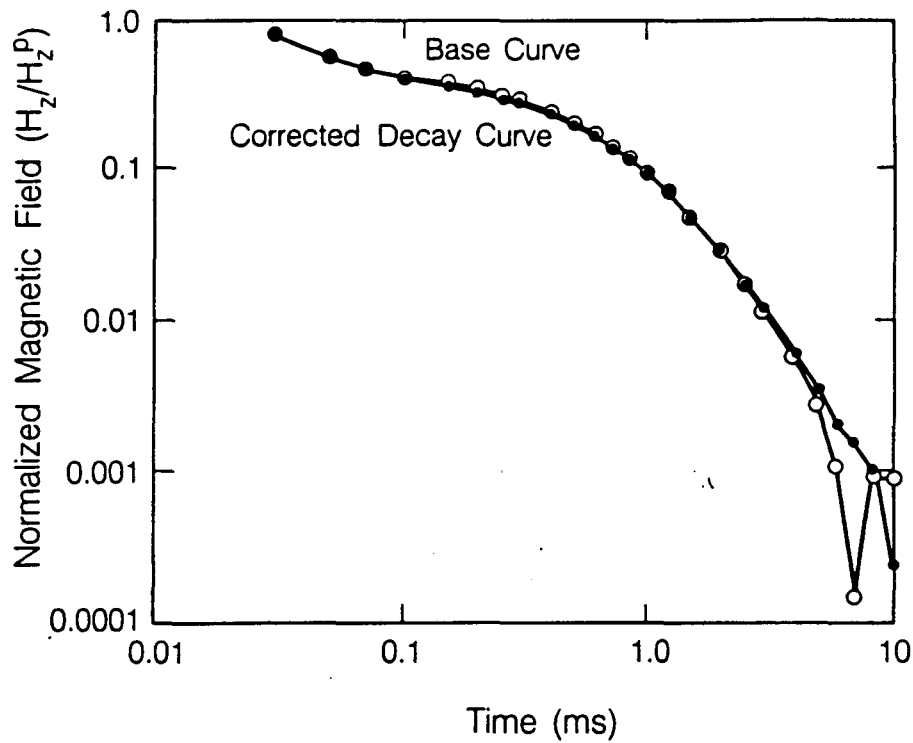

Figure 4.24b Corrected sounding compared to *base* sounding.

anomaly so that the appropriate layered response is revealed for the entire profile. Figure 4.25a shows mid-time vertical field profiles for model G (table 4.1); Figure 4.25b shows the same profiles but with the contact correction applied. The corrected profiles show little effect of the contact except for some noise at the earlier times and for stations adjacent to the contact. In these cases the finite difference approximation for $\partial H_x(t) / \partial z$ is probably not very accurate.

Although we have now demonstrated that the contact effect can be removed for truncated sheet models, of greater interest is the separation of contact effects from an anomaly due to a three-dimensional target body. Since the simplest form of anomaly separation is subtraction, we are interested to know if the anomalies from contacts and other features are additive, i.e. whether the super-position principle holds. Spies and Parker (1984) examined whether the superposition principle is valid for cases of a vertical plate-like conductor located beneath overburden and adjacent to contacts. From scale model results they concluded that superposition holds for the central-loop configuration even for cases when the overburden is in electrical contact with the target body.

To further test our scheme for contact removal we added a deep block-like conductor to the contact model (Figure 4.26). The body is positioned 60 m beneath the overburden and centered 300 m from the edge. The vertical field response of this body beneath the overburden, but well away from the contact, is given in Figure 4.27a; the vertical field anomaly with the overburden response subtracted is given in Figure 4.27b. This figure shows that the anomaly is approximately 0.5 percent of the free-space primary field and only about 15 percent of the observed field at 1 ms. In Figure 4.27c the horizontal field for the model is shown. Because the horizontal field is not coupled to the overburden the anomaly from the target is clear, although it is also low in amplitude.

The vertical field profiles over the model shown in Figure 4.26 are given in Figure 4.28a. The profiles are dominated by the contact response and do not show much evidence of the conductive body (compare with Figure 4.27a). Stripping away the contact anomaly, using the procedure outlined above, results in the profiles shown in Figure 4.28b. Here the presence of the body is a more evident but the profiles are still dominated by the overburden layer response. If we now subtract away the overburden response (Figure 4.28c), the anomaly is similar in shape and size to Figure 4.27b, although it is noisier.
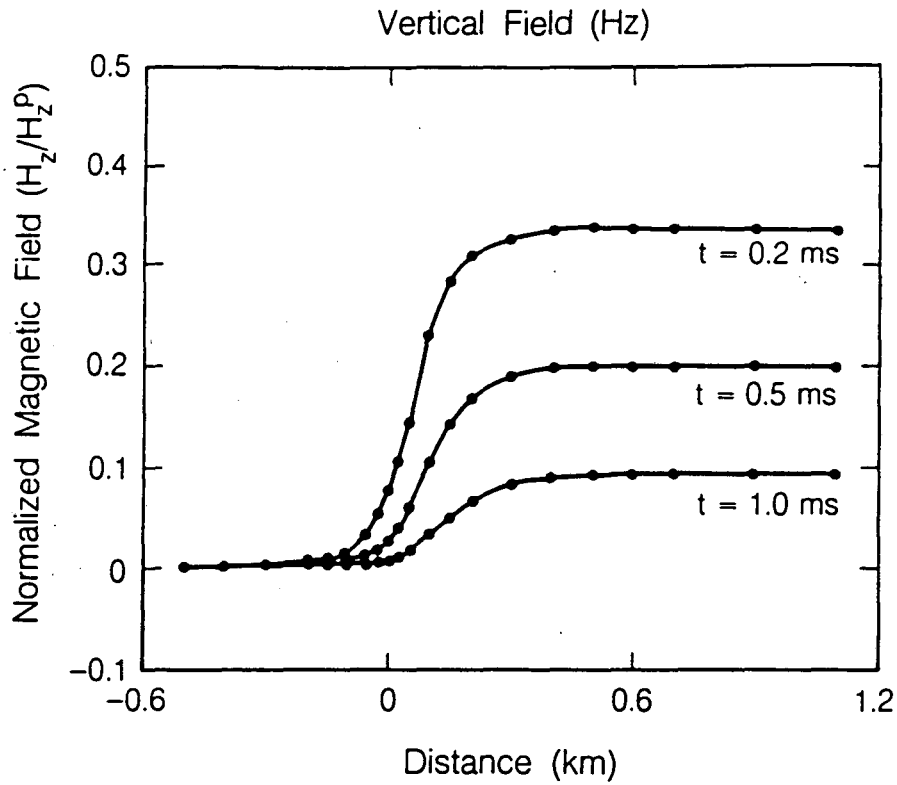
Vertical Field (Hz)

Figure 4.25a Early and middle time vertical magnetic field profiles over contact model G in table 4.1.

Corrected Vertical Field (Hz)
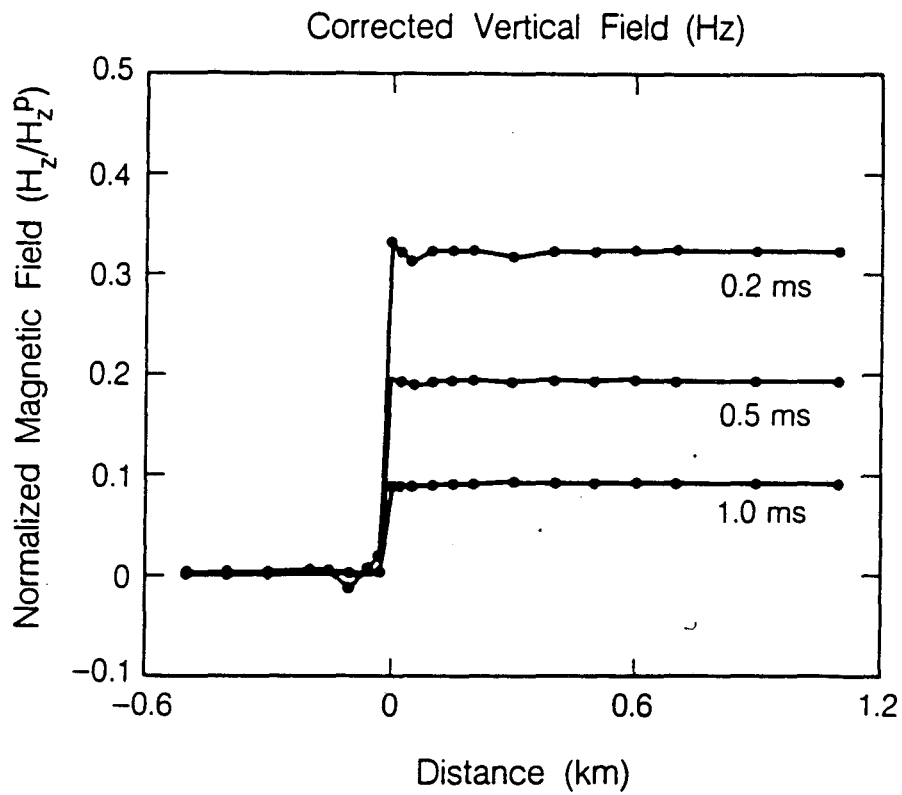

Figure 4.25b Early and middle time profiles with the contact correction applied.
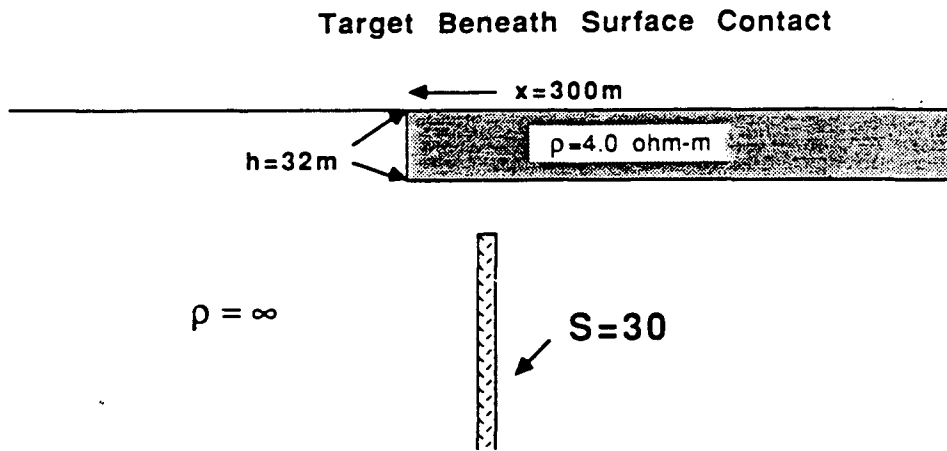
Target Beneath Surface Contact
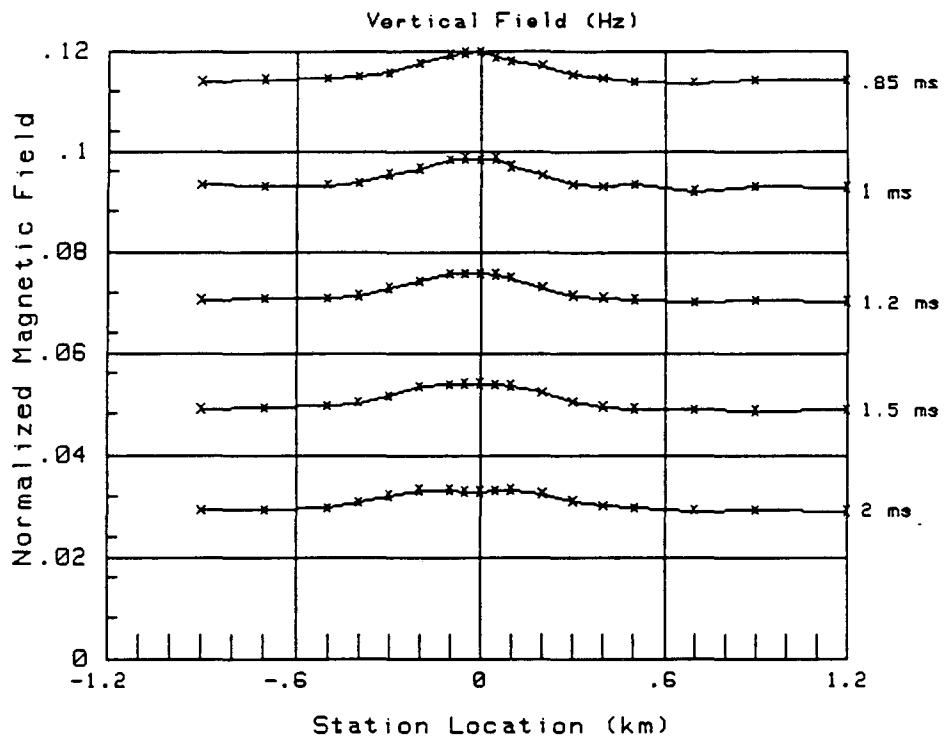

Figure 4.26 Model of a deep conductor beneath surface contact.

Figure 4.27a The vertical field response of the target body in Figure 4.26. beneath a uniform overburden layer.
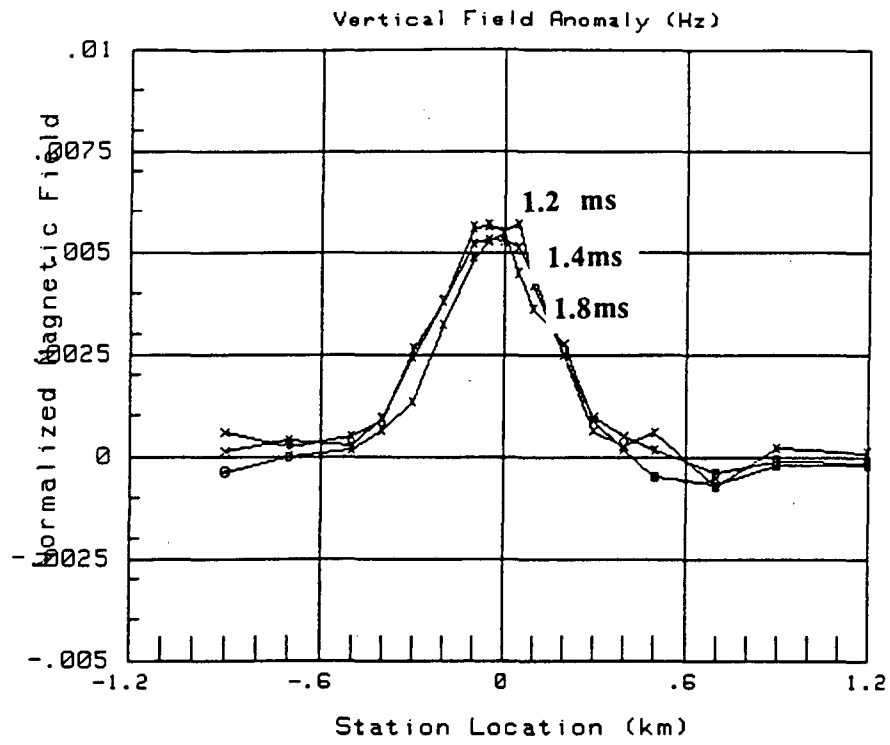
Figure 4.27b Vertical field anomaly with the background response removed.
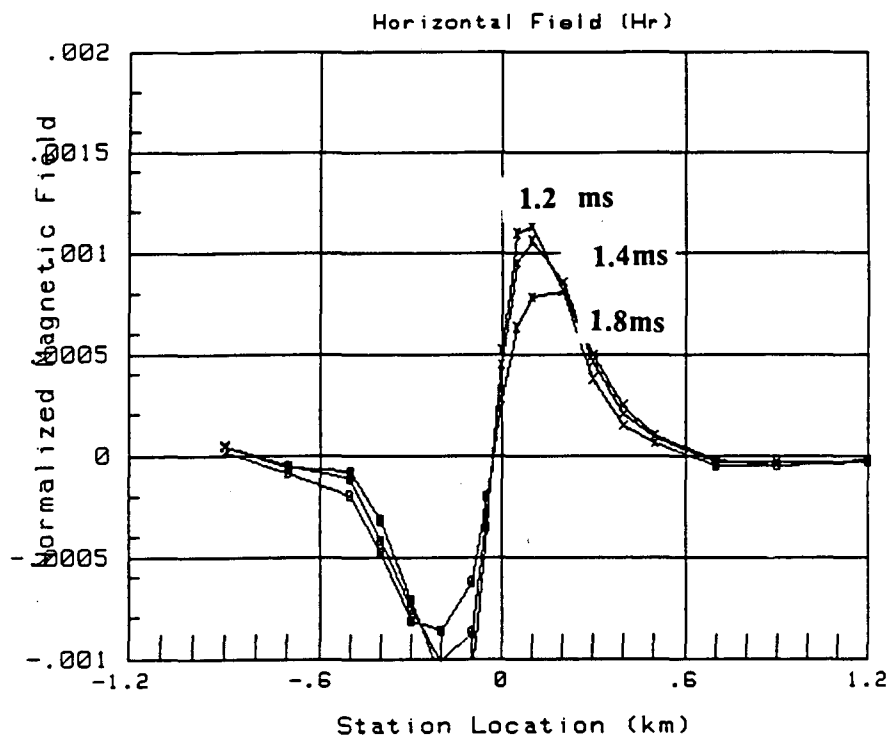

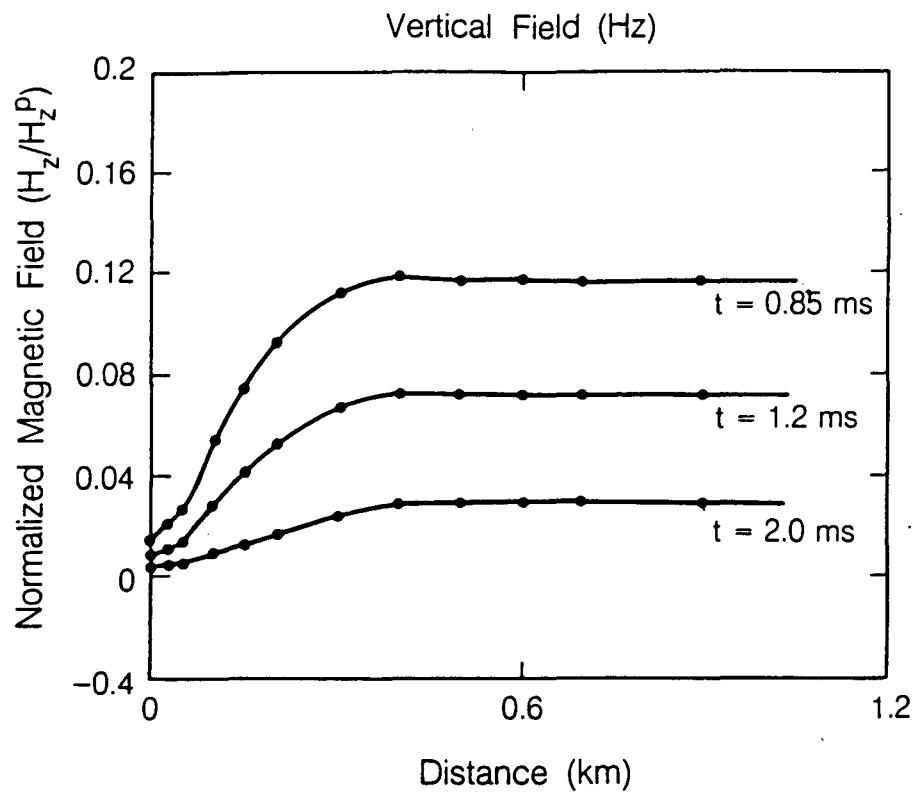Figure 4.27c Horizontal field anomaly over the target body

Vertical Field (Hz)

Figure 4.28a Vertical field time profiles over contact model shown in Figure 4.26.

Corrected Vertical Field (Hz)
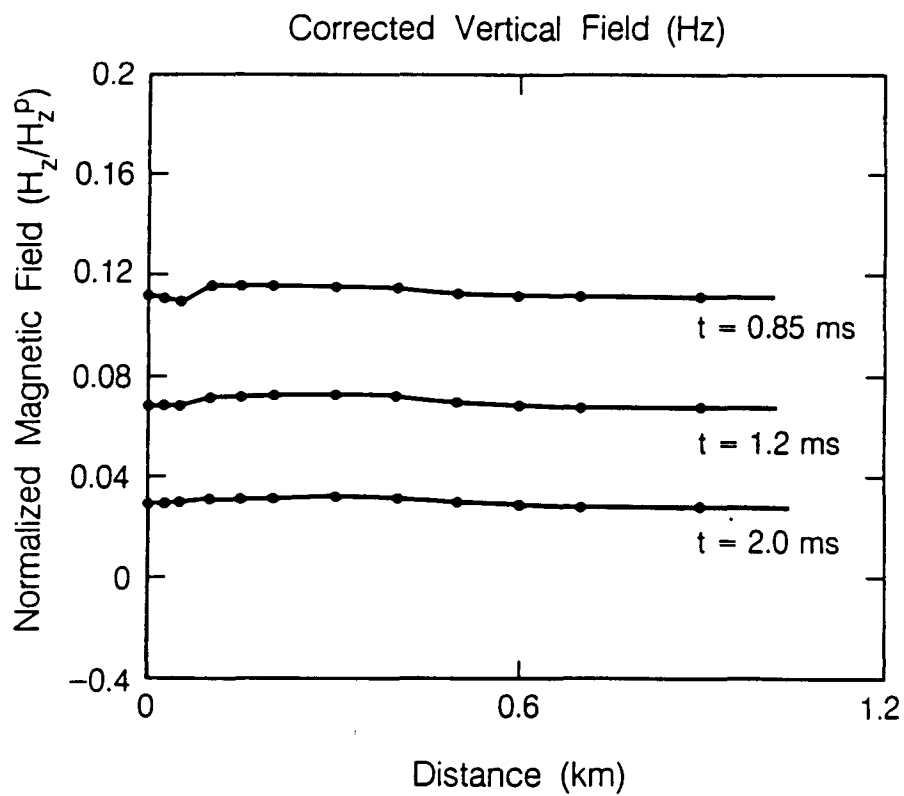
Figure 4.28b Vertical field time profiles for model with the contact correction applied.
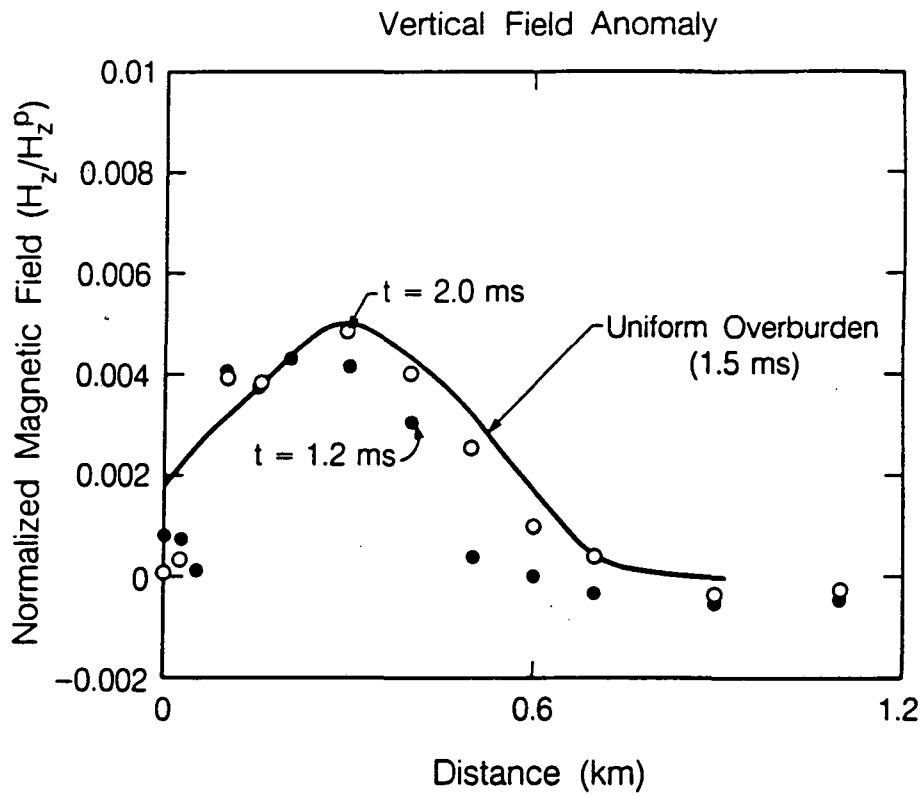
Vertical Field Anomaly

Figure 4.28c Vertical field time profiles for the model with the contact and background responses removed.

This last figure is remarkable if we consider that the anomaly due to the deeper body is less than 15 percent of the contact anomaly and yet it can be reasonably recovered by stripping away the anomaly due to the contact.

4.3 Horizontal Gradient of the Vertical Field

Of the large number of existing central-loop soundings only a small percentage have involved the measurement of the horizontal field component in addition to the usual vertical field measurement. Actually in most surveys only the time derivative of the vertical field (voltage response) is measured. The result is that for these data little of the analysis developed above for the horizontal field has much application. If a series of adjacent central-loop soundings are collected as a profile, however, a quasi-gradient of the field quantity may be constructed. This is made by taking the field difference between adjacent soundings at equivalent time windows and dividing by the station separation. This horizontal "gradient" will only be nonzero if there are lateral variations in conductivity in the profile direction; it should therefore be useful in interpreting these variations.

Because the gradient profiles are similar in appearance to horizontal field profiles, we might expect that this data could be interpreted with much the same approach as was used for the horizontal fields. In this section we develop methods for interpreting vertical field (voltage) TDEM data near contacts that can readily be applied to existing field profiles without much data manipulation. The analysis is given for the horizontal gradient of the vertical field voltages, a quantity that can be easily calculated from the voltages provided by most commercial field instruments.

4.3.1 Numerical Calculations using Program SHEET

For many of the truncated sheet models we found that obtaining the impulse response data from the scale model results is too noisy due to the additional data processing required. To determine the impulse response of the horizontal gradient of the vertical field, for example, we are required to take numerical derivatives of the scale model results in both time and space. As the calculation of each numerical derivative adds noise, this procedure is unsatisfactory for all but the most conductive models. For most of the truncated sheet models we therefore use a numerical code to calculate these responses.

Program SHEET is a FORTRAN code for calculating the vertical and horizontal transient response for a finite loop over a conducting half-plane in air (Weidelt, 1983). The program calculates the secondary vertical and horizontal magnetic fields, for impulse excitation, within or exterior to a finite loop source situated over an arbitrarily dipping truncated sheet. It may also be used to calculate the coincident loop response that is used with the SIROTEM system (Buselli, 1982). The program uses the Wiener-Hopf technique to calculate the response in the frequency domain and uses free-decay modal expansion (instead of Fourier transformation) to calculate the transient response from the harmonic results (Weidelt, 1983).

In Figure 4.29 we compare transient results from program SHEET to numerically differentiated scale model data. The model is a 16 m sheet with a resistivity of 4.6 ohm-m (S=3.52); the transients are shown for a station 300 m from the edge of the sheet on the conductive side. The observations match the computed voltages fairly well, suggesting that the numerical and scale model results can be used interchangeably for the present analysis.

In the section below we examine the horizontal gradient responses for several truncated sheet models. From an analysis of these data we develop some tools that may be applied to field profiles; these will be illustrated in Chapter 5.

4.3.2 Using the Horizontal Gradients to Determine Contact Characteristics

It was shown above that the position of the peak value of the horizontal field transient and its late time slope can be related to the conductance of a truncated sheet and the distance from the source to the edge. In a similar manner the same characteristics for the horizontal gradient of the vertical field transient may also be also related to the contact parameters.

A plot of the horizontal gradient voltage at a site 300 m inward from the edge of a truncated layer is given in Figure 4.30. This transient forms a positive peak at about t=0.5 ms before decaying exponentially at late time. It is similar in appearance to the horizontal field voltage transients described by Dallal (1985).
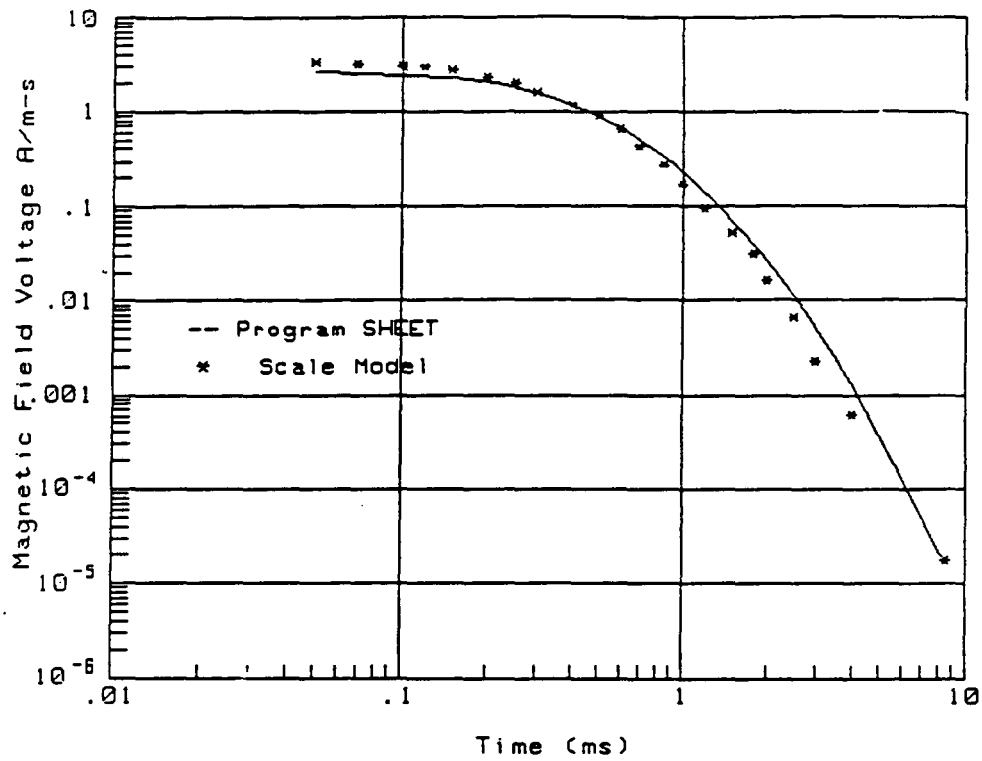
Figure 4.29 Comparison of the vertical field transient from program SHEET to scale model results. The transients are for a station located 300m from the edge.
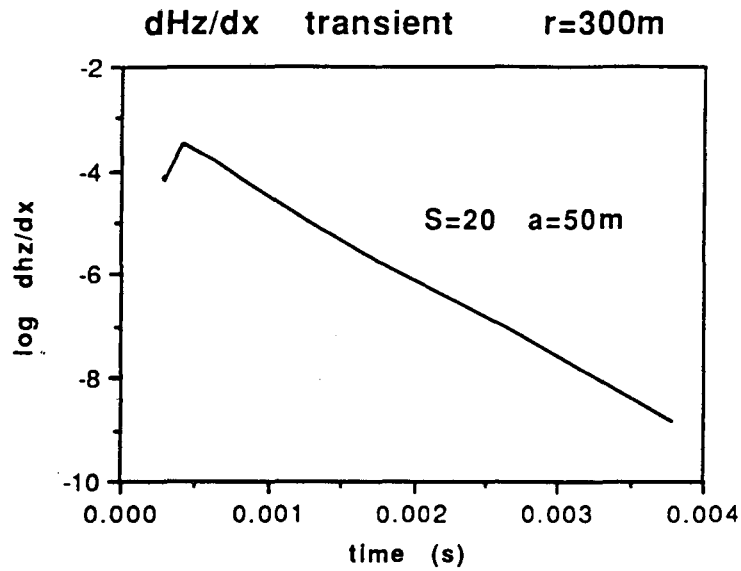
Figure 4.30 Horizontal gradient (psuedogradient) transient voltage for a station 300m inwards from the edge of a 20 S truncated sheet.
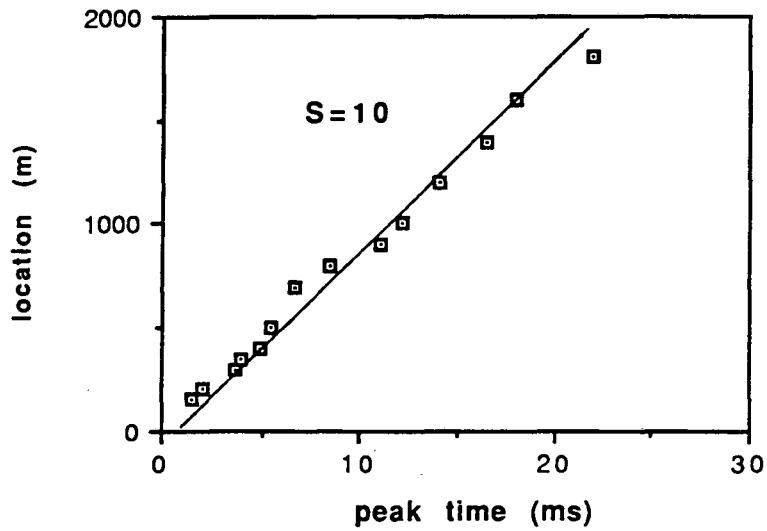

Figure 4.31 Pseudogradient transient peak velocity over a 10 S truncated sheet.

We plot the position of the horizontal gradient positive peak as a function of lag time for a truncated sheet with a conductance of 10 S in Figure 4.31. The velocity of the gradient peak is slightly slower than the horizontal field transient peak; this quantity was empirically found to be

$$V = \frac{1.5}{\mu_0 S}.$$

Note that whereas the velocity of the horizontal field peak may be physically related to the movement of induced currents in the sheet this last relation is simply an empirical result.

The time constant of the horizontal gradient transient is plotted against distance to the edge in Figure 4.32. We have empirically found that this data can be fit to a function given by

$$\tau_1 = \frac{\tau}{\mu_0 Sa} = 0.5(X/a) - 0.5$$

where X is the distance from the center of the loop to the edge and a is the loop radius. Note that this expression is only slightly different from that given for the horizontal field time constant in equation 4.3.

The horizontal gradient time profiles over a truncated sheet are similar in appearance to the horizontal field profiles of Figure 4.2. That is, they form a series of peaks that diminish in amplitude and are centered further from the edge with increasing lag time. We can plot the position and amplitude of these profile peaks against lag time for the gradient data, much as we did for the horizontal fields, to derive relationships to determine sheet conductance and distance to the edge. In Figure 4.33 we show the position of the gradient voltage peaks as a function of lag time for a truncated sheet with a conductance of 5 S. The velocity of the gradient voltage peak is given by

$$V_{gradient} = \frac{0.4}{\mu S}.$$

The amplitude of the horizontal gradient peaks is plotted against normalized time $t_n = \frac{t}{\mu_0 Sa}$ for a truncated sheet model in Figure 4.34. This master curve may be used with gradient data in much the same manner as the earlier curves could be used with horizontal fields. Note that at late-time the gradient voltage decays as t^{-5}.

The above analysis shows that the horizontal gradients of the vertical field for the central-loop
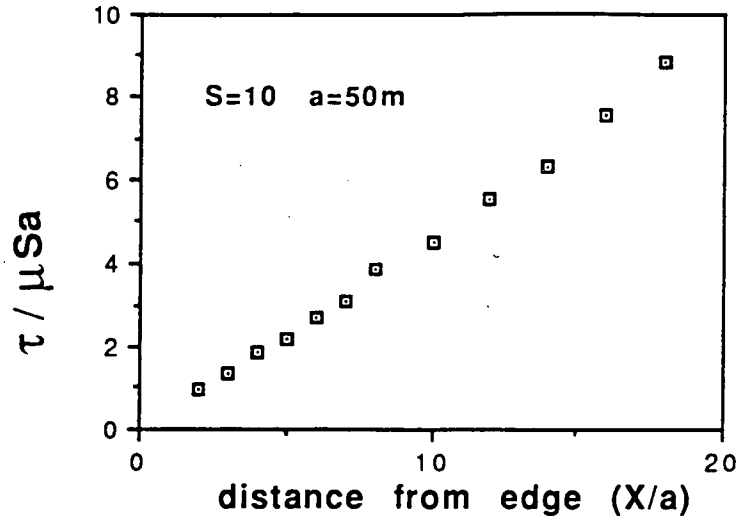
Figure 4.32 Pseudogradient normalized time constant for a truncated sheet.
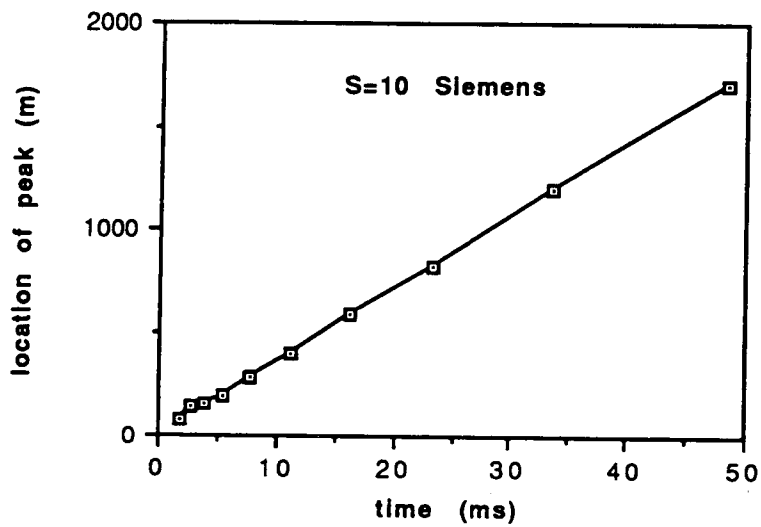

Figure 4.33 Pseudogradient profile peak velocity for a 10 S truncated sheet.
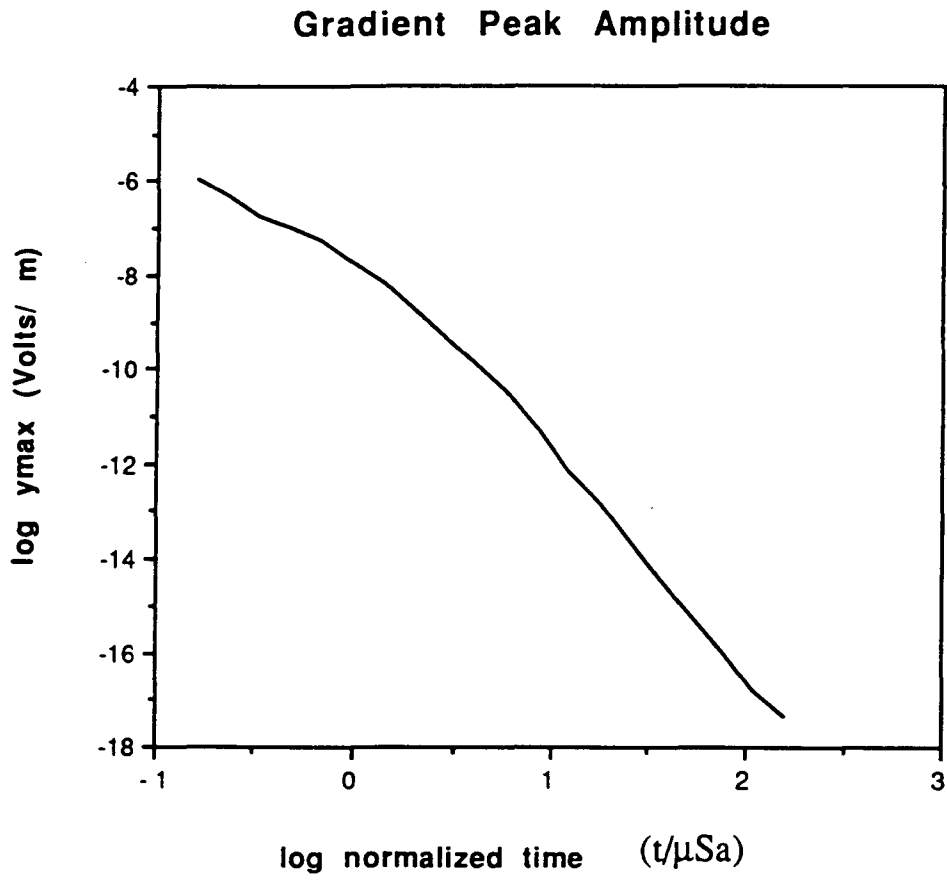
Gradient Peak Amplitude

Figure 4.34 Normalized pseudogradient peak amplitude for a truncated sheet.

profiles may be used in much the same manner as the horizontal fields if several conditions are met. First the gradients must be measured normal to a two-dimensional contact and secondly the stations must be spaced 0.5 to 1.0 loop diameters apart for an accurate calculation of the gradient. In many cases these are reasonable conditions; for such data some of the techniques described above can be applied and we will do so in Chapter 5.

CHAPTER 5: FIELD EXAMPLES

In this chapter we apply some of the methods developed in Chapters 3 and 4 to interpret field data collected over geological contacts. The goal is to demonstrate the techniques and, when possible, to provide some new information or clarify the existing interpretation.

The field data were obtained from published literature (Irvine and Staltari, 1984), from unpublished field surveys collected by exploration companies and from a survey made by the author. Each field example presents a different interpretational problem. All the surveys considered utilize the central-loop or coincident-loop system and/or and the fixed-loop configuration. No field data were available for the electrical dipole system.

5.1 Case 1: Brittania Prospect: Queensland, Austrailia

In Chapter 1 we showed some field profiles from an excellent case history paper by Irvine and Staltari (1984) to illustrate a contact effect that could be mistaken for a vertically dipping sheet-like conductor. In fact, the data, which were collected over the Brittania prospect in Queensland, Australia, were initially interpreted as a vertically dipping sheet. After a series of fruitless drillholes and additional surface EM surveys, however, it was discovered that a surface contact was the main cause of the anomaly. In their conclusions Irvine and Staltari (1984) suggested that in areas of conductive surface layers TDEM prospecting should include coincident loop profiles and fixed-loop profiles made from several loop positions. They state that from this combination of field surveys contact anomalies can readily be distinguished from other anomalies of interest.

Although in many cases the field data profiles over a contact model can resemble those over a vertically dipping sheet (Spies and Parker, 1984), we showed in Chapter 3 that the field "anomaly" never does. In free-space, vortex currents are induced in the plane of a vertically dipping sheet, and the field from these currents may be approximated by a horizontal dipole (McNeill et al. 1984). For a surface thin-sheet contact we showed in Chapter 3 that the anomalous current flows in a horizontal plane and this field more closely resembles a vertical dipole. These the two "anomalies" have distinct signatures and it is a straightforward matter to distinguish between them.

In Figure 5.1 we show fixed-loop vertical field (voltage) profiles along section A-A' over the Brit-tania prospect for lag times from 2.2 to 3.4 ms. The north-south profile trends directly across the main target area. The data were collected using the EM-37 field system (McNeill, 1982) with a 300 by 600 m fixed-loop transmitter centered at station 9450. The figure indicates that the vertical field at these lag times changes polarity at about the same point (near station 9750). This is a characteristic response over a vertically dipping sheet. The zero-crossing in the vertical field for a vertically dipping sheet is due to the fact that the propagation of induced currents has been arrested by the presence of a good conductor; the currents are flowing in vortexes in the vertical plane as they decay.

In areas of conductive overburden a surface contact may be distinguished from a vertically dip-ping sheet if the effect of the surface layer is first removed; otherwise, as shown by Spies and Parker (1984), the responses are easily confused. By subtracting the response of a uniform overburden from the field data the residual may be compared to a contact anomaly or that due to a vertically dipping sheet and as shown in Chapter 3 they are distinct. In the case of the Brittania prospect the resistivities and thicknesses of the surficial sediments are known from a series of Schlumberger resistivity sound-ings. We used the rersistivity data as input to a computer code to generate the fixed-loop response over a layered model for an equivalent configuration to the field data. The layered model calculations were made using program RECTEM (Raiche, 1986).

The calculated data for the appropriate layered models are shown in Figure 5.1b. Note that these data do not show the stationary zero-crossing observed in the field data (Figure 5.1a). In fact, the zero-crossing migrates away from the source with time. However, the magnitude of the model data is simi-lar to that of the field data which suggests that the resistivity model is reasonable.

In Figure 5.2 we plot the difference between the model and field profiles (residual anomaly). The residual profiles are a series of negative anomalies centered over station 9825; these differ from vertical field profiles over a dipping sheet, which would show a crossover anomaly. The data shown in Figure 5.2 are similar to the anomaly profiles produced by a vertical dipole source over a flat-lying truncated sheet that were observed in Chapter 3. These scale model data showed that the edge is located directly beneath the maximum anomaly. Extending these results to the Brittania data we
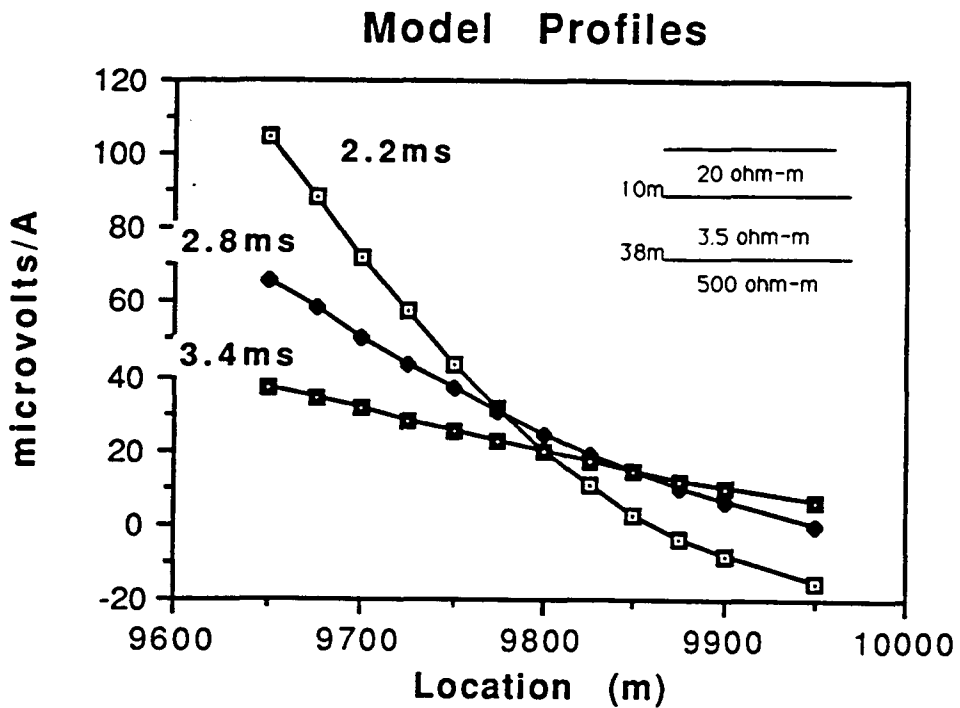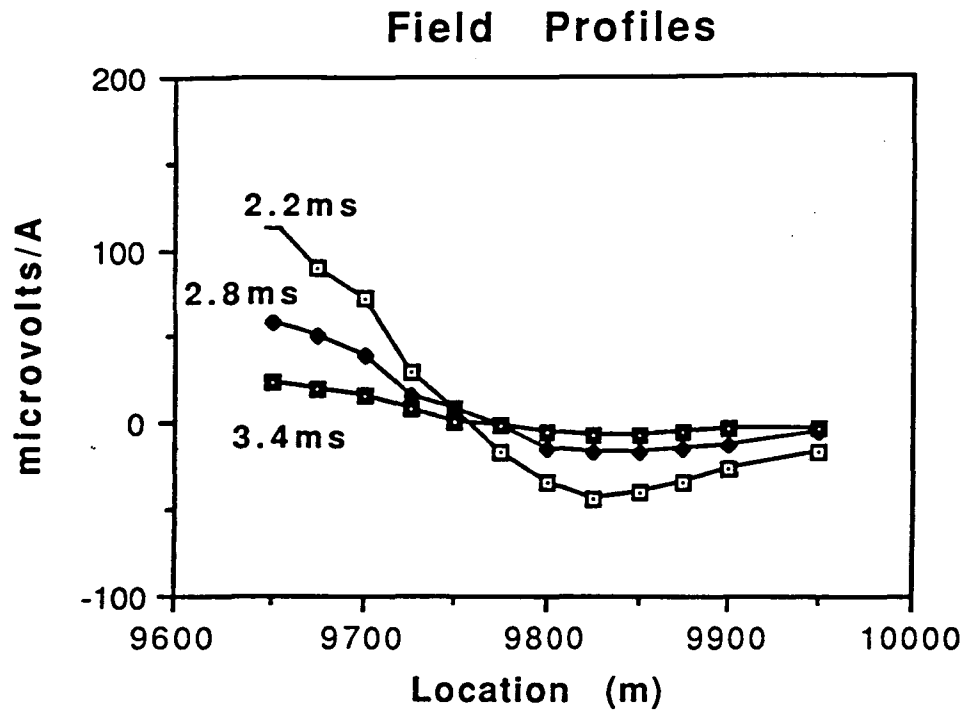
Field   Profiles

Model   Profiles

Figure 5.1a) Fixed loop vertical field profile for line A-A' over the Brittania prospect, Queensland,

Australia (after Irvine and Staltari, 1984). b) Fixed loop model response for the same configuration as
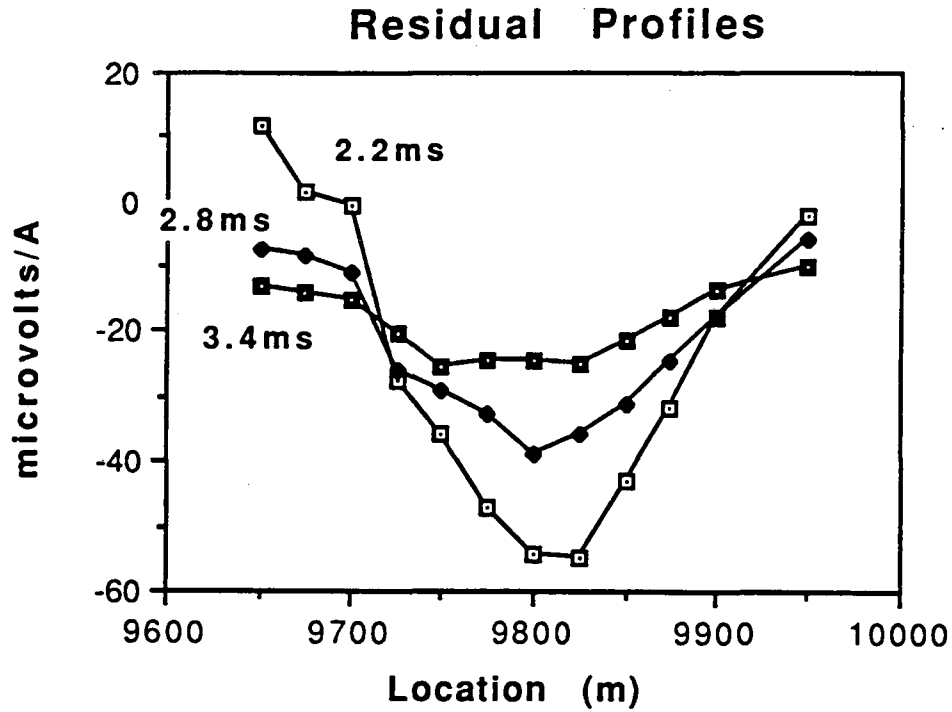
above.

Residual Profiles

Figure 5.2 Residual profiles for the data given in Figure 5.1. The residual is defined as the field profiles (Figure 5.1a) minus the model profiles (Figure 5.1b).
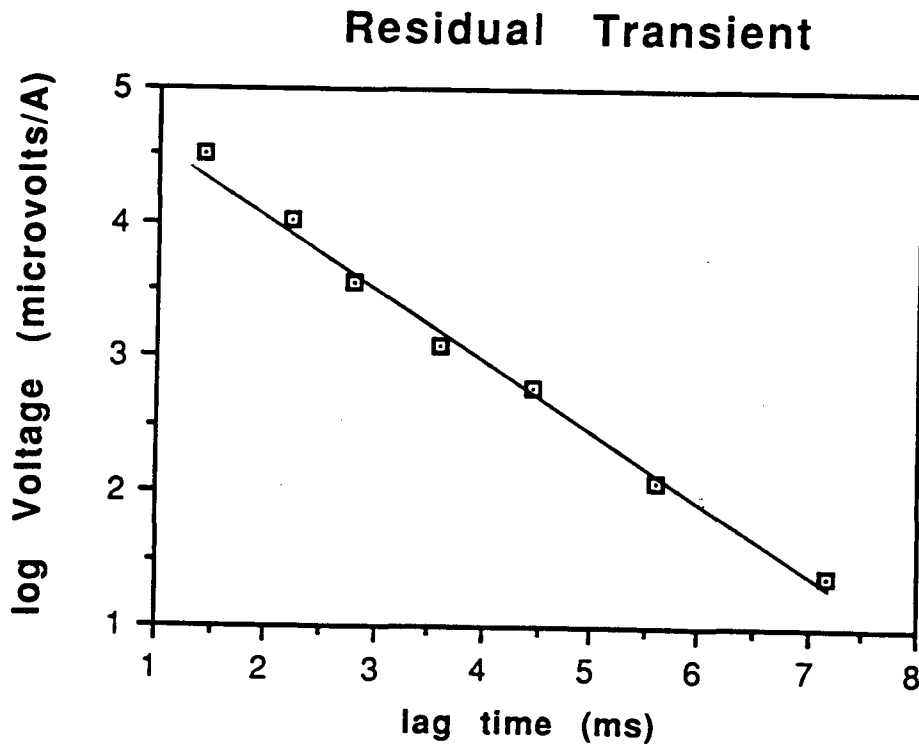
Residual Transient

Figure 5.3 Residual transient for station 9825. The data is fit to an exponential function with a time constant $\tau = 1.4$ ms.

estimate that the contact is located near station 9825. This estimate for the contact location is in close agreement with its interpreted location based on the combined interpretation given in Irvine and Staltari (1984).

In Chapter 3 we also showed that the residual anomaly for a 400 m x 800 m fixed-loop source near a contact should have an exponential form with a time constant given by

$$\tau = \frac{\mu S (X+D)}{3}.$$

Where X is the distance from the loop center to the edge and D is the distance from the receiver to the contact. In Figure 5.3 we plot the residual anomaly for station 9825 on a semilogarithmic plot. The data have a linear slope and with a time constant of 1.4 ms. The distance from the loop center to the edge is 375 m the distance from the receiver to the edge is zero. Solving for S in the above equation and substituting in the above information we can compute the conductance,

$$S = \frac{3\tau}{\mu(X+D)} = \frac{3x(0.0014)}{375 \ x \ 4\pi \ x \ 10^{-7}} = 8.91 \ Siemens.$$

This value is in close agreement with the value for the second (conductive) layer published in the paper based on the Schlumberger resistivity and coincident loop EM interpretations. This indicates that the truncated layer lies beneath the surficial sediments.

Irvine and Staltari (1984) stated that of all the surveys conducted at Brittania, the coincident loop data was the most diagnostic of the contact effect; they also stated, however, that this is not the preferred method for ore prospecting. As shown in Chapter 4, central-loop or coincident-loop profiles show a simple level adjustment across a contact so the edge effect is not so ambiguous as it was for the fixed-loop system. From these profiles, however, it is not clear where is the exact location of the contact nor is the conductance or conductivity contrast for the truncated layer obvious. We showed in Chapter 4, however, that by examining the horizontal gradient of the vertical field this information may be easily obtained.

We plot the coincident loop data and its horizontal gradient for profile A-A' in Figures 5.4a and 5.4b. The gradient data were computed from the coincident loop fields using a forward difference

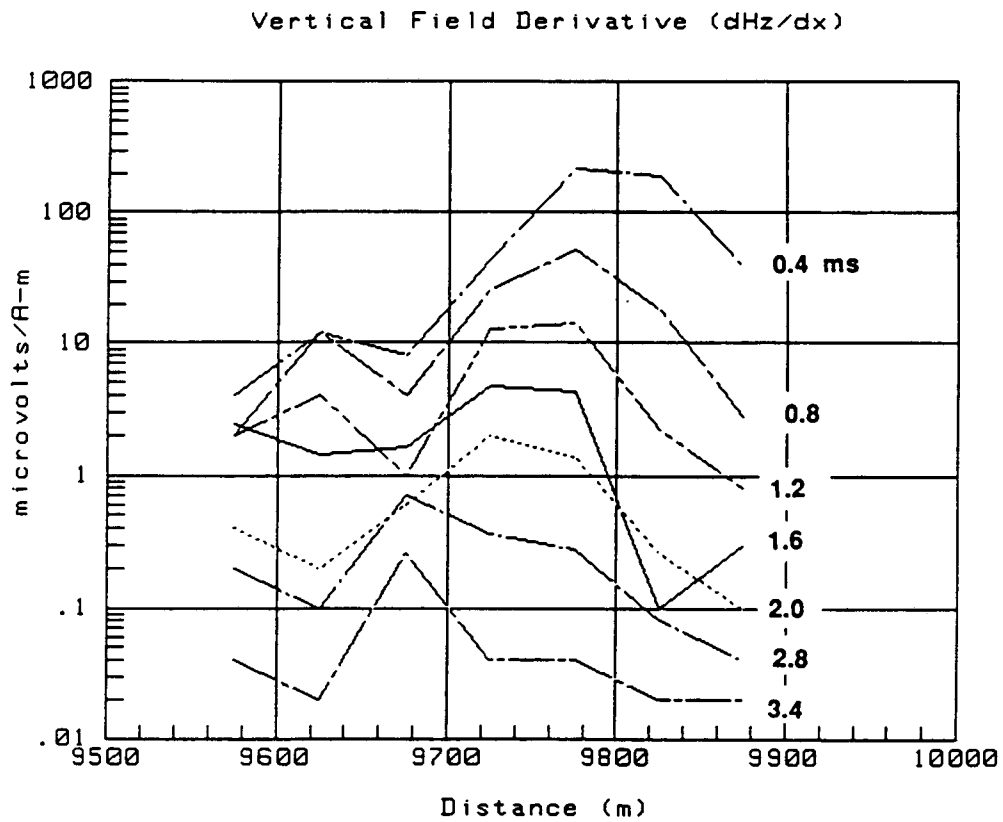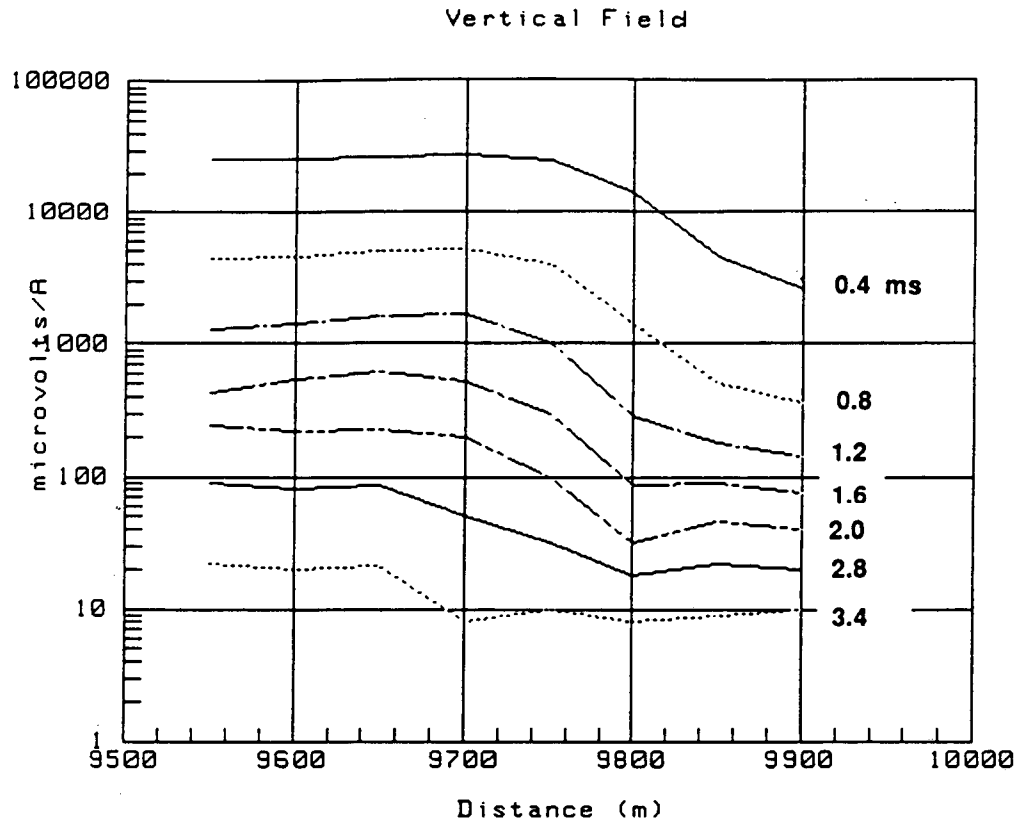Vertical Field

Vertical Field Derivative (dHz/dx)

Figure 5.4a Coincident loop time profiles over line A-A' and b) horizontal gradient of the coincident loop data.

scheme. The coincident loop profiles show a simple field level change across the contact which is characteristic of a surface contact; the gradient profiles form a series of peaks that migrate inwards from the contact at later and later times. The resulting profiles are similar in appearance to the scale model data shown in Chapter 4. In that chapter we suggested that the conductance of the surface layer may be obtained by plotting the location of the peak against the peak time; for a thin-sheet contact this plot has a linear slope. We also showed in Chapter 4 that the slope of this plot is the velocity of the peak and that the sheet conductance may be obtained from this data using the following relation

$$S = \frac{0.4}{\mu V_{pf}}$$

We plot the peak location against peak time for the Brittania horizontal gradient profiles in Figure 5.5; The slope of the plot is linear suggesting a constant velocity equal to 35,000 m/s. Applying this to the above equation we obtain a value of

$$S = \frac{0.4}{35,000 \ x \ 4\pi \ x \ 10^{-7}} = 9.1 \ Siemens$$

which is in close agreement with the value calculated for the fixed-loop profiles.

The location of the edge may be roughly obtained by extrapolating the curve in Figure 5.5 to zero lag time. This occurs near station 9825 which is also in accord with the location obtained from the fixed-loop EM data.

We showed in Chapter 4 that the peak amplitudes of the horizontal gradient profiles are also useful in determining the conductance of the layers forming the contact. We plot the peak amplitudes of the horizontal gradient profile (Figure 5.4) in Figure 5.6. Notice that this curve has the characteristic t^{-4} decay seen in Figure 4.34. The conductance on the more conductive side of the edge may be determined by matching this data to the normalized plot given in Figure 4.34. For example the peak amplitude at 2.0 ms is equal to 3.0 microvolts. Dividing by the loop area (10,000 sq. m) the normalized amplitude is 0.3 nano volts. Matching this voltage to Figure 4.34 we obtain a normalized time of 2.0. The conductance is obtained by solving the time normalization equation for S, that is

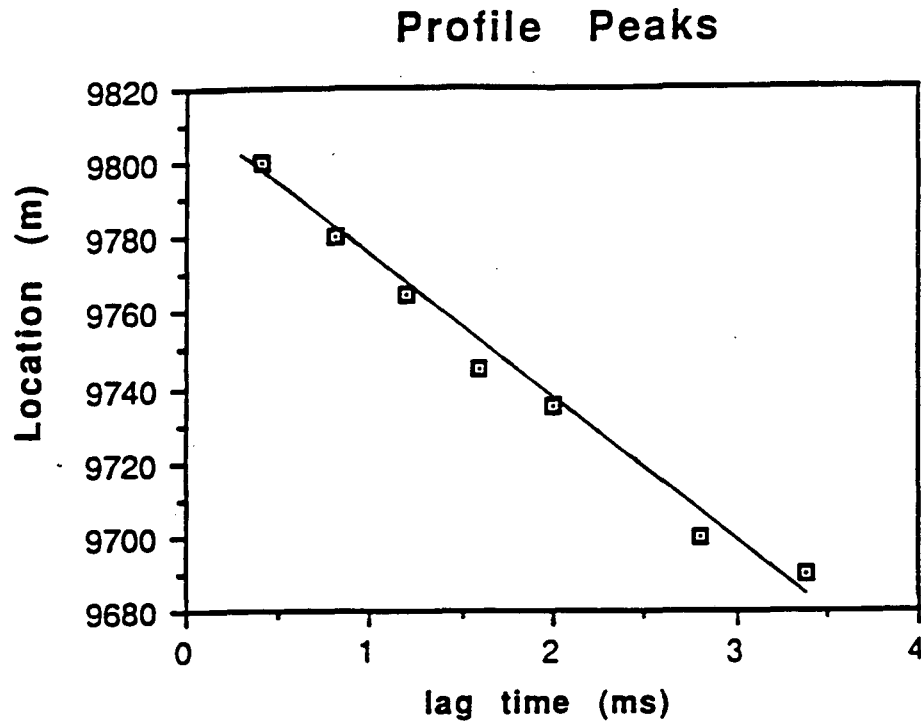$$t_n = \frac{t}{\mu S a} \qquad S = \frac{t}{t_n \mu a}$$

Profile Peaks

Figure 5.5 Location of the horizontal gradient profile peaks plotted against lag time. The slope of the plot is the velocity of the peak.

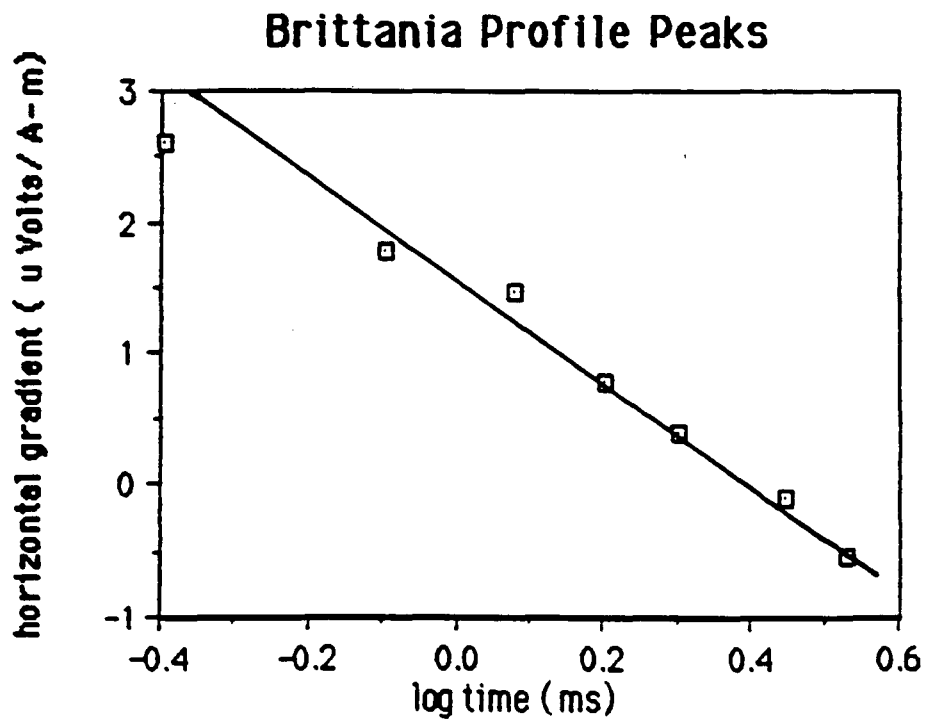## Brittania Profile Peaks

Figure 5.6 Amplitude of horizontal gradient profile peaks for profile A-A' plotted against lag time.

$$S = \frac{0.002}{1.05 \; x \; 4\pi \; x \, 10^{-7} \; x \; 56} = 9.1 \; Siemens$$

where the loop radius a is 56 m. This value is in excellent agreement with the conductance estimates given above.

In Figure 5.7 we compare our contact interpretation to the geologists subsurface model and to the section obtained from the inversion of the Schlumberger resistivity soundings. The TDEM interpretation indicates that the second (conductive) layer is truncated (or pinches out) into poorly conducting rocks near station 9825. Since the surface layer is continuous the location of the discontinuity would not be obvious from the surface geology. Notice that the Schlumberger resistivity soundings, which were expanded parallel to strike, place the contact structure near station 9900, almost 100m northwards from the EM contact interpretation.

Although it is clear that the observed EM anomaly at Brittania may almost be completely explained as an edge effect, contact structures of this type may also be interesting ore prospects. If one can accurately locate the contacts in such cases this information may be of some use in prospecting for the ore bodies. This excellent review paper has allowed us to apply some of our techniques for contact interpretation to field data. Our analysis shows that a) a contact response can be distinguished from that due to a vertically dipping sheet conductor from a single fixed-loop profile and b) the conductance of the truncated layer and edge location may be determined from the same data.

5.2 Case 2: Mapping sulfide vein deposits in the South American Andes

In the first field example the geological and conductivity structure was well known from a combination of surface geology, geophysics and drilling. For the present case only some of this information is known and the surface EM data is expected to provide the answer to a structural puzzle.

The prospect is a metallic sulfide mineral deposit in the South American Andes (Figure 5.8). Sulfide ores occur primarily in a Mesozoic rhyolitic host and at the contact between this rock and the overlying Tertiary volcanics. The northeast-southwest trending veins dip southward approximately 45 degrees near loop 1 (Figure 5.8); and appear as oxidized outcrops in the bands marked "veins".
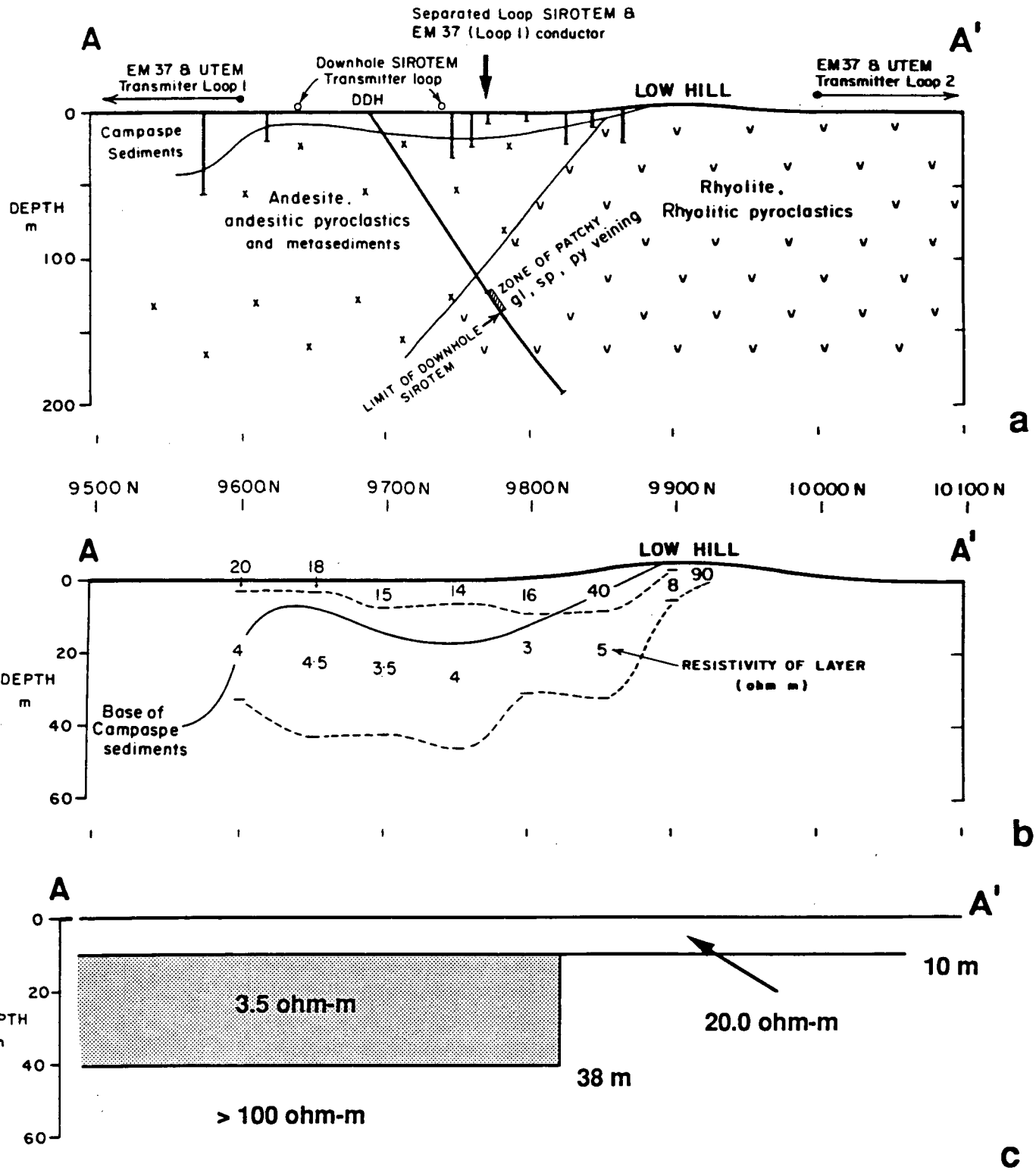
Figure 5.7 Interpreted cross section A-A' for the Brittania prospect. Parts a) and b) show the geological cross-section and the resistivity structure based on Schlumberger resistivity soundings. Part c) shows the interpreted resistivity section based on the present contact interpretation of the EM measurements.
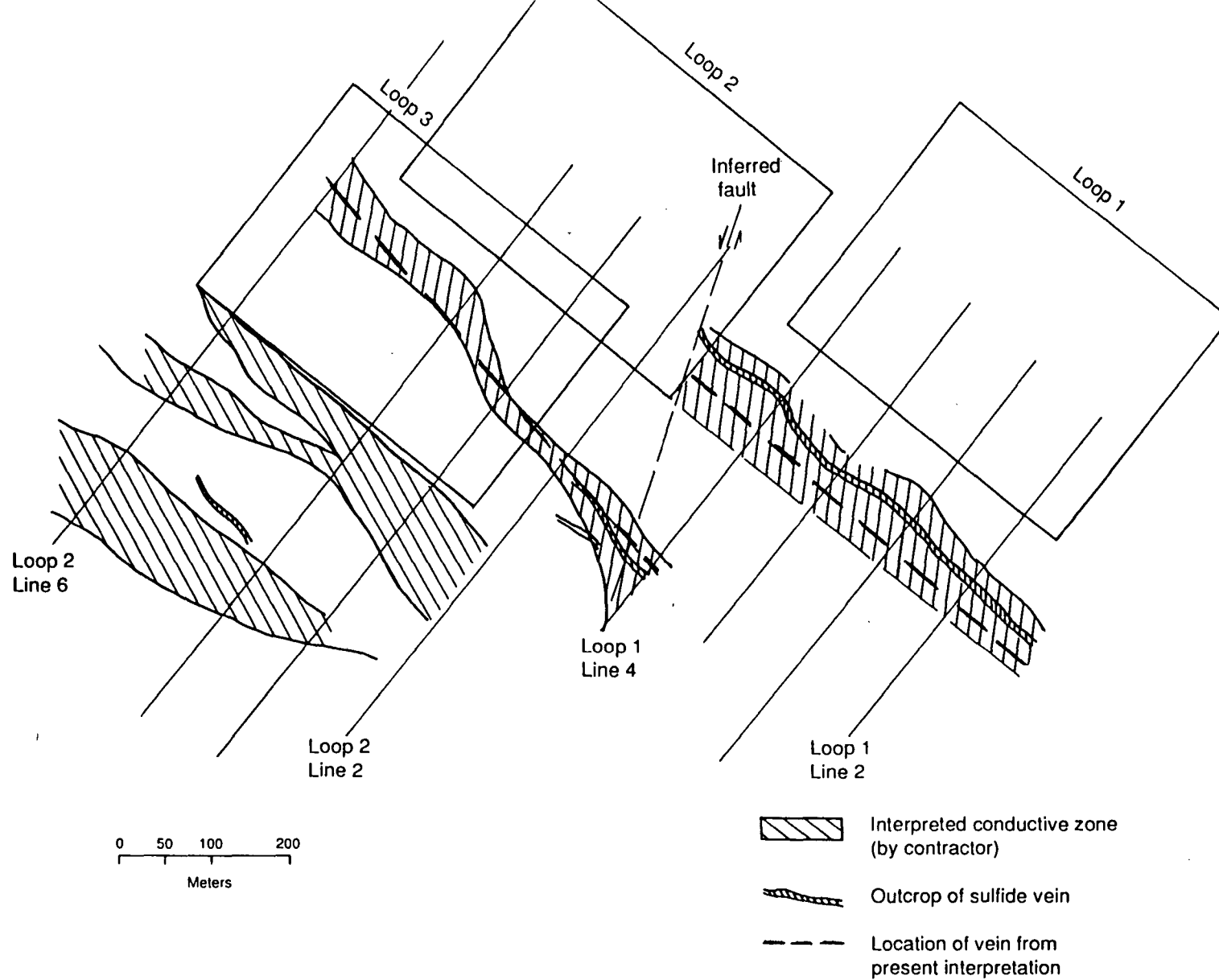
Figure 5.8 Site location map for ore prospect in the South American Andes. The banded markings are the surface location of conductive vein deposits as interpreted by the contractor. The dashed markings are the interpretation by the author.

The depth to unoxidized ore is approximately 130m near the southern edge of loop 1. Adjacent to the outcropping veins the rocks are extensively oxidized and form a discontinuous gossan. At the northwestern edge of loop 1 the veins are offset to the southwest. Across the fault the configuration of the veins is unknown.

Electromagnetic surveys were made over the prospect to trace the vein deposits and help define the structure. Three large rectangular loops (300 m x 400 m) were emplaced in the survey area and time domain horizontal and vertical magnetic field measurements were made along northeast-southwest trending profiles. The survey was done with the CRONE pulse EM system at lag times from 0.1 to 36.0 ms after current extinction (Crone, 1976).

To complicate the interpretation the Mesozoic rhyolites and Tertiary volcanics, which are in contact at the surface southwest of the transmitter loops, have markedly different resistivities. Surface dc resistivity surveys have shown that the Tertiary volcanics are relatively resistive (200 ohm-m) but the rhyolites are 20-60 ohm-m for the upper 150m and lower in resistivity beneath this. The contact between these host rock units will therefore produce an EM anomaly of significant magnitude and since this contact probably extends to considerable depth it will likely produce effects even at later times (see Chapter 3). We expect that contact effects will be superimposed on the anomaly due to the dipping conductor; it is therefore important to distinguish between these two types of anomalies before the vein deposits can be mapped.

The contractor attempted to determine the surface location of the unoxidized vein deposits by picking inflections on the horizontal and vertical field profiles. This is a very effective technique for locating sheet-like conductive mineral deposits in areas of poorly conducting host rocks, and in areas covered by a uniform overburden layers (West et al. 1984). Where the host rock is discontinuous these techniques are less effective and as shown above it is easy to confuse the response from a dipping sheet with that of a contact. The interpreted locations of the conductive zones (vein deposits) are shown in Figure 5.8. In the vicinity of loop 1 the interpretation traces a single conductor coinciding with the known location of the primary vein deposit. Near loops 2 and 3, however, a complex pattern of multiple conductors is indicated. Although it is possible that across the fault the vein deposits have split or

have been reconfigured in a complex manner it is also possible that some of the marked conductors are actually due to surface contacts instead of dipping veins.

To distinguish between these possibilities we use the method described in section 5.1; that is, we calculate the response due to a continuous layered model that best fits the data in the region away from the contact or vein deposits. We then subtract the layered model response from the field profiles. From the residual profiles we can distinguish between anomalies due to a dipping sheet and contact effects.

The background response was determined by fitting the transients measured at the center of the loop transmitters to layered models, using programs RECTEM and RECINV (Raiche, 1986), The best fit for all three transients was a two layer model: a 45 ohm-m layer 170m thick overlying a 25 ohm-m substrate.

Figure 5.9 is a plot of the vertical and horizontal field data profiles for loop 2 line 2 and the difference between these and data profiles calculated for the two layer model (residual profiles). At later times both the field and residual profiles show a clear crossover anomaly in the vertical component and a peak anomaly in the horizontal field near station 300; this is a characteristic type of response for a steeply dipping sheet. Notice that at later times on the horizontal field residual profiles the position of the maximum move slightly southward. This type of peak migration is typical for a dipping sheet (West et al. 1984).

The profiles for loop 2 line 6 are a good illustration of a contact effect (Figure 5.10). They show the characteristic anomaly for a steeply dipping sheet; that is a crossover anomaly in the vertical field and peak in the horizontal component. When the host rock response is removed, however, the residual profiles show a peak anomaly in the vertical field and a crossover in the horizontal component. This is the same type of response described in Chapter 3 for truncated sheet and quarter-space contacts. Since both of these field profiles traverse the trace of the dipping sheet and also across the contact zone and there are indications of both types of anomalies on the residual profiles. For loop 2 line 2 the ore vein response is much stronger than the contact anomaly for loop 2 line 6 the reverse is true.

Vertical field residual transients for both of these anomalies are plotted in Figure 5.11 The figure shows that the transients have slightly different time constants. The time constant for the dipping sheet
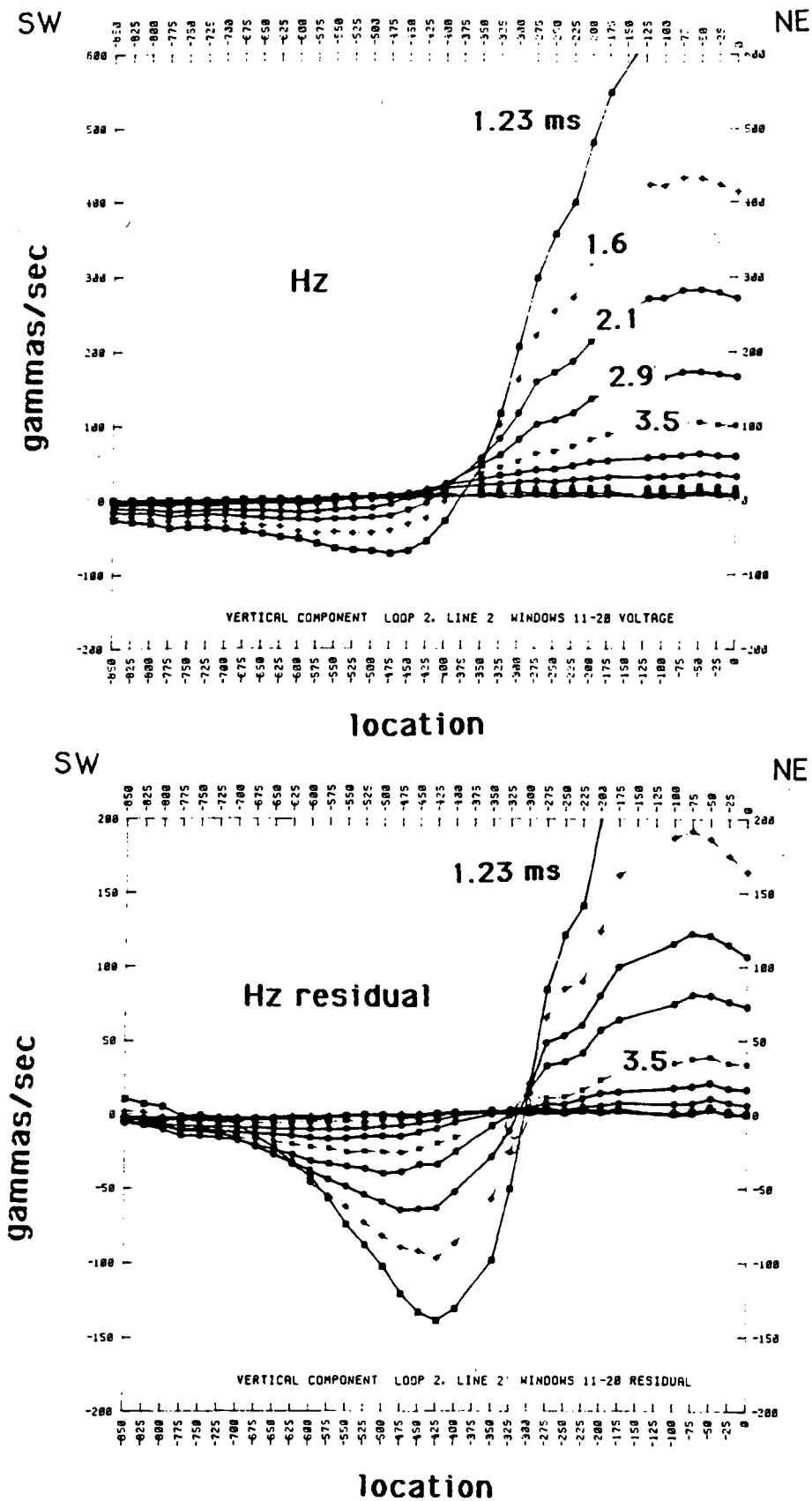
Figure 5.9a Field and residual vertical component profiles for loop 2 line 2. The field and residual profiles both show a crossover anomaly near station 300.
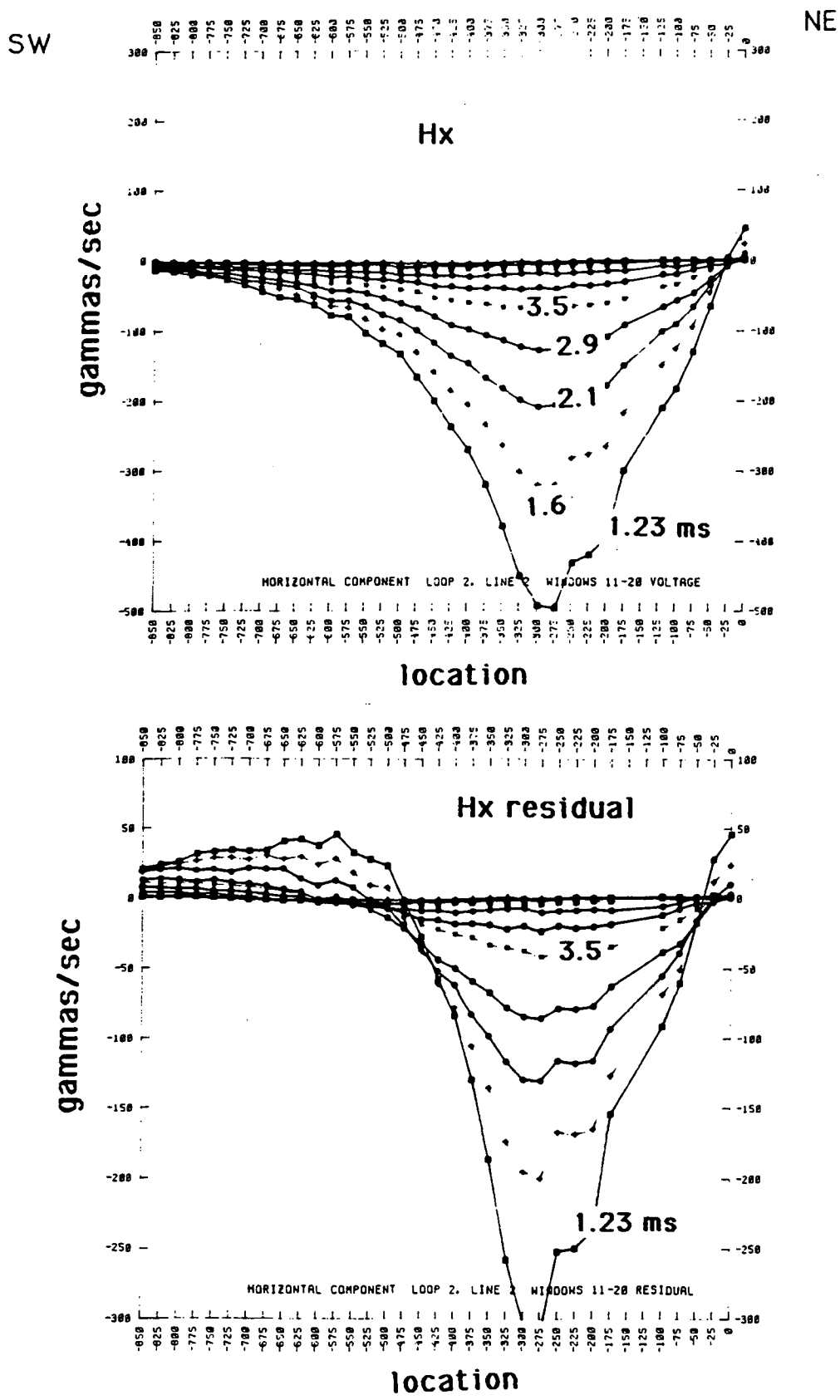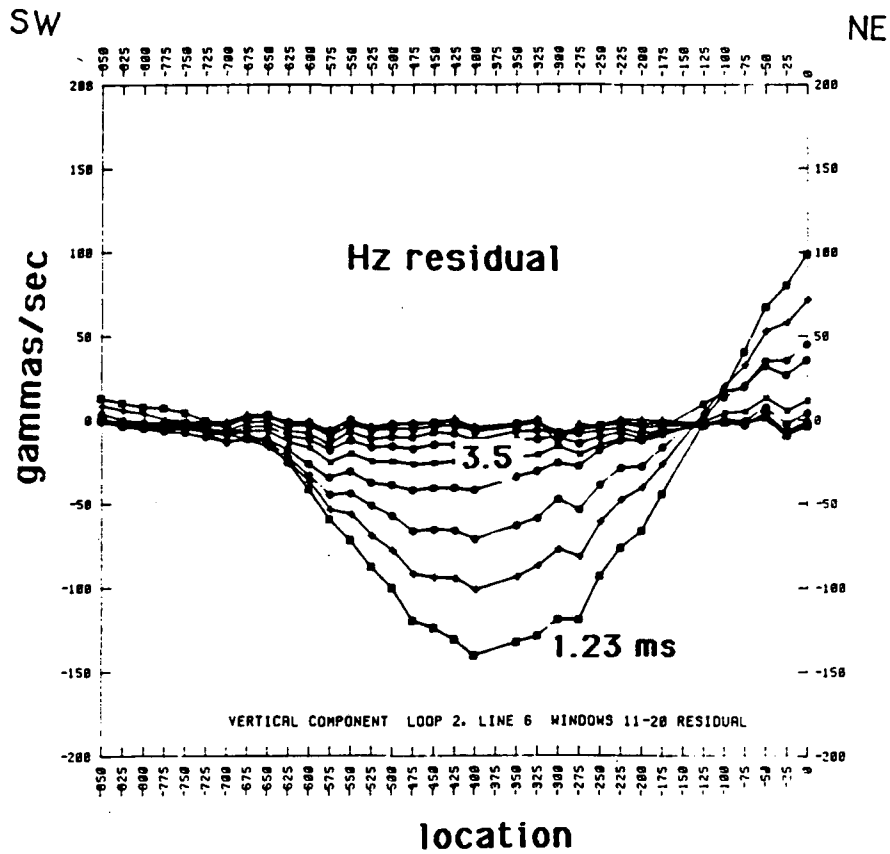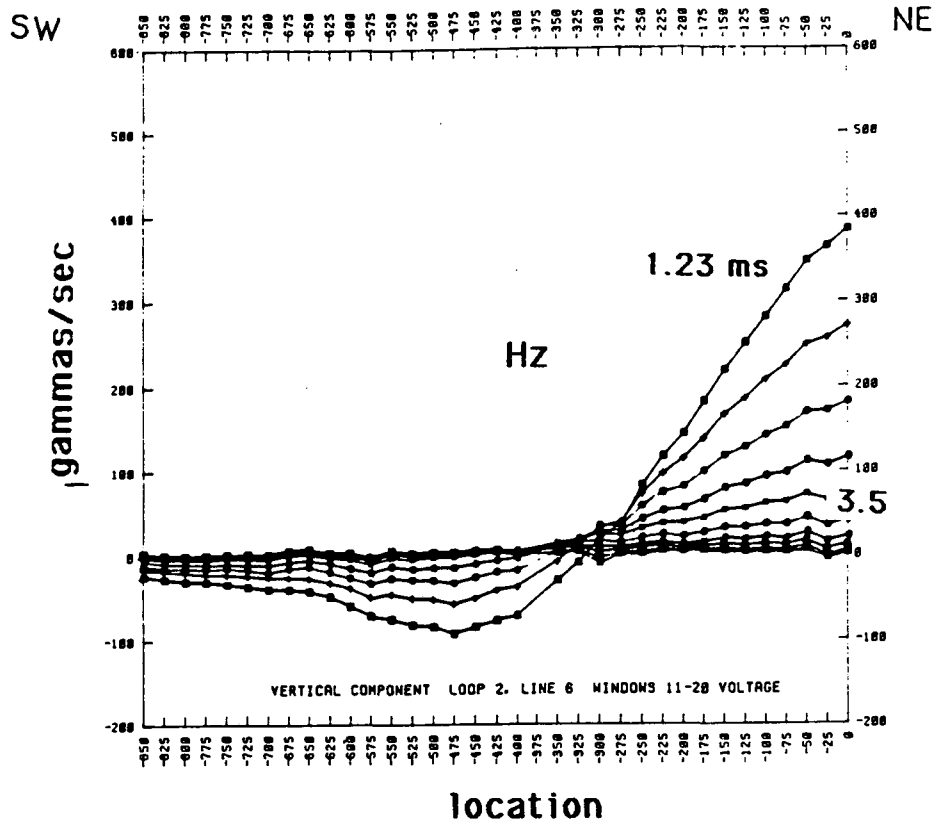
SW

NE

Hx

gammas/sec

HORIZONTAL COMPONENT LOOP 2. LINE 2 WINDOWS 11-28 VOLTAGE

3.5

2.9

2.1

1.6

1.23 ms

location

Hx residual

gammas/sec

3.5

1.23 ms

HORIZONTAL COMPONENT LOOP 2. LINE 2 WINDOWS 11-28 RESIDUAL

location

Figure 5.9b Field and residual horizontal component profiles for loop 2 line 2. The field and residual

profiles both show a peak anomaly near station 300.

Figure 5.10a Field and residual vertical component profiles for loop 2 line 6. The field profiles show a crossover anomaly near station 425 but the residual profiles show a peak.
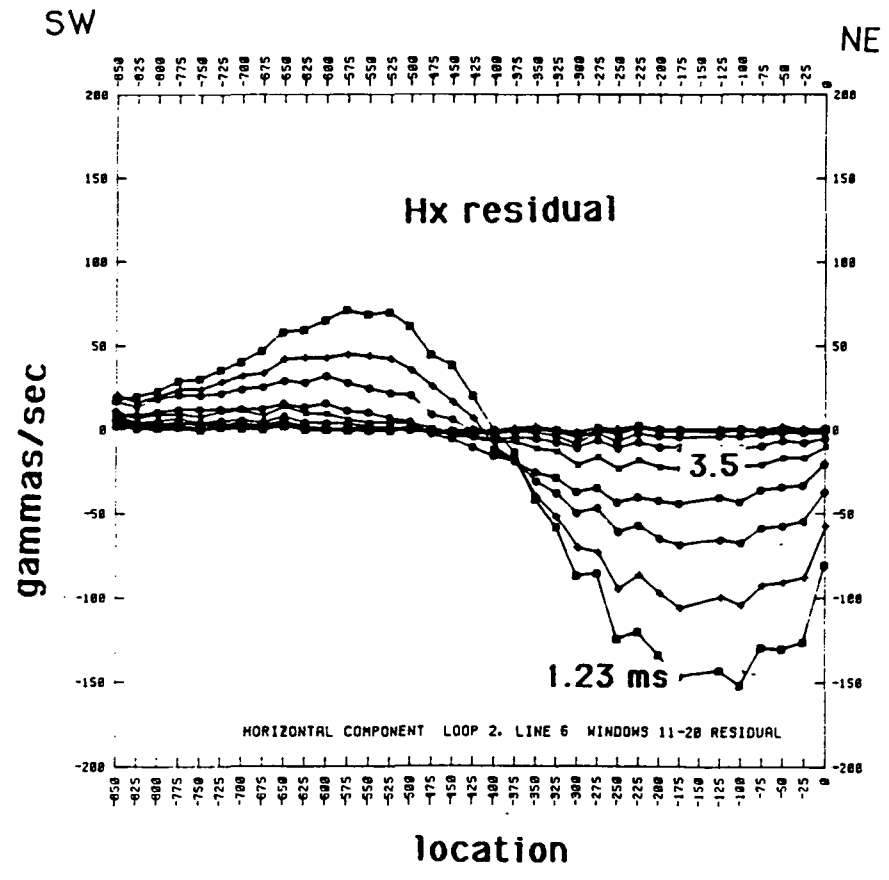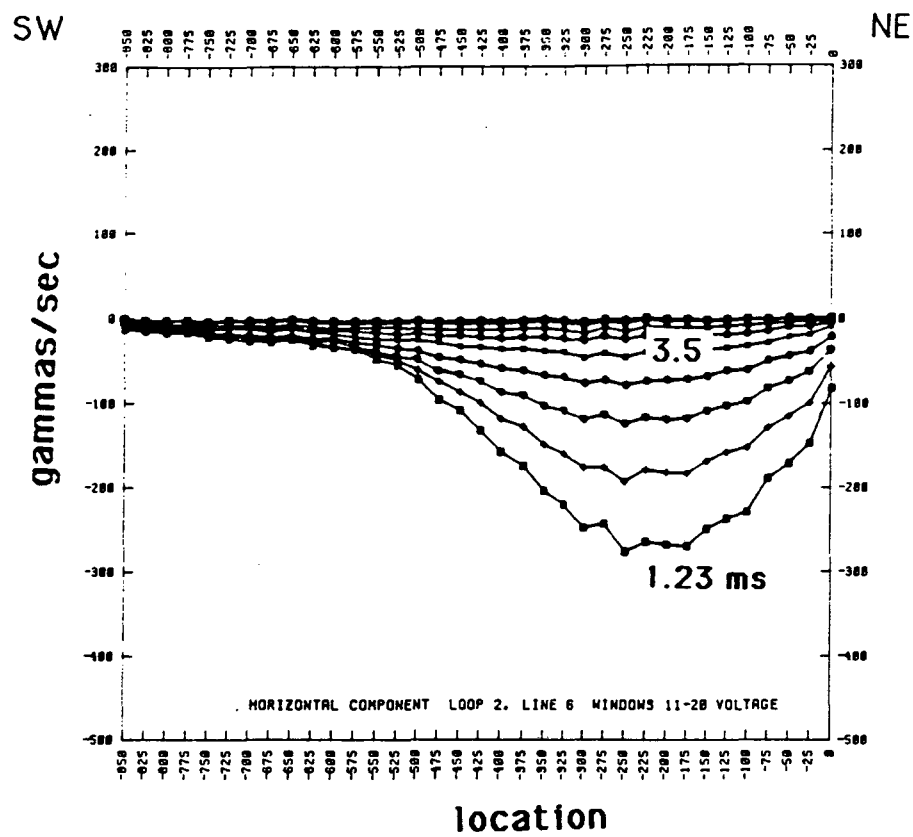
Figure 5.10b Field and residual horizontal component profiles for loop 2 line 6. The field profiles show a peak anomaly near station 425 but the residual profiles show a crossover.

Hz Residual Voltage (sheet)
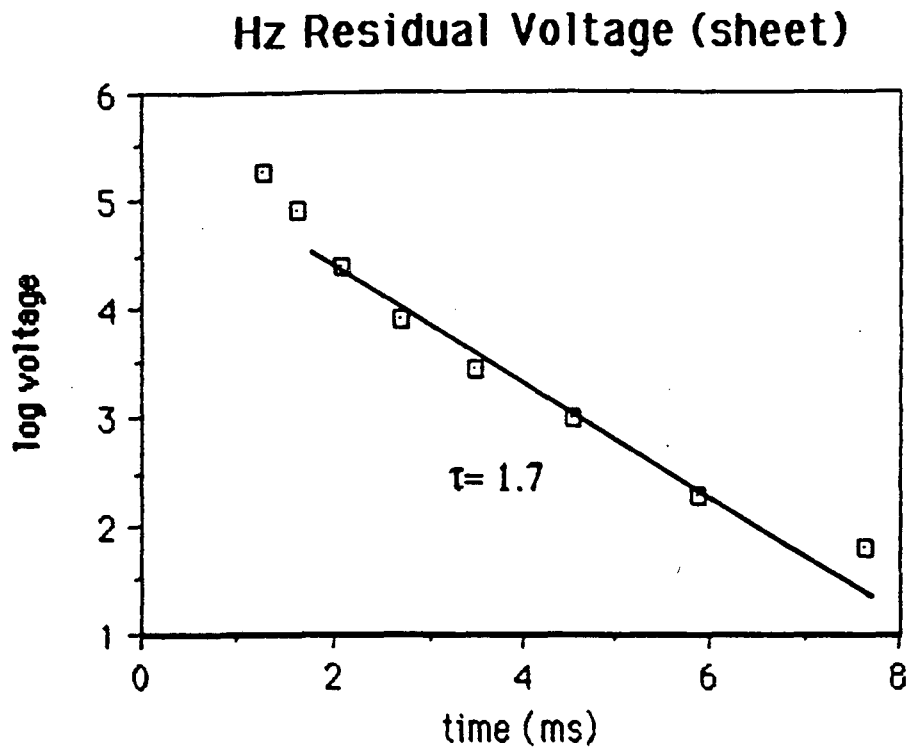
Figure 5.11a Vertical field residual transient from loop 2 line 2 station 425.

Hz Residual Voltage (contact)
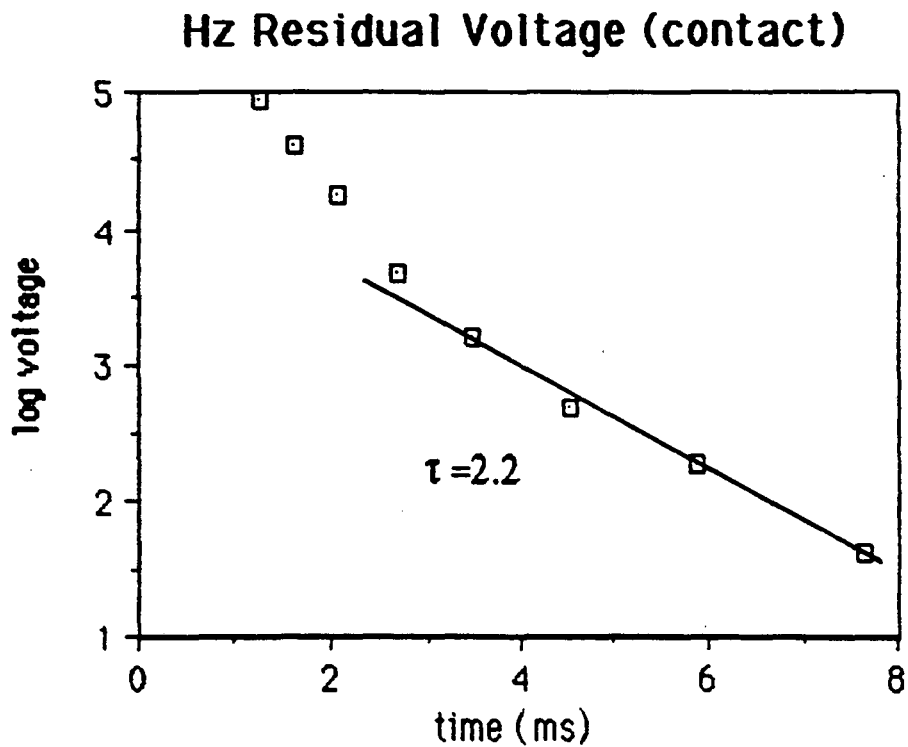
Figure 5.11b Vertical field residual transient from loop 2 line 6 station 400.

is 1.7 ms but for the surficial contact it is 2.2 ms.

The dashed markings on Figure 5.8 indicate the interpreted position of the primary ore zone based on the positions of peaks and crossovers in the residual profiles. These data suggests that the vein was offset southward about 200m near the northwestern edge of loop 2 and continues across the fault with a slightly more northerly trend. The vein anomaly seems to substantially diminish by loop 2 line 6 indicating that the ore content is beginning to weaken. The anomaly near station 400 on loops 2 and 3 is primarily a contact effect. This contact may be the result of oxidation of ore-vein outcrops within the surface rhyolites or it may represent the primary Mesozoic/Tertiary boundary.

The above example, although less quantitative than the first case, shows that separating the EM anomaly from the background response (stripping) is a very useful and not particularly difficult task. It allows for much simpler identification of contact effects and better isolation of target anomalies.

5.3 Case 3: Central-loop sounding in Long Valley, California

A profile of central-loop soundings were made in the Long Canyon region of Long Valley, California to investigate the geological contact zone located at the base of the resurgent dome within Long Valley caldera (Figure 5.9 ; Bailey et al. 1976). A series of ring fractures is known to encompass the dome and within the fracture zone a line of hot springs feeds warm water into shallow aquifers. The resistivity of these shallow aquifers is low (2-5 ohm-m) but rocks of the adjacent resurgent dome are fresh water alluvial sediments and recent volcanics of higher resistivity (10-200 ohm-m) (Stanley et al. 1976). Faults mapped near the contact zone are thought to provide the plumbing for the shallow geothermal system (Sorey, 1985).

The central-loop TDEM profile (A-A') is located at the mouth of Long Canyon beginning approximately 1000m north of the hot springs area and extending southward for 2500m (Figure 5.12). At each station vertical and horizontal field components were measured within a 200m square loop transmitter. The loops were spaced between 100m and 200m apart with the stations more closely spaced in the hot springs region.

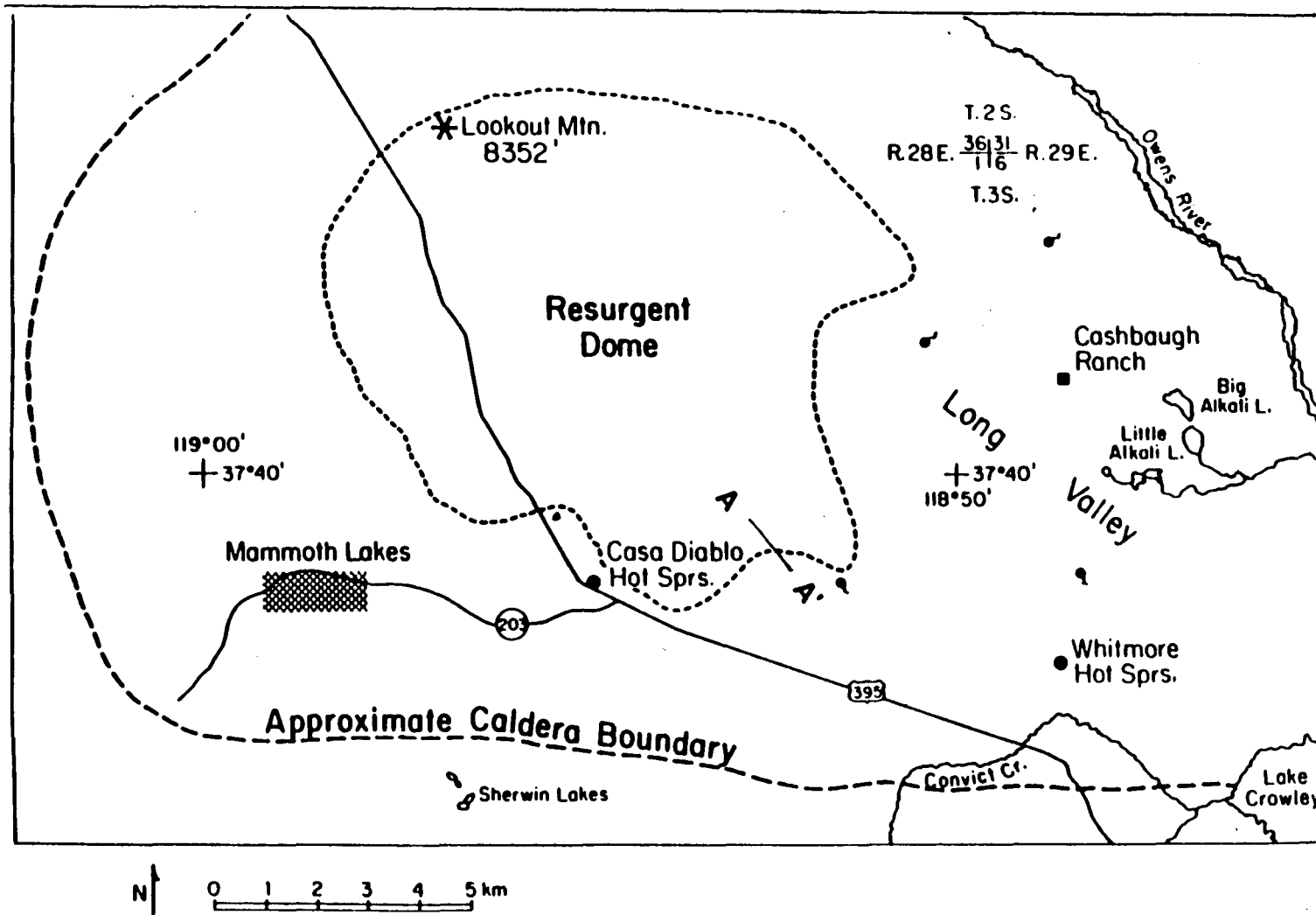Field data were collected using the Geonics EM-37 system, (McNeill, 1982), at fundamental

Figure 5.12 Site location map for the Long Canyon central-loop profile in Long Valley Caldera.

frequencies of 30Hz and 3Hz. This provides transient data at lag times from 0.089 to 72.0 ms after current extinction. The loop centers were located by stretching wire across a diagonal of each loop and marking the position where the wires cross. Along the pre-surveyed line our three person field crew could measure 7-8 sites per field day. This included vertical field measurements and at least one component of the horizontal field. Although the recording time was more than twice as long as normally required for single component data, a complete data set could still be collected within 30 minutes per station.

The horizontal field measurements were typically much noisier than the vertical field data. This is due the higher level of natural field noise and also to leakage of the much stronger vertical component into the horizontal field. Because loop sites are rarely perfectly flat, it is usually not enough to to simply level the horizontal field sensor and make measurements. The best results are obtained when the sensor is aligned perpendicular to the plane of the transmitter loop, otherwise, there is leakage. We did find, however, that it was not important to make horizontal field measurements exactly at the center of the loop; equivalent measurements could be made within 10 m of the center.

Although the horizontal field component is much noisier than the vertical field as shown in Chapters 1 and 4 it is a very important quantity to measure. If the horizontal field is too small to measure in the ambient noise then the geology is reasonably homogeneous and a one dimensional interpretation of the vertical field is probably sufficient to resolve any structure. However, if the horizontal component is a significant percentage of the vertical field then it is necessary to include it in the interpretation.

The Long Canyon TDEM profile was initially interpreted by fitting the vertical field transients to layered models. This was done using computer code NLSTCI (Anderson, 1982); the interpreted cross-section is shown in Figure 5.13. The cross-section shows a transition from the more resistive rocks at the north end of the profile, near the resurgent dome, to the more conductive section near the hot springs area. South of the hot springs the section becomes more resistive again. For the initial 600-800 m at the northern end of the profile the soundings indicate a simple three layer section consisting of a 50 ohm-m layer about 50 m thick overlying a 10 ohm-meter 100 m thick horizon. The basal layer is
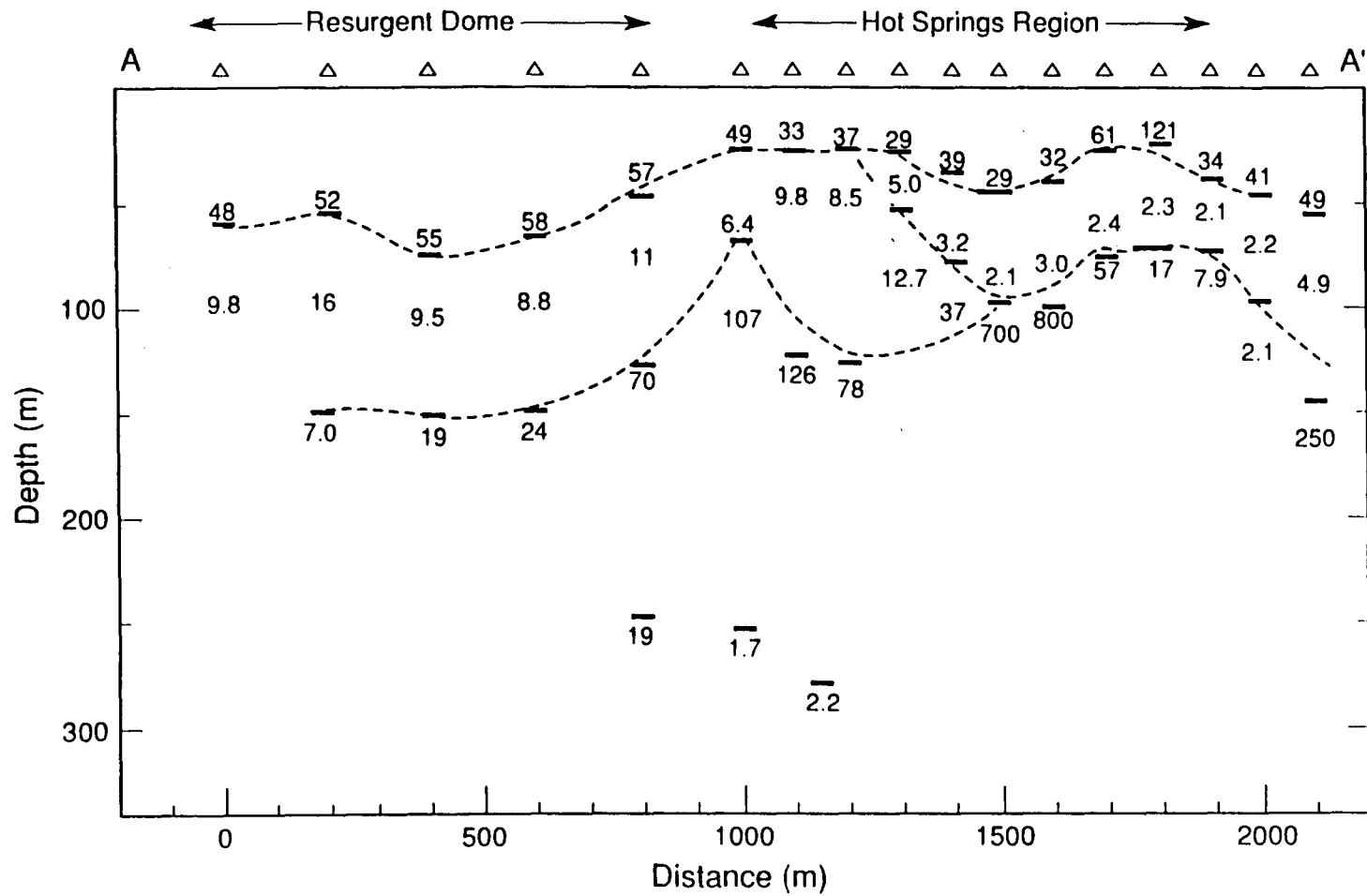
Figure 5.13 Cross-section of layered model interpretations for profile A-A'. The layered models were pieced together along the profile.

10 to 50 ohm-meters. Beginning near station 1000 the inversions suggest a more complex section and the layered models change rapidly from sounding to sounding as the hot springs are approached from the north. The most interesting soundings are located between stations 1200 and 1700 where the resistivity of the second layer changes from 10-15 ohm-m at the northern side of the contact to 2-3 ohm-m on the southern side. The layered models in this area also indicate of a highly resistive third layer beginning near station 1200 and extending to station 1600 and a conductive layer near station 1000 at a depth of 250-300 m. As this layer may have significant implications for geothermal exploration in this area it would be useful to determine if the layer is actually present structure or if it is a manifestation of a contact effect.

In Figure 5.14 we show profiles of the vertical field for line A-A' on semilogarithmic paper at lag times from 0.5 to 20.0 ms. Profiles for the horizontal component of the secondary field and horizontal gradient of the vertical field on linear plots for lag times from 1.4 ms to 10 ms are shown in Figure 5.15. The vertical field profiles are relatively flat at early times but show a field level adjustment reminiscent of a contact at intermediate times. The field levels are higher over the hot springs area but decline outside of this zone.

The horizontal field profiles shown in Figure 5.15b have similar features to the horizontal gradient profiles in Figure 5.15a although the field data are considerably noisier. Both profiles are relatively flat until station 1200, they develop negative peaks near station 1300, cross zero at station 1800, and develop positive peaks near station 2100. These data suggest that there is a lateral change in conductivity beginning near station 1300 and extending to station 2100 and that the region between these stations has a higher conductivity.

Near the center of the profile the peak in the horizontal gradient profiles seems to asymptotically approach station 1300 at earlier times but it migrates southward at later lag times. As shown above, the movement of this peak may be used to estimate the conductance of the second layer on the more conductive side of the contact. Using equation 4.18 we estimate the conductance of the layer to be 12 Siemens; similar values are obtained from the horizontal component. This value of 12 Siemens matches the conductance of the second layer at station 1400, as determined by fitting the vertical field transient
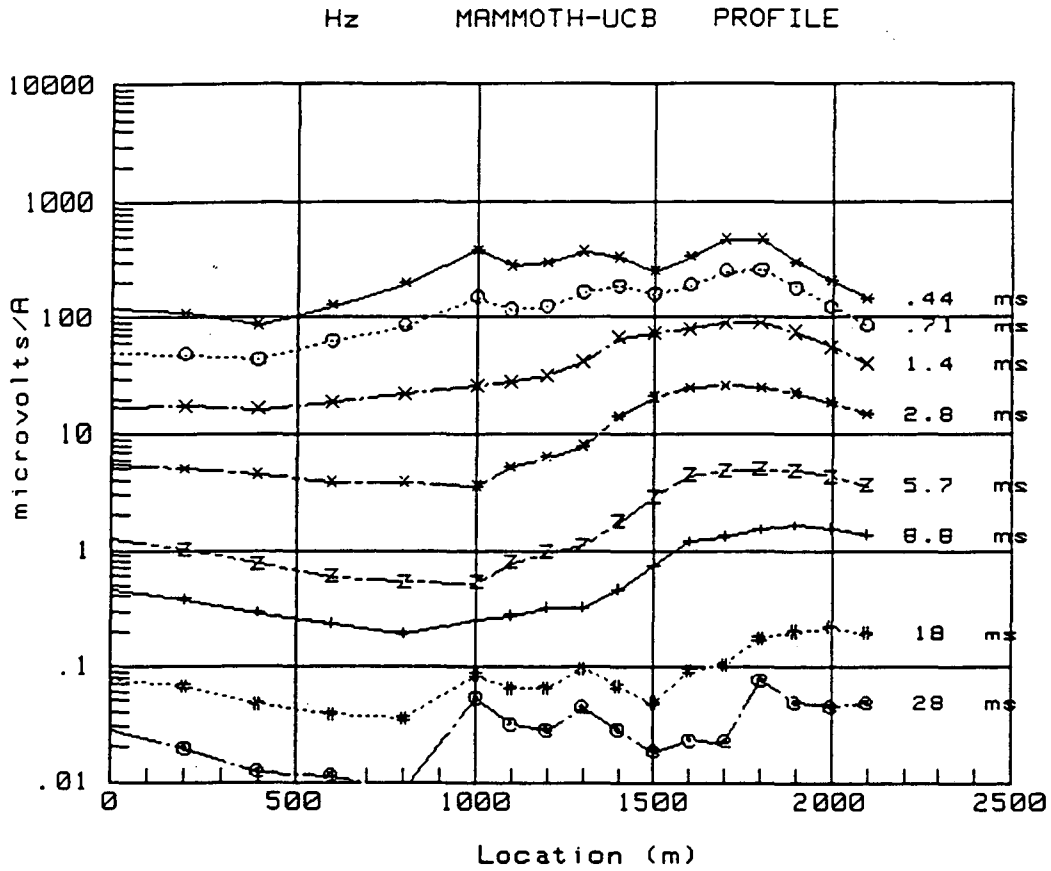
Figure 5.14 Vertical field time profiles for line A-A' for lag time from 0.5 to 28.0 ms after current extinction.
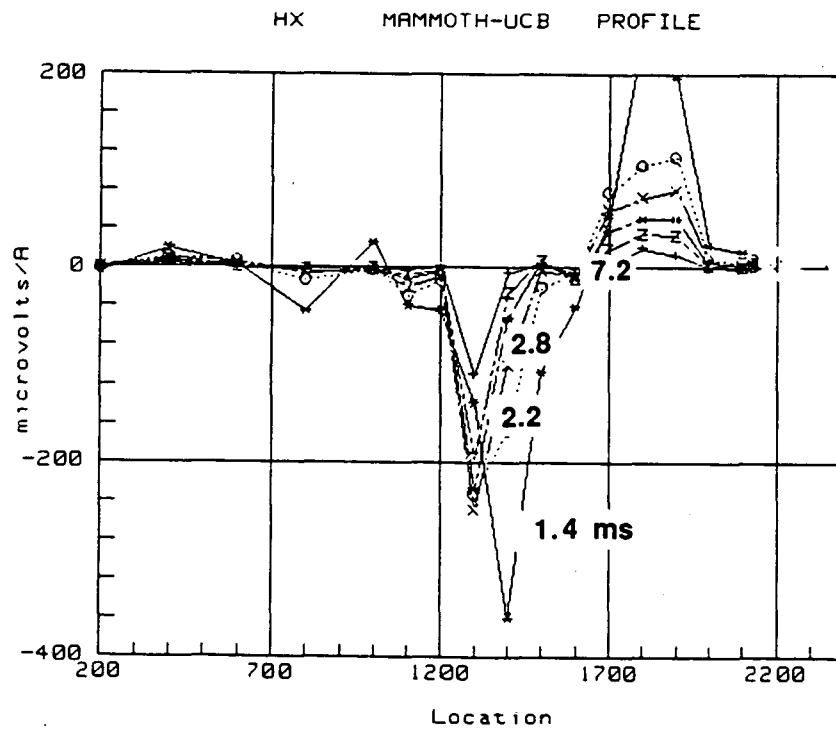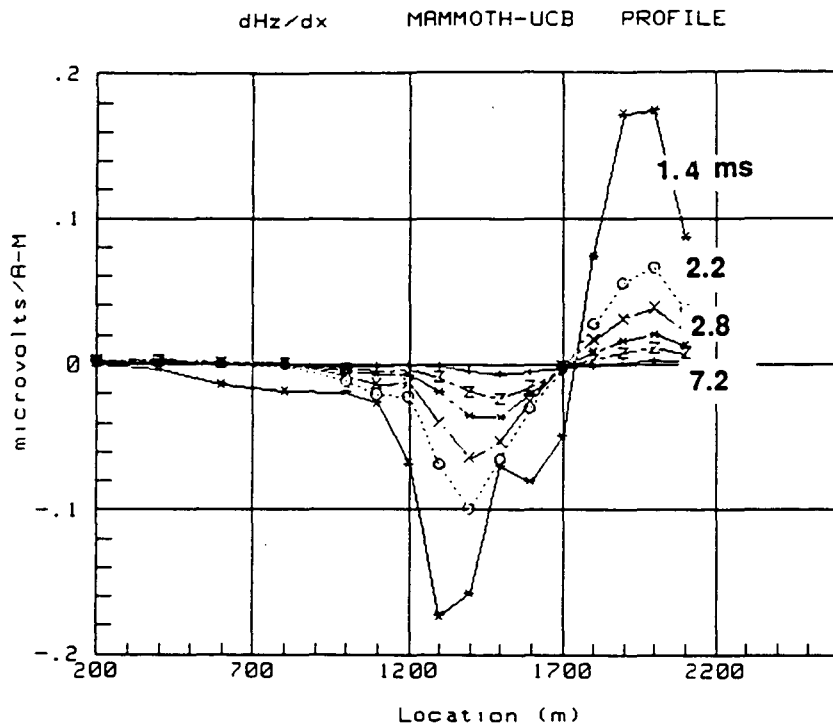
Figure 5.15 a) Horizontal gradient of the vertical field and b) horizontal field for profile A-A' for lag times 1.4 to 7.2 ms after current extinction.

to a layered model. This suggests that the anomaly near the hot springs is mostly due to changes occurring within the second layer and not to any changes occurring at greater depth.

Horizontal component and horizontal gradient transients are given on semilogarithmic plots in Figure 5.16. These plots have linear slopes at late times, and as shown above, this slope may be used to estimate the conductance of the contact and distance to the edge. Fitting the slopes we obtain a time constant of 1.8ms for the horizontal gradient transient and 1.4 ms for the horizontal gradient. Assuming that the contact is located at station 1300m we can use equations 4.4 and 4.18 to estimate the conductance of the truncated layer. From these formulas we obtain estimates of the conductance to be 11 Siemens and 14 Siemens respectively.

This interpretation suggests that the variation of the vertical and horizontal fields across the hot springs area may be explained by an abrupt change in conductivity in the second layer. Although the geology of the region is clearly more complicated than this simple interpretation suggests, the fact that the fields can be well approximated by this simple model casts serious doubt on the existence of a deeper conductor in the hot springs region. In Chapter 1 we showed that layered model inversions for soundings on the conductive side of a quarter-space indicate fictitious resistive layers. In a similar manner the soundings on the resistive side of the edge seem to indicate fictitious conductive horizons.
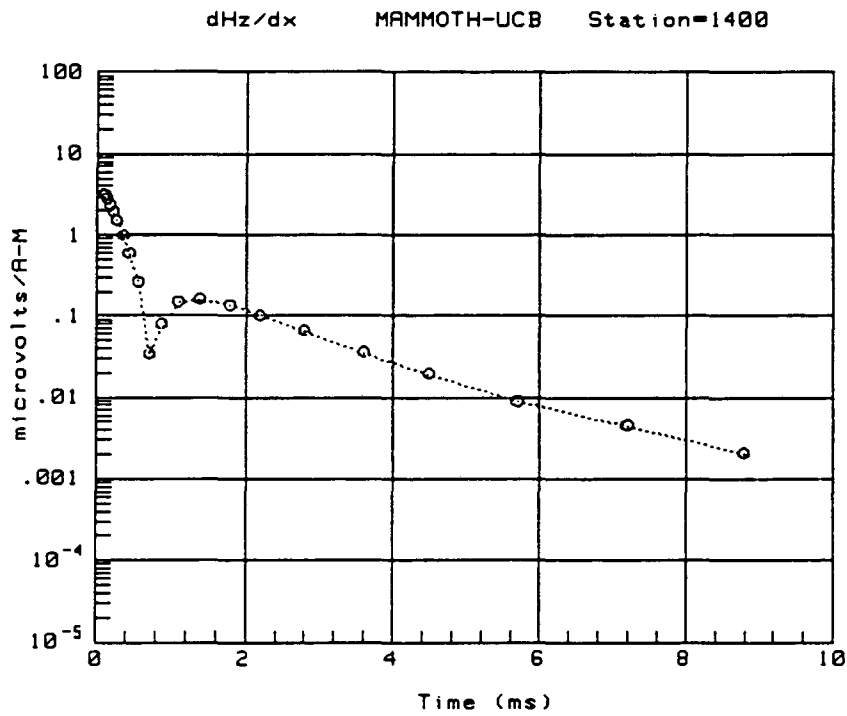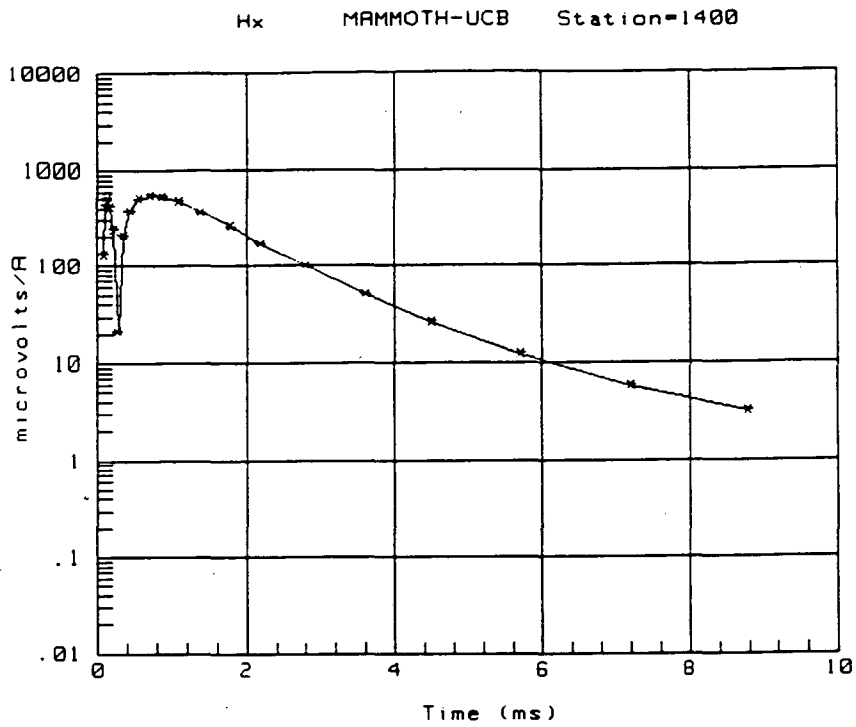
Figure 5.16 a) Horizontal field transient and b) horizontal gradient transient for station 1400 on line A- A'.

CHAPTER 6: CONCLUSIONS AND RECOMMENDATIONS FOR FUTURE WORK

In this thesis we have shown that a geological contact, or even a discontinuous layer of conductive overburden, can have a significant effect on field measurements. These effects, if unaccounted for, can cause serious errors in data interpretation. The goals of the research were to devise means of recognizing a contact effect and where possible to remove it from the observed data.

For a point dipole source near the edge of a truncated surface layer the edge effect is first observed at stations located at the contact. The anomaly forms a maximum during lag times that can be predicted using the propagation velocity for a continuous layer having the same conductance as the truncated sheet. Near the source, however, the anomaly doesn't peak until later lag times and we suggest that the edge anomaly is due to currents that have propagated to the edge and have been reflected back towards the source.

If we define the contact anomaly as the difference between the observable fields, with or without the presence of the contact, the resulting anomaly has a distinctive shape and characteristics. The anomaly builds up approximately linearly with time forms a definite peak and then decays exponentially after the peak. The late-time slope is directly related to the conductance of the truncated layer and the peak time may be related through the propagation velocity to the distance to the edge.

Of all the configurations commonly used in TDEM prospecting, the grounded source (electrical dipole) system is most sensitive to an edge effect and the central-loop configuration is least sensitive. With the latter system the vertical component exhibits a smooth level adjustment across the contact and the horizontal field is zero except near the edge where it forms a peak at times related to the conductance of the truncated sheet and the distance from the edge. Examination of this horizontal component shows that for simple truncated sheet and quarter-space models the sheet conductance or conductivity and distance from the sounding to the edge may be recovered by simple analysis of the field maxima and late-time slopes.

If central-loop horizontal field data is unavailable then much of the same information may be obtained by analyzing a psuedogradient of the vertical field which is formed by taking the differences of the vertical component along a continuous profile and dividing by the separation between soundings.

These "gradient" data are similar in appearance to the horizontal fields and may be analyzed in much the same manner.

The subject of geological contact anomalies in CSEM data is a broad topic and this thesis has only addressed a small portion of the problem. A great deal more needs to be understood on the nature of the contact effect and its relation to the geometrical configuration of the system and the earth model to be studied. In a fundamental sense we need to more fully understand the nature of induced current flow near geological contacts and the formation of galvanic currents and charges. This is a complex topic that should begin with an analysis of simple scale and numerical model data. More needs to be understood on the relation of currents to the conductivity and configuration of subsurface target bodies and on the interaction of the currents flowing in these bodies.

From an explorationists point of view, the fundamental problem is that contacts interfere with the signals related to the targets of interest. The explorationist is therefore interested in separating and removing the contact effects seen in practical geological cases. Although we showed that the effect of a simple surface contact anomaly can be removed to reveal a deeper target it is not clear that the methods used would be effective if the contact was buried, dipping or located in a conductive host. First we need to apply the method developed in the thesis to simple field cases where the geology is well known. If this method is effective on field data then its further development is recommended.

Finally, in a real sense, we should view the geological contact as part of the interpretational puzzle. It is not enough to simply identify it and remove it from the data, we need to incorporate it as part of the geological model. In the area of contact interpretation, much needs to be done on discovering the relation between contact structures and their responses for various CSEM configurations. We should consider the contact as simply a class of geological inhomogeneities. From such a viewpoint, techniques for interpreting contacts should apply to interpreting other structures and vice versa.

The main stumbling block to all this research is the lack of a good inexpensive numerical model that could be used for examining contact effects. With such a tool the above discussed research topics would become more tractable, without it, the research is slow and the results fitful. Development of such a tool should be a top priority for continued research on the effects of geological contacts.

References

Anderson, W.L., 1976, Calculation of transient soundings for a central induction loop system (Program TCILOOP). U.S. Geological Survey open file report 81-1309.

Anderson, W.L., 1982, Nonlinear least-squares inversion of transient soundings for a central induction loop system (Program NLSTCI). U. S. Geological Survey open file report 82-1129.

Annan, A.P., 1974, The equivalent source method for electromagnetic scattering analysis and its geophysical application: Ph. D. thesis Memorial University of Newfoundland.

Bailey, R.A., Dalrymple, G.B., and Lanphere, M.A., 1976, Volcanism, structure and geochronology of Long Valley caldera, Mono County, California: Journal of Geophysical Research **81**, 725-744.

Bartel, D.C., and Becker, A., 1988, Time-domain electromagnetic detection of a hidden target: Geophysics **53**, 537-545.

Bhattacharya, B.K., 1957, Propagation of an electric pulse through a homogeneous and isotropic medium: Geophysics **22**, 905-921.

Bhattacharya, B.K., 1957, Transient electromagnetic waves in a conducting medium: Geophysics **22**, 75-78.

Busselli, G., and O'Neill, B., 1982, SIROTEM a new portable instrument for multi-channel transient electromagnetic measurements: Bulletin Australian Society of Exploration Geophysicists **8**, 82-87.

Buselli, G., McCracken, K.G., and Thornbum, M., 1986, Transient electromagnetic response of the Teufonic orebody: Geophysics **51**, 957-964.

Crone, D., 1975, Pulse electromagnetic- PEM ground method and equipment as applied in mineral exploration. Paper presented at AIME Annual meeting, New York, Feb 16-20.

Dallal, S., 1985, Time domain E.M. for the detection of fractures and cavities. M.S. thesis Engineering

Geoscience, University of California, Berkeley.

Duncan, P.M., Hwang, A., Edwards, R.N., Bailey, R.C., and Garland, G.D., 1980, The development and applications of a wide band electromagnetic sounding system using a psuedo-noise source: Geophysics **45**, 1276-1296.

Eaton, P.A., and Hohmann, G.W., 1986, Technique for rapidly estimating resistivity of the earth from transient electromagnetic soundings: Expanded abstracts Society of Exploration Geophysicists Annual Meeting, Houston, Texas 52-54.

Fitterman, D. V., and Stewart, M.T., 1986, Transient electromagnetic sounding for groundwater: Geophysics **51**, 995-1006.

Fokin, A.F., 1971, The transient method in the search for sulphides. 242p. Nedra, Leningrad (in Russian).

Frischknecht, F.C., 1971, Electromagnetic scale modeling in: Electromagnetic probing in geophysics. (Wait J.R. ed) Boulder Golem Press 265-320.

Frischknecht, F.C., 1988, Electromagnetic physical scale modeling: chapter 6 of " Electromagnetic methods in applied geophysics " Investigations in Geophysics no. 3. ed Misac N. Nabighian Published by the Society of Exploration Geophysicists, Tulsa, Oklahoma.

Frischknecht, F.C. and Raab, P.V., 1984, Time-domain electromagnetic soundings at the Nevada test site, Nevada: Geophysics **49**, 981-993.

Grant, F.S., and West, G.F., 1965, Interpretation theory in applied geophysics: McGraw-Hill Book Co.

Gunderson, B.W., Newman, G.A., and Hohmann, G.W., 1986, Three-dimensional transient electromagnetic responses for a grounded dipole: Geophysics **51** 2117-2130.

Hermance, J.F., 1982, The asymptotic response of three-dimensional basin offsets to magnetotelluric

fields at long periods: the effects of current channeling: Geophysics **47**, 1562-1572.

Hohmann, G.W., 1988, Numerical modeling for electromagnetic methods of Geophysics chapter 5 of " Electromagnetic methods in applied geophysics", Investigations in Geophysics no. 3. ed. Misac N. Nabighian Published by the Society of Exploration Geophysicists, Tulsa, Oklahoma.

Hoversten, G.M. and Morrison, H.F., 1982, Transient fields of a current loop source above a layered earth : Geophysics **47**, 1068-1077.

Irvine, R.J., and Staltari, G., 1984, Case history illustrating interpretation problems in transient electromagnetic surveys: Exploration Geophysics **15**, 155-167.

Joshi, M.S., Gupta, O.P, and Negi, J.G., 1988, On the effects of the half-plane model in HLEM induction prospecting over sulphide dikes in a highly resistive medium: Geophysical Prospecting **36** 551-558.

Kamenetskii, F.M., 1976 Application handbook for the transient process methods in the geophysics of ore bodies. Ministry of Geology, USSR, Leningrad "NEDRA", (in Russian).

Karcher, J.C., and McDermott, E., 1935, Deep electrical prospecting: Bulletin American Association of Petroleum Geologists, **19**, 61-77.

Kaufmann, A.A., 1978, Frequency and transient responses created by currents in confined conductors: Geophysics **43**, 1002-1010.

Kaufmann, A.A., 1985, Tutorial: Distribution of alternating electrical charges in a conducting medium: Geophysical Prospecting **33** 171-184.

Kaufmann, A.A., and Keller, G.V., 1983, Frequency and transient soundings. :Methods in Geochemistry and Geophysics, 16, Amsterdam, Elsevier Pub. Co. 681p.

Keller, G.V., Pritchard, J.I., Jacobson, J.J., and Harthill, N., 1984, Megasource time domain electromagnetic sounding methods: Geophysics **49**, 993-1010.

Lee, K.H., and Morrison, H.F., 1985, A numerical solution for the electromagnetic scattering by a two-dimensional inhomogeneity: Geophysics **50**, 466-472.

Lewis, R., and Lee, T., 1978, The transient electric fields about a loop on a halfspace: Bulletin Australian Society of Exploration Geophysics **9** 173-177.

McCracken, K.G., Oristaglio, M.L., and Hohmann, G.W., 1986, The minimization of noise in electromagnetic exploration systems: Geophysics **51** 819-833.

Macnae, J., and Lamontagne, Y., 1987, Imaging quasi-layered conductive structures by simple processing of transient electromagnetic data: Geophysics **52** 1700-1705.

McNeill, J.D., 1982, EM37 ground transient exploration system: Technical note No. 10. Geonics ltd. Ontario, Canada.

Morrison, H.F., Goldstein, N.E., Hoversten, G.M., Oppliger G., and Riveros, C., 1978, Description, field test and data analysis of a controlled source EM system (EM-60): Lawrence Berkeley Laboratory report no. LBL-7088.

Nabighian, M.N., 1979, Quasi-static transient response of a conducting halfspace: an approximate representation: Geophysics **44**, 845-853.

Nekut, A., Connery, J.E.P., and Kuckes, A.,F., 1977, Deep crustal electrical conductivity: evidence for water in the lower crust: Geophysical Research Letters, **4**, 239-242.

Newman, G.A., Hohmann, G.W., and Anderson, W.L., 1986, Transient electromagnetic responses of a three-dimensional body in a layered earth : Geophysics **51** 1608-1627.

Newman, G.A., 1989, Deep transient electromagnetic soundings with a grounded source over near-surface conductors: Geophysical Journal (in press).

Oristaglio, M.L., and Hohmann, G.W., 1984, Diffusion of electromagnetic fields into a two-dimensional

earth- A finite difference approach: Geophysics **49** 870-894.

Orsinger, A., and VanNostrand, R., 1954, A field evaluation of the electromagnetic reflection method: Geophysics **19,** 478-489.

Pridmore, D.F., Ward, S.H., and Motter, J.W., 1976, Broadband electromagnetic measurements over a massive sulfide prospect: Geophysics **44** 1677-1700.

Raab, P., and Frishknecht, F., 1983, Desktop computer processing of coincident and central loop time domain electromagnetic data: U.S. Geological Survey open file report 83-240.

Raiche, A., 1987, Program RECTEM: Magnetic field calculations for a loop source over an n-layered medium. Code developed at Commonwealth Scientific and Industrial Research Organization (CSIRO) Melbourne, Australia, loaned for use to University of California, Berkeley.

Raiche, A., 1987, Program RECINV: Magnetic field layered model inversion for a loop source over an n-layered medium. Code developed at CSIRO.

Sinclair, G., 1948, Theory of models of electromagnetic systems: Proceedings Institute of Radio Engineering **36**

Slichter, L.B., 1933, An inverse boundary value problem in electrodynamics: Physics **4,** 418

Sorey, M.L., 1985, Evolution and present state of the hydrothermal system in Long Valley Caldera: Journal of Geophysical Research **90** 219-228.

Spies, B.R., 1977, Experience with time domain EM methods in Australia: Abstract, Proceedings Society of Exploration Geophysics Annual meeting, New Orleans, Louisiana.

Spies, B.R., 1980, The application of the transient electromagnetic method in Australian conditions- Field examples and model studies: Ph.D. thesis Macquerie University.

Spies, B.R., 1988, Local noise prediction filtering for central induction transient electromagnetic

sounding: Geophysics, **53,** 1068-1080.

Spies, B.R., and Parker, P.D., 1984, Limitations of large-loop transient electromagnetic surveys in conductive terrains: Geophysics, **49,** 902-913.

Stanley, W.D., Jackson, P.B., and Zohdy, A.A.R., 1976, Deep electrical studies in the Long Valley Caldera, Mono and Inyo Counties, California: Journal of Geophysical Research **81** 810-820.

Tikhonov, A.N., 1946, On the transient electric currents in a homogeneous conducting halfspace: Izv. Akad. SSSR, Ser. Geograf. I. Geofiz. **10** no. 3 (in Russian).

Tikhonov, A.N., 1950, On the transient electric currents in an inhomogeneous layered medium :Izv. Akad. SSSR, Ser. Geograf. I. Geofiz. **14** no. 3 (in Russian).

Vanyan, L.L., Bobrovnikov, L.Z., Dadidov, V.M., Kuznetsov, A.N., Loshenitzina, V.L., Morozova, G.M., and Shtimmer,A.I., 1967, Electromagnetic depth soundings. Selected and translated by G.V. Keller. Consultants Bureau New York.

Wait, J.R., 1951, Oscillating magnetic dipole over a horizontally stratified earth: Canadian Journal of Physics: **29,** 577-592.

Wait, J.R., 1955, Mutual electromagnetic coupling of loops over a homogeneous ground: Geophysics **20,** 630-637.

West, G.F., Macnae, J.C., and Lamontagne Y., 1984, A time-domain electromagnetic system measuring the step response of the ground: Geophysics **49,** 1010-1027.

Wilt, M.J., Goldstein, N.E., Stark, M., Haught, J.R., and Morrison, H.F., 1983, Experience with the EM-60 electromagnetic system for geothermal exploration in Nevada: Geophysics **48,** 1090-1101.

Wilt, M.J., Becker A., and Morrison, H. F., 1985, Electromagnetic Sounding: The effects of vertical contacts. Engineering Geosciences report U.C. contract # 143578.

Wilt, M.J., Becker, A., and Morrison H.F., 1986, Effects of vertical contacts on time domain electromagnetic sounding: Extended abstracts, Society Exploration Geophysicists annual meeting Houston, Texas 177-180.

Yost, W.J., 1952, The interpretation of electromagnetic reflection data in geophysical exploration-Part 1, General theory (oscillating dipole): Geophysics **17,** 806-826.

Appendix 1: Layered Model Inversion Results for a Quarter-Space

Figure A1 shows model and station parameters for layered model inversions of central-loop soundings made over a 4.0 ohm-m quarter-space. Scale model data were collected as described in chapter 1, section 1.5. The data were inverted to a 3 layer model, which includes an air layer, using code NLSTCI (Anderson, 1982). The results are given as transient voltages (mv) for a 200m loop with a current of 1 amp, compared with calculated voltages from the code, and a listing of the model parameters obtained from the inversion. Uncertainty of the model results is not displayed, but note that the computer code was unable to resolve any layers deeper than 400m; when such layers are indicated on the plots they are not meaningful. The importance of the inversion results is the change in the model parameters as the stations are measured closer to the edge of the quarter-space.

conns13

symbols = observed   solid curve = model

transient voltage (mv) vs time (sec)

```
rho(1) = 5000.0000   h( 1 )= 62.00      shift =  0.02703
rho(2) = 3.9837      h( 2 )= 654.23     nobs =  30
rho(3) = 2.7983      h( 3 )= 5529.95    niter = 8
rho(4) = 2.6972
```

conns11

symbols = observed   solid curve = model

```
rho(1) = 5000.0000   h( 1 )= 62.00      shift =  0.02704
rho(2) = 4.1459      h( 2 )= 1329.68    nobs =  30
rho(3) = 2.7961      h( 3 )= 671.21     niter = 8
rho(4) = 7.0752
```

conns7

symbols = observed   solid curve = model

transient voltage (mv) vs time (sec)

```
rho(1) = 5000.0000   h( 1 )= 62.00      shift =  0.02708
rho(2) = 4.0292      h( 2 )= 263.17     nobs =  30
rho(3) = 10.5064     h( 3 )= 2210.83    niter = 8
rho(4) = 0.5296
```

conns5

symbols = observed   solid curve = model

transient voltage (mv) vs time (sec)

```
rho(1) = 5000.0000   h( 1 )= 62.00      shift =  0.02720
rho(2) = 7.3590      h( 2 )= 210.09     nobs =  30
rho(3) = 9.5130      h( 3 )= 7653.23    niter = 6
rho(4) = 3.0548
```

conns4

symbols = observed   solid curve = model

rho(1) = 5000.0000   n(1)= 62.00   shift = 0.02732
rho(2) = 4.0575   n(2)= 195.46   nobs = 70
rho(3) = 28.6090   n(3)= 6372.16   niter = 6
rho(4) = 21.5628

conns3

symbols = observed   solid curve = model

rho(1) = 5000.0000   n(1)= 62.00   shift = 0.02700
rho(2) = 4.3457   n(2)= 137.40   nobs = 30
rho(3) = 4.5167   n(3)= 10.41   niter = 12
rho(4) = 32.4581

conns2

symbols = observed   solid curve = model

rho(1) = 5000.0000   n(1)= 62.00   shift = 0.02673
rho(2) = 5.1634   n(2)= 159.17   nobs = 70
rho(3) = 49.8907   n(3)= 7250.31   niter = 6
rho(4) = 29.5330

conns1.5

symbols = observed   solid curve = model

rho(1) = 5000.0000   n(1)= 62.00   shift = 0.02632
rho(2) = 5.3584   n(2)= 170.03   nobs = 70
rho(3) = 514.3535   n(3)= 7091.22   niter = 6
rho(4) = 0.5360

Appendix 2: Normalized Vertical and Horizontal Fields over a Truncated Sheet

Table A2-1 and Figures A2-1 and A2-2 show central-loop vertical and horizontal fields on the surface of a 3.5 S truncated sheet in an air host in units of milliamps / meter. The data were collected within a 250m radius loop that carries a current of one amp and they are given for offset times from 0.05 to 40 ms after transmitter current extinction. The fields are also corrected for loop height.

In the column labeled "Diff" we give the difference between the observed field and the corresponding thin-sheet reference data. For positive station locations (over the sheet) the difference is with respect to the field measured at the center of the sheet (station 2500m). If the station location is negative (off the edge of the sheet) this difference refers to the free-space field. For the station located at zero the difference is with respect to the average of station 2500m and the free-space measurement.
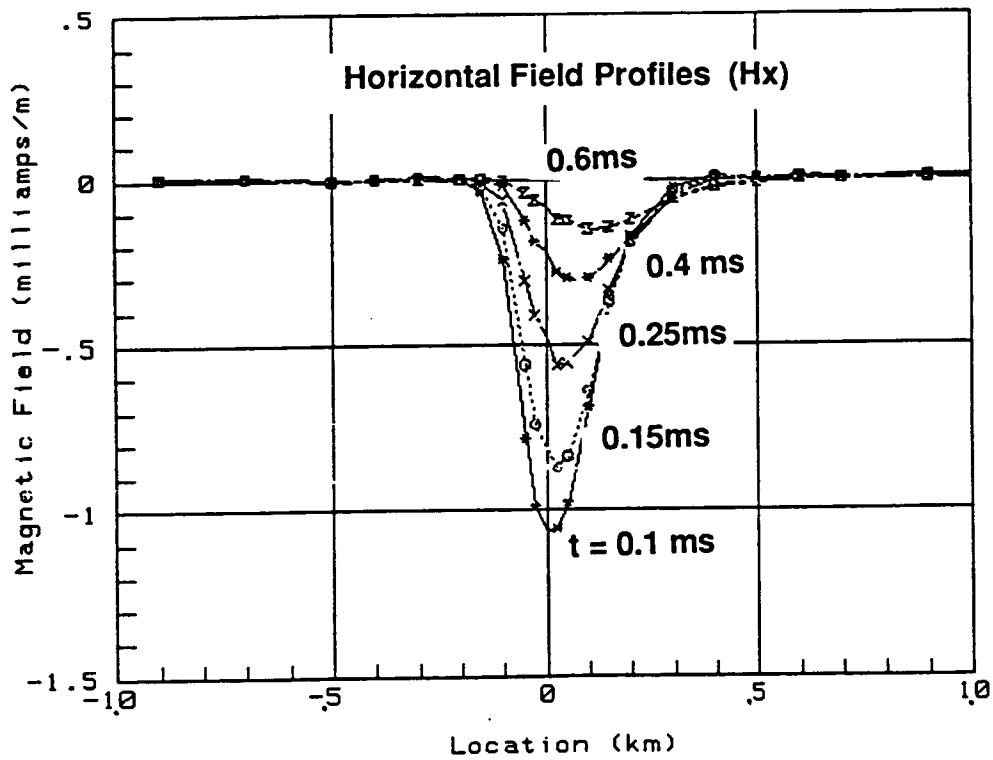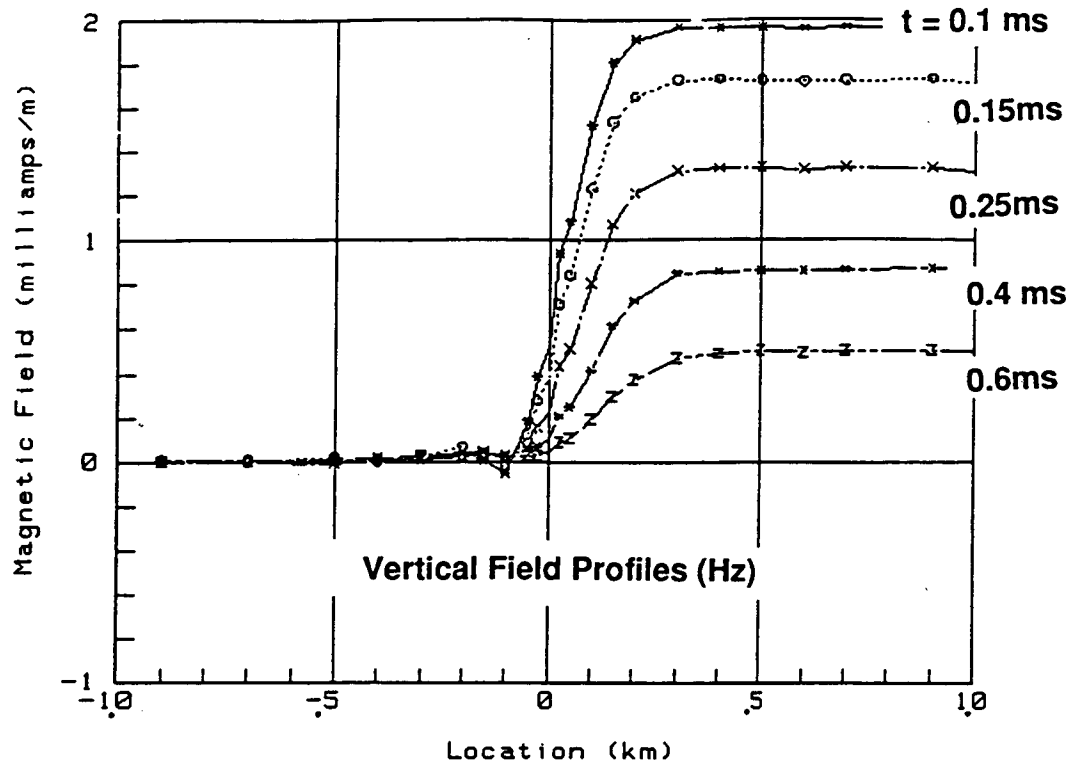
Figure A2.1 Early-time central-loop vertical and horizontal filed profiles over a 3.5 S truncated sheet.

The edge is located at station 0.0
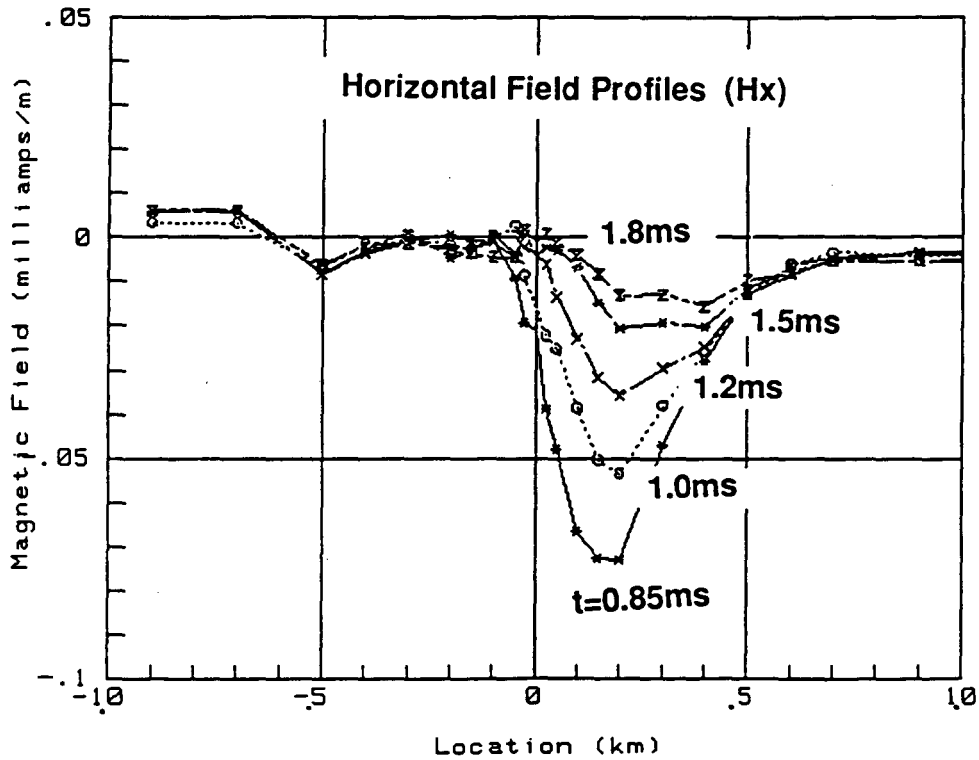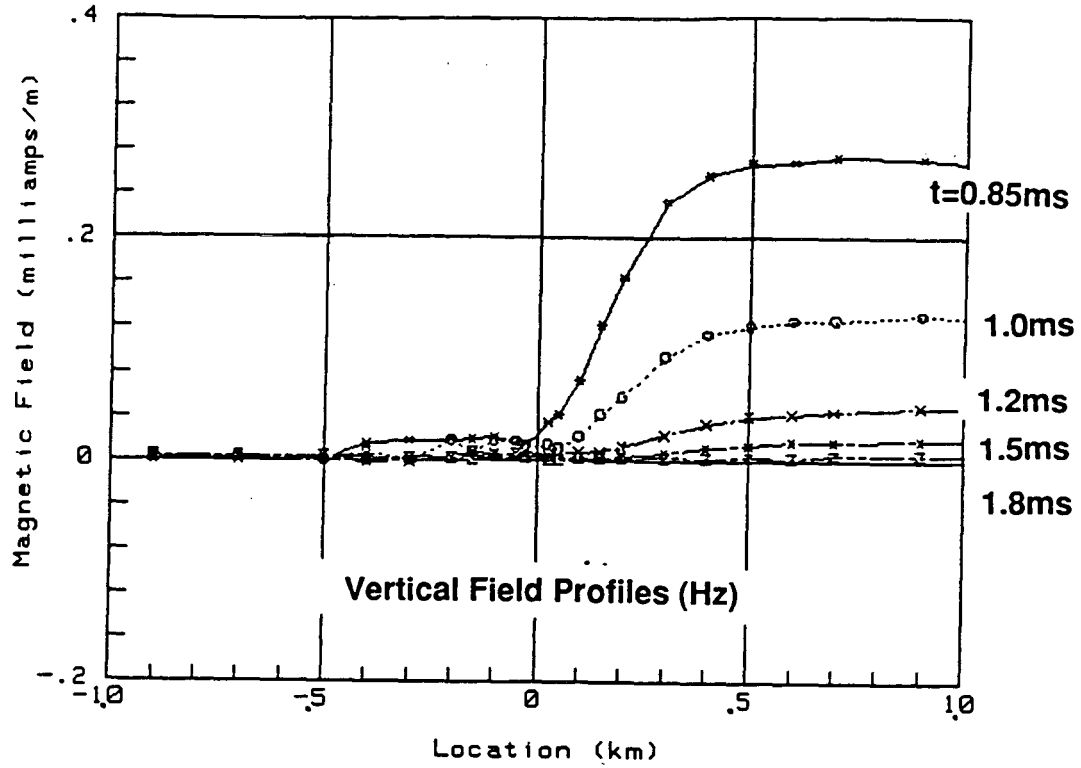
Figure A2.2 Intermediate-time central-loop vertical and horizontal field profiles over a 3.5 S truncated sheet. The edge is located at station 0.0

Table A2-1 Listing of central-loop vertical and horizontal magnetic fields over a 3.5 S truncated sheet.

178

Central-Loop Vertical Magnetic Field   (Hz)

Truncated Sheet model S=3.5 S

	2500m		1800m		1500m	
Time(ms)	Mag Field	Diff	Mag Field	Diff	Mag Field	Diff
.05	2.1719	0.00000	2.1858	.01388	2.1924	.02048
.07	2.1123	0.00000	2.0993	-.01303	2.1118	-.00045
.09	2.0502	0.00000	2.0361	-.01412	2.0400	-.01019
.10	1.9742	0.00000	1.9674	-.00688	1.9746	.00032
.12	1.8815	0.00000	1.8740	-.00748	1.8790	-.00247
.15	1.7358	0.00000	1.7351	-.00065	1.7351	-.00069
.20	1.5308	0.00000	1.5223	-.00855	1.5250	-.00585
.25	1.3294	0.00000	1.3277	-.00166	1.3305	.00117
.30	1.1577	0.00000	1.1589	.00126	1.1579	.00028
.40	.8703	0.00000	.8694	-.00094	.8762	.00589
.50	.6550	0.00000	.6617	.00672	.6654	.01044
.60	.5069	0.00000	.5076	.00076	.5063	-.00055
.70	.3795	0.00000	.3775	-.00204	.3776	-.00188
.85	.2773	0.00000	.2736	-.00377	.2741	-.00327
1.00	.1947	0.00000	.1946	-.00012	.1970	.00229
1.20	.1301	0.00000	.1306	.00052	.1320	.00183
1.50	.0743	0.00000	.0748	.00054	.0751	.00082
1.80	.0465	0.00000	.0459	-.00059	.0473	.00078
2.00	.0346	0.00000	.0328	-.00174	.0329	-.00166
2.50	.0197	0.00000	.0196	-.00016	.0217	.00201
3.00	.0113	0.00000	.0117	.00039	.0132	.00182
4.00	.0056	0.00000	.0056	-.00002	.0055	-.00013
5.00	.0036	0.00000	.0023	-.00133	.0015	-.00214
6.00	.0023	0.00000	.0020	-.00025	.0024	.00014
7.00	.0015	0.00000	.0006	-.00098	.0014	-.00012
8.50	-.0001	0.00000	.0004	.00050	-.0004	-.00024
10.00	.0007	0.00000	-.0002	-.00094	.0010	.00032
12.00	.0006	0.00000	.0003	-.00032	-.0004	-.00096
15.00	-.0007	0.00000	.0001	.00078	-.0004	.00028
18.00	-.0006	0.00000	-.0006	-.00007	-.0012	-.00061
20.00	-.0003	0.00000	.0001	.00036	.0010	.00127
25.00	-.0004	0.00000	-.0003	.00012	-.0003	.00014
30.00	-.0004	0.00000	-.0001	.00027	-.0001	.00032

	1300m		1100m		900m	
Time(ms)	Mag Field	Diff	Mag Field	Diff	Mag Field	Diff
.05	2.2037	.03176	2.1897	.01776	2.1813	.00936
.07	2.0731	-.03923	2.0947	-.02562	2.0947	-.01762
.09	2.0534	.00315	2.0322	-.01800	2.0329	-.01736
.10	1.9758	.00160	1.9674	-.00680	1.9648	-.00942
.12	1.8772	-.00431	1.8682	-.01333	1.8724	-.00910
.15	1.7378	.00208	1.7295	-.00626	1.7315	-.00422
.20	1.5342	.00342	1.5198	-.01099	1.5205	-.01034
.25	1.3321	.00272	1.3254	-.00392	1.3253	-.00411
.30	1.1638	.00614	1.1531	-.00459	1.1548	-.00290
.40	.8661	-.00428	.8689	-.00142	.8714	.00105
.50	.6618	.00685	.6654	.01045	.6576	.00268
.60	.5082	.00129	.5026	-.00426	.5020	-.00481
.70	.3786	-.00092	.3738	-.00566	.3744	-.00508
.85	.2720	-.00534	.2740	-.00331	.2725	-.00489
1.00	.1890	-.00564	.1966	.00190	.1939	-.00077
1.20	.1316	.00143	.1336	.00352	.1309	.00074
1.50	.0746	.00031	.0743	.00005	.0753	.00097
1.80	.0477	.00121	.0480	.00146	.0476	.00105
2.00	.0339	-.00067	.0332	-.00135	.0324	-.00212
2.50	.0190	-.00075	.0188	-.00093	.0179	-.00183
3.00	.0114	.00005	.0086	-.00276	.0100	-.00137
4.00	.0036	-.00206	.0042	-.00141	.0044	-.00128
5.00	.0011	-.00251	.0001	-.00352	.0022	-.00138
6.00	.0017	-.00055	.0004	-.00194	.0008	-.00152
7.00	.0019	.00041	.0024	.00084	.0012	-.00030
8.50	-.0003	-.00015	-.0004	-.00031	-.0001	.00005
10.00	-.0003	-.00095	.0007	-.00004	-.0005	-.00118
12.00	-.0009	-.00145	.0001	-.00050	-.0001	-.00065
15.00	-.0010	-.00030	-.0010	-.00033	-.0005	.00019
18.00	-.0008	-.00022	-.0003	.00029	-.0003	.00029
20.00	-.0003	.00001	.0005	.00084	.0004	.00074
25.00	-.0005	-.00004	-.0001	.00036	.0002	.00062
30.00	.0002	.00061	.0005	.00093	.0004	.00079

	700m		600m		500m	
Time(ms)	Mag Field	Diff	Mag Field	Diff	Mag Field	Diff
.05	2.1986	.02670	2.1765	.00458	2.1808	.00889
.07	2.1008	-.01150	2.1044	-.00785	2.1076	-.00474
.09	2.0356	-.01457	2.0342	-.01602	2.0383	-.01189
.10	1.9715	-.00270	1.9631	-.01119	1.9665	-.00776
.12	1.8742	-.00728	1.8650	-.01646	1.8743	-.00715
.15	1.7302	-.00551	1.7218	-.01397	1.7293	-.00646
.20	1.5272	-.00365	1.5155	-.01533	1.5187	-.01212
.25	1.3300	.00068	1.3195	-.00985	1.3246	-.00479
.30	1.1535	-.00418	1.1468	-.01082	1.1520	-.00571
.40	.8678	-.00252	.8617	-.00867	.8645	-.00586
.50	.6561	.00117	.6544	-.00058	.6543	-.00067
.60	.5029	-.00395	.4959	-.01099	.4985	-.00833
.70	.3761	-.00336	.3694	-.01010	.3674	-.01208
.85	.2732	-.00414	.2691	-.00822	.2677	-.00969
1.00	.1954	.00076	.1944	-.00031	.1865	-.00817
1.20	.1269	-.00317	.1256	-.00456	.1216	-.00848
1.50	.0713	-.00300	.0689	-.00540	.0655	-.00882
1.80	.0438	-.00271	.0415	-.00502	.0388	-.00769
2.00	.0306	-.00391	.0277	-.00683	.0261	-.00846
2.50	.0165	-.00321	.0158	-.00392	.0128	-.00690
3.00	.0085	-.00283	.0091	-.00225	.0075	-.00388
4.00	.0039	-.00171	.0015	-.00414	.0022	-.00342
5.00	.0013	-.00226	.0009	-.00273	.0013	-.00226
6.00	.0005	-.00179	.0001	-.00222	-.0006	-.00288
7.00	.0010	-.00054	.0006	-.00090	.0020	.00045
8.50	-.0004	-.00025	-.0003	-.00020	.0000	.00016
10.00	.0009	.00018	.0002	-.00050	.0004	-.00032
12.00	.0001	-.00046	.0004	-.00020	.0002	-.00043
15.00	-.0001	.00065	-.0001	.00066	-.0004	.00034
18.00	-.0004	.00015	-.0005	.00004	-.0005	.00009
20.00	.0007	.00099	.0004	.00073	.0007	.00099
25.00	-.0006	-.00014	-.0004	.00002	-.0003	.00013
30.00	-.0001	.00030	.0001	.00053	.0004	.00081

	400m		300m		200m	
Time(ms)	Mag Field	Diff	Mag Field	Diff	Mag Field	Diff
.05	2.1925	.02059	2.1965	.02464	2.1565	-.01543
.07	2.0991	-.01323	2.1061	-.00621	2.0731	-.03919
.09	2.0413	-.00896	2.0315	-.01876	1.9915	-.05868
.10	1.9673	-.00693	1.9698	-.00447	1.9122	-.06209
.12	1.8739	-.00759	1.8719	-.00957	1.8069	-.07464
.15	1.7317	-.00406	1.7291	-.00666	1.6532	-.08260
.20	1.5184	-.01240	1.5163	-.01451	1.4238	-.10699
.25	1.3236	-.00573	1.3117	-.01763	1.2104	-.11893
.30	1.1529	-.00480	1.1365	-.02116	1.0182	-.13945
.40	.8581	-.01220	.8500	-.02035	.7283	-.14200
.50	.6497	-.00525	.6282	-.02677	.5145	-.14042
.60	.4893	-.01758	.4640	-.04290	.3685	-.13836
.70	.3597	-.01981	.3335	-.04604	.2518	-.12769
.85	.2560	-.02130	.2326	-.04477	.1647	-.11269
1.00	.1778	-.01682	.1600	-.03470	.1047	-.08996
1.20	.1133	-.01681	.0934	-.03671	.0567	-.07344
1.50	.0558	-.01848	.0436	-.03070	.0233	-.05102
1.80	.0323	-.01419	.0227	-.02378	.0111	-.03543
2.00	.0210	-.01359	.0133	-.02129	.0057	-.02888
2.50	.0107	-.00901	.0062	-.01347	.0029	-.01684
3.00	.0047	-.00666	.0042	-.00716	.0016	-.00974
4.00	.0017	-.00391	.0018	-.00380	.0013	-.00433
5.00	.0005	-.00307	-.0005	-.00414	-.0002	-.00379
6.00	.0002	-.00211	.0005	-.00174	-.0002	-.00254
7.00	.0003	-.00122	.0013	-.00021	.0002	-.00135
8.50	-.0000	.00013	-.0002	-.00005	.0001	.00023
10.00	-.0001	-.00082	.0003	-.00042	-.0005	-.00125
12.00	-.0001	-.00074	-.0001	-.00073	.0001	-.00051
15.00	-.0005	.00017	-.0004	.00029	-.0003	.00041
18.00	-.0004	.00011	-.0009	-.00037	-.0007	-.00014
20.00	.0012	.00148	.0014	.00169	-.0000	.00029
25.00	.0003	.00073	.0000	.00046	-.0003	.00012
30.00	.0005	.00091	.0002	.00059	-.0001	.00032

	150m		100m			
Time(ms)	Mag Field	Diff	Mag Field	Diff	Mag Field	Diff
.05	2.1007	-.07121	1.8585	-.31341	1.4442	-.72768
.07	1.9917	-.12062	1.7054	-.40686	1.2755	-.83680
.09	1.8941	-.15609	1.6194	-.43086	1.1764	-.87383
.10	1.8079	-.16636	1.5219	-.45230	1.0846	-.88968
.12	1.6962	-.18535	1.3966	-.48490	.9828	-.89871
.15	1.5369	-.19887	1.2294	-.50632	.8390	-.89674
.20	1.2898	-.24103	.9926	-.53825	.6584	-.87244
.25	1.0713	-.25807	.8033	-.52606	.5124	-.81698
.30	.8966	-.26106	.6416	-.51604	.3975	-.76018
.40	.6153	-.25501	.4136	-.45673	.2465	-.62379
.50	.4256	-.22940	.2750	-.37994	.1572	-.49771
.60	.2942	-.21267	.1883	-.31852	.1018	-.40502
.70	.1922	-.18730	.1172	-.26232	.0573	-.32218
.85	.1216	-.15573	.0720	-.20535	.0403	-.23706
1.00	.0744	-.12031	.0412	-.15346	.0212	-.17345
1.20	.0411	-.08905	.0200	-.11012	.0100	-.12017
1.50	.0157	-.05862	.0087	-.06562	.0040	-.07026
1.80	.0073	-.03922	.0061	-.04042	.0054	-.04114
2.00	.0033	-.03127	.0017	-.03289	.0032	-.03139
2.50	.0015	-.01825	-.0003	-.02001	.0032	-.01652
3.00	.0029	-.00847	.0021	-.00919	.0023	-.00903
4.00	.0008	-.00487	.0007	-.00490	-.0001	-.00569
5.00	-.0009	-.00445	-.0004	-.00403	.0004	-.00318
6.00	.0005	-.00181	.0016	-.00067	.0003	-.00200
7.00	.0014	-.00014	.0003	-.00124	-.0005	-.00200
8.50	-.0007	-.00055	-.0006	-.00043	-.0004	-.00023
10.00	.0002	-.00050	-.0005	-.00117	-.0000	-.00072
12.00	-.0002	-.00083	.0001	-.00052	-.0011	-.00169
15.00	-.0004	.00035	-.0004	.00036	-.0008	-.00011
18.00	-.0010	-.00044	-.0008	-.00023	-.0007	-.00011
20.00	.0011	.00143	.0006	.00094	.0001	.00043
25.00	.0002	.00062	-.0003	.00011	-.0007	-.00027
30.00	.0002	.00064	.0000	.00044	-.0005	-.00013

	25m		0m		-25m	
Time(ms)	Mag Field	Diff	Mag Field	Diff	Mag Field	Diff
.05	1.2622	-.90968	.7678	-.37338	.5670	.51179
.07	1.1233	-.98902	.6708	-.39112	.4844	.47864
.09	1.0337	-1.01654	.5938	-.43676	.4363	.43078
.10	.9421	-1.03212	.5263	-.46190	.3819	.38080
.12	.8427	-1.03877	.4695	-.47017	.3345	.33564
.15	.7088	-1.02696	.3880	-.48123	.2731	.27176
.20	.5581	-.97272	.2985	-.46855	.2048	.20316
.25	.4286	-.90073	.2246	-.44261	.1510	.14854
.30	.3376	-.82003	.1816	-.40035	.1154	.11222
.40	.2077	-.66258	.0992	-.34040	.0620	.05759
.50	.1251	-.52988	.0553	-.27451	.0301	.02781
.60	.0869	-.41998	.0429	-.21384	.0265	.02321
.70	.0519	-.32759	.0143	-.17429	.0227	.02391
.85	.0336	-.24375	.0222	-.11909	.0133	.01068
1.00	.0266	-.16806	.0138	-.08637	.0094	.00659
1.20	.0138	-.11633	.0120	-.05480	.0123	.01058
1.50	.0040	-.07027	.0045	-.03193	.0040	.00477
1.80	.0038	-.04272	.0047	-.01874	.0063	.00612
2.00	.0012	-.03338	.0054	-.01046	.0035	.00491
2.50	.0033	-.01640	.0029	-.00791	.0019	.00098
3.00	.0038	-.00755	.0067	-.00014	.0000	-.00113
4.00	-.0000	-.00568	.0032	-.00030	.0011	.00043
5.00	-.0017	-.00533	.0015	-.00038	.0001	.00004
6.00	.0018	-.00050	.0018	.00018	.0037	.00324
7.00	.0028	.00132	.0015	-.00044	.0010	-.00022
8.50	-.0004	-.00029	.0017	.00223	.0002	.00060
10.00	.0011	.00037	.0011	.00019	.0015	.00100
12.00	-.0008	-.00138	.0008	.00065	.0020	.00212
15.00	.0002	.00093	.0001	.00105	-.0012	-.00067
18.00	.0004	.00094	-.0000	.00075	.0010	.00150
20.00	.0007	.00099	.0008	.00033	-.0001	-.00072
25.00	.0001	.00056	.0007	.00130	.0001	.00044
30.00	.0004	.00075	.0010	.00101	-.0007	-.00087

	-50m		-100m		-150m	
Time(ms)	Mag Field	Diff	Mag Field	Diff	Mag Field	Diff
.05	.3525	.29726	-.0074	-.06262	.0099	-.04534
.07	.2580	.25228	-.1013	-.10700	-.0153	-.02099
.09	.1848	.17930	-.0902	-.09565	-.0102	-.01569
.10	.1812	.18009	-.0589	-.06001	.0037	.00259
.12	.1532	.15434	-.0530	-.05192	.0155	.01664
.15	.1211	.11981	-.0216	-.02292	.0151	.01378
.20	.0857	.08408	.0103	.00863	.0317	.03012
.25	.0558	.05334	.0246	.02208	.0373	.03481
.30	.0580	.05490	.0032	.00009	.0312·	.02807
.40	.0592	.05481	.0245	.02003	.0413	.03689
.50	.0407	.03841	.0227	.02037	.0303	.02796
.60	.0240	.02074	.0187	.01537	.0293	.02600
.70	.0125	.01369	.0136	.01480	.0165	.01763
.85	.0150	.01236	.0195	.01694	.0177	.01513
1.00	.0338	.03097	.0211	.01826	.0208	.01799
1.20	.0160	.01432	.0165	.01480	.0062	.00453
1.50	.0062	.00691	.0086	.00937	.0068	.00757
1.80	.0042	.00405	.0047	.00458	.0069	.00680
2.00	.0043	.00572	.0045	.00590	.0063	.00766
2.50	.0015	.00062	.0013	-.00040	.0025	.00156
3.00	.0030	-.00186	.0045	-.00330	.0085	.00735
4.00	.0044	.00365	.0028	.00210	-.0010	-.00169
5.00	-.0048	-.00485	.0004	.00031	-.0035	-.00358
6.00	-.0007	-.00117	-.0016	-.00209	.0011	.00065
7.00	.0035	.00230	.0009	-.00032	.0029	.00172
8.50	-.0028	-.00234	-.0019	-.00146	.0002	.00060
10.00	-.0001	-.00064	.0010	.00046	-.0008	-.00128
12.00	-.0011	-.00100	-.0022	-.00202	-.0003	-.00019
15.00	-.0006	-.00004	-.0021	-.00153	.0006	.00115
18.00	-.0008	-.00035	-.0019	-.00142	-.0009	-.00039
20.00	.0020	.00141	.0015	.00090	.0005	-.00006
25.00	-.0008	-.00047	-.0021	-.00178	.0001	.00042
30.00	.0003	.00009	-.0004	-.00063	-.0004	-.00063

	-200m		-300m		-400m	
Time(ms)	Mag Field	Diff	Mag Field	Diff	Mag Field	Diff
.05	.0975	.04228	.0428	-.01242	.0838	.02859
.07	.0248	.01906	.0743	.06858	.0182	.01252
.09	.0462	.04071	.0560	.05046	.0127	.00719
.10	.0403	.03923	.0158	.01476	.0088	.00769
.12	.0480	.04914	.0344	.03556	.0038	.00494
.15	.0611	.05975	.0255	.02422	-.0031	-.00439
.20	.0464	.04476	.0278	.02619	.0236	.02195
.25	.0417	.03924	.0202	.01776	.0136	.01110
.30	.0372	.03403	.0092	.00608	-.0017	-.00487
.40	.0244	.01996	.0016	-.00284	.0153	.01088
.50	.0366	.03427	.0133	.01102	-.0004	-.00268
.60	.0188	.01547	.0163	.01299	.0066	.00335
.70	.0104	.01159	.0076	.00872	.0009	.00208
.85	.0172	.01462	.0172	.01457	.0143	.01171
1.00	.0141	.01130	.0064	.00354	.0041	.00127
1.20	.0172	.01546	-.0013	-.00295	.0061	.00438
1.50	.0005	.00128	.0056	.00636	.0006	.00135
1.80	.0021	.00193	-.0019	-.00201	.0024	.00225
2.00	.0013	.00266	.0005	.00186	.0030	.00435
2.50	.0001	-.00085	-.0000	-.00096	-.0027	-.00363
3.00	.0062	.00501	.0023	.00113	-.0022	-.00333
4.00	.0006	-.00009	.0021	.00142	-.0007	-.00139
5.00	.0009	.00085	.0030	.00291	-.0004	-.00043
6.00	.0011	.00056	.0006	.00007	.0024	.00195
7.00	.0001	-.00111	.0005	-.00067	.0022	.00094
8.50	.0015	.00198	-.0016	-.00115	-.0024	-.00193
10.00	-.0007	-.00118	.0027	.00215	-.0006	-.00109
12.00	-.0006	-.00048	-.0003	-.00021	.0002	.00031
15.00	-.0008	-.00022	-.0005	.00003	-.0036	-.00301
18.00	-.0011	-.00063	.0011	.00157	.0021	.00263
20.00	-.0000	-.00059	-.0002	-.00078	.0010	.00037
25.00	-.0003	.00007	-.0015	-.00115	-.0011	-.00074
30.00	.0007	.00051	.0001	-.00015	-.0007	-.00089

	-500m		-700m		-900m	
Time(ms)	Mag Field	Diff	Mag Field	Diff	Mag Field	Diff
.05	.0549	-.00037	.0608	.00556	.0608	.00556
.07	-.0000	-.00575	-.0091	-.01478	-.0091	-.01478
.09	.0044	-.00105	.0019	-.00356	.0019	-.00356
.10	-.0009	-.00201	-.0010	-.00208	-.0010	-.00208
.12	.0109	.01206	-.0044	-.00326	-.0044	-.00326
.15	.0167	.01534	.0039	.00260	.0039	.00260
.20	.0024	.00075	-.0034	-.00501	-.0034	-.00501
.25	-.0096	-.01211	-.0022	-.00468	-.0022	-.00468
.30	.0115	.00839	-.0010	-.00415	-.0010	-.00415
.40	.0071	.00262	.0036	-.00082	.0036	-.00082
.50	.0075	.00523	.0074	.00510	.0074	.00510
.60	.0030	-.00028	.0004	-.00291	.0004	-.00291
.70	-.0009	.00028	-.0027	-.00154	-.0027	-.00154
.85	-.0016	-.00416	-.0013	-.00392	-.0013	-.00392
1.00	.0085	.00562	.0007	-.00212	.0007	-.00212
1.20	-.0003	-.00200	.0022	.00048	.0022	.00048
1.50	.0021	.00286	-.0019	-.00113	-.0019	-.00113
1.80	.0022	.00210	.0013	.00118	.0013	.00118
2.00	.0020	.00343	-.0016	-.00023	-.0016	-.00023
2.50	.0002	-.00073	.0022	.00128	.0022	.00128
3.00	.0009	-.00028	-.0033	-.00443	-.0033	-.00443
4.00	.0030	.00234	.0023	.00161	.0023	.00161
5.00	.0021	.00207	.0007	.00062	.0007	.00062
6.00	.0027	.00218	.0007	.00023	.0007	.00023
7.00	.0036	.00235	.0026	.00143	.0026	.00143
8.50	-.0008	-.00040	-.0009	-.00046	-.0009	-.00046
10.00	.0013	.00078	.0006	.00010	.0006	.00010
12.00	.0010	.00116	-.0006	-.00046	-.0006	-.00046
15.00	.0021	.00269	.0001	.00064	.0001	.00064
18.00	-.0008	-.00029	-.0011	-.00059	-.0011	-.00059
20.00	.0022	.00160	.0001	-.00045	.0001	-.00045
25.00	.0013	.00165	-.0007	-.00042	-.0007	-.00042
30.00	.0017	.00150	.0004	.00015	.0004	.00015

Central-Loop Horizontal Magnetic Field (Hx)

Truncated Sheet model S=3.5 S

	2500m		1800m		1500m	
Time(ms)	Mag Field	Diff	Mag Field	Diff	Mag Field	Diff
.05	0.0000	0.00000	.0071	.00707	.0029	.00291
.07	0.0000	0.00000	.0031	.00315	-.0027	-.00273
.09	0.0000	0.00000	.0006	.00057	-.0040	-.00396
.10	0.0000	0.00000	.0032	.00317	-.0011	-.00106
.12	0.0000	0.00000	.0038	.00375	-.0004	-.00036
.15	0.0000	0.00000	.0009	.00092	-.0020	-.00195
.20	0.0000	0.00000	.0012	.00118	.0017	.00172
.25	0.0000	0.00000	.0035	.00348	.0020	.00198
.30	0.0000	0.00000	.0018	.00185	.0015	.00146
.40	0.0000	0.00000	.0011	.00113	.0017	.00168
.50	0.0000	0.00000	.0008	.00084	.0000	.00000
.60	0.0000	0.00000	-.0001	-.00008	.0006	.00064
.70	0.0000	0.00000	.0011	.00110	.0012	.00119
.85	0.0000	0.00000	.0015	.00147	.0010	.00095
1.00	0.0000	0.00000	.0010	.00104	.0022	.00215
1.20	0.0000	0.00000	-.0002	-.00024	-.0003	-.00025
1.50	0.0000	0.00000	-.0002	-.00025	-.0007	-.00069
1.80	0.0000	0.00000	-.0007	-.00070	-.0009	-.00089
2.00	0.0000	0.00000	-.0001	-.00008	-.0008	-.00079
2.50	0.0000	0.00000	.0007	.00073	.0001	.00010
3.00	0.0000	0.00000	-.0006	-.00060	-.0009	-.00090
4.00	0.0000	0.00000	.0003	.00026	.0001	.00011
5.00	0.0000	0.00000	-.0002	-.00024	-.0002	-.00021
6.00	0.0000	0.00000	-.0003	-.00031	-.0001	-.00014
7.00	0.0000	0.00000	.0001	.00007	.0004	.00041
8.50	0.0000	0.00000	-.0005	-.00055	-.0000	-.00001
10.00	0.0000	0.00000	-.0001	-.00007	.0003	.00034
12.00	0.0000	0.00000	.0002	.00021	.0005	.00048
15.00	0.0000	0.00000	-.0000	-.00000	.0005	.00047
18.00	0.0000	0.00000	-.0001	-.00013	.0003	.00033
20.00	0.0000	0.00000	.0002	.00016	.0005	.00053
25.00	0.0000	0.00000	.0002	.00016	.0005	.00049
30.00	0.0000	0.00000	.0001	.00012	.0005	.00048

	1300m		1100m		900m	
Time(ms)	Mag Field	Diff	Mag Field	Diff	Mag Field	Diff
.05	.0107	.01069	.0148	.01479	.0147	.01471
.07	.0079	.00795	.0115	.01148	.0100	.00995
.09	.0051	.00515	.0068	.00678	.0067	.00667
.10	.0058	.00578	.0103	.01027	.0089	.00891
.12	.0054	.00537	.0115	.01152	.0083	.00829
.15	.0048	.00479	.0080	.00802	.0049	.00488
.20	.0045	.00451	.0076	.00762	.0030	.00305
.25	.0046	.00458	.0082	.00822	.0046	.00461
.30	.0029	.00289	.0043	.00426	.0028	.00284
.40	.0001	.00006	.0001	.00008	.0004	.00035
.50	.0006	.00061	-.0013	-.00131	-.0016	-.00159
.60	-.0003	-.00028	-.0001	-.00006	-.0031	-.00312
.70	.0001	.00013	-.0019	-.00190	-.0024	-.00243
.85	-.0020	-.00204	-.0017	-.00174	-.0032	-.00316
1.00	-.0027	-.00267	-.0013	-.00126	-.0042	-.00416
1.20	-.0023	-.00227	-.0032	-.00316	-.0038	-.00379
1.50	-.0029	-.00289	-.0043	-.00431	-.0052	-.00524
1.80	-.0032	-.00320	-.0043	-.00434	-.0055	-.00550
2.00	-.0034	-.00344	-.0045	-.00449	-.0046	-.00456
2.50	-.0027	-.00272	-.0031	-.00307	-.0047	-.00468
3.00	-.0038	-.00376	-.0049	-.00486	-.0052	-.00520
4.00	-.0028	-.00284	-.0036	-.00363	-.0039	-.00388
5.00	-.0029	-.00288	-.0038	-.00383	-.0033	-.00327
6.00	-.0029	-.00286	-.0030	-.00300	-.0034	-.00344
7.00	-.0024	-.00236	-.0033	-.00328	-.0031	-.00305
8.50	-.0028	-.00284	-.0041	-.00413	-.0033	-.00326
10.00	-.0025	-.00249	-.0035	-.00351	-.0032	-.00316
12.00	-.0026	-.00255	-.0031	-.00306	-.0029	-.00287
15.00	-.0028	-.00277	-.0035	-.00355	-.0029	-.00290
18.00	-.0027	-.00266	-.0035	-.00355	-.0031	-.00307
20.00	-.0023	-.00233	-.0032	-.00315	-.0029	-.00291
25.00	-.0026	-.00256	-.0032	-.00324	-.0030	-.00301
30.00	-.0024	-.00241	-.0031	-.00314	-.0029	-.00288

	700m		600m		500m	
Time(ms)	Mag Field	Diff	Mag Field	Diff	Mag Field	Diff
.05	.0058	.00583	.0145	.01447	.0042	.00425
.07	.0016	.00158	.0092	.00924	.0006	.00062
.09	-.0003	-.00029	.0086	.00861	-.0018	-.00179
.10	.0026	.00262	.0110	.01103	-.0003	-.00026
.12	.0027	.00270	.0106	.01063	.0002	.00018
.15	-.0005	-.00046	.0088	.00880	-.0024	-.00244
.20	.0029	.00290	.0046	.00462	-.0037	-.00374
.25	.0026	.00259	.0057	.00567	-.0024	-.00245
.30	.0001	.00015	.0003	.00028	-.0056	-.00563
.40	-.0012	-.00121	-.0009	-.00092	-.0070	-.00701
.50	-.0028	-.00279	-.0019	-.00187	-.0094	-.00937
.60	-.0034	-.00336	-.0034	-.00343	-.0119	-.01186
.70	-.0031	-.00308	-.0056	-.00559	-.0119	-.01190
.85	-.0047	-.00472	-.0063	-.00632	-.0134	-.01338
1.00	-.0035	-.00348	-.0062	-.00620	-.0131	-.01314
1.20	-.0049	-.00487	-.0085	-.00848	-.0129	-.01290
1.50	-.0054	-.00542	-.0076	-.00764	-.0116	-.01155
1.80	-.0052	-.00519	-.0081	-.00805	-.0097	-.00966
2.00	-.0052	-.00522	-.0074	-.00741	-.0085	-.00854
2.50	-.0032	-.00317	-.0055	-.00550	-.0050	-.00503
3.00	-.0037	-.00374	-.0045	-.00447	-.0033	-.00330
4.00	-.0015	-.00152	-.0023	-.00230	-.0009	-.00092
5.00	-.0008	-.00076	-.0018	-.00181	-.0005	-.00053
6.00	-.0007	-.00072	-.0016	-.00161	-.0002	-.00016
7.00	-.0000	-.00000	-.0013	-.00132	.0002	.00018
8.50	-.0010	-.00097	-.0021	-.00210	-.0003	-.00030
10.00	-.0005	-.00049	-.0017	-.00165	.0002	.00017
12.00	-.0003	-.00025	-.0014	-.00140	.0001	.00014
15.00	-.0003	-.00030	-.0015	-.00155	.0002	.00016
18.00	-.0006	-.00062	-.0017	-.00167	-.0003	-.00028
20.00	-.0004	-.00041	-.0014	-.00138	.0001	.00010
25.00	-.0004	-.00044	-.0015	-.00151	.0002	.00018
30.00	-.0003	-.00033	-.0016	-.00158	.0001	.00008

	400m		300m		200m	
Time(ms)	Mag Field	Diff	Mag Field	Diff	Mag Field	Diff
.05	.0207	.02073	-.0129	-.01290	-.1211	-.12111
.07	.0175	.01752	-.0189	-.01886	-.1451	-.14508
.09	.0103	.01032	-.0266	-.02656	-.1600	-.15998
.10	.0103	.01025	-.0265	-.02649	-.1676	-.16757
.12	.0088	.00878	-.0298	-.02981	-.1805	-.18053
.15	.0049	.00491	-.0366	-.03658	-.1950	-.19505
.20	.0008	.00075	-.0429	-.04293	-.2031	-.20308
.25	-.0027	-.00273	-.0479	-.04792	-.2007	-.20071
.30	-.0104	-.01035	-.0541	-.05405	-.1948	-.19476
.40	-.0191	-.01908	-.0598	-.05978	-.1739	-.17391
.50	-.0235	-.02350	-.0617	-.06169	-.1480	-.14802
.60	-.0263	-.02626	-.0570	-.05696	-.1219	-.12192
.70	-.0282	-.02820	-.0526	-.05260	-.0978	-.09776
.85	-.0282	-.02818	-.0471	-.04709	-.0733	-.07331
1.00	-.0260	-.02599	-.0383	-.03826	-.0538	-.05378
1.20	-.0250	-.02496	-.0296	-.02960	-.0358	-.03581
1.50	-.0204	-.02042	-.0194	-.01937	-.0208	-.02079
1.80	-.0156	-.01564	-.0130	-.01303	-.0131	-.01315
2.00	-.0135	-.01352	-.0093	-.00932	-.0100	-.01001
2.50	-.0090	-.00902	-.0031	-.00307	-.0050	-.00498
3.00	-.0074	-.00743	-.0019	-.00189	-.0046	-.00455
4.00	-.0050	-.00496	-.0001	-.00009	-.0024	-.00240
5.00	-.0044	-.00437	.0004	.00044	-.0031	-.00311
6.00	-.0044	-.00437	.0001	.00014	-.0032	-.00319
7.00	-.0042	-.00417	.0001	.00007	-.0032	-.00316
8.50	-.0044	-.00438	-.0003	-.00028	-.0033	-.00327
10.00	-.0040	-.00401	.0001	.00007	-.0034	-.00340
12.00	-.0038	-.00384	.0004	.00039	-.0031	-.00305
15.00	-.0042	-.00418	.0005	.00051	-.0031	-.00313
18.00	-.0043	-.00427	.0005	.00045	-.0032	-.00325
20.00	-.0041	-.00409	.0004	.00039	-.0032	-.00321
25.00	-.0043	-.00425	.0004	.00039	-.0032	-.00315
30.00	-.0041	-.00412	.0002	.00016	-.0032	-.00323

Time(ms)	150m Mag Field	150m Diff	100m Mag Field	100m Diff	50m Mag Field	50m Diff
.05	-.3015	-.30152	-.6692	-.66924	-1.0532	-1.05321
.07	-.3359	-.33591	-.6982	-.69822	-1.0504	-1.05037
.09	-.3541	-.35406	-.6962	-.69620	-1.0202	-1.02019
.10	-.3593	-.35926	-.6877	-.68767	-.9792	-.97922
.12	-.3667	-.36667	-.6759	-.67586	-.9254	-.92539
.15	-.3714	-.37139	-.6409	-.64093	-.8412	-.84121
.20	-.3601	-.36008	-.5634	-.56342	-.6870	-.68700
.25	-.3337	-.33367	-.4903	-.49031	-.5548	-.55482
.30	-.3036	-.30359	-.4229	-.42294	-.4631	-.46311
.40	-.2421	-.24210	-.3000	-.30003	-.3001	-.30011
.50	-.1869	-.18689	-.2128	-.21285	-.1941	-.19405
.60	-.1455	-.14555	-.1513	-.15127	-.1254	-.12541
.70	-.1071	-.10714	-.1020	-.10199	-.0797	-.07968
.85	-.0728	-.07283	-.0670	-.06695	-.0482	-.04824
1.00	-.0505	-.05051	-.0388	-.03877	-.0255	-.02545
1.20	-.0319	-.03185	-.0230	-.02301	-.0135	-.01353
1.50	-.0149	-.01492	-.0069	-.00685	-.0028	-.00284
1.80	-.0084	-.00844	-.0040	-.00402	-.0010	-.00105
2.00	-.0059	-.00591	-.0033	-.00333	.0020	.00201
2.50	-.0017	-.00173	-.0007	-.00073	-.0015	-.00149
3.00	-.0030	-.00301	-.0015	-.00147	-.0031	-.00310
4.00	-.0023	-.00231	-.0008	-.00076	-.0005	-.00054
5.00	-.0021	-.00212	-.0012	-.00120	-.0036	-.00365
6.00	-.0017	-.00174	-.0010	-.00103	-.0007	-.00066
7.00	-.0021	-.00211	.0001	.00005	-.0023	-.00228
8.50	-.0023	-.00227	-.0021	-.00206	-.0026	-.00264
10.00	-.0018	-.00182	-.0018	-.00183	-.0021	-.00210
12.00	-.0022	-.00217	-.0019	-.00189	-.0014	-.00142
15.00	-.0022	-.00224	-.0015	-.00145	-.0036	-.00358
18.00	-.0020	-.00204	-.0017	-.00169	-.0017	-.00168
20.00	-.0023	-.00233	-.0022	-.00223	-.0024	-.00244
25.00	-.0025	-.00252	-.0018	-.00180	-.0014	-.00137
30.00	-.0023	-.00231	-.0014	-.00139	-.0020	-.00197

Time(ms)	25m Mag Field	25m Diff	Mag Field	Diff	-25m Mag Field	-25m Diff
.05	-1.1945	-1.19454	-1.3402	-1.34016	-1.3204	-1.32041
.07	-1.1601	-1.16013	-1.2101	-1.21012	-1.1835	-1.18351
.09	-1.1098	-1.10982	-1.1343	-1.13431	-1.0774	-1.07737
.10	-1.0573	-1.05730	-1.0597	-1.05968	-.9913	-.99130
.12	-.9795	-.97946	-.9543	-.95425	-.8810	-.88103
.15	-.8729	-.87286	-.8206	-.82061	-.7439	-.74395
.20	-.7106	-.71059	-.6305	-.63049	-.5590	-.55896
.25	-.5637	-.56371	-.4745	-.47450	-.4132	-.41325
.30	-.4476	-.44761	-.3691	-.36907	-.3109	-.31089
.40	-.2797	-.27974	-.2155	-.21550	-.1915	-.19148
.50	-.1846	-.18456	-.1440	-.14404	-.1110	-.11104
.60	-.1201	-.12015	-.0816	-.08157	-.0633	-.06334
.70	-.0707	-.07069	-.0489	-.04886	-.0336	-.03359
.85	-.0390	-.03903	-.0209	-.02093	-.0195	-.01947
1.00	-.0221	-.02214	-.0163	-.01627	-.0087	-.00870
1.20	-.0060	-.00605	-.0040	-.00400	-.0021	-.00213
1.50	-.0022	-.00224	-.0040	-.00404	.0013	.00128
1.80	.0008	.00080	-.0010	-.00105	.0014	.00144
2.00	.0023	.00225	-.0020	-.00200	.0016	.00155
2.50	.0022	.00218	.0003	.00027	.0008	.00081
3.00	-.0012	-.00124	-.0035	-.00352	-.0008	-.00078
4.00	-.0008	-.00079	-.0066	-.00655	-.0016	-.00164
5.00	.0006	.00064	-.0062	-.00621	-.0010	-.00101
6.00	.0008	.00083	-.0053	-.00532	-.0004	-.00040
7.00	.0008	.00085	-.0054	-.00541	-.0005	-.00049
8.50	-.0022	-.00223	-.0068	-.00680	-.0017	-.00167
10.00	-.0020	-.00205	-.0080	-.00801	-.0034	-.00337
12.00	-.0011	-.00112	-.0058	-.00582	-.0038	-.00379
15.00	-.0012	-.00121	-.0050	-.00495	-.0033	-.00334
18.00	-.0012	-.00117	-.0054	-.00542	-.0028	-.00283
20.00	-.0016	-.00158	-.0050	-.00502	-.0019	-.00191
25.00	-.0015	-.00154	-.0060	-.00600	-.0034	-.00339
30.00	-.0017	-.00171	-.0066	-.00655	-.0021	-.00214

	-50m		-100m		-150m	
Time(ms)	Mag Field	Diff	Mag Field	Diff	Mag Field	Diff
.05	-1.0935	-1.09347	-.3889	-.38885	-.0856	-.08557
.07	-.9528	-.95281	-.3193	-.31933	-.0618	-.06178
.09	-.8712	-.87121	-.2777	-.27769	-.0527	-.05265
.10	-.7843	-.78431	-.2395	-.23947	-.0418	-.04179
.12	-.6881	-.68812	-.1995	-.19953	-.0298	-.02975
.15	-.5633	-.56330	-.1481	-.14813	-.0177	-.01773
.20	-.4068	-.40684	-.0945	-.09452	-.0109	-.01087
.25	-.3078	-.30779	-.0653	-.06534	-.0081	-.00811
.30	-.2293	-.22930	-.0474	-.04736	.0006	.00062
.40	-.1255	-.12550	-.0205	-.02046	-.0005	-.00049
.50	-.0655	-.06547	-.0051	-.00514	.0016	.00164
.60	-.0418	-.04183	-.0042	-.00423	.0020	.00200
.70	-.0232	-.02319	.0009	.00085	-.0022	-.00224
.85	-.0093	-.00932	-.0005	-.00050	-.0008	-.00079
1.00	.0026	.00258	.0003	.00031	-.0027	-.00272
1.20	-.0044	-.00440	-.0009	-.00087	-.0022	-.00222
1.50	-.0037	-.00372	.0006	.00060	-.0029	-.00294
1.80	-.0044	-.00442	-.0046	-.00463	-.0035	-.00351
2.00	-.0043	-.00432	-.0046	-.00462	-.0029	-.00286
2.50	-.0046	-.00456	-.0021	-.00213	-.0039	-.00389
3.00	-.0077	-.00772	-.0019	-.00188	-.0050	-.00501
4.00	-.0053	-.00529	-.0016	-.00161	-.0043	-.00434
5.00	-.0077	-.00775	-.0024	-.00242	-.0040	-.00397
6.00	-.0068	-.00678	-.0035	-.00353	-.0050	-.00500
7.00	-.0097	-.00970	-.0036	-.00357	-.0058	-.00582
8.50	-.0074	-.00741	-.0052	-.00516	-.0046	-.00462
10.00	-.0079	-.00795	-.0046	-.00463	-.0055	-.00547
12.00	-.0083	-.00829	-.0048	-.00479	-.0048	-.00475
15.00	-.0088	-.00885	-.0041	-.00414	-.0056	-.00562
18.00	-.0086	-.00862	-.0044	-.00436	-.0047	-.00467
20.00	-.0085	-.00851	-.0032	-.00315	-.0043	-.00426
25.00	-.0090	-.00902	-.0043	-.00433	-.0048	-.00484
30.00	-.0077	-.00773	-.0043	-.00432	-.0050	-.00501

	-200m		-300m		-400m	
Time(ms)	Mag Field	Diff	Mag Field	Diff	Mag Field	Diff
.05	-.0114	-.01145	.0074	.00737	-.0015	-.00150
.07	-.0018	-.00182	.0118	.01183	-.0029	-.00294
.09	.0004	.00045	.0118	.01184	-.0045	-.00451
.10	.0017	.00166	.0097	.00974	-.0017	-.00173
.12	.0007	.00065	.0041	.00411	.0000	.00002
.15	-.0005	-.00054	.0062	.00623	-.0002	-.00024
.20	.0037	.00370	.0040	.00395	-.0014	-.00135
.25	.0021	.00207	.0006	.00060	-.0021	-.00209
.30	.0059	.00588	.0038	.00380	-.0005	-.00050
.40	.0036	.00363	-.0032	-.00322	-.0005	-.00048
.50	.0033	.00329	.0008	.00083	.0010	.00105
.60	-.0011	-.00107	-.0006	-.00062	.0018	.00182
.70	-.0017	-.00172	-.0019	-.00187	-.0009	-.00092
.85	.0004	.00041	-.0002	-.00025	-.0033	-.00335
1.00	-.0017	-.00171	-.0008	-.00076	-.0014	-.00138
1.20	-.0024	-.00242	-.0013	-.00126	-.0038	-.00382
1.50	-.0047	-.00472	.0012	.00124	-.0020	-.00202
1.80	-.0027	-.00272	-.0013	-.00128	-.0021	-.00212
2.00	-.0020	-.00197	-.0013	-.00130	-.0002	-.00019
2.50	-.0040	-.00405	.0001	.00013	-.0025	-.00251
3.00	-.0046	-.00463	-.0003	-.00029	-.0020	-.00204
4.00	-.0046	-.00456	-.0027	-.00272	-.0023	-.00235
5.00	-.0036	-.00356	-.0006	-.00057	-.0041	-.00412
6.00	-.0037	-.00370	-.0003	-.00030	-.0016	-.00163
7.00	-.0045	-.00449	-.0019	-.00192	-.0021	-.00211
8.50	-.0047	-.00475	-.0017	-.00169	-.0018	-.00183
10.00	-.0042	-.00423	-.0001	-.00014	-.0005	-.00048
12.00	-.0045	-.00448	-.0011	-.00107	-.0017	-.00166
15.00	-.0037	-.00370	-.0008	-.00083	-.0026	-.00256
18.00	-.0038	-.00384	-.0010	-.00104	-.0021	-.00206
20.00	-.0040	-.00396	-.0006	-.00060	-.0019	-.00188
25.00	-.0047	-.00473	-.0013	-.00127	-.0019	-.00193
30.00	-.0045	-.00453	-.0006	-.00060	-.0022	-.00225

Time(ms)	-500m		-700m		-900m	
	Mag Field	Diff	Mag Field	Diff	Mag Field	Diff
.05	-.0056	-.00563	.0008	.00080	.0008	.00080
.07	-.0085	-.00853	.0055	.00553	.0055	.00553
.09	-.0076	-.00763	.0075	.00748	.0075	.00748
.10	-.0061	-.00613	.0075	.00746	.0075	.00746
.12	-.0049	-.00491	.0060	.00603	.0060	.00603
.15	-.0053	-.00527	.0046	.00461	.0046	.00461
.20	-.0067	-.00672	.0069	.00687	.0069	.00687
.25	-.0043	-.00432	.0078	.00776	.0078	.00776
.30	-.0067	-.00673	.0053	.00534	.0053	.00534
.40	-.0068	-.00683	.0066	.00661	.0066	.00661
.50	-.0058	-.00582	.0071	.00709	.0071	.00709
.60	-.0072	-.00725	.0071	.00707	.0071	.00707
.70	-.0058	-.00582	.0064	.00641	.0064	.00641
.85	-.0081	-.00805	.0057	.00565	.0057	.00565
1.00	-.0069	-.00691	.0032	.00325	.0032	.00325
1.20	-.0083	-.00827	.0061	.00613	.0061	.00613
1.50	-.0059	-.00590	.0059	.00590	.0059	.00590
1.80	-.0061	-.00614	.0062	.00617	.0062	.00617
2.00	-.0069	-.00695	.0063	.00632	.0063	.00632
2.50	-.0053	-.00534	.0057	.00574	.0057	.00574
3.00	-.0041	-.00407	.0071	.00706	.0071	.00706
4.00	-.0059	-.00592	.0062	.00623	.0062	.00623
5.00	-.0061	-.00611	.0070	.00703	.0070	.00703
6.00	-.0067	-.00674	.0069	.00694	.0069	.00694
7.00	-.0065	-.00648	.0063	.00625	.0063	.00625
8.50	-.0065	-.00646	.0061	.00608	.0061	.00608
10.00	-.0055	-.00550	.0059	.00588	.0059	.00588
12.00	-.0061	-.00613	.0057	.00565	.0057	.00565
15.00	-.0059	-.00587	.0063	.00632	.0063	.00632
18.00	-.0061	-.00615	.0068	.00683	.0068	.00683
20.00	-.0064	-.00636	.0063	.00632	.0063	.00632
25.00	-.0064	-.00643	.0064	.00638	.0064	.00638
30.00	-.0062	-.00618	.0063	.00635	.0063	.00635